

Experimental and Computational Studies of Secondary Organic Aerosol Formation

Thesis by

Robert John Griffin

In Partial Fulfillment of the Requirements

for the Degree of

Doctor of Philosophy

California Institute of Technology

Pasadena, California

2000

(Defended May 16, 2000)

© 2000
Robert John Griffin
All Rights Reserved

Dedicated with love to Ann
and my Mom and Dad

Money's only paper only ink
We'll destroy ourselves if we can't agree
How the world turns
Who made the sun
Who owns the sea
The world we know will fall piece by piece
Money's only paper only ink

Tracy Chapman

Acknowledgments

Although this thesis bears my name, I was certainly not the only one that contributed to its completion. I would be remiss if I did not take this opportunity to thank those people that helped with the work or that supported me in some way while I was doing it.

First and foremost, I would like to thank my advisor, Professor John Seinfeld. It has been said that an advisor can make or break your graduate school experience, and I was happy and lucky to have one of the great ones. I was fortunate enough to have an advisor who was supportive in every way imaginable and who encouraged me right from the beginning to tackle difficult and interesting projects in both the experimental and computational arenas. Thank you, John, for your advice and support, both professional and personal, over the past five years. Having an advisor you like and respect makes graduate school a lot easier. Count on an invitation to Durham in the future!

I would also like to thank Professor Rick Flagan. Many graduate students are not lucky enough to have two faculty members looking out for them and off of whom to bounce ideas. Rick was particularly instrumental (Yes, that pun was intended.) in the completion of the experimental parts of this thesis, and for that I am grateful to you, Rick.

Professor Donald Dabdub of the University of California at Irvine has been key in teaching me the ins and outs of air quality modeling. His support and willingness to answer even the most mundane questions seemed endless! Donald, thank you also for your role in mentoring me as I made decisions regarding my academic future. Not only

have I come to value you as a collaborator who does great work, but I also consider you a true friend. See the note above about visiting Durham.

I also need to gratefully thank those who have shared my office and lab over the past five years. Not only have we had some great and lively scientific (and not so scientific!) debates, dilemmas, and discussions, but we've also had a heck of a lot of fun, both at work and outside of it. Most of you have seen me at my worst and still haven't held it against me! Jay, Tim, David, Jian, Michele, and Paul – I owe you all a ton! Thanks also to my classmates (particularly Alison – we need a dinner!) who helped me get through transport and the quals and to the Wednesday hoop group (especially Dan and Jason) and my running buddies (Dan, Greg, and Jeff) for giving me regular opportunities to get rid of stress in a healthy way. Jason (Nomar/Andre ... This is just NOT fundamental. She only looks like one!), Peter and Amy (watch out for the Mother Yuccas in Joshua Tree!), and Mike and Nikki (one time at Mammoth...Pose down!), I thank you all for all of the fun over the past years. Thanks to Chris and Shaney (anyone want to invite Jack over next New Year's?) and Jeff and Mina (ever wonder what happened to that couch?) as well. All work and no play make Rob a dull boy, and you all were instrumental in making sure I played every once in a while in graduate school. My Tufts and high school friends, especially Josh (mind if I crash on your couch AGAIN?), Eric (we've come a long way since freshman year, no?), Les (Hermosa rules!), Jen (Squawk!), Larry (San Dieeeeeego!), and Jenn (been rear-ended by a motorcycle lately?) all supported me during grad school, even if they don't know it! Many thanks to all of you, too.

Professor Matt Fraser of Rice University and Professor Mike Kleeman of the University of California at Davis helped out incredibly with the Los Angeles area modeling aspect of this thesis. I hope you both know how much I appreciate your help; thanks for not getting angry when I repeatedly asked for more input! Thanks also for your advice on what it is like to be a young faculty member.

There are many other people whom I feel deserve my gratitude. First, I would like to thank Dr. Mildred Hastbacka of Arthur D. Little, Inc., who not only encouraged me to return to graduate school but also got me interested in atmospheric chemistry through the UNEP/Swedish EPA project. My gratitude also to the support staff in the Engineering Division office (Ann Hilgenfeldt and Elizabeth Hinojos) who were incredibly helpful in getting some of my papers ready for submission. Thanks for always having a smile and taking time to catch up, Ann! In the Chemical Engineering Department, a million thanks to Kathy Bubash for answering a never-ending list of questions about what I needed to do to graduate and to Margie Cormier for always finding extra overheads, clips instead of staples (ha ha!), and time to chat.

To my family, I owe an incredibly huge amount. To Mom and Dad, Jim and Kim, and Gordon, many, many heartfelt thanks for your love and support over the past six years – from the time I decided to leave Boston and head west until now. It means a lot to me that each of you has made the effort to visit me in Pasadena at one point or another. Thanks also to all of you for taking such an interest in my work and future plans. To the McAdam side of my family, thank you for understanding why Ann stayed in California a lot longer than she originally planned! I know NC isn't Rhodey, but I hope it is close enough!

Finally, I have saved the best for last. I would like to thank the best friend that I have ever had, Ann, my beautiful wife. Thank you so much, Ann. Without your love and support throughout this entire process, I know it would not have been as enjoyable and would have been so much more difficult. Thank you for being someone to whom I could vent when our DMA system suddenly had a leak or when I had a bug in my programs that I couldn't find. Thank you for taking such an interest in what I do (and even participating in some of the late weekend nights in lab) and for being so understanding during the last few weeks of crunch time. I owe you everything I have, and your name deserves to be on this thesis just as much as mine does. I am so lucky and proud to be your husband. I love you and always will, and that's a promise.

Abstract

Organic species are important constituents of tropospheric particulate matter in remote, rural, and urban areas. Such aerosol can be primary (emitted in the particle phase as solids or liquids) or secondary (formed *in situ* as condensable vapors) in nature.

Secondary organic aerosol (SOA) is formed when products resulting from the gas-phase oxidation of a parent organic species partition to the particle phase. This partitioning can occur via condensation onto existing inorganic aerosol (heterogeneous-heteromolecular nucleation), absorption into an existing organic aerosol, dissolution to the aerosol aqueous phase, or homogeneous-heteromolecular nucleation.

SOA yield is defined as the amount of SOA formed per the amount of a parent organic species that is oxidized. This yield depends functionally on stoichiometric and partitioning coefficients for each of the oxidation products formed and the total amount of organic aerosol mass available to act as absorptive media. Appropriate yield parameters are developed for a series of parent organics using smog chamber experiments. The effects of parent organic structure and the oxidizing species on SOA yield are also examined during the smog chamber experiments. Such yield parameters are used to model SOA formation from the oxidation of biogenic organic species on a global and annual scale. Yield parameters can also be used to define a new concept, the incremental aerosol reactivity for parent organic species, which is a convenient way of ranking parent organics in terms of their SOA-forming potentials.

Efforts to improve the simulation of SOA formation in the California Institute of Technology three-dimensional air quality model are also described. The Caltech Atmospheric Chemistry Mechanism was designed to predict concentrations of the highly

functionalized secondary organic oxidation products capable of leading to SOA. A module that treats formation of SOA thermodynamically is used to predict the distribution of these products between the gas- and aerosol-phases. The new mechanism and thermodynamic module will be used to simulate a smog episode that occurred in 1993 in the South Coast Air Basin of California.

Contents

Acknowledgments	v
Abstract	ix
List of Figures	xvi
List of Tables	xxi
1. Introduction	1
2. Aerosol formation from the oxidation of biogenic hydrocarbons	15
2.1 Introduction	16
2.2 Mechanism of secondary organic aerosol formation	19
2.3 Fractional aerosol yield	20
2.4 Chamber studies	23
2.5 Experimental procedure	24
2.6 Yields of biogenic organics in photooxidation experiments	29
2.7 Yields of biogenic organics in ozonolysis and nitrate radical experiments	31
2.8 Contribution of individual oxidants to aerosol formation	32
2.9 Conclusions	34
2.10 References	35
3. Estimate of global atmospheric organic aerosol formation from oxidation of biogenic hydrocarbons	60
3.1 Introduction	61
3.2 Secondary organic aerosol formation	62
3.3 Individual oxidant contributions to aerosol formation	63

3.4	Compound-specific emissions inventory for biogenic compounds	65
3.5	Global aerosol formation from biogenic hydrocarbons	67
3.6	References	69
4.	Incremental aerosol reactivity: application to aromatic and biogenic hydrocarbons	75
4.1	Introduction	76
4.2	Theory of secondary organic aerosol formation	78
4.3	Experimental determination of SOA yields	80
4.4	Threshold concentration for SOA formation	85
4.5	Formation of organic aerosol from a mixture of hydrocarbons	86
4.6	Incremental aerosol reactivity	87
4.7	Relative incremental aerosol reactivity	93
4.8	References	95
5.	Secondary organic aerosol: I. Atmospheric chemical mechanism for production of molecular constituents	102
5.1	Introduction	103
5.2	Inorganic chemistry	105
5.3	Organic chemistry	107
5.3.1	Alkanes	108
5.3.1.1	Short chain alkanes	109
5.3.1.2	Medium chain alkanes	110

xiii		
5.3.1.3 Long chain alkanes	111	
5.3.2 Non-biogenic alkenes	112	
5.3.2.1 Ethene	112	
5.3.2.2 Short chain alkenes	113	
5.3.2.3 Long chain alkenes	113	
5.3.3 Aldehydes	114	
5.3.4 Ketones	116	
5.3.5 Alcohols	117	
5.3.6 MTBE	118	
5.3.7 Aromatics	118	
5.3.7.1 Low yield aromatics	119	
5.3.7.2 High yield aromatics	121	
5.3.7.3 Phenolic species	121	
5.3.7.4 Aromatic aldehydes	122	
5.3.7.5 Aromatic acids	124	
5.3.7.6 Polycyclic aromatic hydrocarbons	124	
5.3.8 Biogenics	125	
5.3.8.1 Isoprene	125	
5.3.8.2 Monoterpenes	128	
5.4 Gas-Phase simulation of the SCAQS episode of August 27-29, 1987 in the SOCAB	131	
5.4.1 August 27-29, 1987 SCAQS episode	131	

5.4.2	Ozone simulation	132
5.4.3	Total semi-volatile species	133
5.4.4	Uncertainty analysis	135
5.5	Conclusions	137
5.6	References	138
6.	Secondary organic aerosol: II. Thermodynamic module for gas/particle	
	partitioning of molecular constituents	183
6.1	Introduction	184
6.2	Review of previous techniques to model SOA	185
	6.2.1 Fractional aerosol coefficient	186
	6.2.2 Fixed aerosol yield	187
	6.2.3 Saturation of oxidation products	187
	6.2.4 Dry absorptive partitioning	188
	6.2.5 Henry's law	189
6.3	Partitioning module description	189
	6.3.1 Hydrophobic module description	190
	6.3.2 Hydrophilic module description	195
	6.3.3 Example case studies	199
	6.3.3.1 Hydrophobic module	199
	6.3.3.2 Hydrophilic module	200
6.4	Application to three-dimensional atmospheric models	202
6.5	Discussion	204
6.6	Conclusions	205

6.7	References	206
7.	Conclusions	223
A.	Appendices	
A.1	The atmospheric aerosol-forming potential of whole gasoline vapor	227
A.2	Observation of gaseous and particulate phase products of monoterpane oxidation in forest atmospheres	245
A.3	Gas-phase oxidation of monoterpenes: gaseous and particulate phase products	263

List of Figures

2.1 Chemical structures of the biogenic hydrocarbons investigated.	54
2.2 Secondary organic aerosol yields for the bicyclic olefins tested as a function of organic mass concentration in photooxidation experiments.	55
2.3 Secondary organic aerosol yields for the cyclic diolefins tested as a function of organic mass concentration in photooxidation experiments.	55
2.4 Secondary organic aerosol yields for the sesquiterpenes tested as a function of organic mass concentration in photooxidation experiments.	56
2.5 Secondary organic aerosol yields for the acyclic triolefins and oxygenated terpenes tested as a function of organic mass concentration in photooxidation experiments.	56
2.6 Possible ring-opening mechanism for the reaction between OH and sabinene.	57
2.7 Secondary organic aerosol yields for the bicyclic olefins tested as a function of organic mass concentration in ozonolysis experiments.	58
2.8 Secondary organic aerosol yields for the bicyclic olefins tested as a function of organic mass concentration in NO_3 experiments.	58
2.9 Example output from the SAPRC90b gas-phase chemical mechanism.	59
5.1 An illustrative example of a degradation mechanism for a parent hydrocarbon in CACM.	178
5.2 A map of the SOCAB.	179
5.3 Simulated (solid) versus observed (dashed) NO (blue), NO_2 (red), and O_3 (green) mixing ratios for Pasadena for August 27-29, 1987.	180

5.4 Simulated (solid) versus observed (dashed) NO (blue), NO ₂ (red), and O ₃ (green) mixing ratios for Riverside for August 27-29, 1987.	180
5.5 Mixing ratios simulated by CACM (solid) versus those simulated by the extended LCC mechanism (x) [Harley <i>et al.</i> , 1993] for Pasadena for August 27-29, 1987 [NO (blue), NO ₂ (red), and O ₃ (green)].	181
5.6 Mixing ratios simulated by CACM (solid) versus those simulated by the extended LCC mechanism (x) [Harley <i>et al.</i> , 1993] for Riverside for August 27-29, 1987 [NO (blue), NO ₂ (red), and O ₃ (green)].	181
5.7 Comparison of total predicted SOA precursor concentration in the base case (solid), b/2 case (+), and acid case (dashed) versus observed SOA data (x) in Claremont on August 28, 1987.	182
5.8 Percentage of the total SOA precursor concentration that must partition to account for the observations of <i>Turpin and Huntzicker</i> [1995] for the three cases investigated [base case (solid) b/2 case (+), and acid case (dashed)].	182
6.1 Species that partition into the aerosol phase and the processes that affect them.	216
6.2 Breakdown of aerosol constituents based on their atomic nature, water affinity, and dissociative properties.	217
6.3 Flowsheet for the calculation of the partitioning of hydrophobic organic aerosol constituents between the gas- and aerosol-phases.	218
6.4 Flowsheet for the calculation of the partitioning of hydrophilic organic aerosol constituents between the gas- and aqueous- phases.	219
6.5 Particulate concentrations of octadecanoic acid ($\mu\text{g m}^{-3}$) and its partitioning coefficient ($\text{m}^3 \mu\text{g}^{-1}$) as a function of TSP. Total condensable material =	

1 $\mu\text{g m}^{-3}$.	220
6.6 Particulate concentrations of octadecanoic acid ($\mu\text{g m}^{-3}$) and its partitioning coefficient ($\text{m}^3 \mu\text{g}^{-1}$) as a function of the total amount of condensable material.	
TSP = 50 $\mu\text{g m}^{-3}$.	220
6.7 Sensitivity of the water associated with WSOC (ng m^{-3}) at varying RH. Initial LWC = 1 $\mu\text{g m}^{-3}$, pH = 5, total solute = 1 ng m^{-3} .	221
6.8 Sensitivity of the water associated with WSOC (ng m^{-3}) at varying pH. Initial LWC = 1 $\mu\text{g m}^{-3}$, RH = 0.8, total solute = 1 ng m^{-3} .	221
6.9 Overall flowsheet for the calculation of aerosol water content and the phase distributions of both inorganic and organic aerosol constituents.	222
A.1.1 Secondary organic aerosol yield as a function of total organic aerosol mass concentration (ΔM_o) for 17 individual aromatic species.	242
A.1.2 Plot of $\Delta M_o/\Delta\text{aromatic}$ as a function of ΔM_o for 12 different AQIRP gasolines (Table A1.2).	243
A.1.3 Comparison between observed total SOA concentrations produced from the oxidation of whole gasoline vapor and total SOA concentrations predicted to be formed solely from the fuel's aromatic components.	244
A.2.1 Chemical ionization mass spectrum for the derivative of a C ₉ dioxo carboxylic acid compound detected in aerosol samples.	262
A.2.2 Formation pathways for a C ₉ dioxo carboxylic acid product from oxidation of limonene.	262
A.3.1. Chromatogram of products from β -pinene/O ₃ reaction.	321
A.3.2. Methane CI mass spectra for the derivatives of products from ozone	

oxidation of β -pinene.	322-327
A.3.3. Chromatogram of products from sabinene/O ₃ reaction.	328
A.3.4. Mass spectra for the derivatives of two products (S ₈ and S ₁₂) from ozone oxidation of sabinene.	329
A.3.5. Chromatogram of products from α -pinene/O ₃ reaction.	330
A.3.6. Mass spectra for the derivatives of products from ozone oxidation of α -pinene.	331-334
A.3.7. Chromatogram of products from Δ^3 -carene/O ₃ reaction.	335
A.3.8. Methane CI mass spectra for the derivatives of products from ozone oxidation of Δ^3 -carene.	336-337
A.3.9. Amount of nopinone formed versus the amount of β -pinene reacted.	338
A.3.10. Measured log ($K_{om,i}$) versus estimated log p ^o _L for the major products in the β -pinene/O ₃ and α -pinene/O ₃ systems.	338
A.3.11. Fraction of pinic acid in aerosol phase as a function of organic aerosol mass concentration.	339
A.3.12. Top: Time-dependent secondary organic aerosol yields as a function of organic aerosol mass for two α -pinene/O ₃ experiments. Bottom: α -Pinene mixing ratio and organic aerosol mass concentration as a function of time.	340
A.3.13. Top: Time-dependent secondary organic aerosol yields as a function of organic aerosol mass for the sabinene/O ₃ reaction. Bottom: Sabinene mixing ratio and organic aerosol mass concentration as a function of time.	341
A.3.14. Reaction mechanism of O ₃ / β -pinene reaction.	342
A.3.15. Reaction mechanism of O ₃ /sabinene reaction.	343

A.3.16. Formation mechanism for A ₃ and A ₇ in the O ₃ /α-pinene reaction.	344
A.3.17. Reaction mechanism of O ₃ /Δ ³ -carene reaction.	345

List of Tables

1.1 Concentrations of atmospheric gases.	9
1.2 Properties of atmospheric aerosols.	10
1.3 Previous studies of secondary organic aerosol yields.	11,12
2.1 Reaction rate constants for the oxidation of biogenic hydrocarbons.	42
2.2a Initial conditions and data for photooxidation experiments.	43-45
2.2b Initial conditions and data.	46,47
2.3 Aerosol yield parameters for the photooxidation of biogenic hydrocarbons.	48
2.4 Aerosol yield parameters for the ozonolysis and nitrate radical oxidation of biogenic hydrocarbons.	49
2.5 Simulations of gas-phase chemistry.	50,51
2.6 Individual contributions to aerosol formation.	52,53
3.1 Aerosol yield parameters for biogenic organics.	73
3.2 OH and O ₃ oxidation patterns for bicyclic alkenes.	73
3.3 Estimated species contributions to global emissions.	74
4.1 Aerosol formation parameters α_i and K_i (m ³ μ g ⁻¹) values obtained in the Caltech smog chamber.	98
4.2 Base case mixing ratios (ppb) for the hydrocarbons of interest.	99
4.3 Incremental aerosol reactivities (μ g m ⁻³ ppb ⁻¹) for the parent organic compounds.	100
4.4 Relative incremental aerosol reactivities.	101
5.1 Chemical species represented in CACM.	146-151
5.2 Reactions contained in the Caltech Atmospheric Chemistry Mechanism.	152-172

5.3 Photolysis rate constants.	173
5.4 Three-body kinetics rate constant calculations.	174
5.5 Other rate constant calculations.	175
5.6 Hydroxyl radical rate constants calculated using a structure-reactivity relationship.	176
5.7 Emissions summary in 10^3 kg/day used in CIT for August 27, 1987.	177
5.8 Upwind boundary condition concentrations (ppb).	177
5.9 Statistical analysis of CACM performance on August 28 for O_3 and NO_2 .	177
6.1 Assumed primary organic aerosol composition for validation of the hydrophobic module.	212
6.2 Properties for malic and glyoxalic acids.	212
6.3 Input and output for the evaluation of the hydrophilic module.	213
6.4 Input and output for the evaluation of the hydrophilic module used in conjunction with SCAPE2.	214
6.5 Surrogate organic oxidation products to be used in the partitioning module.	215
A.1.1 Estimation of the contributions by individual species to the SOA formed from the photooxidation of a five-hydrocarbon mixture.	240
A.1.2 Properties of AQIRP reformulated gasolines.	241
A.2.1 Monoterpene oxidation products detected at forest sites.	257-259
A.2.2 Monoterpene oxidation products in filter samples collected in Kejimkujik National Park, Nova Scotia.	260
A.2.3 Gaseous and particulate monoterpene oxidation products in samples collected in San Bernardino National Forest, California.	261

A.3.1 Initial conditions and results of ozone-terpene reactions.	304
A.3.2 Denuder and filter collection efficiencies of selected products.	304
A.3.3 Relative recoveries of select multifunctional compounds vs. recovery standard.	305
A.3.4 Products from ozone oxidation of β -pinene.	306-307
A.3.5 Products from ozone oxidation of sabinene.	308-309
A.3.6 Products from ozone oxidation of α -pinene.	310
A.3.7 Products from ozone oxidation of Δ^3 -carene.	311-312
A.3.8 Products and their surrogates for quantification.	313
A.3.9 Gaseous and particulate product yields in the β -pinene/O ₃ reaction.	314-315
A.3.10 Gaseous and particulate product yields in the sabinene/O ₃ reaction.	316
A.3.11 Gaseous and particulate product yields in the α -pinene/O ₃ reaction.	317
A.3.12 Gaseous and particulate product yields in the Δ^3 -carene/O ₃ reaction.	318
A.3.13 Gas-particle partitioning coefficients (m ³ μ g ⁻¹) of individual products at 306-308K.	319
A.3.14 Sub-cooled liquid vapor pressure estimates.	320

Chapter 1

Introduction

The troposphere is a complex mixture of both naturally occurring and anthropogenic species in both the gas- and the aerosol (liquid or solid particles dispersed in the background gas) phases. While species such as molecular oxygen, molecular nitrogen, and a few noble gases dominate the composition profile of the troposphere, many trace species are also constituents of the mixture called air. Urban, regional, and global air quality issues are of interest to atmospheric scientists because of the detrimental effects associated with many of these trace constituents of the tropospheric system. Methods used to increase our understanding of atmospheric chemistry can be laboratory-based, field-based, theoretical, or computational. While laboratory-based studies allow for investigation of the fundamental physical and chemical processes that occur in the atmosphere, field-based studies allow for identification of the species and phenomena that are dominant in the real world environment. Theoretical studies attempt to explain some of the laboratory and field observations based on new or expanded concepts. Computational studies allow atmospheric scientists to include laboratory measurements in an air quality model to see if the model can match field observations at a given location and time.

Trace gases in the atmosphere have a variety of molecular components. Nitrogen-containing species include the oxides of nitrogen (NO and NO₂), peroxy acyl nitrate compounds (PANs), ammonia (NH₃), nitrous oxide (N₂O) and organo-nitrate compounds. Nitrogen-containing species can have both anthropogenic and biogenic primary sources and can be secondary in nature. The sulfur-containing species in the atmosphere include sulfur dioxide (SO₂, which is oxidized to sulfur trioxide, SO₃, and quickly hydrolyzed to form sulfuric acid, H₂SO₄) carbonyl sulfide (OCS), dimethyl sulfide (CH₃SCH₃), and

hydrogen sulfide (H_2S). Like the nitrogen-containing species discussed previously, sulfur-containing compounds are both primary and secondary and both anthropogenic and biogenic. Carbon-containing species include carbon monoxide (CO), carbon dioxide (CO_2), and organic molecules of both an anthropogenic and a biogenic nature. Organic species include alkanes, alkenes, aromatics, carbonyls, alcohols, and carboxylic acids. Many of the functionalized organics are both primary and secondary. As noted previously, these organic species can also contain sulfur or nitrogen. Other important gas-phase species include ozone (O_3 , a photochemical pollutant) and water, which is the most abundant and perhaps the most important trace gas species in the atmosphere. The processes that govern the concentrations of these species include wind, mixing height, emission rate, formation rate, and consumption rate. Concentrations vary temporally (diurnal and seasonal variations) and spatially. Concentrations of some common gas-phase species are shown in Table 1.1 [*Seinfeld and Pandis*, 1998]. The effects of the trace gases of the troposphere are varied. They include material damage for ozone, health effects on humans for ozone and some of the carbonaceous species, and visibility degradation for NO_2 . Many are considered greenhouse gases as well.

In contrast to gas-phase trace constituents of the atmosphere are those that reside in the aerosol phase. These species can be either solid or amorphous/liquid. Species that contribute to the aerosol burden include sulfate (SO_4^{2-}), nitrate (NO_3^-), ammonium (NH_4^+), water, soil dust, sea salt, elemental carbon, and organic species. As with gas-phase trace constituents of the troposphere, there are many processes that govern the concentrations of particulate matter, including mixing height, emission rates, formation rates, temperature, humidity, wind, and deposition to the earth's surface. Typical

concentrations of atmospheric particulate matter are shown in Table 1.2 [Seinfeld and Pandis, 1998] for a variety of times and locations. It is crucial to understand the formation of atmospheric aerosols because of the well documented effects of these particles. First, increasing aerosol concentrations are statistically linked to regions with increased rates of mortality, pointing to the significant detrimental human health effects of particulate matter. Aerosol particles also participate in radiative forcing. The direct effect of aerosols on the radiative balance of the earth is a result of the reflectance or absorption by aerosol particles of incident sunlight. The indirect effect of aerosols on the radiative balance of the earth results from the change in albedo because of aerosol effects on cloud droplet size and lifetime. Finally, it has been seen in both urban and rural areas that atmospheric particles contribute to visibility degradation because of their light scattering properties.

Of specific interest in the work presented here are the organic aerosol (OA) components of atmospheric particulate matter (PM). OA can have primary (emitted to the atmosphere in the aerosol phase) or secondary (formed *in situ* as condensable vapors) sources. Primary sources of OA include all combustion processes [Schauer, 1998]. Secondary organic aerosol (SOA) is formed when highly functionalized organic oxidation products are absorbed into an organic aerosol phase because of their low volatility [Odum *et al.*, 1996]. Secondary organic products can also partition to the aerosol phase via aqueous dissolution (Henry's law) [Saxena and Hildemann, 1996]. Only those parent organic species with 6 or more carbon atoms are considered capable of forming SOA via the absorptive mechanism. The two groups of compounds that have been investigated the most in terms of their SOA formation potentials are the aromatics

that are constituents of gasoline and the biogenic monoterpenes. The work presented in this thesis discusses each of these compound groups. Previous studies investigating SOA formation from a variety of parent organics are described in Table 1.3.

In contrast to those studies shown in Table 1.3, the work presented here will investigate SOA formation in the context of an absorptive equilibrium theory. The absorption of secondary oxidation products into an absorbing organic aerosol phase is defined by an equilibrium partitioning coefficient, $K_{om,i}$ ($\text{m}^3 \mu\text{g}^{-1}$). This coefficient is defined as

$$K_{om,i} = \frac{A_{i,om}/M_o}{G_i} = \frac{RT}{MW_{om} \zeta_i p_{L,i}^o} \quad (1)$$

where $A_{i,om}$ is the absorbing organic aerosol phase concentration of species i , G_i is its gas phase concentration, M_o is the total amount of organic aerosol (in mass concentration units of $\mu\text{g m}^{-3}$) available to act as the absorptive media, R is the ideal gas constant in appropriate units, T is the temperature in Kelvin, MW_{om} is the average molecular weight of the mixture (g mol^{-1}), ζ is the activity coefficient of i in the mixture, and $p_{L,i}^o$ is the vapor pressure (torr) of i at temperature T . If one combines the definition of $K_{om,i}$ with a mass balance and stoichiometry, it can be shown that the total SOA yield for a parent hydrocarbon (defined as the amount of SOA formed per amount of parent organic that reacts) is given by

$$Y = M_o \sum_i \left(\frac{\alpha_i K_{om,i}}{1 + K_{om,i} M_o} \right) \quad (2)$$

where α_i is the mass-based stoichiometric factor describing the formation of species i from the parent organic of interest.

Chapter 2 discusses a series of outdoor chamber photooxidation experiments that has been used to establish and characterize the significant atmospheric aerosol-forming potentials of 14 biogenic organic species. The effect of structure on aerosol yield for these types of compounds has also been investigated. For bicyclic alkenes (α -pinene, β -pinene, Δ^3 -carene, and sabinene), experiments were also carried out at daytime temperatures in a dark system in the presence of ozone (O_3) or nitrate radicals (NO_3) alone. For ozonolysis experiments, resulting aerosol yields are less dependent on organic mass concentration, when compared to full, sunlight-driven photooxidation. Nitrate radical experiments exhibit extremely high conversion to aerosol for β -pinene, sabinene, and Δ^3 -carene. The relative importance of aerosol formation from each type of reaction for bicyclic alkene photooxidation is elucidated.

The results from this series of outdoor chamber experiments have been used to estimate the annual amount of SOA formed globally from compounds emitted by vegetation. This modeling effort is described in detail in Chapter 3. Because oxidation by NO_3 under ambient, remote conditions is likely to be negligible, parameters describing aerosol formation from hydroxyl radical (OH) and O_3 reaction only are developed. Chamber results, temporally and spatially resolved, compound-specific estimates of biogenic hydrocarbon emissions, and OH and O_3 fields are combined to lead to an estimate for atmospheric SOA formed annually from biogenic precursors of 18.5 Tg, a number considerably smaller than the previously published estimates.

The concept of incremental aerosol reactivity (IAR) is introduced in Chapter 4, and the IARs of a number of important anthropogenic and biogenic organics are investigated for four ambient scenarios. The IAR, defined as a change in the SOA mass produced (in $\mu\text{g m}^{-3}$) per unit change of parent organic reacted (in ppb), is a measure of the aerosol-forming capability of a given parent organic in a prescribed mixture of other organic compounds. The base case scenario is a mixture of both aromatic and biogenic organics. Reactivity values depend on the choice of the initial organic mixture, so cases are also examined in which all biogenic hydrocarbon concentrations are set to zero and all aromatic concentrations are set to zero. The influence of additional organic aerosol is also investigated.

A new atmospheric chemical mechanism, the Caltech Atmospheric Chemistry Mechanism (CACM), is presented in Chapter 5. CACM is designed to represent current ozone chemistry as well as formation of individual surrogate organic oxidation products that are believed to be capable of forming SOA. CACM is used to simulate gas-phase concentrations in the South Coast Air Basin (SOCAB) of Southern California for August 27-29, 1987. Simulated concentrations are compared to those measured as part of the Southern California Air Quality Study (SCAQS). The results for CACM are also compared to previous SCAQS simulation results using the previous chemical mechanism used within the California Institute of Technology three-dimensional atmospheric model (CIT); by doing so, CACM has been validated. Chapter 6 exhibits a module that predicts SOA formation based on the thermodynamic equilibrium partitioning of secondary organic oxidation products to the aqueous phase via Henry's law or to an absorbing organic phase. The modules described in Chapters 5 and 6 will be incorporated into the

next generation of the CIT, which will be applied to the smog episode of September 8-9, 1993, in the SOCAB.

Finally, the Appendices contain papers that describe other areas of work in this field in which the author has been involved. Appendix I describes work investigating the formation of SOA from aromatic species and highly complex mixtures such as gasoline. Appendix II and Appendix III describe respectively field and laboratory observations of the highly functionalized secondary oxidation products of biogenic organics.

Table 1.1. Concentrations of atmospheric gases.

Gas	Average Mixing Ratio (ppm)	Cycle/Source
Ar	9340	No cycle/natural
N ₂	780,840	Biological/microbiological
O ₂	209,460	Biological/microbiological
CH ₄	1.72	Biogenic and chemical
CO ₂	355	Anthropogenic and biogenic
NO/NO ₂	10 ⁻⁶ -10 ⁻²	Anthropogenic, biogenic, and chemical
O ₃	10 ⁻² -10 ⁻¹	Chemical
H ₂ O	Variable	Physicochemical

Table 1.2. Properties of atmospheric aerosols.

Type	Number (cm ⁻³)	PM ₁ (µg m ⁻³)	PM ₁₀ (µg m ⁻³)
Urban (polluted)	10 ⁵ -4x10 ⁶	30-150	100-300
Marine	100-400	1-4	10
Rural	2000-10,000	2.5-8	10-40
Remote continental	50-10,000	0.5-2.5	2-10

PM₁ represents those particles with diameters of 1 µm or less; species that dominate this mode include sulfate, ammonium, nitrate, and organics. PM₁₀ represents those particles with diameters of 10 µm or less; species that dominate this mode include calcium, sodium, and chloride.

Table 1.3. Previous studies of secondary organic aerosol yield*.

COMPOUND	YIELD (%) ^{**}	FAC (%) ^{***}	REFERENCE
<i>Alkanes</i>			
<i>n</i> -heptane		<0.06	McMurtry and Grosjean [1985]
<i>n</i> -octane		<0.001	Wang, et al. [1992]
2,6-dimethylheptane		0.65	O'Brien, et al. [1975]
cyclohexane		<0.017	McMurtry and Grosjean [1985]
methylcyclohexane		9.2	Wang, et al. [1992]
<i>Aromatics</i>			
benzene	0	0	Izumi and Fukuyama [1990]
toluene	2-6 ^b	0.6-1.4	Leone, et al. [1985]
	1.4-6.2 ^b	0.5-1.7	Gery, et al. [1985]
	4.8 ^c	2.1	Stern, et al. [1987]
	3.0 ^d	2.3	Izumi and Fukuyama [1990]
	18.6 ^c	6.4	Wang, et al. [1992]
<i>m</i> -, <i>o</i> -, <i>p</i> -ethyltoluene	3.7, 3.3, 1.5 ^d	1.9, 1.4, 0.6	Izumi and Fukuyama [1990]
<i>o</i> -xylene	8 ^a	6.2	O'Brien, et al. [1975]
<i>m</i> -xylene	3.5 ^c	2.9	Stern, et al. [1987]
<i>m</i> -, <i>o</i> -, <i>p</i> - xylene	2.4-2.6, 2.7,.95 ^d	2.5-3.1, 2.1,	Izumi and Fukuyama [1990]
ethylbenzene	1 ^a	0.78	O'Brien, et al. [1975]
	1.9 ^c	0.6	Stern, et al. [1987]
	3.1 ^d	2	Izumi and Fukuyama [1990]
<i>n</i> -propylbenzene	0.98 ^d	0.2	Izumi and Fukuyama [1990]
isopropylbenzene	2.3 ^d	1	Izumi and Fukuyama [1990]
1,2,3-trimethylbenzene	2.2 ^d	1.4	Izumi and Fukuyama [1990]
1,2,4-trimethylbenzene	1.1 ^d	0.6	Izumi and Fukuyama [1990]
1,3,5-trimethylbenzene	0.5-14 ^a	0.69-1.92	O'Brien, et al. [1975]
	2.4 ^c	2.1	Stern, et al. [1987]
	1.8 ^d	1.2	Izumi and Fukuyama [1990]
<i>o</i> -cresol	5.1-44.5 ^e	0.5-14.0, 0 ^f	McMurtry and Grosjean [1985]
4-hydroxy-2-	57 ^e	8.6	McMurtry and Grosjean [1985]
styrene	0.3 ^d	0.5	Izumi and Fukuyama [1990]
α -, β -methylstyrene	0.7-4.9, 0.57 ^d	1.3-7.6, 1.0	Izumi and Fukuyama [1990]
methoxybenzene	2.7 ^d	0.8	Izumi and Fukuyama [1990]
<i>Olefins</i>			
1-hexene		0.34, 0.24 ^f	McMurtry and Grosjean [1985]
1-heptene		0.85	O'Brien, et al. [1975]
1-octene		4.2	Wang, et al. [1992]
cyclopentene		1.0-5.0 ^f	Hatakeyama, et al. [1987]
cyclohexene		13 ^f	Hatakeyama, et al. [1987]
		18.3	Izumi, et al. [1989]
cycloheptene		4.0-10.0 ^f	Hatakeyama, et al. [1987]
1,5-hexadiene		20.3	O'Brien, et al. [1975]
1,6-heptadiene		69	O'Brien, et al. [1975]
2-methyl-1,5-		47.6	O'Brien, et al. [1975]
1,7-octadiene		68	O'Brien, et al. [1975]
2,6-octadiene		0.9	O'Brien, et al. [1975]

Table 1.3. (continued) Previous studies of secondary organic aerosol yield^{*}.

COMPOUND	YIELD (%) ^{**}	FAC (%) ^{***}	REFERENCE
Biogenics			
α -pinene		55	<i>O'Brien, et al. [1975]</i>
		38-55	<i>Hooker, et al. [1985]</i>
		18.3 ^f	<i>Hatakeyama, et al. [1989]</i>
	10.8 ^c	5.3	<i>Zhang, et al. [1992]</i>
β -pinene		13.8 ^f	<i>Hatakeyama, et al. [1989]</i>
		8	<i>Pandis, et al. [1991]</i>
	10.8 ^c	5.3	<i>Zhang, et al. [1992]</i>
limonene		>50	<i>Schuetzle and Rasmussen [1978]</i>
isoprene		0	<i>Pandis, et al. [1991]</i>

^{*} Does not include the work of the author or of *Odum, et al. [1996]* or *Hoffmann, et al. [1997]* as those works are discussed in the text in detail.

^{**} Yield reported for photooxidation in the presence of NO_x

^{***} FAC: fractional aerosol coefficient (100*ratio of aerosol formed to initial parent organic concentration)

a in terms of aerosol light scattering units

b as fraction of initial carbon present

c assuming aerosol density of 1.0 g cm⁻³

d in terms of carbon mass fraction

e assuming aerosol density of 1.3 g cm⁻³ and accounting for chamber wall losses

f from reaction with ozone only

References

Gery, M.W., D.L. Fox, H.E. Jeffries, L. Stockburger, and W.S. Weathers, A continuous stirred tank reactor investigation of the gas-phase reaction of hydroxyl radicals and toluene, *Intl. J. Chem. Kinet.*, 17, 177-216, 1985.

Hatakeyama, S., K. Izumi, T. Fukuyama, and H. Akimoto, Reactions of ozone with α -pinene and β -pinene in air: yields of gaseous and particulate products, *J. Geophys. Res.*, 96, 947-958, 1989.

Hoffmann, T., J.R. Odum, F. Bowman, D. Collins, D. Klockow, R.C. Flagan, and J.H. Seinfeld, Formation of organic aerosols from the oxidation of biogenic hydrocarbons, *J. Atmos. Chem.*, 26, 189-222, 1997.

Hooker, C.L., H.H. Westberg, and J.C. Sheppard, Determination of carbon balances for smog chamber terpene oxidation experiments using a ^{14}C tracer technique, *J. Atmos. Chem.*, 2, 307-320, 1985.

Izumi, K., and T. Fukuyama, Photochemical aerosol formation from aromatic hydrocarbons in the presence of NO_x , *Atmos. Environ.*, 24A, 1433-1441, 1990.

Leone, J.A., R.C. Flagan, D. Grosjean, and J.H. Seinfeld, An outdoor smog chamber and modeling study of toluene- NO_x photooxidation, *Intl. J. Chem. Kinet.*, 17, 177-216, 1985.

McMurry, P.H., and D. Grosjean, Photochemical formation of organic aerosols: Growth laws and mechanisms, *Atmos. Environ.*, 19, 1445-1451, 1985.

O'Brien, R.J., J.R. Holmes, and A.H. Bockian, Formation of photochemical aerosol from hydrocarbons: Chemical reactions and products, *Environ. Sci. Technol.*, 9, 568-576, 1975.

Odum, J.R., T. Hoffmann, F. Bowman, D. Collins, R.C. Flagan, and J.H. Seinfeld, Gas/particle partitioning and secondary organic aerosol yields, *Environ. Sci. Technol.*, 30, 2580-2585, 1996.

Pandis, S.N., S.E. Paulson, J.H. Seinfeld, and R.C. Flagan, Aerosol formation in the photooxidation of isoprene and β -pinene, *Atmos. Environ.*, 25A, 997-1008, 1991.

Saxena, P., and L.M. Hildemann, Water-soluble organics in atmospheric particles: a critical review of the literature and application of thermodynamics to identify candidate compounds, *J. Atmos. Chem.*, 24, 57-109, 1996.

Schauer, J.J. Source Contributions to Atmospheric Organic Compound Concentrations: Emissions, Measurements, and Model Predictions, Ph.D. Thesis, California Institute of Technology, Pasadena, CA, 1998.

Schuetzle, D., and R.A. Rasmussen, The molecular composition of secondary aerosol particles formed from terpenes, *J. Air. Poll. Control. Assoc.*, 28, 236-240, 1978.

Seinfeld, J.H., and S.N. Pandis, *Atmospheric Chemistry and Physics*, Wiley-Interscience, New York, 1998.

Stern, J.E., R.C. Flagan, D. Grosjean, and J.H. Seinfeld, Aerosol formation and growth in atmospheric aromatic photooxidation, *Environ. Sci. Technol.*, 21, 1224-1231, 1987.

Wang, S.-C., S.E. Paulson, D. Grosjean, R.C. Flagan, and J.H. Seinfeld, Aerosol formation and growth in atmospheric organic/NO_x systems – I. Outdoor smog chamber studies of C₇- and C₈- hydrocarbons, *Atmos. Environ.*, 26A, 403-420, 1992.

Zhang, S.-H., M. Shaw, J.H. Seinfeld, and R.C. Flagan, Photochemical aerosol formation from α -pinene and β -pinene, *J. Geophys. Res.*, 97, 20,717-20,729, 1992.

Chapter 2

Organic Aerosol Formation from the Oxidation of Biogenic Hydrocarbons

Reference: R.J. Griffin, D.R. Cocker III, R.C. Flagan, and J.H. Seinfeld, *J. Geophys. Res.*, 104, 3555-3567, 1999.

2.1 Introduction

A variety of organic compounds are emitted to the atmosphere from both natural and agricultural plants [Isidorov *et al.*, 1985; Arey *et al.*, 1991b; Fehsenfeld *et al.*, 1992; Winer *et al.*, 1992; Arey *et al.*, 1995]. Isoprene (C_5H_8), monoterpenes ($C_{10}H_{16}$), and sesquiterpenes ($C_{15}H_{24}$) comprise the majority of these emissions, although oxygenated and sulfur-containing species have also been identified [Arey *et al.*, 1991a; König *et al.*, 1995; Puxbaum and König, 1997]. Estimates of biogenic organic emissions have been made on global, national (e.g., the United States), and regional (e.g., the South Coast Air Basin of California or the Mediterranean region) bases. Total annual global biogenic organic emissions are estimated to range from 491 to 1150 TgC, greatly exceeding the 98 TgC of total organics estimated to be emitted from anthropogenic sources [Müller, 1992; Guenther *et al.*, 1995]. Averaged over the United States, biogenic emissions are estimated to be of the same order of magnitude of those from anthropogenic sources [Lamb *et al.*, 1993].

Significant uncertainty exists concerning the atmospheric reaction mechanisms of biogenic organics. The presence of unsaturated carbon-carbon bonds in these molecules leads to high reactivities [Atkinson *et al.*, 1995; Shu and Atkinson, 1995; Atkinson, 1997]. Because of the large quantity of emission and because of their atmospheric reactivity, biogenic nonmethane hydrocarbons (NMHCs) are predicted to play an important role in tropospheric chemistry [Chameides *et al.*, 1988; McKeen *et al.*, 1991; Roselle *et al.*, 1991; Fehsenfeld *et al.*, 1992]. Numerous studies investigating the nature of both gas-phase and aerosol-phase products formed from the reactions between biogenic NMHCs and the hydroxyl radical (OH), ozone (O_3), the $O(^3P)$ atom, and the nitrate radical (NO_3)

have been performed [*Stephanou and Stratigakis*, 1993; *Hakola et al.*, 1994; *Calogirou et al.*, 1995, 1997; *Berndt et al.*, 1996; *Grosjean and Grosjean*, 1997; *Hallquist et al.*, 1997; *Shu et al.*, 1997; *Vinckier et al.*, 1997; *Wängberg et al.*, 1997; *Alvarado et al.*, 1998; *Aschmann et al.*, 1998; *Griesbaum et al.*, 1998; *Yu et al.*, 1998].

Went [1960] was apparently the first to suggest the role of biogenic hydrocarbons in the formation of tropospheric aerosols. Higher molecular weight tropospheric hydrocarbons have been shown, upon oxidation, to produce semivolatile products that partition between the gas and aerosol phases [*Pandis et al.*, 1991; *Zhang et al.*, 1992; *Odum et al.*, 1996, 1997ab; *Hoffmann et al.*, 1997]. In the aerosol phase, these products are referred to as secondary organic aerosol (SOA). Among anthropogenic NMHCs, aromatics are the most important source of SOA [*Odum et al.*, 1996, 1997ab]. Among biogenic hydrocarbons, isoprene, because of its small size and the high volatility of its oxidation products, has been shown not to produce SOA at atmospheric levels [*Pandis et al.*, 1991]. Biogenic NMHCs larger than isoprene, however, are effective sources of aerosol [*Pandis et al.*, 1991; *Zhang et al.*, 1992; *Odum et al.*, 1996; *Hoffmann et al.*, 1997].

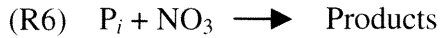
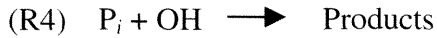
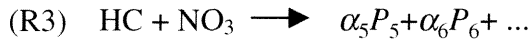
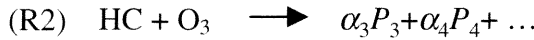
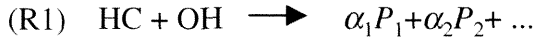
The importance of biogenic NMHCs in tropospheric aerosol formation will vary from area to area depending on climate, amount and nature of vegetation, and other environmental factors. In a Canadian forest, formation and growth of new particles have been attributed to oxidation of biogenic organics [*Leaitch et al.*, 1999]. It has been estimated that under peak photochemical conditions, anywhere from 20-80% of the organic aerosol burden in the South Coast Air Basin of California is secondary in nature [*Turpin and Huntzicker*, 1995; *Schauer et al.*, 1996] and that 16% of the SOA during a specific high-smog episode could be attributed to biogenic precursors [*Pandis et al.*,

1992]. Moreover, *Kaplan and Gordon* [1994] showed that a significant fraction of organic carbon associated with fine particulate matter in the Los Angeles area is not derived from fossil fuel precursors.

Previous experiments have provided limited information on the yields of SOA from α -pinene and β -pinene [*Pandis et al.*, 1991; *Zhang et al.*, 1992]. *Hoffmann et al.* [1997] reported the aerosol-forming potentials of a few other biogenic hydrocarbons, but too few experiments were performed to completely and quantitatively describe resulting aerosol formation. This study reports comprehensive outdoor chamber experiments on aerosol formation from 14 of the most prevalent biogenic organics. Differences in observed aerosol yields among compounds will be addressed on the basis of structural characteristics of the parent hydrocarbon. In sunlight-irradiated chamber experiments, OH, O_3 , and NO_3 all contribute to hydrocarbon consumption and subsequent aerosol formation. To determine the individual contribution of each oxidant to aerosol formation for a parent hydrocarbon, gas-phase chemistry is modeled, from which the fraction of the parent hydrocarbon reacting with each oxidant can be determined. This is coupled with experiments in which O_3 or NO_3 is the only available oxidant. By deriving the quantitative parameters describing aerosol formation in these O_3 -only or NO_3 -only systems, it is possible to unravel the contribution to aerosol formation from each oxidant in full photooxidation experiments. An explanation of the mechanism of SOA formation, a derivation of the functional expression for aerosol yield, an expanded and specific list of the experiments performed, and a detailed experimental protocol all precede the presentation of data from these experiments and the corresponding analysis and discussion.

2.2 Mechanism of Secondary Organic Aerosol Formation

Consider a parent hydrocarbon, HC, reacting with OH, O₃, and NO₃. A variety of products form:



While only two products are indicated for each reaction here, the actual number of products is much greater. (Later, a two-product model is used to quantitatively describe aerosol formation in full photooxidation experiments or ones in which a single oxidant is available.) The parameter α_i represents a stoichiometric factor relating the total amount of product i formed to the total amount of hydrocarbon that reacts. Later, this constant will be expressed on a mass basis, rather than the usual molar basis. As shown in (R4)-(R6), any of these products can, in principle, further react with any of the available oxidants, creating an even more complex and diverse mix of oxidation products.

For parent hydrocarbons containing roughly six or more carbon atoms, these products are semivolatile and, in the presence of sufficient organic aerosol, will partition between the gas and aerosol phases. The fraction of each product that partitions to the

aerosol phase can be described on the basis of an equilibrium coefficient $K_{om,i}$. In principle, if the molecular nature of each product, as well as that of the aerosol organic phase, were known, $K_{om,i}$ could be calculated from first principles. In practice, such molecular-level information is not available, so $K_{om,i}$ values are determined experimentally.

2.3 Fractional Aerosol Yield

Secondary organic aerosol formation has been determined experimentally through investigation of the fractional aerosol yield Y [Pandis *et al.*, 1991; Zhang *et al.*, 1992; Odum *et al.*, 1996, 1997ab; Hoffmann *et al.*, 1997]. Because identification and quantification of individual oxidation products, for example, all the individual products in (R1)-(R6), are difficult, this yield is a convenient overall measure of the aerosol-forming potential of the secondary products of atmospheric oxidation of a parent organic molecule. This yield is defined as the ratio of the amount of SOA formed from the oxidation of a given parent compound to the amount of that compound that reacted:

$$Y = \frac{\Delta M_o}{\Delta HC} \quad (1)$$

where ΔM_o ($\mu\text{g m}^{-3}$) is the organic aerosol mass formed after the consumption of ΔHC ($\mu\text{g m}^{-3}$) of the given parent. The extent of gas/particle absorptive partitioning depends on the amount of the condensed organic phase into which the products can be absorbed. Thus aerosol yield depends on the amount of organic matter present, M_o , into which the semivolatile products may partition. An outcome of this mechanism is that a secondary

product can be absorbed into an organic phase, even if it exists in the gas phase below its own saturation concentration [Pankow, 1994ab; Odum *et al.*, 1996, 1997ab; Hoffmann *et al.*, 1997]. Pankow [1994ab] has defined an absorption equilibrium coefficient $K_{p,i}$ ($\text{m}^3 \mu\text{g}^{-1}$) for the partitioning of such a semivolatile component between the gas and particle phases as

$$K_{p,i} = \frac{F_{i,om}/(\text{TSP})}{A_i} = \frac{760RTf_{om}}{M_{om}10^6\zeta_i p_{L,i}^o} \quad (2)$$

where $F_{i,om}$ (ng m^{-3}) is the mass concentration of compound i in the absorbing organic matter (om) phase, A_i (ng m^{-3}) is its gas-phase mass concentration, TSP ($\mu\text{g m}^{-3}$) is the total suspended particulate concentration, R is the ideal gas constant, T (K) is the temperature, f_{om} is the fraction of the TSP that is absorbing om , M_{om} (g mol^{-1}) is the mean molecular weight of the absorbing phase, ζ_i is the activity coefficient of species i in the om phase, and $p_{L,i}^o$ (torr) is the vapor pressure (subcooled, if necessary) of compound i at temperature T . If only the absorbing organic phase is considered, a similar equilibrium constant can be defined as

$$K_{om,i} = \frac{F_{i,om}/M_{om}}{A_i} = \frac{K_{p,i}}{f_{om}} \quad (3)$$

simply by dividing $K_{p,i}$ by f_{om} . Equation (3) indicates that this new equilibrium constant is a function of the mass of the available organic phase into which a semivolatile product can be absorbed. Thus more of each product partitions to the organic aerosol phase as the total organic aerosol concentration increases. As a result, a parent compound that has

undergone a certain amount of photooxidation, ΔHC , will exhibit a range of SOA yield values depending on the value of M_o . For the experiments described in this paper, $M_o = \Delta M_o$, since all organic aerosol mass is generated by the oxidation of the parent hydrocarbon. By combining the definitions of Y and $K_{om,i}$, a total mass balance, and a stoichiometric constraint, Y can be expressed as a function of ΔM_o by [Odum *et al.*, 1996]

$$Y = \Delta M_o \sum_i \left(\frac{\alpha_i K_{om,i}}{1 + K_{om,i} \Delta M_o} \right) \quad (4)$$

where ΔM_o , $K_{om,i}$ and α_i are defined as above. Yield data for over 30 individual parent compounds obtained in the Caltech outdoor chamber have been fit to (4) using a two product model, that is, with parameters, α_1 , α_2 , $K_{om,1}$ and $K_{om,2}$ [Hoffmann *et al.*, 1997; Odum *et al.*, 1996, 1997ab]. While it was given earlier that many products result from the atmospheric oxidation of a parent hydrocarbon, it has been shown that a two-product model is needed for most compounds to accurately describe the shape of the yield curve described by (4). Use of three or more products in the model has been proven to be superfluous. The four parameters derived in the two-product model can be seen as an adequate description of the stoichiometry and volatility of the complex mix of oxidation products.

It must be noted that this theory assumes that secondary products are unable to form a solution with existing seed aerosol. Accounting for the interactions between the organic compounds themselves allows it to be shown that such products can condense onto seed aerosol at concentrations lower than those predicted by saturation theory alone [Seinfeld and Pandis, 1998]. In this case, the threshold amount of the parent compound

that must react to form SOA in the chamber is defined as ΔHC^* . After consumption of ΔHC^* , products condense onto seed aerosol to form an initial amount of SOA, which can then act as an absorptive medium. At this point, absorption becomes the dominant mechanism governing the partitioning of secondary products and, therefore, determining SOA yield, as in the atmosphere.

2.4 Chamber Studies

In this study the results of extensive outdoor chamber experiments on aerosol formation from 14 biogenic organic compounds are reported. These compounds include monoterpenes of chemical formula $\text{C}_{10}\text{H}_{16}$: α -pinene, β -pinene, Δ^3 -carene, and sabinene, bicyclic olefins that differ in the location of the double bond and the number of carbons associated with the secondary ring; limonene, α -terpinene, γ -terpinene, and terpinolene, cyclic diolefins that differ only in the location of a second double bond; and myrcene and ocimene, acyclic triolefins that differ only in the location of a third double bond. In addition, two sesquiterpenes of structure $\text{C}_{15}\text{H}_{24}$ (β -caryophyllene and α -humulene) and two oxygenated terpenes (linalool and terpinene-4-ol) are investigated. The structure of each of these compounds is shown in Figure 2.1, and their reaction rate constants at 298K with OH , O_3 , and NO_3 are given in Table 2.1.

As noted above, full sunlight-irradiated photooxidation experiments will have, in general, all three of OH , O_3 , and NO_3 present, and, therefore, in general, aerosol yields will be the result of products generated in all three oxidation pathways. Experiments performed in a dark system with O_3 or NO_3 as the only available oxidants, in conjunction with results from gas-phase modeling, can then be used to determine the individual

contributions to SOA formation from each oxidant. Experiments involving NO_3 as the only oxidant need be performed only for bicyclic olefins, as they are the slowest reacting of the compounds studied and will persist long enough for NO_3 to build up in the chamber. The other compounds are consumed completely by OH and O_3 in the sunlight-driven photooxidations prior to significant formation of NO_3 .

2.5 Experimental Procedure

All experiments were performed in a sealed, 50-m³ Teflon chamber that has been described in detail previously [*Odum et al.*, 1996, 1997ab; *Hoffmann et al.*, 1997]. This chamber was normally divided in the center so that two experiments could be run under identical environmental conditions. Each resulting chamber had an estimated volume of 20 m³. Instruments for monitoring gas-phase components and a computer for acquiring aerosol data were operated from a laboratory adjacent to the chamber. Aerosol sampling instruments were operated directly next to the chamber in a closed cart that was maintained at a temperature of approximately 25°C. Between experiments, the chamber was continuously purged with compressed air and allowed to bake in sunlight for at least a day. The compressed air was purified to remove organics, particulate matter, water, and NO_x species. Air in the chamber prior to the experiments contained no detectable hydrocarbons or particles and less than 5 ppb NO_x . Before entering the chamber, the air was passed through a rehumidifier containing distilled and deionized water so that the relative humidity during the experiments was approximately 5%.

At this time, it has not been determined how an increase in humidity influences the formation of SOA. Possible effects include differences in the chemical and physical

nature of the absorbing phase such as a shift from an organic mixture to an aqueous-inorganic-organic mixture, a variation in the mean molecular weight of the absorbing phase, and a change in the activities of secondary products in the absorbing mixture.

Deviation in any or all of these factors would affect the equilibrium partitioning coefficient of each product, thereby affecting the overall SOA yield. These issues are currently under study.

Gas-phase concentrations of the parent hydrocarbons in the chamber were monitored using a Hewlett Packard (Palo Alto, California) 5890 gas chromatograph (GC) equipped with a DB-5 column (J&W Scientific, Davis, California) and a flame ionization detector (FID). The temperature program for the GC began at -60°C, held for 1 min, ramped from -60°C to 150°C at a rate of 40°C min⁻¹, and then held for 1.5 min. Prior to each experiment, known volumes of a solution of the parent hydrocarbon and methylene chloride were vaporized into a small, 60-L Teflon bag filled with compressed air.

Measurements from these bags were then used to calibrate the GC.

Following the GC calibration, seed particles of (NH₄)₂SO₄ were injected into the chamber to obtain initial particle concentrations of approximately 5,000-10,000 particles cm⁻³. (Seed particles were not used in nitrate radical experiments.) The particles were generated by atomizing a solution of (NH₄)₂SO₄ salt in deionized water. The particles flowed through a heated copper tube and a diffusion dryer, resulting in crystalline (NH₄)₂SO₄, and were then passed through a ⁸⁵Kr neutralizer before being injected into the chamber. The initial size distribution of the seed aerosol was centered around a diameter of approximately 100 nm.

Once the number concentration of particles on each side of the chamber had equilibrated, the chamber was divided and covered with a black polyethylene tarpaulin in

order to prevent sunlight from irradiating the contents of the chamber. Propene, NO, NO₂, hexafluorobenzene (C₆F₆), and hydrocarbon were then injected into each side of the chamber through Teflon lines. Propene was used as a photochemical initiator to provide sufficient levels of OH, and C₆F₆ was used as a nonreactive internal standard. NO and NO₂ are added primarily to facilitate the basic photochemical cycle involving O₃ and to participate in the reaction converting peroxy radicals (RO₂) to alkoxy radicals (RO). Therefore, it is expected that the NO_x level in the chamber will have little effect on aerosol yield except through the formation of O₃ and NO₃. Propene and NO_x were injected from certified cylinders of approximately 500 ppm in nitrogen. The target initial mixing ratio of propene in each chamber was 250-300 ppb for each photooxidation experiment, and the amount of NO_x (NO_x = NO + NO₂) injected varied depending on the initial concentration of the parent hydrocarbon. The average hydrocarbon to total NO_x ratio (ppbC/ppb) was approximately 5 to 1, whereas the average ratio of NO to NO₂ was 1.5 to 1. The parent hydrocarbon and the C₆F₆ were injected by vaporizing microliter quantities in a heated glass bulb that was diluted with compressed, purified air that flowed directly to the chamber.

After all of the injections to the chamber had been made and sufficient time had passed to allow mixing within each side of the chamber, measurements of hydrocarbon, O₃, NO_x, and particle concentrations were taken in order to obtain initial values and to ensure that the contents of the chamber were well mixed. Typically, three hydrocarbon readings using the GC method described above were taken from each side of the chamber. Ozone was measured using a Dasibi Environmental Corporation (Glendale, California) Model 1008-PC O₃ analyzer that was calibrated at the beginning of the series

of experiments by Dasibi. The estimated uncertainty in these readings is $\pm 4\%$; a drift of only a few percent in the monitor readings was seen over the course of several months. NO, NO₂, and total NO_x concentrations were monitored using a Thermo Environmental Instruments (Franklin, Massachusetts) Model 42 chemiluminescence NO_x monitor. Prior to each experiment, zero and span checks were performed on this instrument using certified cylinders of NO, NO₂, and N₂. The estimated uncertainty in NO_x monitor readings are $\pm 4\%$ for NO and $\pm 7\%$ for NO₂. After the initial readings were complete, the black tarpaulin was removed, exposing the chamber to sunlight and starting the experiment. During the experiments, O₃ and NO_x were sampled continuously from each side of the chamber in intervals of 10 min, and hydrocarbon samples were taken throughout the experiment from alternating sides of the chamber. Temperature was also tracked continuously throughout the course of each experiment.

Aerosol data included size distributions and total number concentrations for each side of the chamber at a 1-min frequency. Aerosol instrumentation consisted of a TSI (St. Paul, Minnesota) Model 3071 cylindrical scanning electrical mobility spectrometer (SEMS) to measure the size distribution of particles and a TSI Model 3760 condensation nucleus counter (CNC) to count particles. SEMS voltages were ramped exponentially from 40 to 8500 V, and the classifier flows were 2.5 L min⁻¹ for sheath and excess flows and 0.25 L min⁻¹ for inlet and classified aerosol flows. This allowed for the measurement of particles in the diameter range of approximately 30-850 nm. A complete and detailed description of the SEMS operation that includes a description of data analysis techniques has been published previously [*Wang and Flagan, 1990*].

Experiments in which O_3 or NO_3 is the primary oxidant were performed at night to eliminate the possibility of photolysis of secondary products to form OH. (This also avoided high temperatures caused by keeping the chamber covered with the black tarpaulin in direct sunlight, as in the experiments of *Hoffmann et al.*, [1997].) In ozonolysis experiments, an appropriate concentration of 2-butanol was used to scavenge any OH formed in the hydrocarbon- O_3 reaction and to ensure that O_3 was the only oxidant present in the system [*Chew and Atkinson*, 1996].

To compare aerosol formation under the different conditions, it is important that the temperature in the chamber during the dark experiments be close to that of a typical afternoon smog chamber experiment because the partitioning coefficient $K_{om,i}$ is a function of temperature. To achieve this, the entire chamber was covered with an insulating cover as well as the black tarpaulin, neither of which was removed during the course of the experiment. This was done after the seed particles had been injected and the chamber had been divided as described above. In addition, four Holmes (Milford, Massachusetts) Model HFH-501FP space heaters were placed in the open area underneath the chamber. By varying the number of heaters used and their power settings, daytime temperatures of approximately 30°-35°C could be achieved and maintained throughout the course of an experiment.

Injections of hydrocarbon, C_6F_6 , and 2-butanol (if needed) were then made to each side as described above. Once initial readings for both sides had been completed for ozonolysis experiments, O_3 was injected to each side using an Enmet Corporation (Ann Arbor, Michigan) Model 04052-011 O_3 generator until the Dasibi O_3 monitor read approximately 4 times the initial hydrocarbon concentration on the appropriate side. For

NO_3 experiments, sufficient NO_3 was generated via the thermal decomposition of N_2O_5 synthesized by the combination of O_3 and NO_2 [R. Atkinson, personal communication, 1997]. Continuous aerosol, GC, and temperature readings were taken as described above. Initial conditions and resulting data are given for all experiments in Table 2.2.

2.6 Yields of Biogenic Organics in Photooxidation Experiments

Figures 2.2-2.5 show aerosol yields as a function of organic mass concentration for photooxidation experiments with the 14 biogenic compounds tested. Figures 2.2-2.5 also show the theoretical yield curves fit using (4) for each biogenic hydrocarbon. The parameters resulting from the fit of these curves are given in Table 2.3. As seen in Figures 2.2-2.5, there exists a wide range of aerosol yields for biogenic hydrocarbons. Sesquiterpenes have the highest yields of the compounds tested. This behavior is a consequence of the high carbon number of the parent compounds. Limonene, β -pinene, and sabinene are among the compounds with the highest yields, clearly indicating the effect of the presence of a $=\text{CH}_2$ group in a cyclic monoterpene structure. The yields of limonene, Δ^3 -carene, α -pinene, and the terpinene isomers also indicate the significance of double bonds that are internal to ring structures. When oxidants attack unsaturated bonds, carbon atoms may be lost as a result of the decomposition of the resulting radical species [Atkinson, 1997]. However, the two trends noted above suggest that fewer carbon atoms are lost by oxidant attack on $=\text{CH}_2$ double bonds or double bonds that are internal to ring structures. The lower yields of ocimene, myrcene, linalool, and terpinolene also support this hypothesis since three or more carbon atoms can be cleaved by oxidant attack on these molecules. However, terpinene-4-ol, which has an OH group replacing the

second double bond of the terpinene isomers, does not adhere to this trend, in that its yield is significantly lower than that of the terpinene isomers. This is likely a result of the fact that the OH group replaces the more reactive double bond.

For the bicyclic olefins, the number of carbon atoms associated with the secondary ring also seems to have an effect on SOA yield. Δ^3 -carene and α -pinene have an identical structure, outside of a difference in the number of carbon atoms in the secondary ring, yet Δ^3 -carene has a higher aerosol yield than α -pinene (Figure 2.2). Since many of the products of the oxidation of these parent hydrocarbons are expected to be similar and retain their secondary ring structures [Yu *et al.*, 1998], this difference in yield can be explained by the less volatile nature of Δ^3 -carene (boiling point 168°-169°C) compared to α -pinene (boiling point 155°-156°C). However, sabinene (boiling point 163°-164°C), which has an exocyclic methylene group and a secondary three-carbon ring, has lower yields than β -pinene (boiling point 165°-167°C), which has an external methylene group and a secondary four-carbon ring. This is the opposite of the trend seen with Δ^3 -carene and α -pinene. This difference cannot be explained by the slight difference in boiling point of the parent compounds. However, it can possibly be explained by a mechanism that results in the cleavage of both rings in sabinene since open-chain compounds tend to be more volatile than cyclic ones. This mechanism, adapted from the H atom abstraction mechanism of Aschmann *et al.* [1998] for α -pinene, is shown in Figure 2.6. For illustrative purposes, only OH radical reaction is shown. The corresponding mechanism for β -pinene is much less likely to result in the cleavage of both rings.

2.7 Yields of Biogenic Organics in Ozonolysis and Nitrate Radical Experiments

In general, aerosol yields in ozonolysis of the biogenic hydrocarbons are less dependent on organic mass concentration when compared to those under sunlight-irradiated photooxidation, in which the parent hydrocarbon is oxidized by OH, O₃, and NO₃. This indicates that ozonolysis leads to secondary products that are less volatile than those in the full photooxidation system [Hoffmann *et al.*, 1997]. O₃ reactions with β -pinene and sabinene, however, produce significantly lower aerosol yields than the corresponding full photooxidation experiments. The opposite behavior is seen for α -pinene and Δ^3 -carene (Figure 2.7 and Table 2.4). This indicates that compounds with double bonds internal to ring structures are more likely to form condensable products when compared to compounds with external double bonds. (These results cannot be compared to those of Hoffman *et al.* [1997], since those experiments were performed without an OH scavenger and at considerably different temperatures.) Large yields of aerosol result from NO₃ reaction with β -pinene, Δ^3 -carene, and sabinene, indicating possible formation of nitrated products in large yields (Figure 2.8 and Table 2.4). The olefin α -pinene shows insignificant aerosol formation from NO₃ oxidation. This can be explained by the creation in high yield of pinonaldehyde, which is too volatile to partition significantly to the aerosol phase [Wängberg *et al.*, 1997].

Some scatter can be seen in the data sets associated with each type of experiment. This is most likely linked to the uncertainty regarding charging of the aerosol generated in the chamber and slight variations in temperature between experiments.

2.8 Contribution of Individual Oxidants to Aerosol Formation

To identify the amount of parent hydrocarbon consumed by each of the three available oxidants in sunlight-driven photooxidation experiments, the SAPRC90b mechanism [Carter, 1990] was used to model the gas-phase chemistry of the photochemical smog chamber experiments for α -pinene [Odum *et al.*, 1996; Hoffmann *et al.*, 1997], β -pinene, sabinene, and Δ^3 -carene. By using initial concentrations of hydrocarbon, NO_x , and propene and varying model parameters such as sunlight intensity and temperature, it was possible to simulate experimental concentration profiles of hydrocarbon, NO_x , and O_3 , from which it was also possible to infer the amount of hydrocarbon consumed by each oxidant. A sample output is shown in Figure 2.9, and the results for the four hydrocarbons tested are summarized in Table 2.5. As shown in Table 2.5, the fraction of the parent hydrocarbon consumed by each oxidant varies among compounds and within a set of experiments for a single compound depending on initial concentrations of hydrocarbon and NO_x , sunlight intensity, and temperature. In addition, it is confirmed that OH is the primary oxidant for all compounds studied under full photooxidation conditions in the chamber.

The fraction of parent hydrocarbon consumed by each oxidant in each photooxidation experiment has been determined for α -pinene, β -pinene, Δ^3 -carene, and sabinene. Using experimental data from photooxidation experiments (total amount of organic mass formed and total amount of parent hydrocarbon reacted), yield parameters from ozonolysis experiments, and yield parameters from nitrate radical experiments in conjunction with these data, the contribution of each oxidant to aerosol formation in biogenic photooxidation experiments can be estimated.

By adding the contribution of OH, O₃, and NO₃ to organic aerosol formation in equation (1),

$$Y = \frac{\Delta M_{o,\text{OH+}}}{\Delta \text{HC}} + \frac{\Delta M_{o,\text{O}_3}}{\Delta \text{HC}} + \frac{\Delta M_{o,\text{NO}_3}}{\Delta \text{HC}} \quad (5)$$

where OH+ represents OH reaction in addition to any cross reactions (e.g., the reaction of OH with products of initial O₃ reaction). By recognizing that

$$Y_i = \frac{\Delta M_{o,i}}{\Delta \text{HC}_i} \quad (6)$$

with *i* representing each oxidant, it can be shown that the overall yield is

$$Y_i = \frac{\Delta M_{o,\text{OH+}}}{\Delta \text{HC}} + \sum_i f_i Y_i \quad (7)$$

where *f_i* represents the fraction of the parent consumed by oxidant *i* ($\Delta \text{HC}_i / \Delta \text{HC}$) for O₃ and NO₃, which has been determined from the gas-phase modeling. By applying (4) to each oxidant, it can be shown that

$$Y_i = \Delta M_o \sum_j \left(\frac{\alpha_{i,j} K_{om,i,j}}{1 + K_{om,i,j} \Delta M_o} \right) \quad (8)$$

where *j* now represents each product in the two-product model. Therefore, the overall yield is

$$Y = \frac{\Delta M_{o,\text{OH+}}}{\Delta \text{HC}} + \Delta M_o \sum_i f_i \sum_j \left(\frac{\alpha_{i,j} K_{om,i,j}}{1 + K_{om,i,j} \Delta M_o} \right) \quad (9)$$

with the only unknown being the amount of aerosol organic mass formed from OH reactions and cross reactions, which can be determined for each experiment. The fraction of aerosol derived from the reaction of the parent with each oxidant in photooxidation experiments can then be determined from (6), (8), and (9). The results for each experiment are given in Table 2.6. It can be seen that the contribution of each oxidant varies among compounds and within a set of compounds for each oxidant. This variation can be explained mechanistically by differences in temperature (affecting kinetics and gas-particle partitioning of secondary products), incident sunlight intensity (affecting photolysis of NO_3), and initial concentrations (affecting the rate of O_3 and NO_3 formation).

2.9 Conclusions

The atmospheric aerosol forming potential of 14 of the most prevalent terpenoid biogenic hydrocarbons has been elucidated. Yield parameters for each compound tested show that these compounds have a greater potential to form secondary organic aerosol than typical aromatic constituents of gasoline. Although some degree of grouping of the biogenic hydrocarbons based on structural characteristics in terms of their aerosol forming potentials is possible, this is not uniformly the case at this time. As a result, it will be necessary to account individually for most biogenic hydrocarbons when modeling secondary organic aerosol formation in the ambient atmosphere.

Separate ozonolysis and nitrate radical experiments were performed for bicyclic olefins to investigate aerosol formation from reaction with individual oxidants. Yields in ozonolysis experiments are less dependent on organic mass concentration when compared to those in full sunlight-irradiated photooxidation. Sabinene and β -pinene have significantly lower yields from O_3 reaction alone than the corresponding sunlight-driven photooxidation experiments. However, the opposite behavior is seen for α -pinene and Δ^3 -carene. Reaction between NO_3 and β -pinene, Δ^3 -carene, or sabinene leads to high conversion to aerosol, indicating probable ambient aerosol formation at night when monoterpenes continue to be emitted and NO_3 accumulates.

It has been confirmed that OH , O_3 , and NO_3 each contribute to parent hydrocarbon consumption and aerosol formation in chamber photooxidation. Gas-phase chemistry modeling, combined with yield parameters from individual oxidant experiments, allows for the determination of the contribution of each oxidant to aerosol formation.

2.10 References

Alvarado, A., E.C. Tuazon, S.M. Aschmann, R. Atkinson, and J. Arey, Products of the gas-phase reactions of $O(^3P)$ atoms and O_3 with α -pinene and 1,2-dimethyl-1-cyclohexene, *J. Geophys. Res.*, 103, 25,541-25,552, 1998.

Arey, J., A.M. Winer, R. Atkinson, S.M. Aschmann, W.D. Long, and C.L. Morrison, The emission of (Z)-3-hexen-1-ol, (Z)-3-hexenylacetate, and other oxygenated hydrocarbons from agricultural plant species, *Atmos. Environ.*, 25, 1063-1075, 1991a.

Arey, J., A.M. Winer, R. Atkinson, S.M. Aschmann, W.D. Long, C.L. Morrison, and D.M. Olszyk, Terpenes emitted from agricultural species found in California's Central Valley, *J. Geophys. Res.*, 96, 9329-9336, 1991b.

Arey, J., D.E. Crowley, M. Resketo, and J. Lester, Hydrocarbon emissions from natural vegetation in California's South Coast Air Basin, *Atmos. Environ.*, 29, 2977-2988, 1995.

Aschmann, S.M., A. Reissell, R. Atkinson, and J. Arey, Products of the gas-phase reactions of the OH radical with α - and β -pinene in the presence of NO, *J. Geophys. Res.*, 103, 25,553-25,561, 1998.

Atkinson, R., Gas-phase tropospheric chemistry of volatile organic compounds, 1, Alkanes and alkenes, *J. Phys. Chem. Ref. Data*, 26, 215-290, 1997.

Atkinson, R., J. Arey, S.M. Aschmann, S.B. Corchnoy, and Y. Shu, Rate constants for the gas-phase reactions of *cis*-3-hexen-1-ol, *cis*-3-hexenylacetate, *trans*-2-hexenal, and linalool with OH and NO_3 radicals and O_3 at $296 +/ - 2\text{K}$ and OH radical formation yields from the O_3 reactions, *Int. J. Chem. Kinet.*, 27, 941-955, 1995.

Berndt, T., O. Böge, I. Kind, and W. Rolle, Reaction of NO_3 radicals with 1,3-cyclohexadiene, α -terpinene, and α -phellandrene: Kinetics and products, *Ber. Bunsen-Ges. Phys. Chem.*, 100, 462-469, 1996.

Calogirou, A., D. Kotzias, and A. Kettrup, Atmospheric oxidation of linalool, *Naturwissenschaften*, 82, 288-289, 1995.

Calogirou, A., D. Kotzias, and A. Kettrup, Product analysis of the gas-phase reaction of β -caryophyllene with ozone, *Atmos. Environ.*, 31, 283-285, 1997.

Carter, W.P.L., A detailed mechanism for the gas-phase atmospheric reactions of organic compounds, *Atmos. Environ.*, 24, 481-518, 1990.

Chameides, W.L., R.W. Lindsay, J. Richardson, and C.S. Kiang, The role of biogenic hydrocarbons in urban photochemical smog: Atlanta as a case study, *Science*, 241, 1473-1475, 1988.

Chew, A.A., and R. Atkinson, OH radical formation yields from the gas-phase reactions of O₃ with alkenes and monoterpenes, *J. Geophys. Res.*, 101, 28,649-28,653, 1996.

Fehsenfeld, F., et al., Emissions of volatile organic compounds from vegetation and the implications for atmospheric chemistry, *Glob. Biogeochem. Cycles*, 6, 389-430, 1992.

Griesbaum, K., V. Miclaus, and I.C. Jung, Isolation of ozonides from gas-phase ozonolyses of terpenes, *Environ. Sci. Technol.*, 32, 647-649, 1998.

Grosjean, E., and D. Grosjean, The gas phase reaction of unsaturated oxygenates with ozone: Carbonyl products and comparison with the alkene-ozone reaction, *J. Atmos. Chem.*, 27, 271-289, 1997.

Guenther, A., et al., A global model of natural volatile organic compound emissions, *J. Geophys. Res.*, 100, 8873-8892, 1995.

Hakola, H., J. Arey, S.M. Aschmann, and R. Atkinson, Product formation from the gas-phase reactions of OH radicals and O₃ with a series of monoterpenes, *J. Atmos. Chem.*, 18, 75-102, 1994.

Hallquist, M., I. Wängberg, and E. Ljungström, Atmospheric fate of carbonyl oxidation products originating from α -pinene and Δ^3 -carene: Determination of rate of reaction with OH and NO₃ radicals, UV absorption cross sections, and vapor pressures, *Environ. Sci. Technol.*, 31, 3166-3172, 1997.

Hoffmann, T., J.R. Odum, F. Bowman, D. Collins, D. Klockow, R.C. Flagan, and J.H. Seinfeld, Formation of organic aerosols from the oxidation of biogenic hydrocarbons, *J. Atmos. Chem.*, 26, 189-222, 1997.

Isidorov, V.A., I.G. Zenkevich, and B.V. Ioffe, Volatile organic compounds in the atmosphere of forests, *Atmos. Environ.*, 19, 1-8, 1985.

Kaplan, I.R., and R.J. Gordon, Non-fossil-fuel fine-particle organic carbon aerosols in southern California determined during the Los Angeles aerosol characterization and source apportionment study, *Aerosol Sci. Technol.*, 21, 343-359, 1994.

König, G., M. Brunda, H. Puxbaum, C.N. Hewitt, S.C. Duckham, and J. Rudolph, Relative contribution of oxygenated hydrocarbons to the total biogenic VOC emissions of selected mid-European agricultural and natural plant species, *Atmos. Environ.*, 29, 861-874, 1995.

Lamb, B., D. Gay, H. Westberg, and T. Pierce, A biogenic hydrocarbon emission inventory for the U.S.A. using a simple forest canopy model, *Atmos. Environ.*, 27, 1673-1690, 1993.

Leaitch, W.R., J.W. Bottenheim, T.A. Biesenthal, S.M. Li, P.S.K. Liu, K. Asalien, H. Dryfhout-Clark, F. Hopper, and F. Brechtel, A case study of gas-to-particle conversion in an eastern Canadian forest, *J. Geophys. Res.*, 104, 8095-8111, 1999.

McKeen, S.A., E.Y. Hsie, and S.C. Liu, A study of the dependence of rural ozone on ozone precursors in the eastern United States, *J. Geophys. Res.*, 96, 15,377-15,394, 1991.

Müller, J. F., Geographical distribution and seasonal variation of surface emissions and deposition velocities of atmospheric trace gases, *J. Geophys. Res.*, 97, 3787-3804, 1992.

Odum, J.R., T. Hoffmann, F. Bowman, D. Collins, R.C. Flagan, and J.H. Seinfeld, Gas/particle partitioning and secondary organic aerosol yields, *Environ. Sci. Technol.*, 30, 2580-2585, 1996.

Odum, J.R., T.P.W. Jungkamp, R.J. Griffin, R.C. Flagan, and J.H. Seinfeld, The atmospheric aerosol-forming potential of whole gasoline vapor, *Science*, 276, 96-99, 1997a.

Odum, J.R., T.P.W. Jungkamp, R.J. Griffin, H.J.L. Forstner, R.C. Flagan, and J.H. Seinfeld, Aromatics, reformulated gasoline, and atmospheric organic aerosol formation, *Environ. Sci. Technol.*, 31, 1890-1897, 1997b.

Pandis, S.N., S.E. Paulson, J.H. Seinfeld, and R.C. Flagan, Aerosol formation in the photooxidation of isoprene and β -pinene, *Atmos. Environ.*, 25, 997-1008, 1991.

Pandis, S.N., R.A. Harley, G.R. Cass, and J.H. Seinfeld, Secondary organic aerosol formation and transport, *Atmos. Environ., Part A*, 26, 2269-2282, 1992.

Pankow, J.F., An absorption model of the gas/aerosol partitioning of organic compounds in the atmosphere, *Atmos. Environ.*, 28, 185-188, 1994a.

Pankow, J. F., An absorption model of the gas/aerosol partitioning involved in the formation of secondary organic aerosol, *Atmos. Environ.*, 28, 189-193, 1994b.

Puxbaum, H., and G. König, Observation of dipropenyldisulfide and other organic sulfur compounds in the atmosphere of a beech forest with *allium ursinum* ground cover, *Atmos. Environ.*, 31, 291-294, 1997.

Roselle, S.J., T.E. Pierce, and K.L. Schere, The sensitivity of regional ozone modeling to biogenic hydrocarbons, *J. Geophys. Res.*, 96, 7371-7394, 1991.

Schauer, J.J., W.F. Rogge, L.M. Hildemann, M.A. Masurek, G.R. Cass, and B.R.T. Simoneit, Source apportionment of airborne particulate matter using organic compounds as tracers, *Atmos. Environ.*, 30, 3837-3855, 1996.

Seinfeld, J.H., and S.N. Pandis, *Atmospheric Chemistry and Physics*, Wiley-Interscience, New York, 1998.

Shu, Y., and R. Atkinson, Atmospheric lifetimes and fates of a series of sesquiterpenes, *J. Geophys. Res.*, 100, 7275-7281, 1995.

Shu, Y., E.S.C. Kwok, E.C. Tuazon, R. Atkinson, and J. Arey, Products of the gas-phase reactions of linalool with OH radicals, NO₃ radicals, and O₃, *Environ. Sci. Technol.*, 31, 896-904, 1997.

Stephanou, E.G., and N. Stratigakis, Oxocarboxylic and α , ω -dicarboxylic acids: Photooxidation products of biogenic unsaturated fatty acids present in urban aerosols, *Environ. Sci. Technol.*, 27, 1403-1407, 1993.

Turpin, B.J., and J.J. Huntzicker, Identification of secondary organic aerosol episodes and quantitation of primary and secondary organic aerosol concentrations during SCAQS, *Atmos. Environ.*, 29, 3527-3544, 1995.

Vinckier, C., F. Compernolle, and A.M. Saleh, Qualitative determination of the non-volatile reaction products of the α -pinene reaction with hydroxyl radicals, *Bull. Soc. Chim. Belg.*, 106, 501-513, 1997.

Wängberg, I., I. Barnes, and K.H. Becker, Product and mechanistic study of the reaction of NO₃ radicals with α -pinene, *Environ. Sci. Technol.*, 31, 2130-2135, 1997.

Wang, S.C., and R.C. Flagan, Scanning electrical mobility spectrometer, *Aerosol Sci. Technol.*, 13, 230-240, 1990.

Went, F.W., Blue hazes in the atmosphere, *Nature*, 187, 641-643, 1960.

Winer, A.M., J. Arey, R. Atkinson, S.M. Aschmann, W.D. Long, C.L. Morrison, and D.M. Olszyk, Emission rates of organics from vegetation in California's Central Valley, *Atmos. Environ.*, 26, 2647-2659, 1992.

Yu, J., R.C. Flagan, and J.H. Seinfeld, Identification of products containing -COOH, -OH, and -C=O in atmospheric oxidation of hydrocarbons, *Environ. Sci. Technol.*, 32, 2357-2370, 1998.

Zhang, S.H., M. Shaw, J.H. Seinfeld, and R.C. Flagan, Photochemical aerosol formation from α -pinene and β -pinene, *J. Geophys. Res.*, 97, 20,717-20,729, 1992.

Table 2.1. Reaction rate constants for the oxidation of biogenic hydrocarbons.

Parent	$k_{\text{OH}} \times 10^{12}$	$k_{\text{O}_3} \times 10^{18}$	$k_{\text{NO}_3} \times 10^{12}$
Δ^3 -Carene	88	37	9.1
β -Caryophyllene	197	11600	19
α -Humulene	293	11700	35
Limonene	171	200	12.2
Linalool	159	430	11.2
Myrcene	215	470	11
Ocimene	252	540	22
α -Pinene	53.7	86.6	6.2
β -Pinene	78.9	15	2.5
Sabinene	117	86	10
α -Terpinene	363	21100	140
γ -Terpinene	177	140	29
Terpinene-4-ol	170	250	14.6
Terpinolene	225	1880	97

Units are $\text{cm}^3 \text{ molecule}^{-1} \text{ s}^{-1}$. Data are from Atkinson *et al.* [1995], Shu and Atkinson [1995], and Atkinson [1997].

Table 2.2a. Initial conditions and data for photooxidation experiments.

Date	Parent	T, K	ΔHC	ΔM_o	Y	NO	NO_2
			ppb	$\mu\text{g m}^{-3}$		ppb	ppb
07/01/97a	Δ^3 -Carene	310.0	28.8	2.5	0.016	36.9	55.4
07/01/97b	Δ^3 -Carene	310.0	66.8	11.6	0.033	90.5	96.9
08/21/97b	Δ^3 -Carene	312.8	72.5	54.6	0.142	67.5	60.8
08/15/97b	Δ^3 -Carene	308.8	73.6	63.7	0.161	86.2	82.3
08/19/97b	Δ^3 -Carene	312.0	104.6	99.7	0.179	89.6	72.3
09/18/97b	β -Caryophyllene	308.3	5.9	17.6	0.369	18.7	9.4
09/16/97b	β -Caryophyllene	306.6	10.3	64.6	0.775	39.0	14.9
09/17/98b	β -Caryophyllene	308.6	12.9	82.3	0.790	13.1	11.1
09/18/97a	α -Humulene	308.3	5.0	12.9	0.319	16.2	7.8
09/15/97b	α -Humulene	309.3	5.4	28.2	0.648	30.8	23.8
09/16/97a	α -Humulene	306.6	8.6	59.2	0.845	37.6	14.8
09/17/97a	α -Humulene	308.6	9.2	54.2	0.732	19.5	13.5
08/26/97b	Limonene	313.4	20.6	9.5	0.087	43.1	61.8
08/26/97a	Limonene	313.4	35.2	49.6	0.266	17.4	62.8
08/17/97b	Limonene	309.4	49.5	79.1	0.298	73.6	65.8
08/17/97a	Limonene	309.4	65.1	120.2	0.344	75.7	64.4
08/28/97b	Linalool	312.4	71.6	26.7	0.056	164.7	130.1
09/19/97a	Myrcene	311.1	9.8	3.5	0.068	23.5	21.5
09/10/97b	Myrcene	311.9	77.5	57.5	0.168	117.9	79.9
08/24/97a	Ocimene	313.2	45.6	7.3	0.030	96.3	85.7
07/23/97a	Ocimene	315.7	76.5	17.6	0.043	49.0	94.0
07/23/97b	Ocimene	315.7	142.0	50.3	0.066	125.1	168.6

Read 09/18/97 as September 18, 1997.

Table 2.2a. (continued) Initial conditions and data for photooxidation experiments.

Date	Parent	T, K	ΔHC ppb	ΔM_o $\mu\text{g m}^{-3}$	Y	NO ppb	NO_2 ppb
08/15/97a	β -Pinene	308.8	32.3	20.4	0.118	81.4	53.4
07/15/97a	β -Pinene	313.6	33.7	14.6	0.080	49.2	62.5
07/17/97a	β -Pinene	316.2	42.0	7.2	0.032	15.6	43.4
07/27/97a	β -Pinene	313.3	45.0	34.2	0.144	53.1	58.6
07/15/97b	β -Pinene	313.6	62.2	51.4	0.153	87.0	79.7
08/19/97a	β -Pinene	312.0	79.0	109.4	0.260	88.8	64.8
07/21/97a	β -Pinene	313.5	85.5	100.1	0.221	93.7	63.6
07/21/97b	β -Pinene	313.5	96.5	141.6	0.272	93.0	67.0
07/09/97a	Sabinene	316.0	13.9	1.9	0.025	21.3	43.5
07/07/97a	Sabinene	310.3	34.9	14.3	0.076	50.2	52.2
07/05/97a	Sabinene	312.9	53.3	23.9	0.085	91.9	81.4
08/24/97b	Sabinene	313.2	74.0	48.7	0.124	115.3	96.5
07/05/97b	Sabinene	312.9	75.3	51.4	0.129	93.2	61.4
07/07/97b	Sabinene	310.3	77.7	53.4	0.129	106.0	77.9
07/09/97b	Sabinene	316.0	83.3	65.2	0.145	115.5	84.1
09/04/97a	α -Terpinene	316.0	47.0	20.2	0.082	87.1	51.3
09/08/97a	α -Terpinene	314.7	65.2	43.9	0.128	62.8	148.9
09/06/97a	α -Terpinene	313.3	79.6	73.8	0.175	106.0	53.0
09/11/97a	γ -Terpinene	312.4	40.9	21.3	0.098	44.7	45.0
09/10/97a	γ -Terpinene	311.9	77.5	65.9	0.160	132.2	82.7
09/06/97b	Terpinene-4-ol	313.3	116.2	42.6	0.056	216.3	132.2

Read 09/18/97 as September 18, 1997.

Table 2.2a. (continued) Initial conditions and data for photooxidation experiments.

Date	Parent	$T, \text{ K}$	ΔHC ppb	ΔM_o $\mu\text{g m}^{-3}$	Y	NO ppb	NO_2 ppb
09/02/97a	Terpinolene	312.6	25.0	1.9	0.015	47.7	47.3
09/02/97b	Terpinolene	312.6	46.9	5.2	0.021	42.4	64.7
08/28/97a	Terpinolene	312.4	60.1	9.9	0.031	54.7	56.3
09/11/97b	Terpinolene	312.4	92.3	17.8	0.036	128.0	88.8
09/04/97b	Terpinolene	316.0	133.2	28.9	0.041	190.5	122.7

Read 09/18/97 as September 18, 1997.

Table 2.2b. Initial conditions and data.

Date	Parent	$T, \text{ K}$	ΔHC	ΔM_o	Y
			ppb	$\mu\text{g m}^{-3}$	
<i>Nitrate Radical Experiments</i>					
05/20/98a	Δ^3 -Carene	308.0	36.2	24.4	0.125
06/03/98a	Δ^3 -Carene	308.2	51.6	178.8	0.643
05/28/98a	Δ^3 -Carene	310.1	70.2	267.7	0.713
05/18/98a	Δ^3 -Carene	309.2	80.1	310.5	0.722
06/01/98a	β -Pinene	309.9	18.8	32.4	0.322
05/09/98b	β -Pinene	304.0	19.7	46.1	0.428
06/01/98b	β -Pinene	309.9	54.7	243.2	0.830
05/13/98b	β -Pinene	302.0	96.4	467.3	0.891
05/20/98b	Sabinene	308.0	32.8	24.3	0.138
06/03/98b	Sabinene	308.2	41.5	151.5	0.677
05/28/98b	Sabinene	310.1	55.9	223.9	0.749
05/18/98b	Sabinene	309.2	68.2	276.5	0.755

Table 2.2b. (continued) Initial conditions and data.

Date	Parent	$T, \text{ K}$	ΔHC	ΔM_o	Y
			ppb	$\mu\text{g m}^{-3}$	
<i>Ozone Experiments</i>					
06/19/98b	Δ^3 -Carene	308.6	11.8	5.5	0.086
06/21/98b	Δ^3 -Carene	309.3	29.9	18.7	0.117
06/23/98b	Δ^3 -Carene	307.0	47.7	33.1	0.129
06/15/98b	Δ^3 -Carene	306.2	89.9	64.4	0.132
06/05/98a	α -Pinene	309.9	16.7	7.4	0.083
06/05/98b	α -Pinene	309.9	18.2	8.5	0.087
06/07/98a	α -Pinene	303.3	31.0	30.3	0.179
06/07/98b	α -Pinene	303.3	45.5	46.0	0.184
06/09/98a	α -Pinene	308.0	57.0	52.3	0.170
06/09/98b	α -Pinene	308.0	65.0	65.1	0.186
06/13/98a	β -Pinene	308.4	11.9	0.0	0.000
06/13/98b	β -Pinene	308.4	35.2	1.8	0.009
06/11/98a	β -Pinene	306.9	57.6	9.2	0.030
06/11/98b	β -Pinene	306.9	80.1	22.5	0.052
06/19/98a	Sabinene	308.6	12.5	1.4	0.021
06/21/98a	Sabinene	309.3	34.0	5.1	0.028
06/23/98a	Sabinene	307.0	51.6	9.1	0.033
06/15/98a	Sabinene	306.2	92.4	17.9	0.036

Table 2.3. Aerosol yield parameters for the photooxidation of biogenic hydrocarbons.

Parent	α_1	α_2	$K_{om,1}$	$K_{om,2}$
			$m^3 \mu g^{-1}$	$m^3 \mu g^{-1}$
Δ^3 -Carene*	0.054	0.517	0.043	0.0042
β -Caryophyllene*	1.000		0.0416	
α -Humulene	1.000		0.0501	
Limonene	0.239	0.363	0.055	0.0053
Linalool*	0.073	0.053	0.049	0.0210
Ocimene*	0.045	0.149	0.174	0.0041
α -Pinene*	0.038	0.326	0.171	0.0040
β -Pinene*	0.130	0.406	0.044	0.0049
Sabinene	0.067	0.399	0.258	0.0038
α - & γ -Terpinene	0.091	0.367	0.081	0.0046
Terpinene-4-ol*	0.049	0.063	0.159	0.0045
Terpinolene	0.046	0.034	0.185	0.0024

*Includes data from Hoffmann *et al.* [1997].

Table 2.4. Aerosol yield parameters for the ozone and nitrate radical oxidation of bicyclic hydrocarbons.

Parent	α_1	α_2	$K_{om,1}$	$K_{om,2}$
			$m^3 \mu g^{-1}$	$m^3 \mu g^{-1}$
<i>Ozone</i>				
Δ^3 -Carene	0.128	0.068	0.337	0.0036
α -Pinene	0.125	0.102	0.088	0.0788
β -Pinene	0.026	0.485	0.195	0.0030
Sabinene	0.037	0.239	0.819	0.0001
<i>Nitrate Radical</i>				
Δ^3 -Carene	0.743	0.257	0.0088	0.0091
β -Pinene	1.000		0.0163	
Sabinene	1.000		0.0115	

Table 2.5. Simulations of gas-phase chemistry.

Date	Parent	ΔHC ppb	f_{OH} %	f_{O_3} %	f_{NO_3} %	$\Delta\text{HC}_{\text{OH}}$ ppb	$\Delta\text{HC}_{\text{O}_3}$ ppb	$\Delta\text{HC}_{\text{NO}_3}$ ppb
07/01/97a	$\Delta^3\text{-Carene}$	28.8	66.4	13.0	19.3	19.1	3.7	5.6
07/01/97b	$\Delta^3\text{-Carene}$	66.8	68.1	14.6	13.7	45.5	9.8	9.2
08/21/97b	$\Delta^3\text{-Carene}$	72.5	66.0	14.2	18.0	47.8	10.3	13.1
08/15/97b	$\Delta^3\text{-Carene}$	73.6	65.9	15.3	15.9	48.5	11.3	11.7
08/19/97b	$\Delta^3\text{-Carene}$	104.6	63.4	15.3	19.0	66.3	16.0	19.8
08/17/95a	$\alpha\text{-Pinene}$	73.1	38.3	35.1	24.5	28.0	25.6	17.9
09/22/95b	$\alpha\text{-Pinene}$	90.8	46.0	31.5	21.2	41.7	28.6	19.2
09/22/95a	$\alpha\text{-Pinene}$	94.6	47.4	30.9	20.1	44.8	29.3	19.0
09/25/95b	$\alpha\text{-Pinene}$	94.7	47.8	32.7	18.1	45.3	31.0	17.1
09/25/95a	$\alpha\text{-Pinene}$	96.7	53.0	31.3	14.0	51.3	30.3	13.6
08/15/97a	$\beta\text{-Pinene}$	32.3	79.6	8.0	9.8	25.7	2.6	3.2
07/15/97a	$\beta\text{-Pinene}$	33.7	69.0	9.4	19.9	23.2	3.2	6.7
07/17/97a	$\beta\text{-Pinene}$	42.0	56.6	11.2	31.6	23.8	4.7	13.3
07/27/97a	$\beta\text{-Pinene}$	45.0	71.4	9.3	17.5	32.1	4.2	7.9
07/15/97b	$\beta\text{-Pinene}$	62.2	68.6	10.0	18.4	42.7	6.2	11.4
08/19/97a	$\beta\text{-Pinene}$	79.0	72.0	9.5	15.7	56.9	7.5	12.4
07/21/97a	$\beta\text{-Pinene}$	85.5	64.3	9.9	23.6	54.9	8.5	20.2
07/21/97b	$\beta\text{-Pinene}$	96.5	62.9	10.2	24.7	60.7	9.8	23.9

Table 2.5. (continued) Simulations of gas-phase chemistry.

Date	Parent	ΔHC ppb	f_{OH} %	f_{O_3} %	f_{NO_3} %	$\Delta\text{HC}_{\text{OH}}$ ppb	$\Delta\text{HC}_{\text{O}_3}$ ppb	$\Delta\text{HC}_{\text{NO}_3}$ ppb
07/09/97a	Sabinene	13.9	69.4	13.5	16.5	9.6	1.9	2.3
07/07/97a	Sabinene	34.9	78.1	14.1	6.5	27.3	4.9	2.3
07/05/97a	Sabinene	53.3	72.4	14.8	10.9	38.6	7.9	5.8
08/24/97b	Sabinene	74.0	73.6	14.7	8.4	54.5	10.9	6.2
07/05/97b	Sabinene	75.3	71.0	14.7	12.7	53.5	11.1	9.6
07/07/97b	Sabinene	77.7	74.5	16.9	5.3	57.9	13.1	4.1
07/09/97b	Sabinene	83.3	71.1	15.0	11.3	59.3	12.5	9.4

Table 2.6. Individual contributions to aerosol formation.

Date	Parent	ΔM_o $\mu\text{g m}^{-3}$	Percent Contribution		
			OH	O_3	NO_3
07/01/97a	Δ^3 -Carene	2.5	24.14	49.92	25.93
07/01/98b	Δ^3 -Carene	11.6	12.48	48.02	39.50
08/21/97b	Δ^3 -Carene	54.6	45.23	13.24	41.53
08/15/97b	Δ^3 -Carene	63.7	51.52	12.82	35.65
08/19/97b	Δ^3 -Carene	99.7	38.25	12.04	49.71
08/17/95a	α -Pinene	22.7	11.75	88.25	0.00
09/22/95a	α -Pinene	33.0	21.04	78.96	0.00
09/25/95b	α -Pinene	34.2	18.70	81.30	0.00
09/22/95b	α -Pinene	38.2	33.48	66.52	0.00
09/25/95a	α -Pinene	39.3	29.34	70.66	0.00
08/15/97a	β -Pinene	7.2	0.00	7.94	92.06
07/15/97a	β -Pinene	14.6	47.66	4.62	47.72
07/17/97a	β -Pinene	20.4	75.86	3.34	20.79
07/27/97a	β -Pinene	34.2	51.97	4.40	43.63
07/15/97b	β -Pinene	51.4	39.62	5.76	54.62
08/19/97a	β -Pinene	100.0	27.78	6.13	66.09
07/21/97a	β -Pinene	109.4	55.97	5.28	38.76
07/21/97b	β -Pinene	141.6	30.30	6.34	63.36

Table 2.6. (continued) Individual contributions to aerosol formation.

Date	Parent	ΔM_o $\mu\text{g m}^{-3}$	Percent Contribution		
			OH	O ₃	NO ₃
07/09/97a	Sabinene	1.9	74.08	12.01	13.91
07/07/97a	Sabinene	14.3	81.75	6.35	11.90
07/05/97a	Sabinene	23.9	65.98	6.25	27.77
08/24/97b	Sabinene	48.7	71.35	4.41	24.24
07/05/97b	Sabinene	51.4	58.94	4.28	36.78
07/07/97b	Sabinene	53.4	79.33	4.91	15.76
07/09/97b	Sabinene	65.2	62.67	3.92	33.40

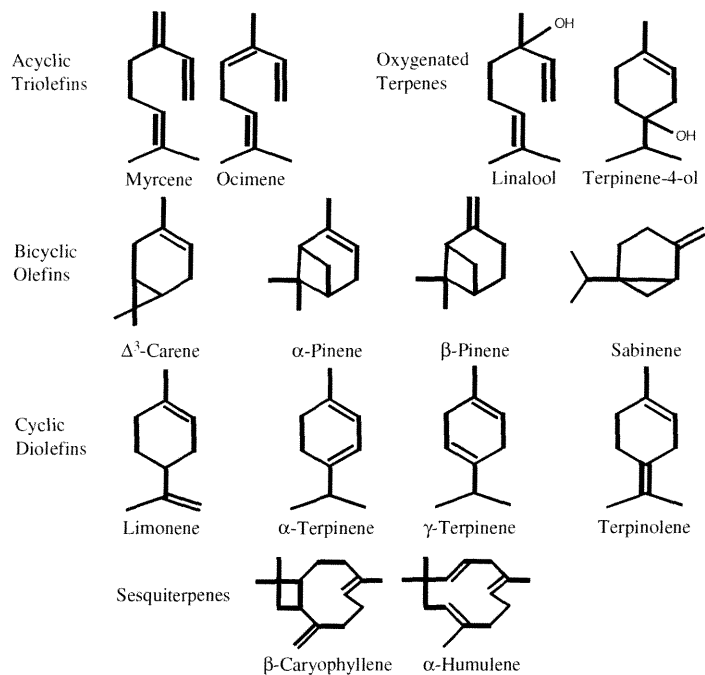


Figure 2.1. Chemical structures of the biogenic hydrocarbons investigated. Bonds between carbon atoms are shown with vertices representing carbon atoms; hydrogen atoms bonded to carbon are not explicitly shown.

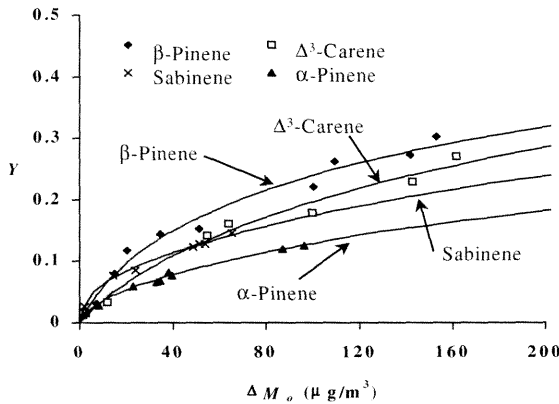


Figure 2.2

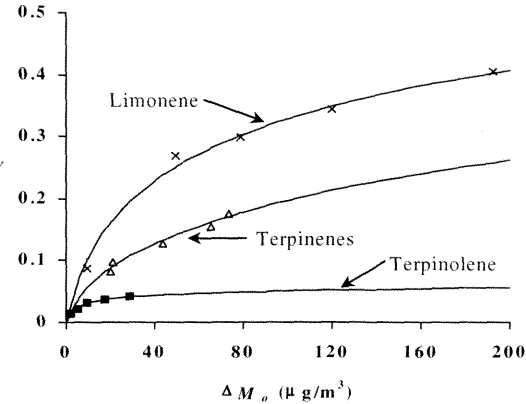


Figure 2.3

Figure 2.2. Secondary organic aerosol yields for the bicyclic olefins tested as a function of organic mass concentration in photooxidation experiments. Data are shown as filled triangles, plus signs, open circles, and filled diamonds for α -pinene, sabinene, Δ^3 -carene, and β -pinene, respectively. The α_1 , α_2 , $K_{om,1}$, and $K_{om,2}$ values used to generate the two-product model fitted curves are given in Table 2.3. Some data were taken from *Hoffmann et al. [1997]*.

Figure 2.3. Secondary organic aerosol yields (data and fitted curves) for the cyclic diolefins tested as a function of organic mass concentration in photooxidation experiments. The α_1 , α_2 , $K_{om,1}$, and $K_{om,2}$ values used to generate the two-product model lines are given in Table 2.3. Some data were taken from *Hoffmann et al. [1997]*.

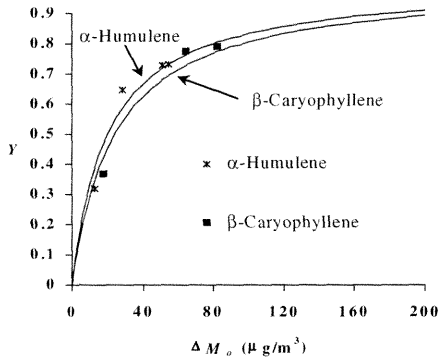


Figure 2.4

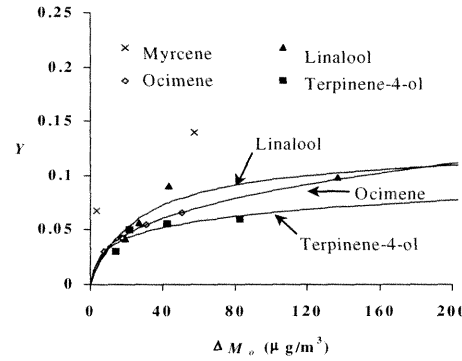


Figure 2.5

Figure 2.4. Secondary organic aerosol yields (data and fitted curves) for the sesquiterpenes tested as a function of organic mass concentration in photooxidation experiments. The α_1 , α_2 , $K_{om,1}$, and $K_{om,2}$ values used to generate the two-product model lines are given in Table 2.3. Some data were taken from Hoffmann *et al.* [1997].

Figure 2.5. Secondary organic aerosol yields (data and fitted curves) for the acyclic triolefins and oxygenated terpenes tested as a function of organic mass concentration in photooxidation experiments. The α_1 , α_2 , $K_{om,1}$, and $K_{om,2}$ values used to generate the two-product model lines are given in Table 2.3. Some data were taken from Hoffmann *et al.* [1997]. No curve is shown for myrcene as only two experiments with myrcene were performed.

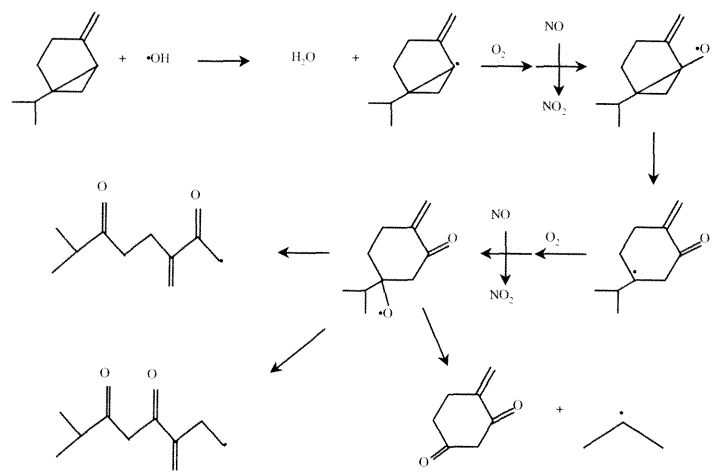


Figure 2.6. Possible ring-opening mechanism for the reaction between OH and sabinene.

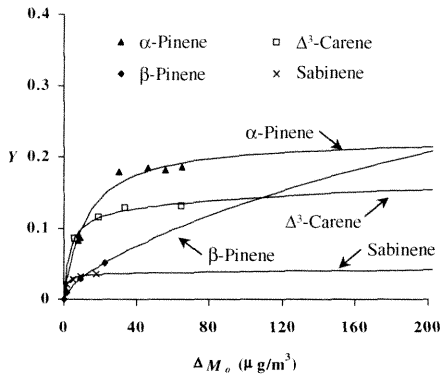


Figure 2.7

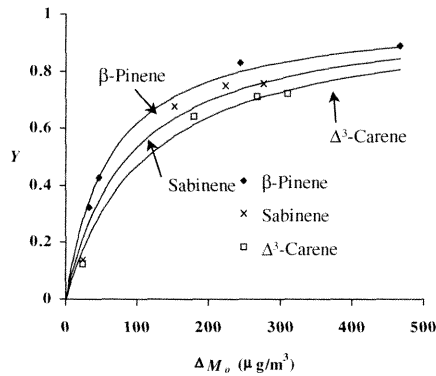


Figure 2.8

Figure 2.7. Secondary organic aerosol yields for the bicyclic olefins tested as a function of organic mass concentration in ozonolysis experiments. Data are shown as filled triangles, plus signs, open circles, and filled diamonds for α -pinene, sabinene, Δ^3 -carene, and β -pinene, respectively. The α_1 , α_2 , $K_{om,1}$, and $K_{om,2}$ values used to generate the two-product model fitted curves are given in Table 2.4.

Figure 2.8. Secondary organic aerosol yields (data and fitted curves) for the bicyclic olefins tested as a function of organic mass concentration in NO_3 experiments. The α_1 , α_2 , $K_{om,1}$, and $K_{om,2}$ values used to generate the two-product model lines are given in Table 2.4.

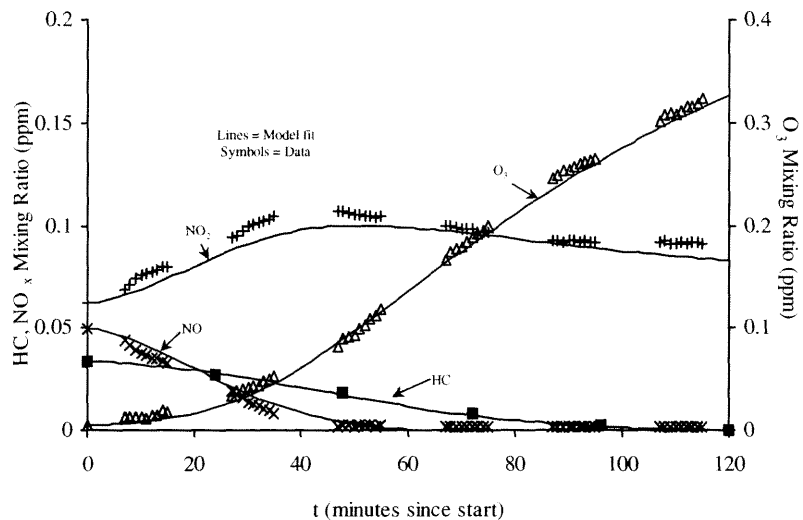


Figure 2.9. Example output (solid curves) from the SAPRC90b [Carter, 1990] gas-phase chemical mechanism. Data (dashes) are shown for the β -pinene experiment performed on July 15, 1997.

Chapter 3

Estimate of Global Atmospheric Organic Aerosol from Oxidation of Biogenic Hydrocarbons

Reference: R.J. Griffin, D.R. Cocker III, J.H. Seinfeld, and D. Dabdub, *Geophys. Res. Lett.*, 26, 2721-2724, 1999.

3.1 Introduction

Biogenic hydrocarbons emitted by vegetation play an important role in the chemistry of the urban- and regional-scale atmosphere [Fehsenfeld *et al.*, 1992]. These compounds are among the most reactive in the atmosphere as measured by their reaction rate constants with ozone (O_3) and the hydroxyl (OH) and nitrate (NO_3) radicals [Atkinson *et al.*, 1995; Shu and Atkinson, 1995; Atkinson, 1997]. Biogenic hydrocarbons contribute to tropospheric ozone formation in regions of extensive vegetation [Chameides *et al.*, 1988; Roselle *et al.*, 1991] and yield relatively non-volatile secondary oxidation products that form aerosols [Hoffmann *et al.*, 1997; Griffin *et al.*, 1999].

The aerosol-forming potential of biogenic hydrocarbons was first noted by Went [1960]. However, a quantitative understanding of aerosol formation from these molecules was lacking until recently [Hoffmann *et al.*, 1997; Griffin *et al.*, 1999]. Griffin *et al.* [1999] investigated the predominant aerosol-forming compounds emitted by vegetation [Arey *et al.*, 1991, 1995; Guenther *et al.*, 1994, 1996; Koenig *et al.*, 1995], the majority of which are monoterpenes that apparently function as defensive agents against herbivory [Lerdau, 1991]. Understanding the aerosol-forming potential of these compounds is imperative to assess the contribution of biogenically derived aerosol to regional particulate levels and the global aerosol burden.

Lioussse *et al.* [1996] included formation of organic aerosol from biogenic precursors in their global study of carbonaceous aerosols; they employed a constant aerosol yield of 5% for all biogenic species except isoprene, which does not form aerosol upon oxidation. Based on previous chamber data, Andreae and Crutzen [1997] provided an estimate of the global amount of aerosol formed annually from biogenic precursors of

30 to 270 Tg yr⁻¹. Recent work has expanded greatly the understanding of secondary organic aerosol (SOA) formation beyond that available to *Andreae and Crutzen* [1997]. Accounting for new data on the aerosol-forming potential of biogenic organics, spatially and temporally resolved, compound-specific global emissions profiles, and the nonlinear nature of SOA formation allows for a sharpening of this estimate.

3.2 Secondary Organic Aerosol Formation

Experiments investigating the aerosol-forming potential of 14 biogenic compounds have been described previously [*Hoffmann et al.*, 1997; *Griffin et al.*, 1999]. SOA forms through adsorptive and/or absorptive condensation or nucleation of products of gas-phase hydrocarbon oxidation [*Pankow*, 1994; *Odum et al.*, 1996]. The SOA yield, Y , defined as the dimensionless ratio of the mass concentration of SOA formed, ΔM_o , to the mass concentration of the parent hydrocarbon reacted, measures the aerosol-forming potential of a compound. Gas-aerosol partitioning of oxidation products depends on the mass concentration of an absorbing organic phase. As a result, Y is a function of the final equilibrium organic mass concentration of this absorbing phase, M_o (μg m⁻³). For the experiments considered, M_o equals ΔM_o as the absorbing medium is generated completely by the parent hydrocarbon oxidation. The relationship between Y and M_o is

$$Y = M_o \sum_i \left(\frac{\alpha_i K_{om,i}}{1 + K_{om,i} M_o} \right) \quad (1)$$

where α_i is the mass-based stoichiometric yield of oxidation product i and $K_{om,i}$ (m³ μg⁻¹) is the gas-particle equilibrium coefficient that describes the partitioning of oxidation

product i between the absorbing organic aerosol phase and the gas phase [Pankow, 1994; Odum *et al.*, 1996]. Yield data for over 30 individual aromatic and biogenic parent hydrocarbons have been fit to equation (1) on the basis of a two-product model, that is, by parameters α_1 , α_2 , $K_{om,1}$, and $K_{om,2}$ [Odum *et al.*, 1996, 1997; Hoffmann *et al.*, 1997; Griffin *et al.*, 1999]. Many products capable of partitioning into the aerosol phase are formed during the atmospheric oxidation of such hydrocarbons [Yu *et al.*, 1998]. However, the remarkably close fit of yield data to equation (1) for the compounds studied indicates that two generic products approximate well the stoichiometry and volatility of the final product mix. While yield scales linearly with M_o in the range of atmospheric applicability (small M_o), experiments must be performed over the entire range of organic mass concentrations to obtain the yield parameters for each parent hydrocarbon (See Table 3.1.). Calculated yields are also shown in Table 3.1 for values of M_o between 5 and 40 $\mu\text{g m}^{-3}$. These yields encompass the range of 5-40% used by Andreae and Crutzen [1997].

3.3 Individual Oxidant Contributions to Aerosol Formation

The unsaturated carbon-carbon bonds inherent to the monoterpene structure induce a high level of reactivity with OH, NO_3 , and O_3 . At NO_x levels characteristic of chamber photooxidation experiments, NO_3 contributes significantly to oxidation if a sufficient amount of NO_3 forms prior to complete consumption of the hydrocarbon by OH and O_3 . Of the compounds of interest, this is the case only for α -pinene, β -pinene, Δ^3 -carene, and sabinene.

In remote areas, NO_3 concentrations are expected to be very low as there is little impact from anthropogenic NO_x sources. Therefore, in order to extrapolate smog

chamber data to ambient conditions for these four bicyclic alkenes, the contribution of NO_3 to chamber aerosol formation must be removed from that measured. To do so, the amount of parent hydrocarbon that reacted with each oxidant in each experiment must be determined. Despite the complexity of the gas-phase chemistry in these experiments, it is possible to simulate hydrocarbon consumption patterns using the SAPRC90b chemical mechanism of *Carter* [1990].

In order to assess the importance of each oxidant to aerosol formation for the bicyclic alkenes, experiments in which either O_3 or NO_3 was the only available oxidant (a scavenger was used to consume any OH formed in the O_3 -alkene reaction) were performed in the dark, but at daytime temperatures. On the basis of the resulting yield information for single-oxidant systems and the gas-phase simulations, it is possible to determine the amount of organic aerosol formed from reaction with each oxidant in full-photooxidation experiments [*Hoffmann et al.*, 1997; *Griffin et al.*, 1999]. By subtracting the NO_3 contribution, yield parameters for aerosol formation in the absence of NO_3 for bicyclic alkenes have been developed (Table 3.1).

In order to extrapolate chamber data to the ambient, it is important to determine if the relative hydrocarbon oxidation by OH and O_3 observed in the chamber is consistent with that expected in the ambient. Global average estimates of 50 ppbv for O_3 and 2.6×10^6 molecules cm^{-3} for OH do lead to relative hydrocarbon consumption patterns similar to those observed in the smog chamber for bicyclic alkenes [*Griffin et al.*, 1999] (Table 3.2). Therefore, we assume that relative consumption patterns for the other biogenic parent compounds studied in the chamber will approximate those expected in the ambient. Because the hydrocarbon oxidation consumption patterns seen in experiments are similar to those derived using global-average oxidant concentrations,

further oxidation of first-generation products in the chamber should mimic appropriately such reactions occurring in the ambient. *Yu et al.* [1998] have shown evidence of these reactions in our chamber. Thus, it can be assumed that the aerosol yield parameters in Table 3.1 can be used to describe ambient aerosol formation even though experimental conditions do not mimic exactly ambient conditions in all situations. While it is expected that aerosol yield will decrease with increasing temperature, there are currently no quantitative data available to describe this phenomenon. Therefore, the parameters given here (derived for an average temperature of 310K) are used in all cases. Given that the majority of biogenic emissions occur in hot, tropical regions, this assumption may not induce a large amount of error.

3.4 Compound-Specific Emissions Inventory for Biogenic Compounds

Because the biogenic species considered exhibit a wide range of SOA yields, it is necessary to assess global-scale emissions of the most important monoterpenes and other reactive volatile organic compounds (ORVOC) in order to estimate the amount of global, biogenically derived SOA formed annually. The global emissions of monoterpenes and ORVOC have been estimated by ecosystem [*Guenther et al.*, 1995]. By determining the predominant plant species associated with these ecosystems and identifying and quantifying the specific monoterpene and ORVOC emissions from these individual species [*Arey et al.*, 1991, 1995; *Guenther et al.*, 1994, 1996; *König et al.*, 1995], the contributions of individual compounds to emissions of monoterpenes or ORVOC on a global scale can be inferred (Table 3.3). Less important compounds are grouped with others expected to have similar aerosol-forming potentials.

By applying the contributions of each species listed in Table 3.3 to the emissions in each $5^\circ \times 5^\circ$ horizontal cell in a global model, a compound-specific and temporally and spatially resolved emissions profile for monoterpenes and ORVOC is established. These emissions are converted to concentration units by using appropriate reactive layer heights specific to each compound. These heights are derived from an estimate of vertical eddy diffusivity [Seinfeld and Pandis, 1998] and appropriate time scales inferred from reaction rate constants and OH and O₃ concentrations simulated by IMAGES [Müller and Brasseur, 1995]. IMAGES oxidant concentrations are given for specific times and, if needed, are scaled by factors ranging from 3 to 10 to reflect values at times when oxidation, and therefore aerosol formation, is expected to be maximum [Mount *et al.*, 1997]. Because biogenic emissions are given as hourly averages for each month, diurnal oxidant concentration is neglected, and each scaled value is used for an entire day. Vertical cells are thus defined by increasing values of the scale heights for the compounds of interest. For example, the lowest three-dimensional cell, in which all compounds are present and well mixed, has a height equal to the scale height of the most reactive compound. The second cell will then extend from the top of the first cell to the scale height of the second most reactive compound. In this second cell, all compounds except the most reactive are present. This development of vertical cell heights is extended until the scale height of the least reactive compound is reached. These vertical cell heights are derived for each surface cell since OH and O₃ levels vary spatially. For simplicity, ground level concentrations of OH and O₃ are used. NO₃ is assumed not to contribute to oxidation.

Since the formation of organic aerosol depends on the relative amounts of monoterpenes and ORVOC emitted, a second emissions scenario was constructed by

using the other major biogenic inventory of *Guenther et al.* [1995]. In the second scenario, emissions of each species in each cell were found simply by using the ratio of emission values predicted by *Müller* [1992] and *Guenther et al.* [1995] (See Table 3.3.). The major difference between these two estimates is that *Guenther et al.* [1995] predict almost three times as much ORVOC emission as *Müller* [1992]. *Andreae and Crutzen* [1997] considered an annual emissions rate of 300-500 Tg C yr⁻¹, which is greater than that predicted by *Müller* [1992] and essentially equal to that predicted by *Guenther et al.* [1995] (See Table 3.3.).

3.5 Global Aerosol Formation from Biogenic Hydrocarbons

Individual α_i and $K_{om,i}$ values have been shown to simulate the amount of SOA formed from mixtures as complex as evaporated gasoline [*Odum et al.*, 1997]. M_{oT} , the mass concentration of SOA formed from the oxidation of the mixture of n hydrocarbons, can be found by solving

$$\sum_j^n \left[\Delta HC_j \sum_i \left(\frac{\alpha_{i,j} K_{om,i,j}}{1 + K_{om,i,j} M_{oT}} \right) \right] = 1 \quad (2)$$

where ΔHC_j is the concentration of parent compound j reacted. To estimate the M_{oT} in each cell from biogenic compounds, equation (2) is used with the yield parameters from Table 3.1 and the daily biogenic concentrations derived in each cell. The yield parameters of sabinene were used for ten-carbon, bicyclic terpenoid ketones because each species exhibits an exocyclic double bond. Yield parameters for aromatics with multiple methyl groups were employed for aromatics [*Odum et al.*, 1997]. First, the compounds

listed in Table 3.1 and these aromatics and ketones are considered. If the left-hand side is greater than unity for M_{oT} equal to zero, equation (2) is solved iteratively to find the appropriate M_{oT} for the cell of interest. (Otherwise, M_{oT} is set to zero for that cell.) In the non-zero cases, additional SOA formation from straight-chain olefins and carbonyls is considered. For these two classes, a flat yield of 5% is assumed for SOA formation [Wang *et al.*, 1991]. The concentration of SOA formed in each cell is thus calculated on a daily basis, converted to mass using cell volume, and summed spatially to provide the global daily amount of SOA formed. At the end of each day, it is assumed that the SOA is released to the free troposphere. The amount of SOA generated from the oxidation of biogenic species annually is found by summing the results of each day of the year.

Using the emissions profiles of both *Guenther et al.* [1995] and *Müller* [1992] to account for possible differences in the distribution between monoterpenes and ORVOC, the estimated range of global biogenically derived SOA is 13-24 Tg yr^{-1} . In the absence of additional information, the best estimate can be taken as the average, 18.5 Tg yr^{-1} . The range estimated here is likely a lower bound since products of biogenic oxidation will partition to primary organic aerosol mass and anthropogenic SOA.

The majority of this biogenically derived SOA will be formed in forested regions. However, because of their extensive conversion to aerosol, biogenic hydrocarbons can also contribute substantially to aerosol burdens in any areas with significant vegetation. On average, if a one-week lifetime is assumed, the predicted burden of SOA from biogenic oxidation is 0.36 Tg, which is slightly less than but of the same order of magnitude as the predicted burdens for primary carbonaceous aerosols from biomass and fossil fuel burning [*Lioussse et al.*, 1996]. This burden is smaller than those predicted for sea salt, soil dust, and sulfate aerosols but is the same order of magnitude as those

predicted for black carbon, nitrate, and ammonium aerosols [Tegen *et al.*, 1997; Adams *et al.*, 1999].

3.6 References

Adams, P.J., J.H. Seinfeld, and D.M. Koch, Global concentrations of tropospheric sulfate, nitrate, and ammonium aerosol simulated in a general circulation model, *J. Geophys. Res.*, 104, 13,791-13,823, 1999.

Andreae, M.O., and P.J. Crutzen, Atmospheric aerosols: Biogeochemical sources and role in atmospheric chemistry, *Science*, 276, 1052-1058, 1997.

Arey, J., D.E. Crowley, M. Crowley, M. Resketo, and J. Lester, Hydrocarbon emissions from natural vegetation in California's South Coast Air Basin, *Atmos. Environ.*, 29, 2977-2988, 1995.

Arey, J., A.M. Winer, R. Atkinson, S.M. Aschmann, W.D. Long, C.L. Morrison, and D.M. Olszyk, Terpenes emitted from agricultural species found in California's Central Valley, *J. Geophys. Res.*, 96, 9329-9336, 1991.

Atkinson, R., Gas-phase tropospheric chemistry of organic compounds, 1, Alkanes and alkenes, *J. Phys. Chem. Ref. Data*, 26, 215-290, 1997.

Atkinson, R., J. Arey, S.M. Aschmann, S.B. Corchnoy, and Y.H. Shu, Rate constants for the gas-phase reactions of *cis*-3-hexen-1-ol, *cis*-3-hexenylacetate, *trans*-2-hexenal, and linalool with OH and NO₃ radicals and O₃ at 296 ±2K and OH radical formation yields from the O₃ reactions, *Int. J. Chem. Kinet.*, 27, 941-955, 1995.

Carter, W.P.L., A detailed mechanism for the gas-phase atmospheric reactions of organic compounds, *Atmos. Environ.*, 24A, 481-518, 1990.

Chameides, W.L., R.W. Lindsay, J. Richardson, and C.S. Kiang, The role of biogenic hydrocarbons in urban photochemical smog: Atlanta as a case study, *Science*, 241, 1473-1475, 1988.

Fehsenfeld, F., et al., Emissions of volatile organic compounds from vegetation and the implications for atmospheric chemistry, *Global Biogeochem. Cycles*, 6, 389-430, 1992.

Griffin, R.J., D.R. Cocker III, R.C. Flagan, and J.H. Seinfeld, Organic aerosol formation from the oxidation of biogenic hydrocarbons, *J. Geophys. Res.*, 104, 3555-3567, 1999.

Guenther, A., et al., A global model of natural volatile organic compound emissions, *J. Geophys. Res.*, 100, 8873-8892, 1995.

Guenther, A., L. Otter, P. Zimmerman, J. Greenberg, R. Scholes, and M. Scholes, Biogenic hydrocarbon emissions from southern African savannas, *J. Geophys. Res.*, 101, 25,859-25,865, 1996.

Guenther, A., P. Zimmerman, and M. Wildermuth, Natural volatile organic compound emission rate estimates for U.S. woodland landscapes, *Atmos. Environ.*, 28, 1197-1210, 1994.

Hoffmann, T., J.R. Odum, F. Bowman, D. Collins, D. Klockow, R.C. Flagan, and J.H. Seinfeld, Formation of organic aerosols from the oxidation of biogenic hydrocarbons, *J. Atmos. Chem.*, 26, 189-222, 1997.

König, G., M. Brunda, H. Puxbaum, C.N. Hewitt, S.C. Duckham, and J. Rudolph, Relative contribution of oxygenated hydrocarbons to the total biogenic VOC emissions of selected mid-European agricultural and natural plants, *Atmos. Environ.*, 29, 861-874, 1995.

Lerdau, M.T., Plant function and biogenic terpene emission, in *Trace Gas Emissions by Plants*, edited by T.D. Sharkey, et al., pp. 121-134, Academic Press, Inc., San Diego, 1991.

Liousse, C., J.E. Penner, C. Chuang, J.J. Walton, H. Eddleman, and H. Cachier, A global three-dimensional model study of carbonaceous aerosols, *J. Geophys. Res.*, **101**, 19,411-19,432, 1996.

Mount, G.H., F.L. Eisele, D.J. Tanner, J.W. Brault, P.V. Johnston, J.W. Harder, E.J. Williams, A. Fried, and R. Shetter, An intercomparison of spectroscopic laser long-path and ion-assisted *in situ* measurements of hydroxyl concentrations during the Tropospheric OH Photochemistry Experiment, fall 1993, *J. Geophys. Res.*, **102**, 6437-6455, 1997.

Müller, J.F., Geographical distribution and seasonal variation of surface emissions and deposition velocities of atmospheric trace gases, *J. Geophys. Res.*, **97**, 3787-3804, 1992.

Müller, J.F., and G.P. Brasseur, IMAGES - a 3-dimensional chemical-transport model of the global troposphere, *J. Geophys. Res.*, **100**, 16445-16490, 1995.

Odum, J.R., T.P.W. Jungkamp, R.J. Griffin, R.C. Flagan, and J.H. Seinfeld, The atmospheric aerosol-forming potential of whole gasoline vapor, *Science*, **276**, 96-99, 1997.

Odum, J.R., T. Hoffmann, F. Bowman, D. Collins, R.C. Flagan, and J.H. Seinfeld, Gas/particle partitioning and secondary organic aerosol yields, *Environ. Sci. Technol.*, **30**, 2580-2585, 1996.

Pankow, J.F., An absorption model of gas/particle partitioning of organic compounds in the atmosphere, *Atmos. Environ.*, **28**, 185-189, 1994.

Roselle, S.J., T.E. Pierce, and K.L. Schere, The sensitivity of regional ozone modeling to biogenic hydrocarbons, *J. Geophys. Res.*, 96, 7371-7394, 1991.

Seinfeld, J.H., and S.N. Pandis, *Atmospheric Chemistry and Physics: From Air Pollution to Climate Change*, John Wiley and Sons, Inc., New York, 1998.

Shu, Y., and R. Atkinson, Atmospheric lifetimes and fates of a series of sesquiterpenes, *J. Geophys. Res.*, 100, 7275-7281, 1995.

Tegen, I., P. Hollrig, M. Chin, I. Fung, D. Jacob, and J. Penner, Contribution of different aerosol species to the global aerosol extinction optical thickness: Estimates from model results, *J. Geophys. Res.*, 102, 23,895-23,915, 1997.

Wang, S.-C., S.E. Paulson, D. Grosjean, R.C. Flagan, and J.H. Seinfeld, Aerosol formation and growth in atmospheric organic/NO_x systems - I. Outdoor smog chamber studies of C₇- and C₈- hydrocarbons, *Atmos. Environ.*, 26A, 403-420, 1992.

Went, F.W., Blue hazes in the atmosphere, *Nature*, 187, 641-643, 1960.

Yu, J., R.C. Flagan, and J.H. Seinfeld, Identification of products containing -COOH, -OH, and -C=O in atmospheric oxidation of hydrocarbons, *Environ. Sci. Technol.*, 32, 2357-2370, 1998.

Table 3.1. Aerosol yield parameters for biogenic organics.

Parent	α_1	α_2	$K_{om,1}$	$K_{om,2}$	Yield
Δ^3 -Carene	0.057	0.476	0.063	0.0042	2.3-10.9%
β -Caryophyllene	1.000	N/A	0.0416	N/A	17.2-62.5%
α -Humulene	1.000	N/A	0.0501	N/A	20.0-66.7%
Limonene	0.239	0.363	0.055	0.0053	6.1-22.8%
Linalool	0.073	0.053	0.049	0.0210	1.9-7.3%
Myrcene ¹	0.100	0.275	0.513	0.0032	7.6-12.7%
Ocimene	0.045	0.149	0.174	0.0041	2.4-6.0%
α -Pinene ²	0.038	0.326	0.171	0.0040	2.4-7.8%
β -Pinene	0.113	0.239	0.094	0.0051	4.2-13.0
Sabinene	0.060	0.376	0.406	0.0038	4.7-10.6%
α - & γ -Terpinene	0.091	0.367	0.081	0.0046	3.4-12.7%
Terpinene-4-ol	0.049	0.063	0.159	0.0045	2.3-5.2%
Terpinolene	0.046	0.034	0.185	0.0024	2.3-4.4%

¹These values are an estimate as only two experiments were performed. ²SOA formation by NO_3 oxidation is negligible [Griffin *et al.*, 1999].

Table 3.2. OH and O_3 oxidation patterns for bicyclic alkenes.

Parent	Chamber		Global Average	
	O_3	OH	O_3	OH
Δ^3 -Carene	18.0%	82.0%	16.2%	83.8%
α -Pinene	41.1%	58.9%	42.5%	57.5%
β -Pinene	12.6%	87.4%	8.0%	92.0%
Sabinene	16.9%	83.1%	25.2%	74.8%

Table 3.3. Estimated species contributions to global emissions.

MONOTERPENES		ORVOC	
Monoterpene ¹	Contribution	ORVOC ²	Contribution
α-Pinene	35%	Terpenoid	9%
β-Pinene	23%	C ₇ -C ₁₀ n-	7%
Limonene	23%	Aromatics	6%
Myrcene	5%	Sesquiterpenes	5%
Sabinene	5%	Terpenoid Ketones	4%
Δ ³ -Carene	4%	Higher Olefins	1%
Ocimene	2%		
Terpinolene	2%		
α- & γ-Terpinene	1%		

¹Guenther *et al.* [1995] estimate a total monoterpene emission rate of 127 TgC yr⁻¹; Mäller [1992] estimates 147 Tg yr⁻¹. ²Only those capable of forming aerosol are included; Guenther *et al.* [1995] estimate an ORVOC emission rate of 260 TgC yr⁻¹; Mäller [1992] estimates 94 Tg yr⁻¹.

Chapter 4

Incremental Aerosol Reactivity: Application to Aromatic and Biogenic Hydrocarbons

Reference: R.J. Griffin, D.R. Cocker III, and J.H. Seinfeld, *Environ. Sci. Technol.*, 33, 2403-2408, 1999.

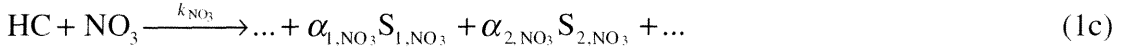
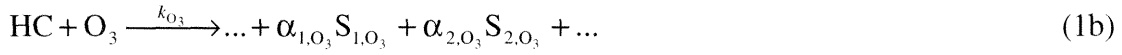
4.1 Introduction

Urban fine particulate matter is comprised of a complex mixture of both primary and secondary organic and inorganic compounds and emanates from a wide variety of sources. An important component that can significantly contribute to the fine particulate burden, especially during severe urban smog episodes, is secondary organic aerosol (SOA). Like ozone, secondary organic aerosol results from the atmospheric oxidation of reactive organic gases (ROGs), but whereas the oxidation of most ROGs results in ozone formation, SOA is generally formed only from the oxidation of ROGs comprised of six or more carbon atoms. This is because oxidation products must have vapor pressures that are sufficiently low to enable them to partition into the aerosol phase.

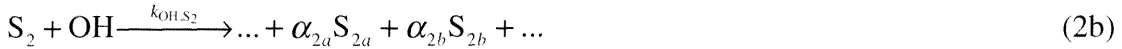
The atmospheric chemical reaction pathways of ROG molecules sufficiently large to lead to SOA are complex, and resulting oxidation products are both numerous and difficult to quantify analytically. The chemical process of organic aerosol formation can be depicted in general terms. Consider the production of semi-volatile organic gases, S_1 , S_2 , ..., from the gas-phase reaction of a parent hydrocarbon, HC, with the OH radical,



where k_{OH} is the OH reaction rate constant, and α_1 , α_2 , ... are the stoichiometric product coefficients. (Later these stoichiometric coefficients will be expressed on a mass basis, rather than the usual molar basis.) If the parent hydrocarbon is an alkene, reactions with O_3 and NO_3 radicals are also possible, providing additional pathways for semi-volatile product formation,



The first-generation products, S_1 , S_2 , ... may subsequently undergo gas-phase reaction themselves, creating second-generation condensable products, S_{1a} , S_{1b} , ... and S_{2a} , S_{2b} , ... etc.,



where k_{OH,S_1} and k_{OH,S_2} are the OH-reaction rate constants for the products, S_1 and S_2 , respectively.

Secondary organic aerosol yields have been measured for many individual ROGs by a number of researchers over the last decade or more [Izumi and Fukuyama, 1990; Pandis *et al.*, 1991; Wang *et al.*, 1992ab; Zhang *et al.*, 1992; Odum *et al.*, 1996; Odum *et al.*, 1997ab; Hoffmann *et al.*, 1997; Forstner *et al.*, 1997ab; Griffin *et al.*, 1999]. Initially it was believed that each ROG should possess a unique value of its SOA yield [Grosjean and Seinfeld, 1989; Pandis *et al.*, 1992; Pandis *et al.*, 1993], but measured yields for an individual ROG exhibited a degree of variation that could not be reconciled in terms of a single, unique SOA yield for each parent ROG. Following Pankow [1994ab], Odum *et al.* [1996] formulated a framework for explaining observed SOA yield data. They

suggested that secondary organic aerosol formation is best described by a gas/aerosol absorptive partitioning model. Within that framework, semi-volatile products from the atmospheric oxidation of an ROG can partition into an absorbing organic aerosol phase at a concentration below their saturation concentration, analogous to the partitioning that occurs between the gas and aqueous phases of a water-soluble atmospheric constituent.

4.2 Theory of Secondary Organic Aerosol Formation

Assuming that absorption is the dominant mechanism describing SOA formation, the equilibrium gas-particle partitioning of a semi-volatile organic species i between the gas phase and an organic phase can be described with the vapor pressure relation [Bowman *et al.*, 1997]

$$p_i = x_i \zeta_i p_i^o \quad (3)$$

where p_i (torr) is the gas-phase partial pressure of species i , x_i is the mole fraction of species i in the organic aerosol phase, ζ_i is the activity coefficient of species i in the aerosol-phase organic mixture, and p_i^o (torr) is the vapor pressure of species i as a pure liquid (subcooled, if necessary). In this scenario, the organic and inorganic portions of the aerosol remain in separate phases. Assuming ideal behavior for air, the gas-phase partial pressure, p_i , can be converted to the gas-phase mass concentration, G_i ($\mu\text{g m}^{-3}$), by the relationship

$$G_i = \frac{p_i m_{wi}}{RT} 10^6 \quad (4)$$

where m_{wi} (g mol⁻¹) is the molecular weight of species i , R (=6.2 x 10⁻² torr m³ mol⁻¹ K⁻¹ = 8.314 J mol⁻¹ K⁻¹) is the ideal gas constant and T (K) is temperature. The factor 10⁶ accomplishes the appropriate unit conversions. For organic species with similar molecular weights (i.e., $m_{wi} = m_w$, the mean molecular weight of the absorbing organic matter) the aerosol mole fraction, x_i , is given by

$$x_i = \frac{A_i}{M_o} \quad (5)$$

where A_i (μg m⁻³) is the aerosol mass concentration of species i and M_o (=Σ A_i) (μg m⁻³) is the total aerosol mass concentration of all the individual semi-volatile organic species.

Equations (4) and (5) can be substituted into equation (3) and rearranged to yield

$$\frac{A_i}{G_i M_o} = \frac{RT}{m_w \zeta_i p_i^o} 10^{-6} = K_i \quad (6)$$

where K_i (m³ μg⁻¹) is defined as the absorption partitioning coefficient of species i [Pankow, 1994ab; Odum *et al.*, 1996]. The absorption partitioning coefficient incorporates vapor pressure, activity coefficient, and molecular weight, providing a single equilibrium parameter for each compound. K_i is analogous to a Henry's law coefficient in relating gas-phase concentration of species i to the mass fraction of species i in the aerosol phase. An important implication of equation (6) is that, since, at a particular temperature, K_i is a constant, a greater fraction of each product must partition to the organic phase as the total organic aerosol concentration increases.

4.3 Experimental Determination of SOA Yields

The approach that has been most successful to estimate the SOA forming capability of an ROG involves the direct measurement of secondary organic aerosol yields. The SOA yield for a given product i , Y_i , is a measure of the mass of aerosol of a species that is produced from the atmospheric oxidation of an ROG and is defined as

$$Y_i = \frac{A_i}{\Delta \text{ROG}} \quad (7)$$

where ΔROG ($\mu\text{g m}^{-3}$) is the reacted amount of the ROG. By this definition, the total SOA yield is just the sum of the individual product yields,

$$Y = \sum_{i=1}^N Y_i \quad (8)$$

In the study of secondary organic aerosol formation, typically a smog chamber is initially filled with a mixture of NO_x , inorganic seed particles, and an aerosol-producing hydrocarbon. The chamber is then exposed to sunlight, or other UV sources, that initiates photooxidation. (Dark experiments can also be conducted when O_3 or NO_3 is the oxidizing species.) As the hydrocarbon reacts it forms semi-volatile products that condense on the seed particles. If mass transport to the available particles cannot keep up with the rate of product formation or when a seed aerosol is not initially present, the semi-volatile products accumulate in the gas phase until supersaturation is reached and nucleation occurs. Studies show that the amount of aerosol produced for a given amount of reacted ROG is independent of whether a seed aerosol is present or not [Bowman *et al.*, 1997]. Reactions are ordinarily run until the entire initial amount of ROG is consumed.

Typically the volume of the initial seed aerosol is small compared to the organic aerosol volume generated.

The total SOA yield from an ROG that generates N semi-volatile products is computed as follows. The total concentration of product i , C_i , is proportional to the total amount of parent organic that reacts, ΔROG ,

$$\alpha_i \Delta\text{ROG} = C_i \quad (9)$$

C_i is also equal at any time to the sum of the gas- (G_i) and aerosol - (A_i) phase concentrations of i ,

$$C_i = A_i + G_i \quad (10)$$

Combining these relations with the definition of the gas-particle partitioning constant, K_i , gives the expression for the total yield in terms of the individual product mass -based stoichiometric coefficients, α_i , and partitioning coefficients, K_i , and the organic aerosol mass concentration, M_o ,

$$Y = M_o \sum_{i=1}^N \frac{\alpha_i K_i}{1 + K_i M_o} \quad (11)$$

Note that in the limit of small organic aerosol mass concentration or high volatility of the products,

$$Y \sim M_o \sum_{i=1}^N \alpha_i K_i \quad (12)$$

the SOA yield is directly proportional to M_o , and that in the limit of large M_o or low volatility of the products

$$Y \sim \sum_{i=1}^N \alpha_i \quad (13)$$

the total yield is independent of M_o and is just the sum of the mass-based stoichiometric coefficients of the products.

It is important to distinguish between aerosol yield, Y , and stoichiometric coefficients, α_i . Stoichiometric coefficients depend on the gas-phase chemical mechanism and represent the total amount of semi-volatile product formed, in both gas and aerosol phases, per amount of parent hydrocarbon reacted. The yield, on the other hand, which measures only the semi-volatile products that have partitioned into the aerosol phase, depends on both the gas-phase reaction mechanism as well as the amount of organic mass available as an absorption medium. Stoichiometric coefficients, by themselves, are therefore not sufficient to predict the amount of aerosol formation (except in the limits discussed previously, as in equation (13)). Partitioning coefficients, stoichiometric coefficients, and organic aerosol mass are required in general to determine the SOA yield.

Ozone-forming potential of organics is determined based on atmospheric reaction mechanisms [Carter, 1994; Carter *et al.*, 1995]. In principle, aerosol-forming potential could be calculated based on a similar atmospheric oxidation mechanism that includes all significant semi-volatile product species. The relative aerosol-forming potential of a group of organics could, this way, be determined based on their oxidation products and the thermodynamic properties of these products. This *ab initio* approach represents a

goal that is not yet attainable because of incomplete knowledge of the semi-volatile oxidation products of the important aerosol-forming compounds. Thus, it is necessary to rely on experimentally measured aerosol yields. Aerosol yields, Y , are expressed theoretically as a function of the available M_o through equation (11). Observed aerosol yields as a function of M_o can be fit to equation (11) by specifying the stoichiometric coefficients, α_i , and gas-particle partitioning coefficients, K_i , of each of the semi-volatile products of oxidation of the parent organic.

Over the last several years, SOA yields for over 30 aromatic and biogenic organics have been measured in the California Institute of Technology outdoor smog chamber (Table 4.1). In these experiments, M_o is generated completely by photooxidation of the parent. In order to fit the observed yields to equation (11), the mix of semi-volatile oxidation products for each parent compound has been represented by two empirical products, characterized by parameters α_1 , K_1 , α_2 , and K_2 . It has been determined that observed yields cannot be fit by assuming only a single product and that use of three products is superfluous [Odum *et al.*, 1996]. (An exception is those compounds with extremely large yields, which can be represented by a single product.) Roughly speaking, one of the empirical semi-volatile products tends to represent a relatively lower vapor pressure compound and the other a relatively higher vapor pressure compound. In Table 4.1, low-yield aromatics (those with multiple methyl substituents) represent those species that fall on the lower of two curves of Y versus M_o described by *Odum et al.* [1997ab]. Correspondingly, high-yield aromatics (those with only one methyl substituent) represent the species falling on the higher of the two curves.

It must be noted that this theory assumes that secondary products are unable to form a solution with existing inorganic seed aerosol. Accounting for the interactions

among the organic compounds themselves allows it to be shown that such products can condense onto seed aerosol at concentrations lower than the saturation concentration of the compound [Seinfeld and Pandis, 1998]. There is a threshold amount of parent compound that must react to form secondary organic aerosol by absorption, defined as ΔROG_j^* ; after consumption of ΔROG_j^* , products condense onto seed aerosol to form an initial organic layer that can then act as an absorptive medium. At this point, absorption becomes the dominant mechanism governing the partitioning of secondary products and, therefore, determining yield, as in the atmosphere. Adsorption of products is not considered here as it has been shown that absorption is the dominant mechanism associated with SOA formation in the ambient [Liang *et al.*, 1997].

Odum et al. [1996, 1997a] showed, moreover, that aerosol formation from the photooxidation of a mixture of parent hydrocarbons can be predicted simply from the SOA yields for the individual parent compounds. This suggests that, at least for the case of a pure organic absorbing phase, oxidation products of different parent hydrocarbons are as soluble in a mixed organic product phase as in an organic phase consisting exclusively of their own oxidation products.

The experimentally determined SOA yields reported by *Odum et al.* [1996, 1997a] and *Griffin et al.* [1999] have been measured at relative humidity (RH) less than 5%. At this level of RH, the seed aerosol, $(\text{NH}_4)_2\text{SO}_4$, is dry and the resulting organic aerosol is water-free. Because organic products will likely be most soluble in their own liquids, SOA yields measured at essentially 0% RH can be expected to represent an upper limit to the aerosol partitioning that will result. While many SOA products are water soluble [Saxena and Hildemann, 1996], they are not expected to be more soluble in an aqueous mixture than in a pure organic phase.

4.4 Threshold Concentration for SOA Formation

For the purpose of illustration, assume that two semi-volatile products are formed from the parent organic ROG_j:



where $\alpha_{i,j}$ represents the mass-based stoichiometric factors described earlier. Therefore by a mass balance,

$$G_1 + A_1 = \alpha_{1j}\Delta\text{ROG}_j \quad (15a)$$

$$G_2 + A_2 = \alpha_{2j}\Delta\text{ROG}_j \quad (15b)$$

where G_i and A_i represent the gas- and aerosol-phase mass concentrations of product i , respectively, and ΔROG_j represents the amount of ROG_j consumed. As shown earlier, their gas phase concentrations would be defined by

$$G_1 = \frac{x_1 \zeta_1 p_1^0 m_{w1}}{RT} 10^6 \quad (16a)$$

$$G_2 = \frac{(1-x_1) \zeta_2 p_2^0 m_{w2}}{RT} 10^6 \quad (16b)$$

where x_1 represents the mole fraction of the first compound in the binary solution. If it is assumed that m_{w1} is approximately equal to m_{w2} , this mole fraction is given by

$$x_1 = \frac{A_1}{A_1 + A_2} \quad (17)$$

Combining equations (15)-(17), replacing vapor pressure with the expression for the equilibrium partitioning coefficient given in equation (6), and setting each ζ_i equal to one, since an ideal solution is assumed, results in a quadratic expression for x_1 in terms of $\alpha_{1,j}$, $\alpha_{2,j}$, $K_{1,j}$, $K_{2,j}$ and ΔROG_j . This expression has real and positive roots. When solved subject to the constraints that A_1 and A_2 are greater than or equal to zero, it can then be shown that the threshold value of the parent organic that must be oxidized to form aerosol, ΔROG_j^* ($\mu\text{g m}^{-3}$), is (21)

$$\frac{1}{\Delta\text{ROG}_j^*} = \sum_{i=1}^2 \alpha_{i,j} K_{i,j} \quad (18)$$

Using the $\alpha_{i,j}$ and $K_{i,j}$ values for the organics given in Table 4.1, it is possible to calculate ΔROG_j^* for each compound. These values will be used to define a base case scenario and are described later.

4.5 Formation of Organic Aerosol from a Mixture of Hydrocarbons

Odum et al. [1996,1997ab] showed that the amount of organic aerosol produced from a mixture of parent hydrocarbons can be predicted as long as each ΔROG_j and the appropriate $\alpha_{i,j}$ and $K_{i,j}$ values are known. For a given M_{oT} (where the subscript T denotes total), the total yield for a parent hydrocarbon j can be calculated from equation (11),

$$Y_j = M_{oT} \sum_i \left(\frac{\alpha_{i,j} K_{i,j}}{1 + M_{oT} K_{i,j}} \right) \quad (19)$$

The amount of aerosol formed specifically from that parent of interest can then be calculated using this yield by

$$M_{oj} = Y_j \Delta \text{ROG}_j \quad (20)$$

Summing the amount of aerosol generated by each parent in the mixture and adding any initial aerosol, M_{init} , gives the total amount of organic aerosol or

$$M_{oT} = \sum_j M_{oj} + M_{init} \quad (21)$$

Finally, combining equations (19)-(21) results in

$$1 = \sum_j \Delta \text{ROG}_j \sum_i \left(\frac{\alpha_{i,j} K_{i,j}}{1 + K_{i,j} M_{oT}} \right) + \frac{M_{init}}{M_o} \quad (22)$$

in which M_{oT} can be found iteratively if M_{init} is known. In this expression, ΔROG_j is actually equal to $\chi_j [\text{ROG}_j]_o$ where χ_j is the fraction of the parent hydrocarbon that reacts and $[\text{ROG}_j]_o$ is the initial concentration of ROG_j . For this study, it is assumed that χ_j is 1 for all species due to the high reaction rates of the species of interest and to avoid the need for complicated gas-phase modeling.

4.6 Incremental Aerosol Reactivity

The incremental ozone reactivity of a parent compound is defined as the ratio of the incremental change in the amount of ozone formed (relative to the ozone formed from oxidation of a base case mixture) that results from an incremental change in the

concentration of the compound of interest in the mixture to the change of the compound's concentration itself [Carter, 1994]. Such measurements are useful when ozone control strategies require some sort of numerical ranking of the parent compounds of interest. Analogously, *incremental aerosol reactivity* for a parent organic ROG_j and a given initial mixture of organics and NO_x, IAR_j ($\mu\text{g m}^{-3}$ ppb⁻¹), can be defined as,

$$\text{IAR}_j = \frac{\delta M_{oT}}{\delta \Delta \text{ROG}_j} \quad (23)$$

the ratio of δM_{oT} ($\mu\text{g m}^{-3}$), the incremental change in total organic aerosol mass that results from an incremental change in the amount of parent hydrocarbon *j* that reacts, $\delta \Delta \text{ROG}_j$ (ppb), to $\delta \Delta \text{ROG}_j$ itself. δM_{oT} is calculated as the difference between the total amount of organic aerosol mass formed when the amount of parent *j* in the mixture is varied incrementally and the total amount of organic aerosol formed in the given initial case (base, base plus initial aerosol, zero-biogenic, or zero-aromatic case in the present situation). Because the initial amount of ROG_j is assumed to react completely, $\delta \Delta \text{ROG}_j$ is just the difference between the initial concentrations of parent reacting in the two scenarios. IAR_j values are then simply found as the slope of a plot δM_{oT} versus $\delta \Delta \text{ROG}_j$ if this ratio is linear.

The challenge in actually computing values of the incremental aerosol reactivity lies in specifying the gas-phase organic parent concentrations. (Since complete consumption of each parent compound is assumed and yield parameters are experimentally determined, the need for gas-phase mechanisms is obviated.) A first choice one might make is a set of typical ambient concentrations in, say, an urban area.

While such a choice can certainly serve to define conditions for the calculation, such an approach lacks the generality desirable in computing IAR_j values. In addition, aerosol formation parameters are available only for a select few of the compounds that are part of the complex mixture of gas-phase organic precursors in the atmosphere. Because the presence of additional organic aerosol precursors increases the potential for aerosol formation, simply using the ambient concentrations of those compounds for which yield data is available would significantly underpredict a compound's ability to form aerosol. However, a unique parameter associated with each organic is its threshold concentration for SOA formation, ΔROG_j^* as defined in equation (18), suggesting specification of the initial mixture based on ΔROG_j^* values. Because less parent is required to react to form aerosol in the presence of other aerosol-forming compounds than when the compound exists by itself, however, the individual ΔROG_j^* values need to be reduced in order to produce an initial mixture that leads to a concentration level relevant to ambient conditions. If ΔROG_j^* are not reduced, the base case would lead to a prediction of organic aerosol concentration that is greater than $650 \mu\text{g m}^{-3}$. The degree to which the ΔROG_j^* values should be reduced to define the initial mixture introduces, however, an unavoidable element of arbitrariness into the specification of the mixture for the IAR calculation. The goal is to select a fraction of the ΔROG_j^* that leads to predicted aerosol levels that are in the range of those observed in ambient atmospheres. By using $\Delta ROG_j^*/4$ for the anthropogenic compounds (the aromatic species listed in Table 4.1) and $\Delta ROG_j^*/8$ for the biogenic compounds, we find that these values are the smallest whole fractions that lead to aerosol formation in the cases when all biogenics equal zero and when all aromatics equal zero, respectively.

Since the biogenic species are more efficient aerosol precursors than the aromatic species, the concentrations of the biogenics need to be decreased from the individual threshold values by a factor of 8, rather than 4. This approach produces a base-case scenario that may be atmospherically realistic for a polluted urban area receiving some influence from biogenic species. These base-case mixing ratios (ppb) that result from this choice of conditions are given in Table 4.2 for 308K (approximately the temperature at which the aerosol yield parameters for each of these compounds were derived). In the base case, anthropogenic species contribute approximately 75% of the total amount of carbon ($\text{ppbC}_{\text{aromatics}} / (\text{ppbC}_{\text{aromatics}} + \text{ppbC}_{\text{biogenics}})$). Since the incremental aerosol reactivities are expected to be dependent on the initial case chosen, to investigate reactivities for a range of scenarios, two additional cases are defined. The first is the so-called zero-biogenics case, in which all biogenic concentrations have been set to zero; correspondingly, in the zero-aromatics case the concentrations of all aromatic species are set to zero. For these cases, M_{init} is assumed to be zero. A fourth case uses base-case concentrations and assumes that M_{init} is equal to $10 \mu\text{g m}^{-3}$.

Solving equation (22) for the four cases results in values of M_{oT} of $37.43 \mu\text{g m}^{-3}$, $5.31 \mu\text{g m}^{-3}$, $6.39 \mu\text{g m}^{-3}$, and $54.97 \mu\text{g m}^{-3}$ respectively. The base case result is not unrealistic for a polluted area during a smog episode. In this base case, 51.1% of the organic aerosol formed is attributable to the oxidation of aromatics, with the remainder resulting from the biogenic precursors. It is interesting to note that simply adding the zero-aromatic and zero-biogenic cases together does not produce the base case value, indicating the nonlinearity associated with SOA formation and the increased potential for

aerosol formation when the products of one parent hydrocarbon interact with products of the oxidation of other compounds.

For each parent organic in each case, individual initial organic concentrations were varied by $\pm 5\%$ and $\pm 10\%$. Equation (22) was used to calculate the total mass of organic aerosol formed in each situation, and IAR_j values were then calculated using equation (23). For example, in the base case, M_{oT} is $37.43 \mu\text{g m}^{-3}$. The M_{oT} values that result from equation (22) if the concentration of *m*-xylene (base case concentration of 46.67 ppb) is decreased by 10%, decreased by 5%, increased by 5%, and increased by 10% are $36.37 \mu\text{g m}^{-3}$, $36.90 \mu\text{g m}^{-3}$, $37.96 \mu\text{g m}^{-3}$ and $38.50 \mu\text{g m}^{-3}$, respectively. The corresponding δM_{oT} values are thus $-1.06 \mu\text{g m}^{-3}$, $-0.53 \mu\text{g m}^{-3}$, $0.53 \mu\text{g m}^{-3}$, and $1.07 \mu\text{g m}^{-3}$. These are associated with $\delta \Delta \text{ROG}_j$ values of -4.667 ppb , -2.334 ppb , 2.334 ppb , and 4.667 ppb . The slope of the plot of δM_{oT} versus $\delta \Delta \text{ROG}_j$ is IAR_j . For *m*-xylene in the base case, this slope is 0.228.

There exists a wide range of IAR_j values for the compounds of interest in each case (Table 4.3). For the base case, IAR_j values range from 0.228 to $0.761 \mu\text{g m}^{-3} \text{ ppb}^{-1}$ for the aromatics considered and from 0.459 to $10.352 \mu\text{g m}^{-3} \text{ ppb}^{-1}$ for the biogenic compounds investigated. These ranges are 0.234 to $0.694 \mu\text{g m}^{-3}$ and 0.399 to $9.446 \mu\text{g m}^{-3}$ respectively when initial organic aerosol is present. Because these represent only small changes (-13 to 5%) compared to the base case, M_{init} is assumed to be zero for the zero-aromatics and zero biogenic cases. In the zero-biogenic case, the IAR_j values for the aromatics exhibit a range of 0.133 to 0.801. It is interesting to note that all of the compounds except diethyl benzene have lower IAR_j values in the zero-biogenic case than in the base case. Diethyl benzene exhibits a 5% decrease in its IAR_j value between the

zero-biogenic and base cases, whereas the other aromatics show a 26-72% increase going from the zero-biogenic to the base case. In the zero-aromatic case, the IAR_j of the biogenic compounds range from 0.456 to 6.923. Similar to the behavior of the aromatics in the zero-biogenic case, all the biogenics except one, terpinolene, have lower IAR_j values in the zero-aromatic case than in the base case. Terpinolene exhibits an IAR_j value that is 7.5% lower in the base case when compared to the zero-aromatic case. The other biogenic compounds exhibit an increase of 10-129%. It should be noted that the R^2 associated with each plot of δM_{oT} versus $\delta \Delta ROG_j$ was essentially unity.

The contrary behavior of diethyl benzene and terpinolene is best explained by considering Y as a function of M_o . While Y increases as the amount of material reacted (and therefore M_o) increases (a positive effect on IAR_j), it becomes less dependent on M_o . This means that $dY/d M_o$ decreases as M_o increases (a negative effect on IAR_j). However, because of the link to α_i and K_i values, the dependence of these effects on M_o varies considerably among the compounds of interest. Diethyl benzene and terpinolene are the two compounds with the fastest decreasing $dY/d M_o$ values, meaning that the negative effect is greatest for these species. For diethyl benzene and terpinolene, this negative effect is greater than the positive effect of increasing M_o , and IAR_j decreases when comparing the zero-biogenic and zero-aromatic cases, respectively, to the base case. Basically, the increase in yield due to increased amount of reaction, and therefore, increased amount of material available to act as an absorptive medium, is not large enough to counteract the change in $dY/d M_o$, as it is for all other compounds. This behavior is also linked to the fact that diethyl benzene and terpinolene are present only in small amounts in the scenarios defined in this study.

4.7 Relative Incremental Aerosol Reactivity

One may also define *relative incremental aerosol reactivities*, where IAR_j is reported relative to that of a reference compound. We can select a single reference compound for the entire mixture of aromatics and biogenics studied, or we can choose one compound from each category as the reference compound. We choose to do the latter because these compounds are emitted from different sources, although one can clearly report all relative incremental aerosol reactivities with respect to a single compound if so desired. *m*-Xylene and α -pinene, compounds that are prevalent in ambient air and that have been investigated extensively experimentally, are convenient reference compounds for aromatics and biogenics, respectively. With these reference compounds, relative incremental aerosol reactivities are defined as either

$$\text{RIAR}_j = \frac{\text{IAR}_j}{\text{IAR}_{m\text{-xylene}}} \quad (24a)$$

$$\text{RIAR}_j = \frac{\text{IAR}_j}{\text{IAR}_{\alpha\text{-pinene}}} \quad (24b)$$

for aromatics and biogenics, respectively (Table 4.4). From this definition, $\text{RIAR}_{m\text{-xylene}}$ and $\text{RIAR}_{\alpha\text{-pinene}}$ are equal to 1.0. It should be noted that the ratio of $\text{IAR}_{\alpha\text{-pinene}}$ to $\text{IAR}_{m\text{-xylene}}$ under the base case conditions considered here is 3.535.

For the base case, RIAR_j values range from 1.153 for low-yield aromatics up to 3.338 for diethyl benzene and from 0.569 for terpinolene up to 12.843 for α -humulene. In the zero-biogenic case the range of values shifts compared to the base case to 1.349 for

the low-yield aromatics up to 6.032 for diethyl benzene. In the zero-aromatic case, RIAR_j values range from 0.882 for linalool up to 13.385 for α -humulene. The RIAR_j value of each aromatic increases in the zero-biogenic case when compared to the base case. This simply means that the other aromatic compounds will form aerosol more readily than *m*-xylene and that this difference is more pronounced at lower values of M_o . The RIAR_j values of these aromatics also retain the same rank when comparing the base and zero-biogenic cases (i.e., low-yield aromatics < high-yield aromatics < methyl propyl benzene < diethyl benzene). The same cannot be said for the biogenic species. Of the compounds investigated, six have RIAR_j values that decrease in the zero-aromatic case when compared to the base case (Δ^3 -carene, β -caryophyllene, limonene, linalool, β -pinene, and the terpinene isomers) and five have values that increase (α -humulene, ocimene, sabinene, terpinene-4-ol, and terpinolene). This shows that relative to α -pinene, the tendency of the biogenic compounds to form aerosol is more strongly dependent on M_o . This is supported by the fact that the relative rank of the RIAR_j values of these compounds varies significantly between the two cases. These differences can be explained using arguments similar to those presented earlier regarding yield as a function of M_o , the behavior of the derivative of this function, and the amount of each compound present in these scenarios.

Because of the link between IAR_j values and the chosen initial conditions, RIAR_j values depend on this choice as well. However, significant changes (a decrease of 20% or an increase of 33%) in the concentrations in the base case chosen here result in small changes (average of 5% and -8%, respectively) in the associated RIAR_j values, indicating the robustness of the methodology used to determine the incremental aerosol reactivity.

The relative ranks of these values in the altered base cases remain virtually unchanged, as well. Only in the case in which concentrations are increased by 33% is there a slight discrepancy; sabinene and Δ^3 -carene, which have very similar RIAR_j values in the base case, switch places in the ranking in this scenario.

4.8 References

Bowman, F.M., J.R. Odum, S.N. Pandis, and J.H. Seinfeld, Mathematical model for gas-particle partitioning of secondary organic aerosols, *Atmos. Environ.*, 31, 3921-3931, 1997.

Carter, W.P.L., Development of ozone reactivity scales for volatile organic compounds, *J. Air Waste Management Assoc.*, 44, 881-899, 1994.

Carter, W.P.L., J.A. Pierce, D. Luo, and I.L. Malkina, Environmental chamber study of maximum incremental reactivities of volatile organic compounds, *Atmos. Environ.*, 18, 2499-2511, 1995.

Forstner, H.J.L., R.C. Flagan, and J.H. Seinfeld, Molecular speciation of the secondary organic aerosol from photooxidation of the higher alkenes: 1-octene and 1-decene, *Environ. Sci. Technol.*, 31, 1345-1358, 1997a.

Forstner, H.J.L., R.C. Flagan, and J.H. Seinfeld, Secondary organic aerosol from photooxidation of aromatic hydrocarbons: molecular composition, *Atmos. Environ.*, 31, 1953-1964, 1997b.

Griffin, R.J., D.R. Cocker III, R.C. Flagan, and J.H. Seinfeld, Organic aerosol formation from the oxidation of biogenic hydrocarbons, *J. Geophys. Res.*, 104, 3555-3567, 1999.

Grosjean, D., and J.H. Seinfeld, Parameterization of the formation potential of secondary organic aerosols, *Atmos. Environ.*, 23, 1733-1747, 1989.

Hoffmann, T., J.R. Odum, F. Bowman, D. Collins, D. Klockow, R.C. Flagan, and J.H. Seinfeld, Formation of organic aerosols from the oxidation of biogenic hydrocarbons, *J. Atmos. Chem.*, 26, 189-222, 1997.

Izumi, K., and T. Fukuyama, Photochemical aerosol formation from aromatic hydrocarbons in the presence of NO_x , *Atmos. Environ.*, 24A, 1433-1441, 1990.

Liang, C., J.F. Pankow, J.R. Odum, and J.H. Seinfeld, Gas/particle partitioning of semivolatile organic compounds to model inorganic, organic, and ambient smog aerosols, *Environ. Sci. Technol.*, 31, 3086-3092, 1997.

Odum, J.R., T.P.W. Jungkamp, R.J. Griffin, H.J.L. Forstner, R.C. Flagan, and J.H. Seinfeld, Aromatics, reformulated gasoline, and atmospheric organic aerosol formation, *Environ. Sci. Technol.*, 31, 1890-1897, 1997a.

Odum, J.R., T.P.W. Jungkamp, R.J. Griffin, R.C. Flagan, and J.H. Seinfeld, The atmospheric aerosol-forming potential of whole gasoline vapor, *Science*, 276, 96-99, 1997b.

Odum, J.R., T. Hoffmann, F. Bowman, D. Collins, R.C. Flagan, and J.H. Seinfeld, Gas/particle partitioning and secondary organic aerosol yields, *Environ. Sci. Technol.*, 30, 2580-2585, 1996.

Pandis, S.N., S.E. Paulson, J.H. Seinfeld, and R.C. Flagan, Aerosol formation in the photooxidation of isoprene and β -pinene, *Atmos. Environ.*, 25, 997-1008, 1991.

Pandis, S.N., R.A. Harley, G.R. Cass, and J.H. Seinfeld, Secondary organic aerosol formation and transport, *Atmos. Environ., Part A*, 26, 2269-2282, 1992.

Pandis, S.N., A.S. Wexler, and J.H. Seinfeld, Secondary organic aerosol formation and transport – 2. Predicting the ambient secondary organic aerosol size distribution, *Atmos. Environ.*, 27, 2403-2416, 1993.

Pankow, J.F. An absorption model of the gas/aerosol partitioning of organic compounds in the atmosphere, *Atmos. Environ.*, 28, 185-188, 1994a.

Pankow, J.F. An absorption model of the gas/aerosol partitioning involved in the formation of secondary organic aerosol, *Atmos. Environ.*, 28, 189-193, 1994b

Saxena, P., and L.M. Hildemann, Water-soluble organics in atmospheric particles: a critical review of the literature and application of thermodynamics to identify candidate compounds, *J. Atmos. Chem.*, 24, 57-109, 1996.

Seinfeld, J.H., and S.N. Pandis, *Atmospheric Chemistry and Physics*, Wiley-Interscience, New York, 1998.

Wang, S.-C., S.E. Paulson, D. Grosjean, R.C. Flagan, and J.H. Seinfeld, Aerosol formation and growth in atmospheric organic/NO_x systems - I. Outdoor smog chamber studies of C₇- and C₈- hydrocarbons, *Atmos. Environ.*, 26A, 403-420, 1992a.

Wang, S.-C., R.C. Flagan, and J.H. Seinfeld, Aerosol formation and growth in atmospheric organic/NO_x systems - II. Aerosol dynamics, *Atmos. Environ.*, 26, 421-434, 1992b.

Zhang, S.-H., M. Shaw, J.H. Seinfeld, and R.C. Flagan, Photochemical aerosol formation from α -pinene and β -pinene, *J. Geophys. Res.*, 97, 20,717-20,729, 1992.

Table 4.1. Aerosol formation parameters α_i and K_i ($\text{m}^3 \mu\text{g}^{-1}$) values obtained in the Caltech smog chamber [*Odum et al.*, 1996, 1997ab; *Hoffmann et al.*, 1997; *Griffin et al.*, 1999].

Hydrocarbon	α_1	K_1	α_2	K_2
<u>Aromatic Compounds</u>				
Low-yield aromatics	0.038	0.042	0.167	0.0014
High-yield aromatics	0.071	0.053	0.138	0.0019
<i>m</i> -Xylene	0.030	0.032	0.167	0.0019
Diethylbenzene	0.083	0.093	0.220	0.0010
Methylpropylbenzene	0.050	0.054	0.136	0.0023
<u>Biogenic Compounds</u>				
Δ^3 -Carene	0.054	0.043	0.517	0.0042
β -Caryophyllene	1.000	0.0416	-	-
α -Humulene	1.000	0.0501	-	-
Limonene	0.239	0.055	0.363	0.0053
Linalool	0.073	0.049	0.053	0.0210
Ocimene	0.045	0.174	0.149	0.0041
α -Pinene	0.038	0.171	0.326	0.0040
β -Pinene	0.130	0.044	0.406	0.0049
Sabinene	0.067	0.258	0.399	0.0038
α - & γ -Terpinene	0.091	0.081	0.367	0.0046
Terpinene-4-ol	0.049	0.159	0.063	0.0045
Terpinolene	0.046	0.185	0.034	0.0024

Table 4.2. Base case mixing ratios (ppb) for the hydrocarbons of interest.

Hydrocarbon	Mixing Ratio
<u>Aromatic Compounds</u>	
Low-yield aromatics	32.58
High-yield aromatics	17.06
<i>m</i> -Xylene	46.67
Diethylbenzene	5.94
Methylpropylbenzene	15.65
<u>Biogenic Compounds</u>	
Δ^3 -Carene	5.17
β -Caryophyllene	0.37
α -Humulene	0.31
Limonene	1.54
Linalool	4.95
Ocimene	2.75
α -Pinene	2.98
β -Pinene	3.01
Sabinene	1.24
α - & γ -Terpinene	2.56
Terpinene-4-ol	2.88
Terpinolene	2.70

Table 4.3. Incremental aerosol reactivities ($\mu\text{g m}^{-3}$ ppb $^{-1}$) for parent organic compounds.

Hydrocarbon	Base Case	Base Case with Initial Aerosol	Zero-biogenic Case	Zero-aromatic Case
<u>Aromatic Compounds</u>				
Low-yield aromatics	0.263	0.260	0.179	na
High-yield aromatics	0.410	0.391	0.326	na
<i>m</i> -Xylene	0.228	0.234	0.133	na
Diethylbenzene	0.761	0.694	0.801	na
Methylpropylbenzene	0.466	0.450	0.358	na
<u>Biogenic Compounds</u>				
Δ^3 -Carene	1.106	1.161	na	0.484
β -Caryophyllene	9.670	9.025	na	6.071
α -Humulene	10.352	9.446	na	6.923
Limonene	2.361	2.257	na	1.388
Linalool	0.751	0.703	na	0.456
Ocimene	0.625	0.581	na	0.531
α -Pinene	0.806	0.806	na	0.517
β -Pinene	1.527	1.527	na	0.777
Sabinene	1.166	1.133	na	0.971
α - & γ -Terpinene	1.310	1.287	na	0.803
Terpinene-4-ol	0.556	0.487	na	0.507
Terpinolene	0.459	0.399	na	0.496

Table 4.4. Relative incremental aerosol reactivities.

Hydrocarbon	Base Case	Zero-biogenic Case	Zero-aromatic Case
<u>Aromatic Compounds</u> (basis: <i>m</i> -xylene)			
Low-yield aromatics	1.153	1.349	na
High-yield aromatics	1.799	2.453	na
<i>m</i> -Xylene	1.000	1.000	na
Diethylbenzene	3.338	6.032	na
Methylpropylbenzene	2.046	2.693	na
<u>Biogenic Compounds</u> (basis: α -pinene)			
Δ^3 -Carene	1.373	na	0.935
β -Caryophyllene	11.997	na	11.737
α -Humulene	12.843	na	13.385
Limonene	2.929	na	2.684
Linalool	0.932	na	0.882
Ocimene	0.775	na	1.026
α -Pinene	1.000	na	1.000
β -Pinene	1.894	na	1.501
Sabinene	1.446	na	1.878
α - & γ -Terpinene	1.626	na	1.553
Terpinene-4-ol	0.690	na	0.981
Terpinolene	0.569	na	0.958

Chapter 5

Secondary Organic Aerosol: I. Atmospheric Chemical Mechanism for Production of Molecular Constituents

5.1 Introduction

Atmospheric urban and regional scale gas-phase chemical mechanisms describe the formation of oxidants such as ozone (O_3), the hydroxyl radical (OH), and the nitrate radical (NO_3), the consumption of reactive organics, and reactions of the resulting organic peroxy radicals with species such as the oxides of nitrogen ($NO_x = NO + NO_2$). Mechanisms that have been used in urban and regional atmospheric models include that of *Lurmann et al.* (LCC) [1987], the Carbon Bond IV Mechanism (CB-IV) [*Gery et al.*, 1989], the Regional Acid Deposition Model (RADM2) [*Stockwell et al.*, 1990], the Regional Atmospheric Chemistry Model (RACM) [*Stockwell et al.*, 1997], and the Statewide Air Pollution Research Center Mechanism (SAPRC-97) [*Carter et al.*, 1997]. In addition, *Jenkin et al.* [1997] have presented a master chemical mechanism consisting of 120 parent organic compounds, 2500 chemical species, and approximately 7000 reactions.

Secondary organic aerosol (SOA) is formed in two steps. First, a sufficiently large parent organic is oxidized, resulting in products that have vapor pressures significantly lower than that of the parent. If their vapor pressures are low enough, these products can partition to the aerosol phase via condensation (adsorptive or absorptive) or homogeneous nucleation. Because low-vapor pressure products are needed to form SOA, in general, only those parent organics with six or more carbon atoms are capable of producing oxidized products that form SOA [*Odum et al.*, 1996]. Existing gas-phase atmospheric chemical mechanisms do not include the detailed organic chemistry necessary for prediction of SOA formation. It should be noted that one reason for this is that much of the chemistry of the larger organics that leads to semi-volatile products is not known.

This paper describes a new chemical mechanism, termed the Caltech Atmospheric Chemistry Mechanism (CACM), that has two goals: (1) to include state-of-the-art treatment of ozone formation chemistry; and (2) to explicitly describe organic chemistry to predict the concentrations of secondary and tertiary semi-volatile oxidation products that have the potential to act as constituents of SOA. In the treatment of O_3 formation chemistry, CACM relies on the recent work of *Stockwell et al.* [1997], *Jenkin et al.* [1997], and *Carter* [1997, 1999]. The new mechanism contains a significant expansion of organic product chemistry in order to predict the formation of multi-functional products of sufficiently low vapor pressure that they can partition between the gas- and particulate phases. In addition to the extension of the mechanism to include more detailed organic chemistry, additional experimental and empirical information on rate constants and product yields (e.g., alkyl nitrate formation versus NO to NO_2 conversion) have been implemented in CACM [*Carter and Atkinson*, 1989; *Atkinson* 1990, 1994, 1997; *Goumri et al.*, 1992; *Lay et al.*, 1996; *Alvarado et al.*, 1998]. While specific organic chemical mechanisms have been developed to model smog chamber SOA data (See, for example, *Barthelme and Pryor* [1999].), we present here the first detailed atmospheric chemical mechanism that is directed toward explicit prediction of formation of the semi-volatile products that could constitute observed SOA and that is designed for use in a three-dimensional air quality model. Because much of this chemistry has yet to be firmly established, the product distributions in the mechanism to be presented are based either on limited observed product data or on extrapolation of the behavior of smaller organics. We recognize, of course, that precise product specifications are likely to change as more is learned about the mechanisms of SOA formation.

CACM includes a total of 191 species: (1) 120 fully integrated species (Fully integrated species have concentrations that are solved for numerically based on kinetics, emission, and deposition.) [15 inorganic, 71 reactive organic, and 34 unreactive organic]; (2) 67 pseudo-steady state species [2 inorganic and 65 organic]; and (3) 4 species that have concentrations that do not change. In comparison, the extended LCC mechanism used by *Harley et al.* [1993] in the California Institute of Technology three-dimensional urban/regional air quality model (CIT) included a total of 46 species: 32 fully integrated species, 9 pseudo-steady state species, and 5 species with concentrations that do not change. Detailed secondary organic oxidation products were not predicted.

Table 5.1 shows a complete list of the species that are included in CACM. Table 5.2 gives the reactions included in CACM with appropriate Arrhenius rate constant expressions. The following text describes the inorganic and organic chemistry in CACM, presents simulations of gas-phase concentrations in the South Coast Air Basin of California (SOCAB) for August 27-29, 1987, and compares these results with observed data and other simulations for this episode. The goals of Part I, therefore, are to present the mechanism and to evaluate its performance in simulating gas-phase chemistry during a well-studied episode in the SOCAB. Part II will derive a module to predict SOA formation based on thermodynamic equilibrium. Future work will include complete gas- and aerosol-phase simulations in the SOCAB for a 1993 episode.

5.2 Inorganic Chemistry

Inorganic chemistry within CACM (Reactions 1-42 in Table 5.2) is derived primarily from the SAPRC-99 mechanism of *Carter* [1999]. Only a brief overview of the inorganic chemistry need be given here. Photolysis rate constants are given in Table 5.3,

and rate constants determined by three-body kinetics are listed in Table 5.4. Additional rate constants not falling into one of the previously mentioned categories are shown in Table 5.5.

Tropospheric inorganic chemistry is driven by a few relatively well understood reactions acting in a cycle. The first step is the emission of NO and organic species from anthropogenic or biogenic sources. NO is converted to NO₂ primarily via the reaction of NO with O₃ (reaction 5), hydroperoxy radicals (HO₂) (reaction 26), or alkylperoxy radicals (RO₂) (multiple reactions). These peroxy radicals are formed by the reaction of OH with organic species (multiple reactions), CO (reaction 24), O₃ (reaction 25), or H₂O₂ (reaction 37). Photolysis of NO₂ (reaction 1) results in the formation of O(³P) and NO, with O(³P) combining with O₂ to form O₃ (reaction 2). Photolysis of O₃ (reactions 15 and 16) leads to some formation of both O(³P) and O(¹D) with O₂, and O(¹D) can then react with water (reaction 17) to form OH, the primary tropospheric oxidant. O(¹D) can also be collisionally stabilized to form O(³P) (reaction 18). Other reactions that produce OH and that are included are the photolysis of HONO (reaction 20), the reaction between O₃ and HO₂ (reaction 30), and the photolysis of H₂O₂ (reaction 36). HONO is formed by the reaction of OH and NO (reaction 19) or by the reaction of NO₂ and H₂O (reaction 21), and H₂O₂ is formed by the self-combination of HO₂ (reactions 31 and 32).

The nitrate radical, NO₃, is formed primarily by the combination of NO₂ and O₃ (reaction 6). NO₃ is relatively unimportant during the day because of its high rate of photolysis (reactions 13 and 14) to either NO and O₂ or NO₂ and O(³P). Other sources include the reaction of NO₂ with O(³P) (reaction 4) and the oxidation of HNO₃ by OH (reaction 23). HNO₃ is formed in the reaction of NO₂ with OH (reaction 22), by the

combination of HO_2 and NO_3 (reaction 33), or by the hydrolysis of N_2O_5 (reaction 11).

The kinetics of reaction 22 [*Dransfield et al.*, 1999] have been significantly updated as compared with those in the extended LCC mechanism used by *Harley et al.* [1993].

HNO_4 is formed by the reaction of NO_2 with HO_2 (reaction 27). Sinks for HNO_4 include decomposition back to NO_2 and HO_2 (reaction 28) and reaction with OH (reaction 29).

Oxidation of SO_2 by OH to form SO_3 (reaction 35) must be included in any gas-aerosol mechanism since SO_3 rapidly forms sulfuric acid (H_2SO_4) which, in turn, transfers to the aerosol phase [*Seinfeld and Pandis*, 1998].

5.3 Organic Chemistry

In existing gas-phase mechanisms, organic chemistry has been focused primarily on predicting the total concentration of peroxy radicals that are generated as a result of hydrocarbon oxidation. In an effort to address the computational demands of gas-phase mechanisms to be used in three-dimensional atmospheric models, parent organics are often lumped into surrogate groups so that both the number of species and the number of reactions are reduced. Recently, *Stockwell et al.* [1997] developed a detailed lumped gas-phase mechanism (RACM) that tracks the formation of 18 highly aggregated organic products. Specific multi-functional products needed for SOA prediction are not tracked. Prediction of specific products is important because gas-particle partitioning, through the link to vapor pressure, is highly dependent on molecular size and degree of functionality [*Yu et al.*, 1999].

In CACM, primary organic compounds are lumped in a manner similar to that described by *Stockwell et al.* [1997]. The result is a set of surrogate compounds designed to represent the entire array of gas-phase organic species emitted to the atmosphere.

Oxidation reactions of the surrogate parents are tracked individually, with multiple pathways being represented by the dominant reaction [Kwok and Atkinson, 1995; Atkinson, 1997]. Reactions of the resulting alkyl peroxy radicals are also included. From the reactions of these alkyl peroxy radicals, it is possible to predict the formation of surrogate oxidation products. If a product is considered reactive, it can go on to form tertiary (and so on) oxidation products. Concentrations of the secondary, tertiary, etc., oxidation products then allow for prediction of the partitioning of organic molecules between the gas- and aerosol phases (Part II).

In CACM, the lumped model compound corresponding to a given individual parent hydrocarbon is determined by considering the size of the molecule, its structural characteristics (e.g., branched versus cyclic versus straight chain), its functionality (both location and type), its reactivity, and its experimentally determined potential for forming SOA, if available. Taking the ‘average’ structure of the compounds within a group (a group being appropriately defined) yields the surrogate for each group. Twenty-three individual groups, either surrogates or those described explicitly, are used (See Table 5.1). Instead of generating an aggregate rate constant for the surrogates as described by Stockwell *et al.* [1997], the rate constant for the model parent (either based on experimental data or calculated using structure-reactivity relationships) is used. (See Tables 5.2 and 5.6.)

5.3.1 Alkanes

Alkanes are found in significant quantity in urban atmospheres [Fraser *et al.*, 1997; Schauer, 1998; Schauer *et al.*, 1999ab]. Methane chemistry is included explicitly in CACM, but because of its large mixing ratio, the concentration of methane remains

unchanged. The main tropospheric loss process for methane is the well documented oxidation by OH (reaction 43) to form the methyl peroxy radical ($\text{RO}_2\text{1}$). $\text{RO}_2\text{1}$ can then react with NO (reaction 110) in the presence of O_2 to form HO_2 , formaldehyde (HCHO), and NO_2 , with other peroxy radicals (represented henceforth as RO_2T) (reaction 111) to yield HCHO and HO_2 , or with HO_2 to form HCHO (reaction 112). Throughout CACM, alkyl peroxy radical reactions with RO_2T are assumed, for simplicity, to form the same products as the NO reaction that results in the conversion of NO to NO_2 . In addition, reactions with HO_2 are assumed to form the degradation products of the corresponding intermediate hydroperoxide in an effort to limit the number of fully integrated species since hydroperoxides are relatively reactive and often form very similar products [Seinfeld and Pandis, 1998]. The main purpose of including alkyl peroxy radical reactions with RO_2T and HO_2 is to capture accurately alkyl peroxy radical concentrations using the pseudo-steady state approximation. Both HO_2 and RO_2T are fully integrated species in CACM. To account accurately for RO_2T (which is formed along with every individual RO_2i species) concentrations, its reactions with NO, HO_2 , and itself are also included in CACM (reactions 94-96).

5.3.1.1 Short Chain Alkanes

Short chain alkanes (ALKL) are considered as those with between 2 and 6 carbon atoms. Based on the structural aggregation, 2-methyl-butane is used to represent these compounds, as shown in Table 5.1. In general, alkanes with more than one carbon atom are oxidized by OH abstraction of an H-atom with the subsequent addition of O_2 to form the alkyl peroxy radical [Atkinson, 1997]. As discussed above, the alkyl peroxy radical further reacts with NO, HO_2 , or RO_2T . In the case of ALKL, oxidation by OH (reaction

58) results in the formation of RO₂5, which is a lumped alkyl peroxy radical formed by other parent hydrocarbons as well. RO₂5 is treated as a primary peroxy radical with three carbon atoms. Upon reaction with NO (reaction 122), RO₂5 can form the corresponding alkyl nitrate or NO₂, HO₂, and the corresponding aldehyde. The yield of alkyl nitrate formation versus NO to NO₂ conversion is calculated based on *Carter and Atkinson* [1989]. The HO₂ and RO₂T reactions also form HO₂ and an aldehyde (ALD2) (reactions 123 and 124). In this case, the alkyl nitrate formed in the NO reaction is treated as ALKL. When reactive small chain compounds that are not expected to contribute to SOA (either by dissolving in an aqueous phase or by absorption into an organic phase) are formed, they are reclassified within parent groups according to their size and most reactive functional group.

5.3.1.2 Medium Chain Alkanes

Medium chain alkanes (ALKM) are taken as those with between 7 and 12 carbon atoms and are represented by 3,5-dimethyl-heptane. Initial OH oxidation of this species forms RO₂20 (reaction 78). Like the corresponding RO₂5, RO₂20 is formed by more than one parent species and is represented by a lumped structure, 3-methyl-4-heptyl-peroxy radical. RO₂20 also reacts with NO (reaction 176), HO₂ (reaction 178), and RO₂T (reaction 177). Reaction 176 forms an alkyl nitrate (AP3). The alkoxy radical formed in reactions 176-178 has sufficient chain length that the dominant mechanism involving this radical proceeds by isomerization through a 1,5-H shift [Atkinson, 1997]. The result is RO₂18, a hydroxy alkyl peroxy radical. RO₂18 can react via the NO pathway or with HO₂ and RO₂T (reactions 170-172) to form a hydroxy alkyl nitrate (AP2), HO₂, and a hydroxy ketone (UR16). (Products that are considered nonreactive or whose oxidation

products do not have vapor pressures estimated to be an order of magnitude less than the first product itself are labeled as unreactive, UR_i , in CACM). In this case, the alkyl nitrate products (denoted as AP_i) have sufficiently high carbon number that they or their oxidation products could potentially participate in SOA formation. The oxidation of such alkyl nitrate products proceeds by OH abstraction of the H-atom closest to the nitrooxy group. Subsequent decomposition reactions and reactions with O_2 result in the release of NO_2 and formation of functionalized products. In the case of AP_2 (reaction 351), UR_{16} is assumed to form. In the case of AP_3 (reaction 352), a ketone (UR_{32}) is formed.

5.3.1.3 Long Chain Alkanes

Long chain alkanes (ALKH) are represented by *n*-hexadecane since hexadecane exhibits the approximate average number of carbons of those long chain *n*-alkanes that reside at least partially in the gas-phase. Oxidation proceeds as above (reaction 93) and results in the formation of RO_232 . RO_232 is formed only from the oxidation of ALKH; therefore, the structure of RO_232 is 8-hexadecyl peroxy radical. Reaction of RO_232 with NO (reaction 215) forms either 8-hexadecyl nitrate (AP_{11}) or NO_2 and RO_241 (8-hydroxy-11-hexadecyl-peroxy radical) via the 1,5-H shift. The reaction of RO_232 with HO_2 and RO_2T (reactions 216 and 217) also results in the formation of RO_241 . Similarly, RO_241 and NO combine (reaction 218) to form either 8-hydroxy-11-hexadecyl nitrate (AP_{12}) or NO_2 , HO_2 , and 11-hydroxy-8-hexadecanone (UR_{20}) via a second isomerization followed by reaction with O_2 . The HO_2 and RO_2T reactions (reactions 219 and 220) also result in the formation of UR_{20} . Oxidation of AP_{11} and AP_{12} (reactions 360 and 361) results in the formation of 8-hexadecanone (UR_{34}) and UR_{20} , respectively.

5.3.2 Non-biogenic Alkenes

5.3.2.1 Ethene

Despite their high reactivity [Atkinson, 1997], alkenes are still found in high concentration in the ambient [Fraser *et al.*, 1997], which is indicative of significant emissions [Schauer, 1998; Schauer *et al.*, 1999ab]. Ethene (ETHE) is the smallest alkene. Given that its atmospheric chemistry is relatively well understood and that this chemistry is unique [Atkinson, 1997], ETHE is treated explicitly. Reaction of alkenes with OH, NO₃, O₃, and O(³P) (reactions 49-52 respectively for ETHE) are taken into account. In the case of ETHE, reaction with OH results in the formation of RO₂2, a lumped 2-hydroxy, 4-carbon, primary peroxy radical. RO₂2 can undergo peroxy radical reactions similar to those described in the alkanes section above (reactions 113-115). However, in the case of the NO reaction, an alkyl nitrate product is not formed because of the small carbon number [Carter and Atkinson, 1989]. Products of these reactions are HCHO, ALD2, and HO₂. Reaction of ETHE with NO₃ leads to the formation of RO₂3 via addition of NO₃ to the double bond. RO₂3 is a lumped radical similar to RO₂2 with ONO₂ replacing the OH group. Similar to the reactions of RO₂2, those of RO₂3 (reactions 116-118) create HCHO, ALD2, and HO₂. In addition, NO₂ is liberated from RO₂3 upon reaction. The reaction of ETHE with O₃ is initiated by O₃ attack of the double bond in the well known bridging mechanism. The decomposition of this highly energetic intermediate leads to formation of a short chain *n*-carboxylic acid (ACID), HO₂, CO, OH, HCHO, and H₂O. Yields of these products are shown in Table 5.2 and are derived from Jenkin *et al.* [1997]. The final reaction of ETHE is that with O(³P), leading to formation of RO₂1, CO, HO₂, and RO₂4, where RO₂4 is an aldehydic 2-carbon peroxy

radical. The yields of these products are also shown in Table 5.2 and are derived from Atkinson [1997]. As with previous organic peroxy radicals, RO₂4 can further react with NO, RO₂T, and HO₂ (reactions 119-121). Radicals that exhibit an α -carbonyl are assumed not to form alkyl nitrate products [Jenkin *et al.*, 1997]. Thus, the products of reactions 119 through 121 include HCHO, CO, HO₂, and NO₂ (in the NO reaction only).

5.3.2.2 Short Chain Alkenes

Short chain alkenes with between 3 and 6 carbon atoms (OLEL) are represented by 1-pentene because of the high occurrence of straight chain α -alkenes in this group. Similar to ETHE, OLEL is consumed by OH, NO₃, O₃, and O(³P) (reactions 54-57). As with ETHE, OH and NO₃ reaction lead to RO₂2 and RO₂3, respectively. OLEL reaction with O₃ leads to formation of HCHO, ALD2, ACID, CO, OH, carbon dioxide (CO₂), HO₂, ALKL (a reclassified reactive product), and RO₂5 in yields shown in Table 5.2 and derived from Jenkin *et al.* [1997]. The OLEL reaction with O(³P) leads to ALKL (a reclassified reactive product), ALD2, RO₂4, and RO₂5 in yields also shown in Table 5.2 and derived from Atkinson [1997].

5.3.2.3 Long Chain Alkenes

Longer chain alkenes (OLEH) are taken as those with more than 6 carbon atoms and are represented by 4-methyl-1-octene because of the high occurrence of branched α -alkenes. As before, OH, NO₃, O₃, and O(³P) can react with OLEH (reactions 74-77 respectively). Reactions with OH and NO₃ lead to RO₂18 and RO₂19, respectively. RO₂18 is represented by a lumped structure exhibiting a 7-carbon chain, a methyl group in the 2-position, a hydroxy group in the 2-position, and the peroxy radical group in the

5-position. Its reactions are described above. RO₂19 is formed exclusively by OLEH and is the corresponding radical with the nitrooxy group in the 1-position and the peroxy radical at the 2-position. Reactions of RO₂19 (reactions 173-175) result in the formation of HCHO and 3-methyl-heptanal (RPR1) (Reactive products that are capable of participating in SOA formation and that do not exhibit a nitrooxy group are labeled RPR_i or RP_i). The reactions typical of RPR1 will be discussed in the next section. Oxidation or photolysis of RPR1 (reactions 300-302) leads to formation of RO₂20 or the corresponding acyl peroxy radical (RO₂55). The corresponding peroxy nitrate compound (PAN7), RO₂20, and 3-methyl-heptanoic acid (UR1) are formed in the reactions of RO₂55 (reactions 303-307). Details of acyl peroxy radical reactions will be given in the next section. The reaction of OLEH with O₃ leads to the formation of HCHO, RPR1, ACID, UR1, CO, OH, HO₂, CO₂, ALKM (a reclassified reactive product), and RO₂20 in yields described in Table 5.2 and derived via *Jenkin et al.* [1997]. The OLEH-O(³P) reaction forms ALKM, RPR1, RO₂4, and RO₂20 in yields described in Table 5.2 and derived via *Atkinson* [1997].

5.3.3 Aldehydes

Unlike alkanes and alkenes, aldehydes are both emitted in large amounts and formed via atmospheric chemistry. Aldehydes contribute significantly to the overall reactivity of the urban atmosphere [*Grosjean et al.*, 1996].

Formaldehyde is the only aldehyde with one carbon atom; its atmospheric chemistry is well understood. Degradation of HCHO occurs by photolysis (reactions 44 and 45) and oxidation by OH (reaction 46) and NO₃ (reaction 47). Higher *n*-aldehydes (ALD2) are represented by *n*-pentanal. Because of the importance of aldehyde reactions

(with respect to RPR species leading to UR species capable of forming SOA), a general aldehyde mechanism is discussed here. Like HCHO, higher aldehydes are degraded by OH, NO₃, or photolysis. OH and NO₃ degradation proceed via abstraction of the aldehydic H-atom and result in the formation of an acyl radical (RC(O)O₂•) after the subsequent addition of O₂. Photolysis is assumed to form a primary alkyl radical, CO, and an H-atom radical. The alkyl radical and the H-atom radical each react immediately with O₂ to form an alkyl peroxy radical and a hydroperoxy radical, respectively.

The acyl peroxy radical can then undergo reaction with NO, NO₂, HO₂, and RO₂T. In the NO reaction, NO is converted to NO₂, resulting in decomposition of the remainder of the original radical to form CO₂ and a primary alkyl radical which immediately forms an alkyl peroxy radical upon addition of O₂. CO₂ and a primary alkyl peroxy radical are also formed in the RO₂T reaction. NO₂ adds to the radical to form a peroxy acyl nitrate species (denoted as PANi) that can thermally decompose back to RC(O)O₂• and NO₂. Acyl peroxy radicals are converted to organic acids in the reaction with HO₂. This pathway is less likely to occur relative to the NO or NO₂ reactions under high NO_x conditions typical of urban atmospheres [Niki *et al.*, 1985; Moortgat *et al.*, 1989] but accounts for one path of secondary formation of the organic acids observed in the atmosphere [Fraser *et al.*, 1999; Nolte *et al.*, 1999]. At present, the known routes of organic acid formation in the atmosphere cannot account for measured ambient concentrations and are not well understood [Jacob and Wofsy, 1988; Seinfeld and Pandis, 1998].

The photolysis of ALD2 (reaction 59) leads to the formation of RO₂5, CO, and HO₂. The reactions with OH (reaction 60) and with NO₃ (reaction 61) result in the

formation of RO₂6, the corresponding acyl radical. RO₂6 reacts with NO or RO₂T (reactions 125 and 129) to form NO₂ (in the NO case), CO₂, and RO₂5 and with NO₂ (reaction 126) to form the corresponding PAN compound (PAN1, which thermally decomposes in reaction 127). The reaction between RO₂6 and HO₂ (reaction 128) yields ACID and O₃.

5.3.4 Ketones

Atmospheric ketones are less abundant than aldehydes [Fraser *et al.*, 1997], but like aldehydes, they have both primary [Schauer, 1998; Schauer *et al.*, 1999b] and secondary sources. Ketones in CACM are broken down into two groups: short chain ketones with between 3 and 6 carbons (KETL) and long chain ketones with more than 6 carbons (KETH). Sinks of ketones include photolysis and reaction with OH.

Ketones (for example, R₁CH₂C(O)R₂) either photolyze or are oxidized by OH [Atkinson, 1994]. It is assumed that the OH reaction proceeds via abstraction of the H-atom in the position α - to the carbonyl functionality. After addition of O₂, this results in the formation of R₁CH(O₂ \bullet)C(O)R₂, a keto-alkyl peroxy radical. Photolysis yields cleavage of the carbon-carbon bond adjacent to the carbonyl. After addition of O₂, the results are R₁CH₂O₂ \bullet , a simple alkyl peroxy radical, and R₂C(O)O₂ \bullet , an acyl peroxy radical. The keto-alkyl peroxy radical, of course, reacts with NO, HO₂, and RO₂T to form an alkoxy radical in the position α - to the carbonyl. This radical will decompose to form a higher aldehyde (R₁C(O)H) and the acyl peroxy radical described above.

In CACM, KETL is represented by 2-pentanone because of the frequent occurrence of small chain ketones that have the functional group in the 2-position. Following the mechanism described above, the reaction of KETL with OH (reaction 62)

yields RO₂7, a keto-alkyl peroxy radical that is represented by a lumped structure with 4 carbons, the keto group in the 2-position, and the peroxy radical in the 3-position. Analogously, the photolysis of KETL (reaction 63) results in RO₂5 and a 2-carbon acyl radical, RO₂8. Because RO₂8 is formed in so many reactions in CACM, it is treated as a fully integrated species. RO₂7 follows the reaction patterns (reactions 130-132) discussed earlier for alkyl peroxy radicals with carbonyls in the α -position. The resulting products include NO₂ (for the NO reaction only), ALD2, and RO₂8. RO₂8 follows the reaction patterns (reactions 133-137) discussed earlier for acyl peroxy radicals. The resulting products include NO₂ (for the NO reaction only), CO₂, RO₂1, and peroxy acetyl nitrate (PAN2). Similarly, 2-heptanone represents KETH. Photolysis of KETH (reaction 71) also yields RO₂5 and RO₂8. Oxidation of KETH by OH (reaction 70) results in the formation of RO₂16, 2-keto-3-heptyl peroxy radical. Further reactions of RO₂16 (reactions 164-166) also result in NO₂, ALD2, and RO₂8. Because the final products formed by KETL and KETH are similar, separating them into two groups is based solely on kinetics.

5.3.5 Alcohols

Alcohols have both anthropogenic and biogenic sources [*Harley et al.*, 1992; *Goldan et al.*, 1993; *Sharkey*, 1996]. Hydroxyl groups, which characterize alcohols, are also present in multi-functional secondary organic oxidation products [*Yu et al.*, 1999].

Methanol (MEOH) and ethanol (ETOH) have well understood atmospheric chemistry [*Atkinson*, 1994]. Degradation of these compounds proceeds via OH abstraction of an H-atom from either a C-H or O-H bond. For MEOH (reaction 48), the resulting intermediates react instantaneously with O₂ to form HCHO and HO₂. For

ETOH (reaction 53), the split between C-H and O-H abstraction is determined from the rate constants of each pathway [Kwok and Atkinson, 1995]. If the H-atom is abstracted from an O-H bond, the resulting intermediate immediately reacts with O₂ to form ALD2 and HO₂. If the H-atom is abstracted from a C-H bond, the result is either ALD2 or RO₂ depending on the location of the abstraction. 2-Hexanol represents alcohols with three or more carbon (ALCH). Abstraction by OH of an H-atom from the carbon chain is expected to be the dominant sink for ALCH (reaction 69). The resulting radical is RO₂2.

5.3.6 MTBE

Because methyl-*tert*-butyl ether (MTBE) is a constituent of reformulated gasoline sold in the region during the period of interest, it is the only ether explicitly tracked in CACM. (Others are included in ALKL or ALKM as in *Stockwell et al.* [1997].) Reaction of MTBE with OH (reaction 68) proceeds via H-atom abstraction and forms RO₂15. RO₂15 reacts with NO, HO₂, or RO₂T (reactions 161-163) to form ALD2, ALKL, KETL, and HCHO in yields described in Table 5.2 and based on the work of *Japar et al.* [1990] and the estimates of *Harley et al.* [1993].

5.3.7 Aromatics

Aromatic species comprise a significant portion of motor vehicle emissions [*Harley et al.*, 1992] and have been identified as the most likely class of anthropogenic precursors that are important with respect to SOA formation [*Odum et al.*, 1996, 1997]. Aromatics are found in relatively high concentrations in the urban atmosphere [*Fraser et al.*, 1999] and come from a variety of sources [*Schauer, 1998; Schauer et al., 1999ab*].

Aromatic species are aggregated depending on their reactivity, their degree and nature of substitution, and their potential for SOA formation, as determined by *Odum et al.* [1996, 1997]. Low yield aromatics (AROL, represented by 1,2,3-trimethylbenzene) are those with two or more methyl side groups and no functional side groups (such as phenols, aldehydes, acids, or nitro groups); high yield aromatics (AROH, represented by 3-*n*-propyl-toluene) have one or fewer methyl side groups and no functional side groups. Phenolic species (AROO, represented by 2,6-dimethyl-phenol) may have one or more alkyl side groups and one or more phenolic substituents. Aldehydic aromatics (ARAL, represented by *p*-tolualdehyde) have one aldehydic functional group; acidic aromatics (ARAC, represented by *p*-toluic acid) have one carboxylic functional group. Gas-phase polycyclic aromatic hydrocarbons (PAHs, represented by 1,2-dimethyl-naphthalene) have multiple aromatic rings. Generally, only PAHs with two aromatic rings remain in the gas-phase; those with more partition between the gas- and aerosol-phases [*Fraser et al.*, 1999].

5.3.7.1 Low Yield Aromatics

AROL chemistry is initiated by reaction with OH (reaction 79), which can occur either by addition to the aromatic ring (to form a phenolic product, AROO, or a cyclohexadienyl radical, RAD3) or abstraction of an H-atom from a methyl group (to form RO₂21). The yields of these products are described in Table 5.2 and are derived from *Atkinson* [1990, 1994]. Like other organic peroxy radicals, RO₂21 reacts with NO (reaction 179) to form a methyl nitrooxy substituted aromatic (AP4) or NO₂ and an aldehydic aromatic product (ARAL). Upon OH oxidation (reaction 353), AP4 is assumed to form ARAL as well. The reactions of RO₂21 with HO₂ and RO₂T (reactions

180 and 181) also lead to the formation of ARAL. RAD3 can react either with NO_2 (reaction 105) to form nitro-trimethylbenzene (UR12) or predominantly with O_2 (reaction 98) to form a cyclohexadienyl peroxy radical (RO₂34). RO₂34 can then isomerize (reaction 228) to form a bicyclic peroxy radical (RO₂43) or react with NO, HO_2 , and RO₂T (reactions 229-231) [Klotz *et al.*, 1997]. If RO₂34 reacts, as opposed to isomerizes, the dominant product is represented by 4,5-dimethyl-6-keto-2,4-heptadienal, RP11. RO₂43 can also react with NO, HO_2 , and RO₂T (reactions 232-234) to form ring cleavage products such as methyl glyoxal (MGLY). The remaining unreactive ring cleavage products in this second pathway do not contribute to SOA formation so they are grouped together for all aromatic parents except PAH. They are represented by 2-methylbutenalic acid, RP10. In an effort to account for acid formation in aromatic oxidation (and the subsequent formation of SOA), RP11 reacts with OH (reaction 334) to form directly the corresponding acid (UR26) and O_3 with the loss of HO_2 (as in the acyl radical reaction mechanism described in detail above), instead of undergoing the full range of aldehyde reactions. RP10 can either react with OH (reaction 332) to form the corresponding anhydride (UR24) or photolyze (reaction 333) to form the corresponding furan (UR25). MGLY is modeled to behave as an aldehyde, and follows the reaction pattern described earlier. Photolysis of MGLY (reaction 265) leads to formation of RO₂8, CO, and HO_2 while H-atom abstraction by OH (reaction 263) or NO_3 (reaction 264) leads to RO₂48, a 3-carbon, keto-acyl radical. RO₂48 follows the acyl radical reaction pattern described above and forms NO_2 (NO reaction only), CO_2 , and RO₂8 upon reaction with NO (reaction 266) or RO₂T (reaction 270). Upon reaction with NO_2 (reaction 267), RO₂48 forms keto-peroxy-propionyl nitrate (PAN4), which thermally

decomposes (reaction 268). The reaction between RO₂48 and HO₂ (reaction 269) forms keto-propanoic acid (UR21), which is considered capable of forming SOA because of its solubility in the aqueous phase. The chemistry of AROL is shown in Figure 5.1.

5.3.7.2 High Yield Aromatics

OH also initiates AROH oxidation (reaction 80). However, because of the degree of substitution, only ring addition is taken into account [Atkinson, 1994]. The products of this first step are AROO, HO₂, and a cyclohexadienyl (RAD4) radical similar to that formed in AROL oxidation. Yields are given in Table 5.2. Upon reaction with NO₂ (reaction 106), RAD4 forms the nitro-form of AROH (UR13). However, RAD4 predominantly reacts with O₂ (reaction 99) to form RO₂35, another cyclohexadienyl peroxy radical. RO₂35 can isomerize (reaction 235) to form RO₂44 or can react with NO, HO₂, or RO₂T (reactions 236-238) to form primarily RP11. RO₂44 reacts with NO, HO₂, or RO₂T (reactions 239-241) to form MGLY and RP10. The yield of the ring fragmentation products and kinetics are the only differences between the chemistry of AROL and AROH.

5.3.7.3 Phenolic Species

In contrast to AROL and AROH, both NO₃ and OH can initiate oxidation of AROO. NO₃ abstracts the H-atom from the phenolic functional group (reaction 72) to form RAD1, a dimethyl-benzoxy radical. In an effort to account for observed concentrations of nitro-phenols [Fraser *et al.*, 1999], it is assumed that RAD1 reacts only with NO₂ (reaction 103) to form dimethyl-nitro-phenol (RPR4). OH oxidation of AROO (reaction 73) proceeds via side chain abstraction (RO₂17) or addition to the ring to reform

AROO or another cyclohexadienyl radical (RAD2). Yields for this reaction are presented in Table 5.2. RO₂17 reacts similarly to other organic peroxy radicals with the primary products including a nitrooxy derivative of AROO (AP1) and NO₂ from the reaction of NO. Reaction with NO, HO₂, and RO₂T (reactions 167-169) lead to formation of hydroxy-tolualdehyde (RPR2). As before, RAD2 reacts predominantly with O₂ (reaction 97) to form a cyclohexadienyl peroxy radical (RO₂33) or can react with NO₂ (reaction 104) to form RPR4. RO₂33 can isomerize to RO₂42 (reaction 221) or can react with NO, HO₂, or RO₂T (reactions 222-224) to form primarily 4-hydroxy-3,5-dimethyl-2,4-hexadienial, RPR9. RO₂42 will react (reactions 225-227) to yield MGLY and RP10. Upon oxidation (reaction 350), AP1 will yield RPR2. Similarly to RP11, RPR2 reacts with OH (reaction 308) to form directly the corresponding acid (UR2) and O₃ with the loss of HO₂. RPR9 also forms directly the corresponding acid (RP17) (reaction 331), which further reacts to form the corresponding diacid (UR29) (reaction 347).

5.3.7.4 Aromatic Aldehydes

The degradation of ARAL by NO₃ (reaction 81) proceeds via abstraction of the aldehydic H-atom, resulting in the formation of HNO₃. In an effort to account for ambient concentrations of aromatic acids [Rogge *et al.*, 1993; Fraser *et al.*, 1999], it is assumed that the resulting acyl radical immediately reacts with HO₂ to form the corresponding aromatic acid (ARAC) and O₃. Degradation of ARAL by OH (reaction 82) can proceed via three distinct pathways: abstraction of the H-atom from the aldehyde group, abstraction of an H-atom from the methyl side group, or ring addition. The split between these is determined kinetically assuming that OH adds directly to the ring to form a phenolic compound in the same yield as discussed previously. As with the NO₃

reaction, abstraction of the aldehydic H-atom leads directly to acid formation.

Abstraction of an H-atom from the methyl group leads to the formation of RO₂22 which can proceed to react with NO, RO₂T, and HO₂ (reactions 182-184) and form primarily an aromatic compound with either one aldehyde and one nitrooxy-methyl side chain (AP5) or two substituent aldehyde side groups (RPR6). Upon oxidation (reaction 354), AP5 is converted to RPR6. Again in an effort to account for ambient formation of aromatic acids and diacids [Rogge *et al.*, 1993; Fraser *et al.*, 1999], the aldehyde groups of RPR6 are converted directly to acids with formation of O₃ and loss of HO₂ (reactions 320 and 321). RPR7 describes an aromatic ring with one aldehyde and one acid substituent group. ADAC describes the aromatic species with two acid groups. (The UR*i* notation is not used with ADAC, as aromatic diacids are also constituents of primary aerosol.) As with the other aromatic species discussed so far, addition of OH to the aromatic ring in ARAL results in the formation of a cyclohexadienyl radical, RAD5. As before, RAD5 can react with NO₂ (reaction 107) to form the corresponding nitro-tolualdehyde (RPR5) or with O₂ (reaction 100) to form the cyclohexadienyl peroxy radical, RO₂36. The aldehyde group of RPR5 can be converted directly to the acid (reaction 319) to form methyl-nitro-benzoic acid (UR14). Similar to the radicals formed from other aromatic species, RO₂36 can isomerize (reaction 242) to RO₂45 or undergo reaction with NO, RO₂T, and HO₂ (reactions 243-245) to form 2-methyl-5-formyl-2,4-hexadienial, RP12. RO₂45 reacts (reactions 246-248) to form MGLY and RP10. The three aldehyde groups of RP12 subsequently can be converted directly to acids forming, in order, RP13, RP18, and UR30 (reactions 335, 336, and 348).

5.3.7.5 Aromatic Acids

Because the carboxylic acid moieties in CACM are considered unreactive, the degradation of ARAC is driven by reaction with OH (reaction 83) via either side chain H-atom extraction (RO₂23) or addition to the ring (UR2 or RAD6). Reactions of RO₂23 (reactions 185-187) yield either the methyl-nitrooxy derivative (AP6) or RPR7. When oxidized by OH (reaction 355), AP6 yields RPR7. Similar to other cyclohexadienyl radicals, RAD6 reacts predominantly with O₂ (reaction 101) to form the corresponding cyclohexadienyl peroxy radical (RO₂37) but can also react with NO₂ (reaction 108) to form the nitro derivative of ARAC (UR14). Isomerization of RO₂37 (reaction 249) leads to the formation of RO₂46, which reacts (reactions 253-255) to form RP10 and MGLY. Reaction of RO₂37 (reactions 250-252) leads to the formation of RP13.

5.3.7.6 Polycyclic Aromatic Hydrocarbons

The final lumped aromatic compound considered in CACM is PAH. The sink for PAH is reaction with OH (reaction 92), which can lead to RO₂31 (H-atom abstraction from the side chain), UR11 (hydroxy-PAH), or an aromatic cyclohexadienyl radical (RAD7) similar to those formed by monoaromatic compounds. RO₂31 reacts (reactions 212-214) as before to form the methyl-nitrooxy derivative (AP10) and the aldehyde derivative (UR19). AP10 forms UR19 upon oxidation by OH (reaction 359). RAD7 reacts with O₂ (reaction 102) to form RO₂38 or with NO₂ (reaction 109) to form nitro-PAH (UR15). RO₂38 can isomerize (reaction 256) to RO₂47 or react (reactions 257-259) to form 2-(dimethyl propenal)-benzaldehyde (RP14). The aldehyde groups in RP14 can be converted successively to acids, RP19 and UR31 (reactions 337 and 349). The

reactions of RO₂47 (reactions 260-262) lead to MGLY and 2-formyl-acetophenone (RP15). The aldehyde group in RP15 can be converted to acid (reaction 338) resulting in the formation of 2-carboxy-acetophenone (UR27).

5.3.8 Biogenics

Biogenic organics play an important role in atmospheric chemistry [*Lamb et al.*, 1993; *Guenther et al.*, 1995]. (In the SOCAB, anthropogenic emissions of organic carbon are expected to be approximately an order of magnitude greater than those from biogenic sources [*Benjamin et al.*, 1997].) Isoprene (ISOP) and the monoterpenes are considered in CACM; sesquiterpenes are ignored because of their low emission rate relative to those of isoprene and the monoterpenes and since little is known about their oxidation patterns.

5.3.8.1 Isoprene

Because its structure (2-methyl-1,3-butadiene, C₅H₈) is unique compared to other biogenic species, ISOP is treated explicitly in CACM. The atmospheric behavior of isoprene has been studied in detail [*Paulson et al.*, 1992ab; *Yu et al.*, 1995; *Kwok et al.*, 1995]. ISOP does not contribute significantly to SOA formation [*Pandis et al.*, 1992]. Like other unsaturated molecules, ISOP is oxidized by OH, NO₃, O₃, and O(³P) (reactions 64-67). The mechanism in CACM assumes that OH and NO₃ addition to the double bonds occurs only at the two most probable spots, as determined by the stability of the resulting radicals [*Atkinson, 1997*]. The split between these locations is determined kinetically. The most preferred OH attack occurs first (approximately 2/3) in the 1-position and second (approximately 1/3) in the 4-position, resulting in a tertiary

peroxy radical, RO₂9, and a secondary peroxy radical, RO₂10, respectively. The reactions of RO₂9 (reactions 138-140) are assumed to result in the formation of methyl-vinyl-ketone (MVK), HCHO, HO₂, and NO₂ (NO₂ in the NO case only). Correspondingly, the reactions of RO₂10 (reactions 141-143) result in the formation of methacrolein (MCR), HCHO, HO₂, and NO₂ (NO₂ in the NO case only). The NO₃ oxidation pattern is analogous, with RO₂11 and RO₂12 having a nitrooxy group instead of an OH group. Upon reaction (reactions 144-146), RO₂11 liberates NO₂ and forms MVK, HCHO, HO₂, and NO₂. Similarly, RO₂12 reactions (reaction 147-149) liberate NO₂ and form MCR, HCHO, HO₂, and NO₂. The ISOP-O₃ reaction forms MVK, MCR, HCHO, OLEL (a reclassified small product), CO₂, ACID, CO, OH, HO₂, RO₂13, and RO₂14 in yields shown in Table 5.2 and derived from *Jenkin et al.* [1997]. RO₂13 is a 4-carbon, unsaturated peroxy radical with a keto group; the unsaturated bond is in the 1-position, the keto group is in the 3-position, and the peroxy radical is in the 4-position. The reactions of RO₂13 (reactions 150-152) lead to HCHO and a 3-carbon, unsaturated acyl radical (RO₂39); NO₂ is also formed in the NO reaction. RO₂39 follows the previously discussed reaction pattern for acyl radicals and results in the formation of RO₂14 and CO₂ (NO and RO₂T reactions; reactions 153 and 157), an unsaturated peroxy nitrate compound, PAN3 (NO₂ reaction; reaction 154), which thermally decomposes (reaction 155), and OLEL, ACID, and O₃ (HO₂ reaction; reaction 156). RO₂14 is a 2-carbon, unsaturated peroxy radical that is converted to OLEL or RO₂7 upon reaction (reactions 158-160). The ISOP-O(³P) reaction yields OLEL (reclassified) and ALD2 in yields shown in Table 5.2 and derived from *Atkinson* [1997].

MCR and MVK are major oxidation products of ISOP, and their chemistry is described explicitly in CACM. MVK reacts with OH, O₃, and O(³P) (reactions 271-273); the NO₃ reaction is not considered because of its comparatively small rate constant [Carter, 1999]. OH reaction leads to the formation of RO₂49, a 4-carbon, 2-keto, 3-peroxy, 4-hydroxy radical. Reactions of RO₂49 (reactions 274-276) lead to MGLY, HCHO, and HO₂ (and NO₂ in the NO reaction). The MVK-O₃ reaction results in the formation of MGLY, HCHO, ACID, UR21, ALD2, CO, CO₂, HO₂, OH, water, and RO₂8 in yields shown in Table 5.2 and derived from *Jenkin et al.* [1997]. Reaction between MVK and O(³P) leads to KETL (reclassified), RO₂4, and RO₂8 in yields shown in Table 5.2 and derived from *Atkinson* [1997]. MCR can also react with OH, NO₃, O₃, and O(³P) (reactions 277-280). The OH and NO₃ reactions can proceed via addition to the double bond (RO₂51 and RO₂52 respectively) or via H-atom abstraction from the aldehyde group (RO₂50). RO₂50 behaves similarly to the acyl radicals that have been described previously (reactions 281-285). Products include NO₂, CO₂, and RO₂14 (NO or RO₂T reaction), PAN5 (NO₂ reactions), and ACID and OLEL (HO₂ reaction). Similarly to RO₂49, RO₂51 and RO₂52 (reactions 286-288 and 289-291 respectively) lead to the formation of HCHO and MGLY. Reaction between MCR and O₃ leads to HCHO, MGLY, OH, CO, HO₂, ACID, and RO₂53 as shown in Table 5.2 with yields derived from *Jenkin et al.* [1997]. RO₂53 is a primary, 3-carbon, dicarbonyl peroxy radical. Its reactions (reactions 292-294) lead to the formation of RO₂54, an aldehydic, 2-carbon acyl radical. RO₂54 follows the reactions characteristic of acyl radicals (reactions 295-299). Products include NO₂, CO₂, CO, and HO₂ (NO and RO₂T reactions), glyoxalic acid (RP16; HO₂ reaction), and the corresponding peroxy nitrate compound (PAN6).

Degradation of RP16 proceeds via photolysis (reaction 341) which leads to OH, HO₂, and CO or abstraction of the aldehydic H-atom by OH or NO₃ (reactions 339 and 340, respectively). The abstraction pathway leads to the formation of the corresponding acyl radical (RO₂58). As before, RO₂58 will react with NO, NO₂, HO₂, or RO₂T (reactions 342-346) to form products that include NO₂, CO₂, CO, OH, the corresponding peroxy nitrate species (PN10), and the corresponding acid (oxalic acid, UR28).

5.3.8.2 Monoterpenes

Despite evidence that monoterpenes are not easily aggregated according to SOA formation potentials [Griffin *et al.*, 1999], we lump them in this way in CACM because the uncertainties associated with monoterpene chemistry preclude representation at any greater level of detail. α -Terpineol, which represents relatively low yield monoterpenes (BIOL), encompasses the carbon number, structural characteristics, and reactivity of the group members as well. BIOL is oxidized by OH, NO₃, O₃, and O(³P) (reactions 84-87). OH addition to the double bond leads to RO₂24, a dihydroxy, tertiary peroxy radical (NO₃ addition results in the analogous radical, RO₂25, with NO₃ replacing the hydroxy group in the 2-position). Reaction of NO with RO₂24 (reaction 188) results in the nitrooxy product (AP7) or the keto-aldehyde (2-hydroxy-3-isopropyl-6-keto-heptanal, RPR3) caused by ring cleavage. The reactions between RO₂24 and RO₂T or HO₂ (reactions 189 and 190) also result in RPR3 formation. Upon oxidation (reaction 356), AP7 forms RPR3 as well. The reactions of RO₂25 (reactions 191-193) liberate NO₂ and form RPR3. Oxidation of BIOL by O(³P) is assumed to result in two products (epoxide, UR5, and carbonyl, UR6) in yields estimated from Alvarado *et al.* [1998] and shown in Table 5.2. The attack by O₃ and resulting decomposition result in the formation of UR3,

UR4, CO, RPR3, HO₂, H₂O₂, OH, and RO₂26 in yields shown in Table 5.2 and derived from *Jenkin et al.* [1997]. UR3 and UR4 are the resulting hydroxy-keto-acid and keto-aldehyde respectively. RO₂26 is a trisubstituted (hydroxy group, aldehyde, and ketone) organic peroxy radical. The reactions of RO₂26 (reactions 194-196) lead primarily to the formation of RO₂8 and UR17, a hydroxy dial. Reactions of RPR3 follow the reaction pattern assumed for aldehydes, as it assumed that the aldehyde is the most reactive moiety within RPR3. These reactions (reactions 309-311) result in the formation of the corresponding acyl radical (RO₂56) or UR4. The acyl radical reaction pattern followed by RO₂56 leads to formation of NO₂, CO₂, and UR4 (NO reaction; reaction 312), PAN8 (NO₂ reaction; reaction 313) which thermally decomposes (reaction 314), UR3 and O₃ (HO₂ reaction; reaction 315), or CO₂ and UR4 (RO₂T reaction; reaction 316).

CACM also incorporates a class (BIOH) for those monoterpenes that have relatively high SOA yield parameters [*Griffin et al.*, 1999]. The structure chosen to represent this group is γ -terpinene because of its high reactivity and large SOA formation potential. As with all other unsaturated compounds, BIOH is oxidized by OH, NO₃, O₃, and O(³P) (reactions 88-91). OH addition is assumed to occur so that the peroxy radical is at the most stable possible location. The result is a cyclic, unsaturated, hydroxy peroxy radical (RO₂27). NO₃ oxidation occurs analogously to form the corresponding nitrooxy peroxy radical (RO₂28). Reaction of RO₂27 with NO (reaction 197) results in either the corresponding nitrooxy compound (AP8) or the keto-aldehyde ring cleavage product (UR7). The HO₂ and RO₂T reactions (reactions 198 and 199) also result in the formation of UR7, as do the reactions of RO₂28 (reactions 200-202). The RO₂28 reactions also liberate NO₂. UR7 is also formed by the reaction of AP8 with OH (reaction 357). In the

$O(^3P)$ reaction, UR9 (epoxide) and UR10 (ketone) are formed in yields shown in Table 5.2 and derived from *Alvarado et al.* [1998]. The O_3 -BIOH reaction leads to UR7, UR8, CO, OH, H_2O_2 , RO₂29, and RO₂30 in yields shown in Table 5.2 and derived from *Jenkin et al.* [1997]. UR8 is the corresponding keto-acid ring cleavage product. RO₂29 is a primary peroxy radical with an unsaturated bond and a ketone moiety. Its reactions (reactions 203-205) lead to the appropriate nitrooxy product (AP9) or another peroxy radical (RO₂40). RO₂40 is formed by isomerization and exhibits an unsaturated carbon-carbon bond, a hydroxy group, a ketone, and the peroxy radical in a secondary position. Upon oxidation (reaction 358), AP9 yields the corresponding unsaturated keto-aldehyde (UR33). The reactions of RO₂40 (reactions 206-208) lead to decomposition and the formation of RO₂8 and an unsaturated hydroxy aldehyde (RPR8). The corresponding reactions of RO₂30 (reactions 209-211), which exhibits an unsaturated bond, a ketone group, and an aldehyde, lead to the formation of UR18 (an unsaturated dial). Two photolysis pathways (reactions 324 and 325) are given for RPR8, one in which CO, HO_2 , and RO₂9 are formed and another in which the corresponding acyl radical, RO₂57, is formed. (This is due to the α -position of the aldehyde relative to the unsaturated bond.) RO₂57 is also formed by the OH and NO_3 abstraction of the aldehydic H-atom from RPR8 (reactions 322 and 323 respectively). Following the behavior of other acyl radicals (in reactions 326-330), RO₂57 leads to RO₂9, CO₂, and NO_2 (NO reaction), the corresponding peroxy nitrate compound, PAN9 (NO₂ reaction), the corresponding acid (UR23) and O_3 (HO_2 reaction), and CO₂ and RO₂9 (RO₂T reaction).

5.4 Gas-Phase Simulation of the SCAQS Episode of August 27-29, 1987 in the SOCAB

Up to this point we have presented a chemical mechanism for urban/regional atmospheric chemistry of ozone and SOA precursors. In its ozone formation chemistry, the mechanism builds upon previous work of *Stockwell et al.* [1997], *Jenkin et al.* [1997], and *Carter* [1997,1999]. The mechanism is intended for use in three-dimensional urban/regional atmospheric models, where both ozone formation and SOA production are to be predicted. As a prelude to these comprehensive simulations, it is of importance to establish the performance of the mechanism in ozone prediction, to ensure that that performance is consistent with the current state-of-the-art in ozone simulation. Consequently, we present here a simulation of gas-phase chemistry in the SOCAB of California. We will evaluate ozone predictions of the new mechanism against both observed data and the earlier simulations of *Harley et al.* [1993]. The CIT model will be used as the basic three-dimensional model [*Harley et al.*, 1993; *Meng et al.*, 1998]. The CIT model conforms with the latest three-dimensional model structure, such as that embodied in the U.S. Environmental Protection Agency's Models 3 [*United States Environmental Protection Agency*, 1999], so modules presented in the present series of papers can be used in that framework as well.

5.4.1 August 27-29, 1987 SCAQS Episode

During the summer and fall of 1987, an intensive monitoring program known as the Southern California Air Quality Study (SCAQS) took place in the SOCAB [Lawson, 1990], which is shown graphically in Figure 5.2. The meteorological and air quality measurements made during this program provide a detailed ambient data set that has been

used a number of times to evaluate atmospheric models. Previous simulations of the episode of August 27-29, 1987 include those of *Harley et al.* [1993], *Harley and Cass* [1995], *Jacobson et al.* [1996], and *Meng et al.* [1998]. We will consider this episode as well. *Harley et al.* [1993] give emissions and boundary and initial conditions information for this episode. Therefore, only summary tables need be given here. Table 5.7 shows a highly aggregated emissions profile for one of the days simulated, and Table 5.8 gives the upwind boundary conditions. *Harley et al.* [1993] also describe the deposition module and meteorology used in CIT.

5.4.2 Ozone Simulation

Predicted (solid) mixing ratios of O_3 (green), NO (blue), and NO_2 (red) in Pasadena and Riverside are compared to data observed (dashed) at those locations in Figures 5.3 and 5.4, respectively. For Pasadena it is seen that O_3 is underpredicted on each day and that NO_2 is both under- and overpredicted depending on the time of day. NO simulations match observed data reasonably well except on the third day, when NO is significantly overpredicted at rush hour times (even though the third day is a Saturday). In Riverside, O_3 is underpredicted on the first day and matched well on the second and third days. Peak NO is underpredicted, but NO is slightly over predicted at night. NO_2 is generally overpredicted. These trends typify locations throughout the SOCAB. Pasadena and Riverside are chosen because they are downwind of major emissions sites and, thus, represent locations that are expected to display secondary species in higher concentrations.

A statistical analysis of simulated results versus observed data has been performed for NO_2 and O_3 (Table 5.9). Statistics considered include bias, normalized

bias, standard deviation, gross error, and normalized gross error. The methodology for these calculations is described in *Harley et al.* [1993]. It is seen that these numbers are comparable to those of *Harley et al.* [1993] and, moreover, are typical of the level of agreement achieved in current three-dimensional modeling studies [*Harley and Cass*, 1995; *Jacobson et al.*, 1996; *Meng et al.*, 1998]. CACM predictions (solid) compared to those of *Harley et al.* [1993] (x) are shown for Pasadena and Riverside in Figures 5.5 and 5.6, respectively (using the same color scheme as Figures 5.3 and 5.4). In each case, O_3 and NO_2 CACM predictions usually exceed those from *Harley et al.* [1993]. Correspondingly, NO predictions are generally lower. Since the emissions, meteorology, and model structure are identical to those of *Harley et al.* [1993], the differences seen in Figures 5.5 and 5.6 can be ascribed solely to changes in the chemical mechanism.

5.4.3 Total Semi-volatile Species

A principal goal of CACM is to predict concentrations of those surrogate organic products that have the potential to partition to the aerosol phase. Based on known or estimated vapor pressures or solubility, a product is considered to have the potential to partition to the aerosol phase if it meets one or more of the following criteria: (1) it is known to be partially soluble; (2) it is an aromatic acid; (3) it is an aromatic with two functional groups that are not aldehydes; (4) it has 12 or more carbon atoms (excluding primary gas-phase emission of ALKH and PAH); (5) it has at least 10 carbons and two functional groups; (6) it has at least 6 carbon atoms and two functional groups, one of which is an acid; or (7) it is trifunctional. The products considered capable of forming SOA based on these criteria are marked with a plus sign in Table 5.1. The total concentration of those products in the base case (solid) is compared in Figure 5.7 to

observed concentrations of SOA (x) for August 28, 1987 in Claremont [*Turpin and Huntzicker, 1995*]. Figure 5.7 shows that the predicted temporal behavior of the total mass available to partition to SOA tracks well the pattern observed for SOA in the ambient. Figure 5.7 also shows that the base case predictions result in sufficient mass to account for the observed SOA concentrations.

Reliable techniques for estimating/measuring ambient concentrations of SOA lag behind those for inorganic aerosol. Therefore, it must be noted that observed SOA data do have associated uncertainties. The data of *Turpin and Huntzicker [1995]* presented here were generated by a technique that delineates organic carbon (OC) and elemental carbon (EC) aerosol concentrations under conditions when production of SOA should be low. The assumption made with this technique is that EC and primary OC have the same sources, so that a representative ratio of primary OC to EC for a given region exists. In order to determine this ratio, ambient measurements of the OC/EC ratio are made on days when photochemical activity is expected to be low or an average ratio is obtained by determining the ratio at individual emissions sites. Subsequent ambient measurements are then made during times when photochemical activity is expected to occur, and it is assumed that if the ambient value of OC/EC is greater than the characteristic primary OC/EC value, the excess OC consists of SOA [*Turpin and Huntzicker, 1995*]. The main advantage of this approach is its simplicity; however, there are associated problems. First, the primary OC/EC ratio varies from source to source and may be dependent on factors such as meteorology, time of day, and season. It must also be noted that obtaining an average primary OC/EC ratio is a difficult task because of problems associated with sampling of semi-volatile organics, and it has been shown that different sample collection

and analysis techniques result in different values for this ratio at the same location and time [McMurtry, 1989; Turpin and Huntzicker, 1995]. Finally, even on days when there is little potential for photochemical activity, previously formed SOA may be present because it has remained in the region from prior days.

5.4.4 Uncertainty Analysis

Historically, when conducting three-dimensional urban/regional atmospheric simulations, the largest uncertainties are those associated with the emissions inventory. From a chemical mechanism perspective, uncertainty lies in the rate constants, the product yields, and the mechanisms of degradation of second-, third-, and further generation products. These issues have been discussed in detail previously [Harley *et al.*, 1993; Jacobson *et al.*, 1996; Stockwell *et al.*, 1997]. While there are a number of areas of uncertainty in the chemical mechanism that one might select for analysis, space does not permit a lengthy analysis of such uncertainties, especially with regard to ozone formation. However, it is informative to investigate aspects of the chemical mechanism to which prediction of semi-volatile products might be especially sensitive. Because aromatics are known to be an important source of anthropogenic SOA [Odum *et al.*, 1996] and because uncertainties in aromatic chemistry have been well documented [Atkinson, 1994], an issue is the sensitivity of SOA predicted from aromatic precursors to key aspects of aromatic photooxidation. One particular rate constant that has the potential to be especially influential is that which describes the isomerization of radicals formed in aromatic-OH chemistry (reactions 221, 228, 235, 242, 249, and 256) [Lay *et al.*, 1996]. This rate constant affects SOA formation because slower isomerization will lead to less MGLY and RP10 formation and more formation of semi-volatile products. Because

earlier models generally underpredicted organic aerosol [Meng *et al.*, 1997, 1998], we consider only the effect of halving the isomerization rate constant in an uncertainty analysis. Changes between the two cases are very small for NO, NO₂, and O₃. General trends are a slight decrease in O₃, a slight increase in NO, and mixed results for NO₂. Figure 5.7 also compares the total amount of organic material available to partition to SOA in Claremont on August 28, 1987 in the base case (solid) and that in which the bridging rate constant is halved (b/2 case, +). It is seen that decreasing the bridging rate constant results in a significant increase in the amount of organic mass with the potential to form SOA, especially in the early morning and early afternoon.

A second source of uncertainty in the chemical mechanism is the direct conversion of aldehydes to acid groups in certain reactive products. Although the exact mechanism of this conversion remains elusive, such a step attempts to account for observed ambient concentrations of semi-volatile organic acids [Rogge *et al.*, 1993; Nolte *et al.*, 1999]. Since assuming 100% conversion certainly overestimates the acid formation, this yield is also halved (reactions 81, 82, 308, 319, 320, 321, 331, 336, 337, 338, 347, 348, and 349). Figure 5.7 also shows the results for this scenario (acid case, dashed) for August 28, 1987 in Claremont. While there are essentially no changes in the simulations for O₃ and NO_x in this case, predictions of total SOA material are seen to decrease as expected. However, the magnitude of these changes is not as large as that of the b/2 case (+). Figure 5.8 shows the percentage of the total SOA precursor concentration that must partition to account for the observations of *Turpin and Huntzicker* [1995] in the base case (solid), the b/2 case (+), and the acid case (dashed). It

is seen that in each case, sufficient concentrations of SOA precursor material are predicted to account for the observations of *Turpin and Huntzicker* [1995].

5.5 Conclusions

Previous gas-phase mechanisms describing urban/regional atmospheric chemistry have focused primarily on describing the formation of ozone with reduced attention to organic chemistry beyond the initial consumption of the parent organic. This paper describes a new chemical mechanism, the Caltech Atmospheric Chemistry Mechanism (CACM), that describes explicitly organic chemistry in an effort to predict the concentrations of secondary and tertiary organic oxidation products that can act as constituents of secondary organic aerosol. Parent organics in CACM must be aggregated into lumped surrogate structures. In total, CACM includes 191 species: 120 fully integrated species (15 inorganic, 71 reactive organic, and 34 unreactive organic), 67 pseudo-steady state species (2 inorganic and 65 organic), and 4 species that have concentrations that do not change because of reaction. These species participate in over 360 reactions.

CACM has been used to predict gas-phase concentrations in the South Coast Air Basin of California for August 27-29, 1987. As part of the Southern California Air Quality Study, ambient measurements were taken during these dates, providing data to which the model results can be compared. As shown in this paper, the mixing ratios of O₃, NO, and NO₂ predicted by CACM are statistically comparable to those predicted by the extended mechanism of *Lurmann et al.* [1987], which has been used in the California Institute of Technology three-dimensional air quality model previously [*Harley et al.*, 1993]. In addition, CACM predicts secondary and tertiary organic oxidation products.

Concentrations of those products capable of forming secondary organic aerosol will be passed to a model designed to predict equilibrium gas-aerosol partitioning of organic oxidation products (Part II). The development of CACM is a first step in allowing for more rigorous treatment of secondary organic aerosol formation in atmospheric models than has been possible previously.

5.6 References

Alvarado, A., E.C. Tuazon, S.M. Aschmann, R. Atkinson, and J. Arey, Products of the gas-phase reactions of O(³P) atoms and O₃ with α -pinene and 1,2-dimethyl-1-cyclohexene, *J. Geophys. Res.*, 103, 25,541-25,552, 1998.

Atkinson, R., Gas-phase tropospheric chemistry of volatile organic compounds: 1. Alkanes and alkenes, *J. Phys. Chem. Ref. Data*, 26, 215-290, 1997.

Atkinson, R., Gas-phase tropospheric chemistry of organic compounds, *J. Phys. Chem Ref. Data, Monograph 2*, 1994.

Atkinson, R., Gas-phase tropospheric chemistry of organic compounds: a review, *Atmos. Environ.*, 24A, 1-41, 1990.

Barthelmie, R.J., and S.C. Pryor, A model mechanism to describe oxidation of monoterpenes leading to secondary organic aerosol, *J. Geophys. Res.*, 104, 23,657-23,669, 1999.

Benjamin, M.T., M. Sudol, D. Vorsatz, and A.M. Winer, A spatially and temporally resolved biogenic hydrocarbon emissions inventory for the California South Coast Air Basin, *Atmos. Environ.*, 31, 3087-3100, 1997.

Carter, W.P.L., SAPRC-99, available via ftp (<http://helium.ucr.edu/~carter/>), 1999.

Carter, W.P.L., SAPRC-97, available via ftp (<http://helium.ucr.edu/~carter/>), 1997.

Carter, W.P.L., and R. Atkinson, Alkyl nitrate formation from the atmospheric photooxidation of alkanes: a revised estimation method, *J. Atmos. Chem.*, 8, 165-173, 1989.

Dransfield, T.J., K.K. Perkins, N. M. Donahue, J.G. Anderson, M.M. Sprengnether, and K.L. Demerjian, Temperature and pressure dependent kinetics of the gas-phase reaction of the hydroxyl radical with nitrogen dioxide, *Geophys. Res. Letters*, 26, 687-690, 1999.

Fraser, M.P., G.R. Cass, and B.R.T. Simoneit, Particulate organic compounds emitted from motor vehicle exhaust and in the urban atmosphere, *Atmos. Environ.*, 33, 2715-2724, 1999.

Fraser, M.P., G.R. Cass, B.R.T. Simoneit, and R.A. Rasmussen, Air quality model evaluation data for organics 4. C₂-C₃₆ aromatic hydrocarbons, *Environ. Sci. Technol.*, 31, 2356-2367, 1997.

Gery, M.W., G.Z. Whitten, J.P. Killus, and M.C. Dodge, A photochemical mechanism for urban and regional scale computer modeling, *J. Geophys. Res.*, 94, 12,925-12,956, 1989.

Goldan, P.D., W.C. Kuster, F.C. Fehsenfeld, and S.A. Montzka, The observation of a C₅ alcohol emission in a North American pine forest, *Geophys. Res. Lett.*, 20, 1039-1042, 1993.

Goumri, A., L. Elmaimouni, J.-P. Sawyersyn, and P. Devolder, Reaction rates at (297 +/- 3)K of four benzyl-type radicals with O₂, NO, and NO₂ by discharge flow/laser induced fluorescence, *J. Phys. Chem.*, 96, 5395-5400, 1992.

Griffin, R.J., D.R. Cocker III, R.C. Flagan, and J.H. Seinfeld, Organic aerosol formation from the oxidation of biogenic hydrocarbons, *J. Geophys. Res.*, 104, 3555-3567, 1999.

Grosjean, E., D. Grosjean, M.P. Fraser, and G.R. Cass, Air quality model evaluation data for organics 2. C₁-C₁₄ carbonyls in Los Angeles, *Environ. Sci. Technol.*, 30, 2687-2703, 1996.

Guenther, A., et al., A global model of natural volatile organic compound emissions, *J. Geophys. Res.*, 100, 8873-8892, 1995.

Harley, R.A., and G.R. Cass, Modeling the atmospheric concentrations of individual volatile organic compounds, *Atmos. Environ.*, 29, 905-922, 1995.

Harley, R.A., A.G. Russell, G.J. McRae, G.R. Cass, and J.H. Seinfeld, Photochemical modeling of the Southern California Air Quality Study, *Environ. Sci. Technol.*, 27, 378-388, 1993.

Harley, R.A., M.P. Hannigan, and G.R. Cass, Respeciation of organic gas emissions and the detection of excess unburned gasoline in the atmosphere, *Environ. Sci. Technol.*, 26, 2395-2408, 1992.

Hoffmann, T., J.R. Odum, F. Bowman, D. Collins, D. Klockow, R.C. Flagan, and J.H. Seinfeld, Formation of organic aerosols from the oxidation of biogenic hydrocarbons, *J. Atmos. Chem.*, 26, 189-222, 1997.

Jacob, D.J., and S.C. Wofsy, Photochemistry of biogenic emissions over the Amazon forest, *J. Geophys. Res.*, 93, 1477-1486, 1988.

Jacobson, M.Z., R. Lu, R.P. Turco, and O.B. Toon, Development and application of a new air pollution modeling system 1. Gas-phase simulations, *Atmos. Environ.*, 30, 1939-1963, 1996.

Japar, S.M., T.J. Wallington, J.F.O. Richert, and J.C. Ball, The atmospheric chemistry of oxygenated fuel additives: *tert*-butyl alcohol, dimethyl ether, and methyl-*tert*-butyl ether, *Intl. J. Chem. Kinetics*, 22, 1257-1269, 1990.

Jenkin, M.E., S.M. Saunders, and M.J. Pilling, The tropospheric degradation of volatile organic compounds: a protocol for mechanism development, *Atmos. Environ.*, 31, 81-104, 1997.

Klotz, B., I. Barnes, K.H. Becker, and B.T. Golding, Atmospheric chemistry of benzene oxide/oxepin, *J. Chem. Soc., Faraday Trans.*, 93, 1507-1516, 1997.

Kwok, E.S.C., S.M. Aschmann, J. Arey, and R. Atkinson, Product formation from the reaction of the NO₃ radical with isoprene and rate constants for the reactions of methacrolein and methyl vinyl ketone with the NO₃ radical, *Intl. J. Chem. Kinetics*, 28, 925-934, 1995.

Kwok, E.S.C., and R. Atkinson, Estimation of hydroxyl radical reaction rate constants for gas-phase organic compounds using a structure-reactivity relationship: an update, *Atmos. Environ.*, 29, 1685-1695, 1995.

Lamb, B., D. Gay, H. Westberg, and T. Pierce, A biogenic hydrocarbon emission inventory for the U.S.A. using a simple forest canopy model, *Atmos. Environ.*, 27, 1673-1690, 1993.

Lawson, D.R., The Southern California Air Quality Study, *J. Air Waste Mgmt. Assoc.*, 40, 156-165, 1990.

Lay, T.H., J.W. Bozzelli, and J.H. Seinfeld, Atmospheric photochemical oxidation of benzene: benzene + OH and the benzene-OH adduct (hydroxyl-2,4-cyclohexadienyl) + O₂, *J. Phys. Chem.*, 100, 6543-6554, 1996.

Lurmann, F.W., W.P.L. Carter, and L.A. Coyner, A surrogate species chemical reaction mechanism for urban-scale air quality simulation models. Volumes I and II. Report to the U.S. Environmental Protection Agency under Contract 68-02-4104. ERT, Inc., Newbury Park, CA, and Statewide Air Pollution Research Center, University of California, Riverside, CA, 1987.

McMurry, P.H., Final report to the California Air Resources Board under contract A732-075, 1989.

Meng Z., D. Dabub, and J.H. Seinfeld, Size-resolved and chemically resolved model of atmospheric aerosol dynamics, *J. Geophys. Res.*, 103, 3419-3435, 1998.

Meng, Z., D. Dabub, and J.H. Seinfeld, Chemical coupling between atmospheric ozone and particulate matter, *Science*, 277, 116-119, 1997.

Moortgat, G.K., B. Veyret, and R. Lesclaux, Kinetics of the reaction of HO₂ with CH₃C(O)O₂ in the temperature range 253-368K, *Chem. Phys. Lett.*, 160, 443-447, 1989.

Niki, H., P.D. Maker, C.M. Savage, and L.P. Breitenbach, FTIR study of the kinetics and mechanism of Cl-atom-initiated reactions of acetaldehyde, *J. Phys. Chem.*, 89, 588-591, 1985.

Nolte, C.G., M.P. Fraser, and G.R. Cass, Gas-phase C₂-C₁₀ organic acid concentrations in the Los Angeles atmosphere, *Environ. Sci. Technol.*, 33, 540-545, 1999.

Odum, J.R., T.P.W. Jungkamp, R.J. Griffin, R.C. Flagan, and J.H. Seinfeld, The atmospheric aerosol-forming potential of whole gasoline vapor, *Science*, 276, 96-99, 1997.

Odum, J.R., T. Hoffmann, F. Bowman, D. Collins, R.C. Flagan, and J.H. Seinfeld, Gas/particle partitioning and secondary organic aerosol yields, *Environ. Sci. Technol.*, 30, 2580-2585, 1996.

Pandis S.N., S.E. Paulson, J.H. Seinfeld, and R.C. Flagan, Aerosol formation in the photooxidation of isoprene and β -pinene, *Atmos. Environ.*, 25, 997-1008, 1991.

Paulson, S.E., R.C. Flagan, and J.H. Seinfeld, Atmospheric photooxidation of isoprene: 1. The hydroxyl radical and ground-state atomic oxygen reactions, *Intl. J. Chem. Kinetics*, 24, 79-101, 1992a.

Paulson, S.E., R.C. Flagan, and J.H. Seinfeld, Atmospheric photooxidation of isoprene: 2. The ozone-isoprene reaction, *Intl. J. Chem. Kinetics*, 24, 103-125, 1992b.

Rogge, W.F., M.A. Mazurek, L.M. Hildemann, G.R. Cass, and B.R.T. Simoneit, Quantification of urban organic aerosols at a molecular-level-identification, abundance and seasonal-variation, *Atmos. Environ.*, 27A, 1309-1330, 1993.

Schauer, J.J., M.J. Kleeman, G.R. Cass, and B.R.T. Simoneit, Measurement of emissions from air pollution sources 1. C₁ through C₂₉ organic compounds from meat charbroiling, *Environ. Sci. Technol.*, 33, 1566-1577, 1999a.

Schauer, J.J., M.J. Kleeman, G.R. Cass, and B.R.T. Simoneit, Measurement of emissions from air pollution sources 2. C₁ through C₃₀ organic compounds from medium duty diesel trucks, *Environ. Sci. Technol.*, 33, 1578-1587, 1999b.

Schauer, J.J. *Source Contributions to Atmospheric Organic Compound Concentrations: Emissions, Measurements, and Model Predictions*, Ph.D. Thesis, California Institute of Technology, Pasadena, CA, 1998.

Seinfeld, J.H., and S.N. Pandis, *Atmospheric Chemistry and Physics*, Wiley-Interscience, New York, 1998.

Sharkey, T.D., Emission of low-molecular mass hydrocarbons from plants, *Trends Plant Sci.*, 1, 78-82, 1996.

Stockwell, W.R., F. Kirchner, M. Kuhn, and S. Seefeld, A new mechanism for regional atmospheric chemistry modeling, *J. Geophys. Res.*, 102, 25,847-25,879, 1997.

Stockwell, W.R., P. Middleton, J.S. Chang, and X. Tang, The second generation Regional Acid Deposition Model chemical mechanism for regional air quality modeling, *J. Geophys. Res.*, 95, 16,343-16,367, 1990.

Turpin, B.J., and J.J. Huntzicker, Identification of secondary organic aerosol episodes and quantitation of primary and secondary organic aerosol concentrations during SCAQS, *Atmos. Environ.*, 29, 3527-3544, 1995.

United States Environmental Protection Agency, Web site for Models 3 (<http://www.epa.gov/asmdnerl/models3/index.html>), 1999

Yu, J., D.R. Cocker III, R.J. Griffin, R.C. Flagan, and J.H. Seinfeld, Gas-phase ozone oxidation of monoterpenes: gaseous and particulate products, *J. Atmos. Chem.*, 34, 207-258, 1999.

Yu, J., H.E. Jeffries, and R.M. LeLacheur, Identifying airborne carbonyl-compounds in isoprene atmospheric photooxidation products by their PFBHA oximes using gas-

chromatography ion-trap mass spectrometry, *Environ. Sci. Technol.*, 29, 1923-1932, 1995.

Table 5.1. Chemical species represented in CACM.

Inorganic, Fully Integrated Species			
NO	Nitric oxide	NO ₂	Nitrogen dioxide
O ₃	Ozone	HONO	Nitrous acid
HNO ₃	Nitric acid	HNO ₄	Pernitric acid
N ₂ O ₅	Nitrogen pentoxide	NO ₃	Nitrate radical
HO ₂	Hydroperoxy radical	CO	Carbon monoxide
CO ₂	Carbon dioxide	H ₂ O ₂	Hydrogen peroxide
SO ₂	Sulfur dioxide	SO ₃	Sulfur trioxide
OH	Hydroxyl radical		

Reactive, Fully Integrated Parent Organic Species (* denotes those that are also formed in CACM)			
ETHE	Ethene		
OLEL	Lumped alkenes C ₃ -C ₆ * (1-pentene)		
OLEH	Lumped alkenes >C ₆ (4-methyl-1-octene)		
ALKL	Lumped alkanes C ₂ -C ₆ * (2-methyl-butane)		
ALKM	Lumped alkanes C ₇ -C ₁₂ * (3,5-dimethyl-heptane)		
ALKH	Lumped alkanes >C ₁₂ (n-hexadecane)		
AROH	Lumped high SOA yield aromatic species (3-n-propyl-toluene)		
AROL	Lumped low SOA yield aromatic species (1,2,3-trimethyl-benzene)		
AROO	Lumped phenolic species* (2,6-dimethyl-phenol)		
ARAL	Lumped aromatic monoaldehydes* (p-tolualdehyde)		
ARAC ⁺	Lumped aromatic monoacids* (p-toluic acid)		
PAH	Lumped gas-phase polycyclic aromatic hydrocarbons (1,2-dimethyl-naphthalene)		
HCHO	Formaldehyde*		
ALD2	Lumped higher aldehydes* (n-pentanal)		
KETL	Lumped ketones C ₃ -C ₆ * (2-pentanone)		
KETH	Lumped ketones >C ₆ (2-heptanone)		
MEOH	Methanol		
ETOH	Ethanol		
ALCH	Lumped higher alcohols (2-hexanol)		
ISOP	Isoprene		
BIOL	Lumped low SOA yield monoterpene species (α-terpineol)		
BIOH	Lumped high SOA yield monoterpene species (γ-terpinene)		
MTBE	Methyl- <i>tert</i> -butyl ether		

Table 5.1. (continued) Chemical species represented in CACM.

Non-reacting, Fully Integrated Organic Species

ADAC ⁺	Lumped aromatic diacids (terephthalic acid)
ACID	Lumped organic acids <C ₆
UR1	3-Methyl-heptanoic acid
UR2 ⁺	3-Hydroxy-4-methyl-benzoic acid
UR3 ⁺	2-Hydroxy-3-isopropyl-6-keto-heptanoic acid
UR4	2-Isopropyl-5-keto-hexanal
UR5 ⁺	1-Methyl-3-hydroxy-4-isopropyl-1, 2-cyclohexane epoxide
UR6 ⁺	2-Hydroxy-3-isopropyl-6-methyl-cyclohexanone
UR7 ⁺	3, 7-Dimethyl-6-keto-3-octenal
UR8 ⁺	3-Isopropyl-6-keto-3-heptenoic acid
UR9	1-Methyl-4-isopropyl-1, 2-cyclo-4-hexene epoxide
UR10	3-Isopropyl-6-methyl-3-cyclohexenone
UR11 ⁺	1, 2-Dimethyl-3-hydroxy-naphthalene
UR12	1, 2, 3-Trimethyl-5-nitro-benzene
UR13	3- <i>n</i> -Propyl-4-nitro-toluene
UR14 ⁺	2-Nitro-4-methyl-benzoic acid
UR15 ⁺	1, 2-Dimethyl-3-nitro-naphthalene
UR16	2-Methyl-2-hydroxy-5-heptanone
UR17 ⁺	2-Hydroxy-3-isopropyl-hexadial
UR18	3-Isopropyl-2-pentendial
UR19 ⁺	1-Methyl-2-formyl-naphthalene
UR20 ⁺	11-Hydroxy-8-hexadecanone
UR21 ⁺	Keto-propanoic acid
UR22 ⁺	2,6-Dimethyl-3,4-dinitro-phenol
UR23 ⁺	3-Isopropyl-4-hydroxy-2-butenoic acid
UR24	Maleic anhydride
UR25	3H-Furan-2-one
UR26 ⁺	4, 5-Dimethyl-6-keto-2, 4-heptadienoic acid
UR27 ⁺	2-Carboxy-acetophenone
UR28 ⁺	Oxalic acid
UR29 ⁺	4-Hydroxy-3, 5-dimethyl-2, 4-hexadienoic acid
UR30 ⁺	2-Methyl-5-carboxy-2, 4-hexadienoic acid
UR31 ⁺	2-(Dimethyl-propenoic acid)-benzoic acid
UR32	3-Methyl-4-heptanone
UR33	2-Isopropyl-5-keto-2-hexenal
UR34 ⁺	8-Hexadecanone

Table 5.1. (continued) Chemical species represented in CACM.

Reactive, Fully Integrated Secondary Organic Species

PAN1	Peroxy pentionyl nitrate
PAN2	Peroxy acetyl nitrate (PAN)
PAN3	Unsaturated peroxy propionyl nitrate (PPN)
PAN4	Keto-PPN
PAN5	Methylene-PPN
PAN6	Peroxy nitrate derived from glyoxal
PAN7	Peroxy 3-methyl-heptionyl nitrate
PAN8 ⁺	Peroxy 2-hydroxy-3-isopropyl-6-keto-heptionyl nitrate
PAN9	Peroxy 3-isopropyl-4-hydroxy-2-butenionyl nitrate
PN10	Peroxy nitrate derived from glyoxalic acid
MGLY	Methyl glyoxal
MVK	Methyl-vinyl-ketone
MCR	Methacrolein
RPR1	3-Methyl-heptanal
RPR2	3-Hydroxy-4-methyl-benzaldehyde
RPR3 ⁺	2-Hydroxy-3-isopropyl-6-keto-heptanal
RPR4 ⁺	2,6-Dimethyl-4-nitro-phenol
RPR5	2-Nitro-4-methyl-benzaldehyde
RPR6	Benzene-1, 4-dialdehyde
RPR7 ⁺	4-Formyl-benzoic acid
RPR8	3-Isopropyl-4-hydroxy-2-butenal
RPR9 ⁺	4-Hydroxy-3, 5-dimethyl-2, 4-hexadienial
RP10	2-Methyl-butenalic acid
RP11	4, 5-Dimethyl-6-keto-2, 4-heptadienal
RP12 ⁺	2-Methyl-5-formyl-2, 4-hexadienial
RP13 ⁺	2-Carboxyl-5-methyl-2, 4-hexadienial
RP14 ⁺	2-(Dimethyl-propenal)-benzaldehyde
RP15	2-Formyl-acetophenone
RP16	Glyoxalic acid
RP17 ⁺	4-Hydroxy-3, 5-dimethyl-2, 4-hexadienalic acid
RP18 ⁺	2-Methyl-5-formyl-2, 4-hexadiendioic acid
RP19 ⁺	2-(Dimethyl-propenal)-benzoic acid
AP1 ⁺	2-Nitrooxymethyl-6-methyl-phenol
AP2	2-Methyl-2-hydroxy-5-heptylnitrate
AP3	3-Methyl-4-heptylnitrate
AP4	1, 2-Dimethyl-3-nitrooxymethyl-benzene
AP5	4-Nitrooxymethyl-benzaldehyde
AP6 ⁺	4-Nitrooxymethyl-benzoic acid
AP7 ⁺	1-Methyl-1-nitro-2, 3-dihydroxy-4-isopropyl-cyclohexane
AP8 ⁺	1-Methyl-4-nitro-4-isopropyl-5-hydroxy-cyclohexene
AP9	5-Isopropyl-6-nitro-4-hexen-2-one
AP10 ⁺	1-Methyl-2-nitrooxymethyl-naphthalene

Table 5.1. (continued) Chemical species represented in CACM.

Reactive, Fully Integrated Secondary Organic Species

AP11 ⁺	8-Hexadecylnitrate
AP12 ⁺	8-Hydroxy-11-hexadecylnitrate
RO ₂ T	Total organic peroxy radical
RO ₂ 8	Acetyl peroxy radical

Reactive, Inorganic Pseudo-Steady State Species

OSD	O (¹ D)	O	O (³ P)
-----	---------------------	---	---------------------

Reactive, Organic Pseudo-Steady State Species

RO ₂ 1	Methyl peroxy radical from oxidation of CH ₄
RO ₂ 2	Hydroxy alkyl peroxy radical <C ₆ from oxidation of ETHE, ETOH, OLEL, and ALCH (C ₄ , 1-peroxy, 2-hydroxy)
RO ₂ 3	Nitroso alkyl peroxy radical <C ₆ from oxidation of ETHE and OLEL (C ₄ , 1-nitroso, 2-peroxy)
RO ₂ 4	Aldehydic alkyl peroxy radical from oxidation of ISOP and ETHE (C ₂)
RO ₂ 5	Alkyl peroxy radical <C ₆ from oxidation of KETL, ISOP, ALKL, BIOH, and OLEL (C ₃ , 1-peroxy)
RO ₂ 6	Acyl radical from aldehydic H abstraction of ALD2
RO ₂ 7	Keto alkyl peroxy radical <C ₆ from oxidation of ISOP and KETL (C ₄ , 2-keto, 3-peroxy)
RO ₂ 9	Branched hydroxy alkenyl peroxy radical from oxidation of ISOP (C ₄ chain, 1-hydroxy, 2-methyl, 2-peroxy)
RO ₂ 10	Branched hydroxy alkenyl peroxy radical from oxidation of ISOP (C ₄ chain, 2-methyl, 3-peroxy, 4-hydroxy)
RO ₂ 11	Branched nitroso alkenyl peroxy radical from oxidation of ISOP (C ₄ chain, 1-nitroso, 2-methyl, 2-peroxy)
RO ₂ 12	Branched nitroso alkenyl peroxy radical from oxidation of ISOP (C ₄ chain, 2-methyl, 3-peroxy, 4-nitroso)
RO ₂ 13	Keto alkenyl peroxy radical from oxidation of ISOP (C ₄ , 3-keto, 4-peroxy)
RO ₂ 14	Alkenyl peroxy radical from oxidation of ISOP (C ₂)
RO ₂ 15	Ether alkyl peroxy radical from oxidation of MTBE (C ₅ , accounts for attack on both sides of the ether bond)
RO ₂ 16	Keto alkyl peroxy radical from oxidation of KETH (C ₇ , 2-keto, 3-peroxy)
RO ₂ 17	Aromatic peroxy radical from side chain oxidation of AROO
RO ₂ 18	Branched hydroxy alkyl peroxy radical >C ₆ from oxidation of OLEH and ALKM (C ₇ chain, 2-methyl, 2-hydroxy, 5-peroxy)

Table 5.1. (continued) Chemical species represented in CACM.

Reactive, Organic Pseudo-Steady State Species

RO ₂ 19	Branched nitrato alkyl peroxy radical from oxidation of OLEH (C ₈ chain, 4-methyl, 1-nitro, 2-peroxy)
RO ₂ 20	Branched alkyl peroxy radical >C ₆ from oxidation of OLEH and ALKM (C ₇ chain, 3-methyl, 4-peroxy)
RO ₂ 21	Aromatic peroxy radical from side chain oxidation of AROL
RO ₂ 22	Aromatic peroxy radical from side chain oxidation of ARAL
RO ₂ 23	Aromatic peroxy radical from side chain oxidation of ARAC
RO ₂ 24	Cyclic dihydroxy alkyl peroxy radical from OH oxidation of BIOL (C ₆ cycle, 1-methyl, 1-peroxy, 2, 3-dihydroxy, 4-isopropyl)
RO ₂ 25	Cyclic hydroxy nitrato alkyl peroxy radical from NO ₃ oxidation of BIOL (C ₆ cycle, 1-methyl, 1-peroxy, 2-nitro, 3-hydroxy, 4-isopropyl)
RO ₂ 26	Branched keto hydroxy aldehydic peroxy radical from oxidation of BIOL (C ₇ chain, 2-hydroxy, 3-isopropyl, 5-peroxy, 6-keto)
RO ₂ 27	Cyclic hydroxy alkenyl peroxy radical from oxidation of BIOH (C ₆ cycle, 1-methyl, 1-ene, 4-peroxy, 4-isopropyl, 5-hydroxy)
RO ₂ 28	Cyclic nitrato alkenyl peroxy radical from oxidation of BIOH (C ₆ cycle, 1-methyl, 1-ene, 4-peroxy, 4-isopropyl, 5-nitro)
RO ₂ 29	Branched keto alkenyl peroxy radical from oxidation of BIOH (C ₆ chain, 1-peroxy, 2-isopropyl, 2-ene, 5-keto)
RO ₂ 30	Branched keto aldehydic peroxy radical from oxidation of BIOH (C ₇ chain, 3-isopropyl, 3-ene, 5-peroxy, 6-keto)
RO ₂ 31	Aromatic peroxy radical from side chain oxidation of PAH
RO ₂ 32	Alkyl peroxy radical from oxidation of ALKH (8-peroxy)
RO ₂ 33	Peroxy radical from addition of O ₂ to RAD2
RO ₂ 34	Peroxy radical from addition of O ₂ to RAD3
RO ₂ 35	Peroxy radical from addition of O ₂ to RAD4
RO ₂ 36	Peroxy radical from addition of O ₂ to RAD5
RO ₂ 37	Peroxy radical from addition of O ₂ to RAD6
RO ₂ 38	Peroxy radical from addition of O ₂ to RAD7
RO ₂ 39	Unsaturated acyl peroxy radical from oxidation of ISOP (C ₃)
RO ₂ 40	Branched hydroxy keto alkenyl peroxy radical from oxidation of BIOH (C ₆ chain, 1-hydroxy, 2-isopropyl, 2-ene, 4-peroxy, 5-keto)
RO ₂ 41	Hydroxy alkyl peroxy radical from oxidation of ALKH (8-hydroxy, 11-peroxy)
RO ₂ 42	Bicyclic peroxy radical from the O ₂ bridging in RO ₂ 31
RO ₂ 43	Bicyclic peroxy radical from the O ₂ bridging in RO ₂ 32
RO ₂ 44	Bicyclic peroxy radical from the O ₂ bridging in RO ₂ 33
RO ₂ 45	Bicyclic peroxy radical from the O ₂ bridging in RO ₂ 34
RO ₂ 46	Bicyclic peroxy radical from the O ₂ bridging in RO ₂ 35
RO ₂ 47	Bicyclic peroxy radical from the O ₂ bridging in RO ₂ 36
RO ₂ 48	Acyl radical from aldehydic H abstraction of MGLY
RO ₂ 49	Peroxy radical formed from OH oxidation of MVK

Table 5.1. (continued) Chemical species represented in CACM.

Reactive, Organic Pseudo-Steady State Species

RO ₂ 50	Acyl radical from aldehydic H abstraction of MCR
RO ₂ 51	Peroxy radical from OH addition to double bond in MCR
RO ₂ 52	Peroxy radical from NO ₃ addition to double bond in MCR
RO ₂ 53	Dicarbonyl peroxy radical from MCR/O ₃ reaction (C ₃ chain, 1-peroxy, 2-keto, 3-aldehydic)
RO ₂ 54	Acyl radical from decomposition of RO ₂ 53
RO ₂ 55	Acyl radical from aldehydic H abstraction of RPR1
RO ₂ 56	Acyl radical from aldehydic H abstraction of RPR3
RO ₂ 57	Acyl radical from aldehydic H abstraction of RPR7
RO ₂ 58	Acyl acid peroxy radical from aldehydic H abstraction of RP16 (C ₂)
RAD1	Radical from NO ₃ oxidation of AROO
RAD2	Hexadienyl radical from OH oxidation of AROO
RAD3	Hexadienyl radical from OH oxidation of AROL
RAD4	Hexadienyl radical from OH oxidation of AROH
RAD5	Hexadienyl radical from OH oxidation of ARAL
RAD6	Hexadienyl radical from OH oxidation of ARAC
RAD7	Hexadienyl radical from OH oxidation of PAH
RAD8	Radical from NO ₃ oxidation of RPR4

Species with Concentrations not Affected by Reaction

H ₂ O	Water vapor	O ₂	Oxygen
M	Third body	CH ₄	Methane

Table 5.2. Reactions contained in the Caltech Atmospheric Chemistry Mechanism.

Reaction	Reactants	Products	Rate Constants (ppm-min units)*	References, Comments
1	$\text{NO}_2 + h\nu$	$\text{NO} + \text{O}$	See Table 5.3	1
2	$\text{O} + \text{O}_2 + \text{M}$	$\text{O}_3 + \text{M}$	$3.32\text{E+18}/\text{TEMP}^{4.8}$	2
3	$\text{O} + \text{NO}_2$	$\text{NO} + \text{O}_2$	$2.86\text{E+6}/\text{TEMP}^*\text{EXP}$ (119.8/TEMP)	2
4	$\text{O} + \text{NO}_2 + \text{M}$	$\text{NO}_3 + \text{M}$	See Table 5.4	2
5	$\text{NO} + \text{O}_3$	$\text{NO}_2 + \text{O}_2$	$7.92\text{E+5}/\text{TEMP}^*\text{EXP}$ (-1368.9/TEMP)	2
6	$\text{NO}_2 + \text{O}_3$	$\text{NO}_3 + \text{O}_2$	$6.16\text{E+4}/\text{TEMP}^*\text{EXP}$ (-2471.1/TEMP)	2
7	$\text{NO} + \text{NO}_3$	2NO_2	$7.92\text{E+6}/\text{TEMP}^*\text{EXP}$ (110.7/TEMP)	2
8	$\text{NO} + \text{NO} + \text{O}_2$	2NO_2	$2.24/\text{TEMP}^{2*}\text{EXP}$ (528.4/TEMP)	2
9	$\text{NO}_2 + \text{NO}_3 + \text{M}$	$\text{N}_2\text{O}_5 + \text{M}$	See Table 5.4	2
10	N_2O_5	$\text{NO}_2 + \text{NO}_3$	See Table 5.4	2
11	$\text{N}_2\text{O}_5 + \text{H}_2\text{O}$	2HNO_3	$1.14\text{E-4}/\text{TEMP}$	2
12	$\text{NO}_2 + \text{NO}_3$	$\text{NO} + \text{NO}_2 + \text{O}_2$	$1.98\text{E+4}/\text{TEMP}^*\text{EXP}$ (-1258.2/TEMP)	2
13	$\text{NO}_3 + h\nu$	$\text{NO} + \text{O}_2$	See Table 5.3	1
14	$\text{NO}_3 + h\nu$	$\text{NO}_2 + \text{O}$	See Table 5.3	1
15	$\text{O}_3 + h\nu$	$\text{O} + \text{O}_2$	See Table 5.3	1
16	$\text{O}_3 + h\nu$	$\text{OSD} + \text{O}_2$	See Table 5.3	1
17	$\text{OSD} + \text{H}_2\text{O}$	2OH	$9.68\text{E+7}/\text{TEMP}$	2

Table 5.2. (continued) Reactions contained in the Caltech Atmospheric Chemistry

Mechanism.

Reaction	Reactants	Products	Rate Constants (ppm-min units) [*]	References, Comments
18	OSD + M	O + M	9.2E+12/TEMP*EXP	2
			(95.6/TEMP)	
19	NO + OH + M	HONO + M	See Table 5.4	2
20	HONO + <i>h</i> v	0.9 NO + 0.1 NO ₂ + 0.9 OH + 0.1 HO ₂	See Table 5.3	1
21	NO ₂ + H ₂ O	HONO - NO ₂ + HNO ₃	1.76E-6/TEMP	1
22	NO ₂ + OH + M	HNO ₃ + M	See Table 5.4	3
23	HNO ₃ + OH	NO ₃ + H ₂ O	See Table 5.5	2
24	CO + OH	HO ₂ + CO ₂	See Table 5.5	2
25	O ₃ + OH	HO ₂ + O ₂	8.36E+5/TEMP*EXP	2
			(-1001.5/TEMP)	
26	NO + HO ₂	NO ₂ + OH	1.5E+6/TEMP*EXP	2
			(271.8/TEMP)	
27	NO ₂ + HO ₂ + M	HNO ₄ + M	See Table 5.4	2
28	HNO ₄	NO ₂ + HO ₂	See Table 5.4	2
29	HNO ₄ + OH	NO ₂ + O ₂ + H ₂ O	6.6E+5/TEMP*EXP	2
			(362.4/TEMP)	
30	O ₃ + HO ₂	OH + 2 O ₂	6.16E+3/TEMP*EXP	2
			(-598.9/TEMP)	
31	HO ₂ + HO ₂	H ₂ O ₂	See Table 5.5	2
32	HO ₂ + HO ₂ + H ₂ O	H ₂ O ₂ + O ₂ + H ₂ O	See Table 5.5	2

Table 5.2. (continued) Reactions contained in the Caltech Atmospheric Chemistry

Mechanism.

Reaction	Reactants	Products	Rate Constants (ppm-min units) [*]	References, Comments
33	NO ₃ + HO ₂	0.8 NO ₂ + 0.2 HNO ₃ + 0.8 OH + O ₂	1.76E+6/TEMP	2
34	O + O ₃	2 O ₂	3.52E+6/TEMP*EXP (-2058.4/TEMP)	2
35	SO ₂ + OH	H ₂ SO ₄ (via SO ₃) + HO ₂	See Table 5.4	2
36	H ₂ O ₂ + <i>hν</i>	2 OH	See Table 5.3	1
37	H ₂ O ₂ + OH	HO ₂ + H ₂ O	1.28E+6/TEMP*EXP (-161/TEMP)	1
38	O + NO + M	NO ₂ + M	2.97E+12/TEMP ^{3.6}	2
39	HONO + OH	NO ₂ + H ₂ O	1.19E+6/TEMP*EXP (261.7/TEMP)	2
40	NO ₃ + OH	NO ₂ + HO ₂	8.8E+6/TEMP	2
41	NO ₃ + NO ₃	2 NO ₂ + O ₂	3.74E+5/TEMP*EXP (-2450.9/TEMP)	2
42	OH + HO ₂	H ₂ O + O ₂	2.11E+7/TEMP*EXP (251.6/TEMP)	2
43	CH ₄ + OH	RO ₂ 1 + RO ₂ T + H ₂ O	1.17E+6/TEMP*EXP (-1800.2/TEMP)	2
44	HCHO + <i>hν</i>	CO + 2 HO ₂	See Table 5.3	1
45	HCHO + <i>hν</i>	CO + H ₂	See Table 5.3	1
46	HCHO + OH	CO + HO ₂ + H ₂ O	5.28E+3* EXP(286.9/TEMP)	4
47	HCHO + NO ₃	HNO ₃ + CO + HO ₂	8.8E+5/TEMP*EXP (-2430.8/TEMP)	2

Table 5.2. (continued) Reactions contained in the Caltech Atmospheric Chemistry Mechanism.

Reaction	Reactants	Products	Rate Constants (ppm-min units) [*]	References, Comments
48	MEOH + OH	HO ₂ + HCHO + H ₂ O	2.64*TEMP*EXP (170.1/TEMP)	4
49	ETHE + OH	RO ₂ 2 + RO ₂ T	8.62E+5/TEMP*EXP (437.8/TEMP)	5
50	ETHE + NO ₃	RO ₂ 3 + RO ₂ T	2.15*TEMP*EXP (-2282.3/TEMP)	5
51	ETHE + O ₃	0.315 CO + 0.06 HO ₂ + 0.06 OH + 0.185 ACID + 0.5 HCHO + 0.07 H ₂ O	4.02E+3/TEMP*EXP (-2580.3/TEMP)	5
52	ETHE + O	0.6 CO + HO ₂ + 0.6 RO ₂ 1 + 0.4 RO ₂ 4 + RO ₂ T	3.21E+5/TEMP	5
53	ETOH + OH	CF(1) HO ₂ + CF(1) ALD2 + CF(2) RO ₂ 2 + CF(2) RO ₂ T + H ₂ O	2.72*TEMP*EXP (532/TEMP)	4
54	OLEL + OH	RO ₂ 2 + RO ₂ T	2.58E+6/TEMP*EXP (500.3/TEMP)	4
55	OLEL + NO ₃	RO ₂ 3 + RO ₂ T	4.4E+4/TEMP*EXP (-800.2/TEMP)	5
56	OLEL + O ₃	0.56 CO + 0.2 CO ₂ + 0.36 OH + 0.28 HO ₂ + 0.5 HCHO + 0.5 ALD2 + 0.24 ACID + 0.1 ALKL + 0.28 RO ₂ 5 + 0.28 RO ₂ T	4.4/TEMP	5
57	OLEL + O	0.5 ALKL + 0.4 ALD2 + 0.1 RO ₂ 4 + 0.1 RO ₂ 5 + 0.2 RO ₂ T	2.05E+6/TEMP	5
58	ALKL + OH	RO ₂ 5 + RO ₂ T + H ₂ O	1.72E+6/TEMP	4

Table 5.2. (continued) Reactions contained in the Caltech Atmospheric Chemistry

Mechanism.

Reaction	Reactants	Products	Rate Constants (ppm-min units) [*]	References, Comments
59	ALD2 + <i>hν</i>	CO + HO ₂ + RO ₂ 5 + RO ₂ T	See Table 5.3	1
60	ALD2 + OH	RO ₂ 6 + RO ₂ T + H ₂ O	3.039E+6/TEMP* EXP(250/TEMP)	1
61	ALD2 + NO ₃	HNO ₃ + RO ₂ 6 + RO ₂ T	1.32E+5/TEMP*EXP (-1427/TEMP)	1
62	KETL + OH	RO ₂ 7 + RO ₂ T + H ₂ O	2.16E+06/TEMP	6
63	KETL + <i>hν</i>	RO ₂ 5 + RO ₂ 8 + 2 RO ₂ T	See Table 5.3	1
64	ISOP + OH	0.66 RO ₂ 9 + 0.34 RO ₂ 10 + RO ₂ T	1.12E+7/TEMP*EXP (410.2/TEMP)	5
65	ISOP + NO ₃	0.66 RO ₂ 11 + 0.34 RO ₂ 12 + RO ₂ T	1.33E+6/TEMP*EXP (-445.9/TEMP)	5
66	ISOP + O ₃	0.068 CO ₂ + 0.461 CO + 0.5 HCHO + 0.664 OH + 0.366 HO ₂ + 0.054 OLEL + 0.121 ACID + 0.389 MVK + 0.17 MCR + 0.271 RO ₂ 13 + 0.095 RO ₂ 14 + 0.366 RO ₂ T	3.46E+3/TEMP*EXP (-1912.9/TEMP)	5
67	ISOP + O	0.925 OLEL + 0.075 ALD2	1.54E+7/TEMP	5
68	MTBE + OH	RO ₂ 15 + RO ₂ T + H ₂ O	1.41E+6/TEMP	7
69	ALCH + OH	RO ₂ 2 + RO ₂ T + H ₂ O	See Table 5.6	8
70	KETH + OH	RO ₂ 16 + RO ₂ T + H ₂ O	See Table 5.6	8
71	KETH + <i>hν</i>	RO ₂ 5 + RO ₂ 8 + 2 RO ₂ T	See Table 5.3	1
72	AROO + NO ₃	HNO ₃ + RAD1	1.66E+6/TEMP	2
73	AROO + OH	0.16 HO ₂ + 0.16 AROO + 0.1 RO ₂ 17 + 0.1 RO ₂ T + 0.74 RAD2 + 0.1 H ₂ O	See Table 5.6	8

Table 5.2. (continued) Reactions contained in the Caltech Atmospheric Chemistry

Mechanism.

Reaction	Reactants	Products	Rate Constants (ppm-min units) [*]	References, Comments
74	OLEH + OH	RO ₂ 18 + RO ₂ T	See Table 5.6	8
75	OLEH + NO ₃	RO ₂ 19 + RO ₂ T	$k_{74} * k_{55} / k_{54}$	Estimated k
76	OLEH + O ₃	0.56 CO + 0.2 CO ₂ + 0.36 OH + 0.28 HO ₂ + 0.5 HCHO + 0.5 RPR1 + 0.12 ACID + 0.12 UR1 + 0.1 ALKM + 0.28 RO ₂ 20 + 0.28 RO ₂ T	$k_{74} * k_{56} / k_{54}$	Estimated k
77	OLEH + O	0.5 ALKM + 0.4 RPR1 + 0.1 RO ₂ 4 + 0.1 RO ₂ 20 + 0.2 RO ₂ T	$k_{74} * k_{57} / k_{54}$	Estimated k
78	ALKM + OH	RO ₂ 20 + RO ₂ T + H ₂ O	See Table 5.6	8
79	AROL + OH	0.16 HO ₂ + 0.16 AROO + 0.06 RO ₂ 21 + 0.78 RAD3 + 0.06 RO ₂ T+ + 0.06 H ₂ O	1.44E+7/TEMP	4
80	AROH + OH	0.16 HO ₂ + 0.16 AROO + 0.84 RAD4	See Table 5.6	8
81	ARAL + NO ₃	HNO ₃ + O ₃ - HO ₂ + ARAC	6.16E+5/TEMP*EXP (-1872.2/TEMP)	2
82	ARAL + OH	(0.16-CF(39)) HO ₂ + CF(39) O ₃ + CF(39) ARAC + CF(45) RO ₂ 22 + CF(40) RAD5 + CF(45) RO ₂ T + (CF(39) + CF(45))H ₂ O	5.68E+06/TEMP	2
83	ARAC + OH	0.16 HO ₂ + 0.16 UR2 + 0.1 RO ₂ 23 + 0.74 RAD6 + 0.1 RO ₂ T+ 0.1 H ₂ O	See Table 5.6	8
84	BIOL + OH	RO ₂ 24 + RO ₂ T	7.48E+7/TEMP	9
85	BIOL + NO ₃	RO ₂ 25 + RO ₂ T	6.42E+6/TEMP	9

Table 5.2. (continued) Reactions contained in the Caltech Atmospheric Chemistry

Mechanism.

Reaction	Reactants	Products	Rate Constants (ppm-min units) [*]	References, Comments
86	BIOL + O ₃	0.445 CO + 0.055 H ₂ O ₂ + 0.445 HO ₂ + 0.89 OH + 0.055 UR3 + 0.445 UR4 + 0.055 RPR3 + 0.445 RO ₂ 26 + 0.445 RO ₂ T	1.1E+2/TEMP	9
87	BIOL + O	0.75 UR5 + 0.25 UR6	$k_{84} * k_{57} / k_{54}$	Estimated k
88	BIOH + OH	RO ₂ 27 + RO ₂ T	7.79E+7/TEMP	5
89	BIOH + NO ₃	RO ₂ 28 + RO ₂ T	1.28E+7/TEMP	5
90	BIOH + O ₃	0.445 CO + 0.055 H ₂ O ₂ + 0.89 OH + 0.055 UR7 + 0.055 UR8 + 0.445 RO ₂ 29 + 0.445 RO ₂ 30 + 0.89 RO ₂ T	6.16E+1/TEMP	5
91	BIOH + O	0.75 UR9 + 0.25 UR10	3.78E+7/TEMP	5
92	PAH + OH	0.16 HO ₂ + 0.16 UR11 + 0.1 RO ₂ 31 + 0.74 RAD7 + 0.1 RO ₂ T + 0.1 H ₂ O	3.39E+7/TEMP	6
93	ALKH + OH	RO ₂ 32 + RO ₂ T + H ₂ O	See Table 5.6	8
94	RO ₂ T + HO ₂	HO ₂	1.5E+5/TEMP*EXP (800.2/TEMP)	2
95	RO ₂ T + NO	NO	1.85E+6/TEMP*EXP (181.2/TEMP)	2
96	RO ₂ T + RO ₂ T	RO ₂ T	4.4E+2/TEMP	2
97	RAD2 + O ₂	RO ₂ 33 + RO ₂ T	4.62E+7/TEMP	10
98	RAD3 + O ₂	RO ₂ 34 + RO ₂ T	k_{97}	
99	RAD4 + O ₂	RO ₂ 35 + RO ₂ T	k_{97}	
100	RAD5 + O ₂	RO ₂ 36 + RO ₂ T	k_{97}	
101	RAD6 + O ₂	RO ₂ 37 + RO ₂ T	k_{97}	

Table 5.2. (continued) Reactions contained in the Caltech Atmospheric Chemistry

Mechanism.

Reaction	Reactants	Products	Rate Constants (ppm-min units)*	References, Comments
102	RAD7 + O ₂	RO ₂ 38 + RO ₂ T	k_{97}	
103	RAD1 + NO ₂	RPR4	1.32E+7/TEMP	10
104	RAD2 + NO ₂	RPR4 + H ₂ O	k_{103}	
105	RAD3 + NO ₂	UR12 + H ₂ O	k_{103}	
106	RAD4 + NO ₂	UR13 + H ₂ O	k_{103}	
107	RAD5 + NO ₂	RPR5 + H ₂ O	k_{103}	
108	RAD6 + NO ₂	UR14 + H ₂ O	k_{103}	
109	RAD7 + NO ₂	UR15 + H ₂ O	k_{103}	
110	RO ₂ 1 + NO	NO ₂ + HO ₂ + HCHO	1.8E+6/TEMP*EXP (180.2/TEMP)	11
111	RO ₂ 1 + RO ₂ T	HO ₂ + HCHO + RO ₂ T + O ₂	k_{96}	
112	RO ₂ 1 + HO ₂	HO ₂ + OH + HCHO	k_{94}	
113	RO ₂ 2 + NO	NO ₂ + HO ₂ + HCHO + ALD2	1.08E+6/TEMP*EXP (180.2/TEMP)	11
114	RO ₂ 2 + RO ₂ T	HO ₂ + HCHO + ALD2 + RO ₂ T + O ₂	k_{96}	
115	RO ₂ 2 + HO ₂	OH + HO ₂ + HCHO + ALD2	k_{94}	
116	RO ₂ 3 + NO	2 NO ₂ + HCHO + ALD2	k_{113}	
117	RO ₂ 3 + RO ₂ T	NO ₂ + HO ₂ + HCHO + ALD2 + O ₂ + RO ₂ T	k_{96}	
118	RO ₂ 3 + HO ₂	NO ₂ + HO ₂ + OH + HCHO + ALD2	k_{94}	
119	RO ₂ 4 + NO	NO ₂ + CO + HO ₂ + HCHO	1.52E+6/TEMP*EXP (180.2/TEMP)	11
120	RO ₂ 4 + RO ₂ T	CO + HO ₂ + HCHO + RO ₂ T + O ₂	k_{96}	
121	RO ₂ 4 + HO ₂	CO + HO ₂ + OH + HCHO	k_{94}	

Table 5.2. (continued) Reactions contained in the Caltech Atmospheric Chemistry Mechanism.

Reaction	Reactants	Products	Rate Constants (ppm-min units)*	References, Comments
122	$\text{RO}_25 + \text{NO}$	$\text{CF}(3) \text{ ALKL} + \text{CF}(4) \text{ NO}_2 + \text{CF}(4)$ $\text{HO}_2 + \text{CF}(4) \text{ ALD2}$	$1.28\text{E+6}/\text{TEMP}^*\text{EXP}$ (180.2/TEMP)	11
123	$\text{RO}_25 + \text{RO}_2\text{T}$	$\text{HO}_2 + \text{ALD2} + \text{RO}_2\text{T} + \text{O}_2$	k_{96}	
124	$\text{RO}_25 + \text{HO}_2$	$\text{HO}_2 + \text{OH} + \text{ALD2}$	k_{94}	
125	$\text{RO}_26 + \text{NO}$	$\text{NO}_2 + \text{CO}_2 + \text{RO}_25 + \text{RO}_2\text{T}$	$4.87\text{E+6}/\text{TEMP}^*\text{EXP}$ (180.2/TEMP)	11
126	$\text{RO}_26 + \text{NO}_2 + \text{M}$	$\text{PAN1} + \text{M}$	See Table 5.4	12
127	PAN1	$\text{NO}_2 + \text{RO}_26 + \text{RO}_2\text{T}$	See Table 5.4	12
128	$\text{RO}_26 + \text{HO}_2$	$\text{O}_3 + \text{ACID}$	k_{94}	
129	$\text{RO}_26 + \text{RO}_2\text{T}$	$\text{CO}_2 + \text{RO}_25 + 2 \text{RO}_2\text{T} + \text{O}_2$	k_{96}	
130	$\text{RO}_27 + \text{NO}$	$\text{NO}_2 + \text{ALD2} + \text{RO}_28 + \text{RO}_2\text{T}$	k_{113}	
131	$\text{RO}_27 + \text{RO}_2\text{T}$	$\text{ALD2} + \text{RO}_28 + 2 \text{RO}_2\text{T} + \text{O}_2$	k_{96}	
132	$\text{RO}_27 + \text{HO}_2$	$\text{OH} + \text{ALD2} + \text{RO}_28 + \text{RO}_2\text{T}$	k_{94}	
133	$\text{RO}_28 + \text{NO}$	$\text{NO}_2 + \text{CO}_2 + \text{RO}_21 + \text{RO}_2\text{T}$	k_{125}	
134	$\text{RO}_28 + \text{NO}_2 + \text{M}$	$\text{PAN2} + \text{M}$	k_{126}	
135	PAN2	$\text{NO}_2 + \text{RO}_28 + \text{RO}_2\text{T}$	k_{127}	
136	$\text{RO}_28 + \text{HO}_2$	$\text{O}_3 + \text{ACID}$	k_{94}	
137	$\text{RO}_28 + \text{RO}_2\text{T}$	$\text{CO}_2 + \text{RO}_21 + 2 \text{RO}_2\text{T} + \text{O}_2$	k_{96}	
138	$\text{RO}_29 + \text{NO}$	$\text{CF}(5) \text{ OLEL} + \text{CF}(6) \text{ NO}_2 + \text{CF}(6)$ $\text{HO}_2 + \text{CF}(6) \text{ HCHO} + \text{CF}(6) \text{ MVK}$	$9.14\text{E+5}/\text{TEMP}^*\text{EXP}$ (180.2/TEMP)	11
139	$\text{RO}_29 + \text{RO}_2\text{T}$	$\text{HO}_2 + \text{MVK} + \text{HCHO} + \text{RO}_2\text{T} + \text{O}_2$	k_{96}	
140	$\text{RO}_29 + \text{HO}_2$	$\text{HO}_2 + \text{OH} + \text{MVK} + \text{HCHO}$	k_{94}	

Table 5.2. (continued) Reactions contained in the Caltech Atmospheric Chemistry Mechanism.

Reaction	Reactants	Products	Rate Constants (ppm-min units) [*]	References, Comments
141	RO ₂ 10 + NO	NO ₂ + HO ₂ + HCHO + MCR	k_{138}	
142	RO ₂ 10 + RO ₂ T	HO ₂ + HCHO + MCR + RO ₂ T + O ₂	k_{96}	
143	RO ₂ 10 + HO ₂	HO ₂ + OH + HCHO + MCR	k_{94}	
144	RO ₂ 11 + NO	2 NO ₂ + HCHO + MVK	k_{138}	
145	RO ₂ 11 + RO ₂ T	NO ₂ + HCHO + MVK + RO ₂ T + O ₂	k_{96}	
146	RO ₂ 11 + HO ₂	NO ₂ + OH + HCHO + MVK	k_{94}	
147	RO ₂ 12 + NO	2 NO ₂ + HCHO + MCR	k_{138}	
148	RO ₂ 12 + RO ₂ T	NO ₂ + HCHO + MCR + RO ₂ T + O ₂	k_{96}	
149	RO ₂ 12 + HO ₂	NO ₂ + OH + HCHO + MCR	k_{94}	
150	RO ₂ 13 + NO	NO ₂ + HCHO + RO ₂ 39 + RO ₂ T	k_{113}	
151	RO ₂ 13 + RO ₂ T	HCHO + RO ₂ 39 + 2 RO ₂ T + O ₂	k_{96}	
152	RO ₂ 13 + HO ₂	HCHO + OH + RO ₂ 39 + RO ₂ T	k_{94}	
153	RO ₂ 39 + NO	NO ₂ + CO ₂ + RO ₂ 14 + RO ₂ T	k_{125}	
154	RO ₂ 39 + NO ₂ + M	PAN3 + M	k_{126}	
155	PAN3	NO ₂ + RO ₂ 39 + RO ₂ T	k_{127}	
156	RO ₂ 39 + HO ₂	O ₃ + 0.5 OLEL + 0.5 ACID	k_{94}	
157	RO ₂ 39 + RO ₂ T	CO ₂ + RO ₂ 14 + 2 RO ₂ T + O ₂	k_{96}	
158	RO ₂ 14 + NO	CF(7) OLEL + CF(8) NO ₂ + CF(8) RO ₂ 7 + CF(8) RO ₂ T	k_{122}	
159	RO ₂ 14 + RO ₂ T	RO ₂ 7 + 2 RO ₂ T + O ₂	k_{96}	
160	RO ₂ 14 + HO ₂	OH + RO ₂ 7 + RO ₂ T	k_{94}	

Table 5.2. (continued) Reactions contained in the Caltech Atmospheric Chemistry

Mechanism.

Reaction	Reactants	Products	Rate Constants (ppm-min units)*	References, Comments
161	$\text{RO}_215 + \text{NO}$	$\text{NO}_2 + \text{HO}_2 + \text{CF}(9)$ $\text{ALD2} + \text{CF}(10)$ $\text{HCHO} + \text{CF}(11)$ $\text{KETL} +$ $\text{CF}(12)$ ALKL	k_{138}	
162	$\text{RO}_215 + \text{RO}_2\text{T}$	$\text{HO}_2 + \text{CF}(13)$ $\text{ALD2} + \text{CF}(14)$ $\text{HCHO} + \text{CF}(15)$ $\text{KETL} + \text{CF}(16)$ $\text{ALKL} + \text{RO}_2\text{T} + \text{O}_2$	k_{96}	
163	$\text{RO}_215 + \text{HO}_2$	$\text{OH} + \text{HO}_2 + \text{CF}(13)$ $\text{ALD2} + \text{CF}(14)$ $\text{HCHO} + \text{CF}(15)$ $\text{KETL} +$ $\text{CF}(16)$ ALKL	k_{94}	
164	$\text{RO}_216 + \text{NO}$	$\text{NO}_2 + \text{ALD2} + \text{RO}_28 + \text{RO}_2\text{T}$	$6.51\text{E}+5/\text{TEMP}^*\text{EXP}$ (180.2/TEMP)	11
165	$\text{RO}_216 + \text{RO}_2\text{T}$	$\text{ALD2} + \text{RO}_28 + 2 \text{RO}_2\text{T} + \text{O}_2$	k_{96}	
166	$\text{RO}_216 + \text{HO}_2$	$\text{OH} + \text{ALD2} + \text{RO}_28 + \text{RO}_2\text{T}$	k_{94}	
167	$\text{RO}_217 + \text{NO}$	$\text{CF}(21)$ $\text{AP1} + \text{CF}(22)$ $\text{NO}_2 + \text{CF}(22)$ $\text{HO}_2 + \text{CF}(22)$ RPR2	$5.49\text{E}+5/\text{TEMP}^*\text{EXP}$ (180.2/TEMP)	11
168	$\text{RO}_217 + \text{RO}_2\text{T}$	$\text{HO}_2 + \text{RPR2} + \text{RO}_2\text{T} + \text{O}_2$	k_{96}	
169	$\text{RO}_217 + \text{HO}_2$	$\text{HO}_2 + \text{OH} + \text{RPR2}$	k_{94}	
170	$\text{RO}_218 + \text{NO}$	$\text{CF}(19)$ $\text{AP2} + \text{CF}(20)$ $\text{NO}_2 + \text{CF}(20)$ $\text{HO}_2 + \text{CF}(20)$ UR16	k_{167}	
171	$\text{RO}_218 + \text{RO}_2\text{T}$	$\text{HO}_2 + \text{UR16} + \text{RO}_2\text{T} + \text{O}_2$	k_{96}	
172	$\text{RO}_218 + \text{HO}_2$	$\text{HO}_2 + \text{OH} + \text{UR16}$	k_{94}	
173	$\text{RO}_219 + \text{NO}$	$2 \text{NO}_2 + \text{HCHO} + \text{RPR1}$	$4.63\text{E}+5/\text{TEMP}^*\text{EXP}$ (180.2/TEMP)	11

Table 5.2. (continued) Reactions contained in the Caltech Atmospheric Chemistry

Mechanism.

Reaction	Reactants	Products	Rate Constants (ppm-min units) [*]	References, Comments
174	RO ₂ 19 + RO ₂ T	NO ₂ + HCHO + RPR1 + RO ₂ T + O ₂	k_{96}	
175	RO ₂ 19 + HO ₂	NO ₂ + OH + HCHO + RPR1	k_{94}	
176	RO ₂ 20 + NO	CF(17) AP3 + CF(18) NO ₂ + CF(18) RO ₂ T + CF(18) RO ₂ T	k_{167}	
177	RO ₂ 20 + RO ₂ T	RO ₂ 18 + 2 RO ₂ T + O ₂	k_{96}	
178	RO ₂ 20 + HO ₂	OH + RO ₂ 18 + RO ₂ T	k_{94}	
179	RO ₂ 21 + NO	CF(23) AP4 + CF(24) NO ₂ + CF(24) HO ₂ + CF(24) ARAL	k_{173}	
180	RO ₂ 21 + RO ₂ T	HO ₂ + ARAL + RO ₂ T + O ₂	k_{96}	
181	RO ₂ 21 + HO ₂	HO ₂ + OH + ARAL	k_{94}	
182	RO ₂ 22 + NO	CF(41) AP5 + CF(42) NO ₂ + CF(42) HO ₂ + CF(42) RPR6	k_{167}	
183	RO ₂ 22 + RO ₂ T	HO ₂ + RPR6 + RO ₂ T + O ₂	k_{96}	
184	RO ₂ 22 + HO ₂	HO ₂ + OH + RPR6	k_{94}	
185	RO ₂ 23 + NO	CF(43) AP6 + CF(44) NO ₂ + CF(44) HO ₂ + CF(44) RPR7	k_{167}	
186	RO ₂ 23 + RO ₂ T	HO ₂ + RPR7 + RO ₂ T + O ₂	k_{96}	
187	RO ₂ 23 + HO ₂	HO ₂ + OH + RPR7	k_{94}	
188	RO ₂ 24 + NO	CF(25) AP7 + CF(26) NO ₂ + CF(26) HO ₂ + CF(26) RPR3	3.91E+5/TEMP*EXP (180.2/TEMP)	11
189	RO ₂ 24 + RO ₂ T	HO ₂ + RPR3 + RO ₂ T + O ₂	k_{96}	
190	RO ₂ 24 + HO ₂	HO ₂ + OH + RPR3	k_{94}	
191	RO ₂ 25 + NO	2 NO ₂ + RPR3	k_{188}	
192	RO ₂ 25 + RO ₂ T	NO ₂ + RPR3 + RO ₂ T + O ₂	k_{96}	

Table 5.2. (continued) Reactions contained in the Caltech Atmospheric Chemistry

Mechanism.

Reaction	Reactants	Products	Rate Constants (ppm-min units) [*]	References, Comments
193	RO ₂ 25 + HO ₂	NO ₂ + OH + RPR3	k_{94}	
194	RO ₂ 26 + NO	NO ₂ + UR17 + RO ₂ 8 + RO ₂ T	k_{188}	
195	RO ₂ 26 + RO ₂ T	UR17 + RO ₂ 8 + 2 RO ₂ T + O ₂	k_{96}	
196	RO ₂ 26 + HO ₂	UR17 + OH + RO ₂ 8 + RO ₂ T	k_{94}	
197	RO ₂ 27 + NO	CF(27) AP8 + CF(28) NO ₂ + CF(28) HO ₂ + CF(28) UR7	k_{188}	
198	RO ₂ 27 + RO ₂ T	HO ₂ + UR7 + RO ₂ T + O ₂	k_{96}	
199	RO ₂ 27 + HO ₂	HO ₂ + OH + UR7	k_{94}	
200	RO ₂ 28 + NO	2 NO ₂ + UR7	k_{188}	
201	RO ₂ 28 + RO ₂ T	NO ₂ + UR7 + RO ₂ T + O ₂	k_{96}	
202	RO ₂ 28 + HO ₂	NO ₂ + OH + UR7	k_{94}	
203	RO ₂ 29 + NO	CF(29) AP9 + CF(30) NO ₂ + CF(30) RO ₂ 40 + CF(30) RO ₂ T	k_{173}	
204	RO ₂ 29 + RO ₂ T	RO ₂ 40 + 2 RO ₂ T + O ₂	k_{96}	
205	RO ₂ 29 + HO ₂	OH + RO ₂ 40 + RO ₂ T	k_{94}	
206	RO ₂ 40 + NO	NO ₂ + RPR8 + RO ₂ 8 + RO ₂ T	k_{173}	
207	RO ₂ 40 + RO ₂ T	RPR8 + RO ₂ 8 + 2 RO ₂ T + O ₂	k_{96}	
208	RO ₂ 40 + HO ₂	OH + RPR8 + RO ₂ 8 + RO ₂ T	k_{94}	
209	RO ₂ 30 + NO	NO ₂ + UR18 + RO ₂ 8 + RO ₂ T	k_{188}	
210	RO ₂ 30 + RO ₂ T	UR18 + RO ₂ 8 + 2 RO ₂ T + O ₂	k_{96}	
211	RO ₂ 30 + HO ₂	OH + UR18 + RO ₂ 8 + RO ₂ T	k_{94}	
212	RO ₂ 31 + NO	CF(31) AP10 + CF(32) NO ₂ + CF(32) HO ₂ + CF(32) UR19	2.78E+5/TEMP*EXP (180.2/TEMP)	11
213	RO ₂ 31 + RO ₂ T	HO ₂ + UR19 + RO ₂ T + O ₂	k_{96}	

Table 5.2. (continued) Reactions contained in the Caltech Atmospheric Chemistry

Mechanism.

Reaction	Reactants	Products	Rate Constants (ppm-min units)*	References, Comments
214	RO ₂ 31 + HO ₂	HO ₂ + OH + UR19	k_{94}	
215	RO ₂ 32 + NO	CF(33) AP11 + CF(34) NO ₂ + CF(34) RO ₂ 41 + CF(34) RO ₂ T	1.41E+5/TEMP*EXP (180.2/TEMP)	11
216	RO ₂ 32 + RO ₂ T	RO ₂ 41 + 2 RO ₂ T + O ₂	k_{96}	
217	RO ₂ 32 + HO ₂	OH + RO ₂ 41 + RO ₂ T	k_{94}	
218	RO ₂ 41 + NO	CF(35) AP12 + CF(36) NO ₂ + CF(36) HO ₂ + CF(36) UR20	k_{215}	
219	RO ₂ 41 + RO ₂ T	HO ₂ + UR20 + RO ₂ T + O ₂	k_{96}	
220	RO ₂ 41 + HO ₂	HO ₂ + OH + UR20	k_{94}	
221	RO ₂ 33	RO ₂ 42 + RO ₂ T	9.84E+43/TEMP ^11.4*EXP (-9460/TEMP)	13
222	RO ₂ 33 + NO	NO ₂ + HO ₂ + RPR9	k_{167}	
223	RO ₂ 33 + RO ₂ T	HO ₂ + RPR9 + RO ₂ T + O ₂	k_{96}	
224	RO ₂ 33 + HO ₂	HO ₂ + OH + RPR9	k_{94}	
225	RO ₂ 42 + NO	NO ₂ + HO ₂ + RP10 + MGLY	k_{167}	
226	RO ₂ 42 + RO ₂ T	HO ₂ + RP10 + MGLY + O ₂ + RO ₂ T	k_{96}	
227	RO ₂ 42 + HO ₂	HO ₂ + OH + RP10 + MGLY	k_{94}	
228	RO ₂ 34	RO ₂ 43 + RO ₂ T	k_{221}	
229	RO ₂ 34 + NO	NO ₂ + HO ₂ + RP11	k_{173}	
230	RO ₂ 34 + RO ₂ T	HO ₂ + RP11 + RO ₂ T + O ₂	k_{96}	
231	RO ₂ 34 + HO ₂	HO ₂ + OH + RP11	k_{94}	
232	RO ₂ 43 + NO	NO ₂ + HO ₂ + RP10 + MGLY	k_{173}	
233	RO ₂ 43 + RO ₂ T	HO ₂ + RP10 + MGLY + O ₂ + RO ₂ T	k_{96}	

Table 5.2. (continued) Reactions contained in the Caltech Atmospheric Chemistry

Mechanism.

Reaction	Reactants	Products	Rate Constants (ppm-min units) [*]	References, Comments
234	RO ₂ 43 + HO ₂	HO ₂ + OH + RP10 + MGLY	<i>k</i> ₉₄	
235	RO ₂ 35	RO ₂ 44 + RO ₂ T	<i>k</i> ₂₂₁	
236	RO ₂ 35 + NO	NO ₂ + HO ₂ + RP11	<i>k</i> ₁₈₈	
237	RO ₂ 35 + RO ₂ T	HO ₂ + RP11 + RO ₂ T + O ₂	<i>k</i> ₉₆	
238	RO ₂ 35 + HO ₂	HO ₂ + OH + RP11	<i>k</i> ₉₄	
239	RO ₂ 44 + NO	NO ₂ + HO ₂ + RP10 + MGLY	<i>k</i> ₁₈₈	
240	RO ₂ 44 + RO ₂ T	HO ₂ + RP10 + MGLY + O ₂ + RO ₂ T	<i>k</i> ₉₆	
241	RO ₂ 44 + HO ₂	HO ₂ + OH + RP10 + MGLY	<i>k</i> ₉₄	
242	RO ₂ 36	RO ₂ 45 + RO ₂ T	<i>k</i> ₂₂₁	
243	RO ₂ 36 + NO	NO ₂ + HO ₂ + RP12	<i>k</i> ₁₆₇	
244	RO ₂ 36 + RO ₂ T	HO ₂ + RP12 + RO ₂ T + O ₂	<i>k</i> ₉₆	
245	RO ₂ 36 + HO ₂	HO ₂ + OH + RP12	<i>k</i> ₉₄	
246	RO ₂ 45 + NO	NO ₂ + HO ₂ + RP10 + MGLY	<i>k</i> ₁₆₇	
247	RO ₂ 45 + RO ₂ T	HO ₂ + RP10 + MGLY + O ₂ + RO ₂ T	<i>k</i> ₉₆	
248	RO ₂ 45 + HO ₂	HO ₂ + OH + RP10 + MGLY	<i>k</i> ₉₄	
249	RO ₂ 37	RO ₂ 46 + RO ₂ T	<i>k</i> ₂₂₁	
250	RO ₂ 37 + NO	NO ₂ + HO ₂ + RP13	<i>k</i> ₁₆₇	
251	RO ₂ 37 + RO ₂ T	HO ₂ + RP13 + RO ₂ T + O ₂	<i>k</i> ₉₆	
252	RO ₂ 37 + HO ₂	HO ₂ + OH + RP13	<i>k</i> ₉₄	
253	RO ₂ 46 + NO	NO ₂ + HO ₂ + RP10 + MGLY	<i>k</i> ₁₆₇	
254	RO ₂ 46 + RO ₂ T	HO ₂ + RP10 + MGLY + O ₂ + RO ₂ T	<i>k</i> ₉₆	
255	RO ₂ 46 + HO ₂	HO ₂ + OH + RP10 + MGLY	<i>k</i> ₉₄	
256	RO ₂ 38	RO ₂ 47 + RO ₂ T	<i>k</i> ₂₂₁	
257	RO ₂ 38 + NO	NO ₂ + HO ₂ + RP14	<i>k</i> ₂₁₂	

Table 5.2. (continued) Reactions contained in the Caltech Atmospheric Chemistry

Mechanism.

Reaction	Reactants	Products	Rate Constants (ppm-min units) [*]	References, Comments
258	RO ₂ 38 + RO ₂ T	HO ₂ + RP14 + RO ₂ T + O ₂	k_{96}	
259	RO ₂ 38 + HO ₂	HO ₂ + OH + RP14	k_{94}	
260	RO ₂ 47 + NO	NO ₂ + HO ₂ + RP15 + MGLY	k_{212}	
261	RO ₂ 47 + RO ₂ T	HO ₂ + RP15 + MGLY + O ₂ + RO ₂ T	k_{96}	
262	RO ₂ 47 + HO ₂	HO ₂ + OH + RP15 + MGLY	k_{94}	
263	MGLY + OH	RO ₂ 48 + RO ₂ T + H ₂ O	7.57E+6/TEMP	5
264	MGLY + NO ₃	HNO ₃ + RO ₂ 48 + RO ₂ T	6.16E+5/TEMP*EXP (-1897.3/TEMP)	2
265	MGLY + <i>hν</i>	CO + HO ₂ + RO ₂ 8 + RO ₂ T	See Table 5.3	1
266	RO ₂ 48 + NO	NO ₂ + CO ₂ + RO ₂ 8 + RO ₂ T	k_{125}	
267	RO ₂ 48 + NO ₂ + M	PAN4 + M	k_{126}	
268	PAN4	NO ₂ + RO ₂ 48 + RO ₂ T	k_{127}	
269	RO ₂ 48 + HO ₂	O ₃ + UR21	k_{94}	
270	RO ₂ 48 + RO ₂ T	CO ₂ + RO ₂ 8 + 2 RO ₂ T + O ₂	k_{96}	
271	MVK + OH	RO ₂ 49 + RO ₂ T	1.82E+6/TEMP*EXP (452.9/TEMP)	2
272	MVK + O ₃	0.56 CO + 0.2 CO ₂ + 0.28 HO ₂ + 0.36 OH + 0.5 MGLY + 0.5 HCHO + 0.12 ACID + 0.1 ALD2 + 0.12 UR21 + 0.28 RO ₂ 8 + 0.28 RO ₂ T + 0.2 H ₂ O	3.3E+2/TEMP*EXP (-1519.9/TEMP)	2
273	MVK + O	0.85 KETL + 0.15 RO ₂ 4 + 0.15 RO ₂ 8 + 0.3 RO ₂ T	1.9E+6/TEMP	2

Table 5.2. (continued) Reactions contained in the Caltech Atmospheric Chemistry

Mechanism.

Reaction	Reactants	Products	Rate Constants (ppm-min units)*	References, Comments
274	RO ₂ 49 + NO	NO ₂ + HO ₂ + MGLY + HCHO	k_{113}	
275	RO ₂ 49 + RO ₂ T	HO ₂ + MGLY + HCHO + RO ₂ T + O ₂	k_{96}	
276	RO ₂ 49 + HO ₂	HO ₂ + OH + MGLY + HCHO	k_{94}	
277	MCR + OH	CF(46) RO ₂ 50 + CF(46) H ₂ O + CF(47) RO ₂ 51 + RO ₂ T	8.18E+6/TEMP*EXP (176.1/TEMP)	2
278	MCR + NO ₃	CF(46) HNO ₃ + CF(46) RO ₂ 50 + CF(47) RO ₂ 52 + RO ₂ T	6.6E+5/TEMP*EXP (-1726.2/TEMP)	2
279	MCR + O ₃	0.41 CO + 0.41 HO ₂ + 0.82 OH + 0.5 HCHO + 0.59 MGLY + 0.09 ACID + 0.41 RO ₂ 53 + 0.41 RO ₂ T	5.98E+2/TEMP*EXP (-2113.7/TEMP)	2
280	MCR + O	0.15 CO + 0.15 HO ₂ + 0.85 ALD2 + 0.15 RO ₂ 7 + 0.15 RO ₂ T	2.79E+6/TEMP	2
281	RO ₂ 50 + NO	CO ₂ + NO ₂ + RO ₂ 14 + RO ₂ T	k_{125}	
282	RO ₂ 50 + NO ₂	PAN5 + M + M	k_{126}	
283	PAN5	NO ₂ + RO ₂ 50 + RO ₂ T	k_{127}	
284	RO ₂ 50 + HO ₂	O ₃ + 0.5 ACID + 0.5 OLEL	k_{94}	
285	RO ₂ 50 + RO ₂ T	CO ₂ + RO ₂ 14 + 2 RO ₂ T + O ₂	k_{96}	
286	RO ₂ 51 + NO	NO ₂ + HO ₂ + HCHO + MGLY	k_{113}	
287	RO ₂ 51 + HO ₂	HO ₂ + HCHO + MGLY + RO ₂ T + O ₂	k_{94}	
288	RO ₂ 51 + RO ₂ T	HO ₂ + OH + MGLY + HCHO	k_{96}	
289	RO ₂ 52 + NO	2 NO ₂ + MGLY + HCHO	k_{113}	

Table 5.2. (continued) Reactions contained in the Caltech Atmospheric Chemistry

Mechanism.

Reaction	Reactants	Products	Rate Constants (ppm-min units) [*]	References, Comments
290	$\text{RO}_252 + \text{HO}_2$	$\text{NO}_2 + \text{MGLY} + \text{HCHO} + \text{RO}_2\text{T} + \text{O}_2$	k_{94}	
291	$\text{RO}_252 + \text{RO}_2\text{T}$	$\text{NO}_2 + \text{OH} + \text{MGLY} + \text{HCHO}$	k_{96}	
292	$\text{RO}_253 + \text{NO}$	$\text{NO}_2 + \text{HCHO} + \text{RO}_254 + \text{RO}_2\text{T}$	k_{122}	
293	$\text{RO}_253 + \text{HO}_2$	$\text{HCHO} + \text{RO}_254 + 2 \text{RO}_2\text{T} + \text{O}_2$	k_{94}	
294	$\text{RO}_253 + \text{RO}_2\text{T}$	$\text{OH} + \text{HCHO} + \text{RO}_254 + \text{RO}_2\text{T}$	k_{96}	
295	$\text{RO}_254 + \text{NO}$	$\text{CO}_2 + \text{CO} + \text{NO}_2 + \text{HO}_2$	k_{125}	
296	$\text{RO}_254 + \text{NO}_2$ + M	PAN6 + M	k_{126}	
297	PAN6	$\text{NO}_2 + \text{RO}_254 + \text{NO}_2$	k_{127}	
298	$\text{RO}_254 + \text{HO}_2$	$\text{O}_3 + \text{RP16}$	k_{94}	
299	$\text{RO}_254 + \text{RO}_2\text{T}$	$\text{CO}_2 + \text{CO} + \text{HO}_2 + \text{RO}_2\text{T} + \text{O}_2$	k_{96}	
300	RPR1 + OH	$\text{RO}_255 + \text{RO}_2\text{T} + \text{H}_2\text{O}$	See Table 5.6	8
301	RPR1 + NO_3	$\text{HNO}_3 + \text{RO}_255 + \text{RO}_2\text{T}$	$k_{61} * k_{300} / k_{60}$	Estimated k
302	RPR1 + $h\nu$	$\text{CO} + \text{HO}_2 + \text{RO}_220 + \text{RO}_2\text{T}$	See Table 3	1
303	$\text{RO}_255 + \text{NO}$	$\text{NO}_2 + \text{CO}_2 + \text{RO}_220 + \text{RO}_2\text{T}$	k_{125}	
304	$\text{RO}_255 + \text{NO}_2$ + M	PAN7 + M	k_{126}	
305	PAN7	$\text{NO}_2 + \text{RO}_255 + \text{RO}_2\text{T}$	k_{127}	
306	$\text{RO}_255 + \text{HO}_2$	$\text{O}_3 + \text{UR1}$	k_{94}	
307	$\text{RO}_255 + \text{RO}_2\text{T}$	$\text{CO}_2 + \text{RO}_220 + \text{RO}_2\text{T} + \text{O}_2$	k_{96}	
308	RPR2 + OH	$\text{O}_3 - \text{HO}_2 + \text{UR2} + \text{H}_2\text{O}$	k_{82}	
309	RPR3 + OH	$\text{RO}_256 + \text{RO}_2\text{T} + \text{H}_2\text{O}$	See Table 5.6	8
310	RPR3 + NO_3	$\text{HNO}_3 + \text{RO}_256 + \text{RO}_2\text{T}$	$k_{61} * k_{300} / k_{60}$	Estimated k

Table 5.2. (continued) Reactions contained in the Caltech Atmospheric Chemistry

Mechanism.

Reaction	Reactants	Products	Rate Constants (ppm-min units) [*]	References, Comments
311	RPR3 + <i>hν</i>	CO + 2 HO ₂ + UR4	See Table 5.3	1
312	RO ₂ 56 + NO	NO ₂ + CO ₂ + HO ₂ + UR4	<i>k</i> ₁₂₅	
313	RO ₂ 56 + NO ₂ + M	PAN8 + M	<i>k</i> ₁₂₆	
314	PAN8	NO ₂ + RO ₂ 56 + RO ₂ T	<i>k</i> ₁₂₇	
315	RO ₂ 56 + HO ₂	O ₃ + UR3	<i>k</i> ₉₄	
316	RO ₂ 56 + RO ₂ T	CO ₂ + HO ₂ + UR4 + RO ₂ T + O ₂	<i>k</i> ₉₆	
317	RPR4 + NO ₃	HNO ₃ + RAD8	1.66E+6/TEMP	2
318	RAD8 + NO ₂	UR22 + H ₂ O	1.01E+7/TEMP*EXP (151.0/TEMP)	2
319	RPR5 + OH	O ₃ - HO ₂ + UR14 + H ₂ O	<i>k</i> ₈₂	
320	RPR6 + OH	O ₃ - HO ₂ + RPR7 + H ₂ O	<i>k</i> ₈₂	
321	RPR7 + OH	O ₃ - HO ₂ + ADAC + H ₂ O	<i>k</i> ₈₂	
322	RPR8 + OH	RO ₂ 57 + RO ₂ T + H ₂ O	See Table 5.6	8
323	RPR8 + NO ₃	HNO ₃ + RO ₂ 57 + RO ₂ T	<i>k</i> ₆₁ * <i>k</i> ₃₂₂ / <i>k</i> ₆₀	Estimated <i>k</i>
324	RPR8 + <i>hν</i>	CO + HO ₂ + RO ₂ 9 + RO ₂ T	See Table 5.3	1
325	RPR8 + <i>hν</i>	HO ₂ + RO ₂ 57 + RO ₂ T	See Table 5.3	1
326	RO ₂ 57 + NO	NO ₂ + CO ₂ + RO ₂ 9 + RO ₂ T	<i>k</i> ₁₂₅	
327	RO ₂ 57 + NO ₂ + M	PAN9 + M	<i>k</i> ₁₂₆	
328	PAN9	NO ₂ + RO ₂ 57 + RO ₂ T	<i>k</i> ₁₂₇	
329	RO ₂ 57 + HO ₂	UR23 + O ₃	<i>k</i> ₉₄	
330	RO ₂ 57 + RO ₂ T	CO ₂ + RO ₂ 9 + 2 RO ₂ T + O ₂	<i>k</i> ₉₆	
331	RPR9 + OH	O ₃ - HO ₂ + RP17 + H ₂ O	See Table 5.6	8

Table 5.2. (continued) Reactions contained in the Caltech Atmospheric Chemistry

Mechanism.

Reaction	Reactants	Products	Rate Constants (ppm-min units) [*]	References, Comments
332	RP10 + OH	HO ₂ + UR24 + H ₂ O	See Table 5.6	8
333	RP10 + <i>hν</i>	UR25	See Table 5.3	1
334	RP11 + OH	O ₃ - HO ₂ + UR26 + H ₂ O	See Table 5.6	8
335	RP12 + OH	O ₃ - HO ₂ + RP13 + H ₂ O	See Table 5.6	8
336	RP13 + OH	O ₃ - HO ₂ + RP18 + H ₂ O	See Table 5.6	8
337	RP14 + OH	O ₃ - HO ₂ + RP19 + H ₂ O	See Table 5.6	8
338	RP15 + OH	O ₃ - HO ₂ + UR27 + H ₂ O	See Table 5.6	8
339	RP16 + OH	RO ₂ 58 + RO ₂ T + H ₂ O	<i>k</i> ₂₆₃	
340	RP16 + NO ₃	HNO ₃ + RO ₂ 58 + RO ₂ T	<i>k</i> ₂₆₄	
341	RP16 + <i>hν</i>	2 CO + OH + HO ₂	See Table 5.3	1
342	RO ₂ 58 + NO	CO + CO ₂ + NO ₂ + OH	<i>k</i> ₁₂₅	
343	RO ₂ 58 + NO ₂ + M	PN10 + M	<i>k</i> ₁₂₆	
344	PN10	NO ₂ + RO ₂ 58 + RO ₂ T	<i>k</i> ₁₂₇	
345	RO ₂ 58 + HO ₂	O ₃ + UR28	<i>k</i> ₉₄	
346	RO ₂ 58 + RO ₂ T	CO + CO ₂ + OH + RO ₂ T + O ₂	<i>k</i> ₉₆	
347	RP17 + OH	O ₃ - HO ₂ + UR29 + H ₂ O	See Table 5.6	8
348	RP18 + OH	O ₃ - HO ₂ + UR30 + H ₂ O	See Table 5.6	8
349	RP19 + OH	O ₃ - HO ₂ + UR31 + H ₂ O	See Table 5.6	8
350	AP1 + OH	NO ₂ + RPR2 + H ₂ O	See Table 5.6	8
351	AP2 + OH	NO ₂ + UR16 + H ₂ O	See Table 5.6	8
352	AP3 + OH	NO ₂ + UR32 + H ₂ O	See Table 5.6	8
353	AP4 + OH	NO ₂ + ARAL + H ₂ O	See Table 5.6	8
354	AP5 + OH	NO ₂ + RPR6 + H ₂ O	See Table 5.6	8

Table 5.2. (continued) Reactions contained in the Caltech Atmospheric Chemistry Mechanism.

Reaction	Reactants	Products	Rate Constants (ppm-min units) [*]	References, Comments
355	AP6 + OH	NO ₂ + RPR7 + H ₂ O	See Table 5.6	8
356	AP7 + OH	NO ₂ + RPR3 + H ₂ O	See Table 5.6	8
357	AP8 + OH	NO ₂ + UR7 + H ₂ O	See Table 5.6	8
358	AP9 + OH	NO ₂ + UR33 + H ₂ O	See Table 5.6	8
359	AP10 + OH	NO ₂ + UR19 + H ₂ O	See Table 5.6	8
360	AP11 + OH	NO ₂ + UR34 + H ₂ O	See Table 5.6	8
361	AP12 + OH	NO ₂ + UR20 + H ₂ O	See Table 5.6	8

^{*}If reaction rates depend on concentrations of O₂, these rate constants already take this into account by being multiplied by 2.1E+5. The CF(*i*) factors represent product stoichiometric yields estimated or determined kinetically [*Carter and Atkinson et al.*, 1989; *Japar et al.*, 1990; *Kwok and Atkinson et al.*, 1995]. Rate constant references: 1. *Harley et al.* [1993]/*Lurmann et al.* [1987]; 2. *Carter* [1997, 1999]; 3. *Dransfield et al.* [1999]; 4. *Atkinson* [1994]; 5. *Atkinson* [1997]; 6. *Atkinson* [1990]; 7. *Japar et al.* [1990]; 8. *Kwok and Atkinson* [1995]; 9. *Hoffmann et al.* [1997]; 10. *Goumri et. al.* [1992]; 11. *Jenkin et al.* [1997]; 12. *Stockwell et al.* [1997]; 13. *Lay et al.* [1996].

Table 5.3. Photolysis rate constants*.

Photolyzed Species (Reaction #)	Products	Typical Value of j_i (min ⁻¹)	Comments
NO ₂ (1)	NO + O	4.01E-1	
NO ₃ (13)	NO + O ₂	9.90E-1	
NO ₃ (14)	NO ₂ + O	8.7	
O ₃ (15)	O + O ₂	2.34E-2	
O ₃ (16)	OSD + O ₂	9.96E-4	
HONO (20)	0.9 NO + 0.1 NO ₂ + 0.1 HO ₂ + 0.9 OH	7.77E-2	
H ₂ O ₂ (36)	2 OH	3.04E-4	
HCHO (44)	HO ₂ + CO	1.18E-3	
HCHO (45)	CO + H ₂	2.03E-3	
ALD2 (59)	CO + HO ₂ + RO ₂ 5 + RO ₂ T	2.67E-4	
KETL (63)	RO ₂ 5 + RO ₂ 8 + 2 RO ₂ T	5.62E-5	
KETH (71)	RO ₂ 5 + RO ₂ 8 + 2 RO ₂ T	5.62E-5	assumed equal to j_{KETL}
MGLY (265)	CO + HO ₂ + RO ₂ 8 + RO ₂ T	7.89E-3	
RPR1 (302)	CO + HO ₂ + RO ₂ 20 + RO ₂ T	2.67E-4	assumed equal to j_{ALD2}
RPR3 (311)	CO + 2 HO ₂ + UR4	2.67E-4	assumed equal to j_{ALD2}
RPR8 (324)	CO + HO ₂ + RO ₂ 9 + RO ₂ T	2.67E-4	assumed equal to j_{ALD2}
RPR8 (325)	HO ₂ + RO ₂ 57 + RO ₂ T	2.67E-4	assumed equal to j_{ALD2}
RP10 (333)	UR25	2.67E-4	assumed equal to j_{ALD2}
RP16 (341)	CO + OH + HO ₂	7.89E-3	assumed equal to j_{MGLY}

*Photolysis rate constants as a function of zenith angle are calculated by integrating over ultraviolet wavelengths the product (actinic irradiance * absorption cross section * quantum yield).

Table 5.4. Three-body kinetics rate constant calculations*.

Reaction	k_o^{300}	n	k_{inf}^{300}	m	F
4	9.0E-32	2	2.2E-11	0	0.8
9	2.8E-30	3.5	2.0E-12	0.2	0.45
10	In equilibrium with reaction (9)				
19	7.0E-31	2.6	3.6E-11	0.1	0.6
22 [†]	2.85E-30	2.67	3.13E-11	0	See below
27	1.8E-31	3.2	4.7E-12	0	0.6
28	In equilibrium with reaction (27)				
35	4.1E-31	3.3	2.0E-12	0	0.45
126	9.7E-29	5.6	9.3E-12	1.5	0.6
127	In equilibrium with reaction (126)				

*Three-body rate constants at temperature T (K) and pressure corresponding to $[M]$ (molecule cm^{-3}) are found via the following formulae:

$$k_o(T) = k_o^{300}(T) \left(\frac{T}{300} \right)^{-n} (\text{cm}^6 \text{ molecule}^{-2} \text{ s}^{-1})$$

$$k_{\text{inf}}(T) = k_{\text{inf}}^{300}(T) \left(\frac{T}{300} \right)^{-m} (\text{cm}^3 \text{ molecule}^{-1} \text{ s}^{-1})$$

$$k(T, z) = \left(\frac{k_o(T)[M]}{1 + (k_o(T)[M]/k_{\text{inf}}(T))} \right)^{F^{(1 + \log_{10}(k_o(T)[M]/k_{\text{inf}}(T)))^{-1}}} (\text{cm}^3 \text{ molecule}^{-1} \text{ s}^{-1})$$

To convert to $\text{ppm}^{-1} \text{ min}^{-1}$ units, multiply by $(4.4E+17/T)$

[†]The rate constant expression for reaction 22 has small correction factors incorporated into it. It is found as in *Dransfield et al. [1999]*.

Table 5.5. Other rate constant calculations.

Reaction	Expression*	k_1	k_2	k_3
23	a	7.2E-15 *EXP(785.1/TEMP)	4.1E-16 *EXP(1439.4/TEMP)	1.9E-33 *EXP(724.7/TEMP)
24	b	1.3E-13	3.19E-33	-
31	b	2.2E-13 *EXP(598.9/TEMP)	1.85E-33 *EXP(981.4/TEMP)	-
32 [†]	b	3.08E-34 *EXP(2798.2/TEMP)	2.59E-54 *EXP(3180.7/TEMP)	-

*Three-body rate constants at temperature TEMP (K) and pressure corresponding to $[M]$ (molecule cm^{-3}) are found via the following formulae:

a) $k (\text{cm}^3 \text{ molecule}^{-1} \text{ s}^{-1}) = k_1 + k_2[M]$ or b) $k (\text{cm}^3 \text{ molecule}^{-1} \text{ s}^{-1}) = k_1 + k_3[M](1 + k_3[M]/k_2)$

[†]Reaction 32 is third order.

To convert to $\text{ppm}^{-1} \text{ min}^{-1}$ units, multiply by $(4.4\text{E}+17/\text{TEMP})$; to convert to $\text{ppm}^{-2} \text{ min}^{-1}$, multiply by $(3.23\text{E}+33/\text{TEMP}^2)$.

Table 5.6. Hydroxyl radical rate constants calculated using a structure-reactivity relationship [Kwok and Atkinson, 1995]. *See below for a simple example calculation.

Reaction	k (ppm ⁻¹ min ⁻¹) at 300 K	Reaction	k (ppm ⁻¹ min ⁻¹) at 300 K
69 (ALCH)	1.88E+4	338 (RP15)	1.91E+4
70 (KETH)	7.54E+3	347 (RP17)	3.22E+5
73 (AROO)	3.32E+5	348 (RP18)	2.89E+5
74 (OLEH)	5.09E+4	349 (RP19)	1.96E+5
78 (ALKM)	1.51E+4	350 (AP1)	3.23E+5
80 (AROH)	2.23E+4	351 (AP2)	7.96E+3
83 (ARAC)	1.55E+3	352 (AP3)	1.13E+4
93 (ALKH)	2.89E+4	353 (AP4)	4.85E+4
300 (RPR1)	5.19E+4	354 (AP5)	1.94E+4
309 (RPR3)	6.22E+4	355 (AP6)	2.05E+3
322 (RPR8)	1.68E+5	356 (AP7)	4.47E+4
331 (RPR9)	3.54E+5	357 (AP8)	1.51E+5
332 (RP10)	1.61E+5	358 (AP9)	1.33E+5
334 (RP11)	2.88E+5	359 (AP10)	1.14E+5
335 (RP12)	3.53E+5	360 (AP11)	2.76E+4
336 (RP13)	3.21E+5	361 (AP12)	4.07E+4
337 (RP14)	2.13E+5		

*As shown in Kwok and Atkinson [1995], the rate constant for OH oxidation of an organic species is dependent on the number and type of structural components and the location of these groups relative to other groups. For example, ALKH is represented by *n*-hexadecane. There are three types of structural components associated with this molecule: -CH₃ positioned next to -CH₂- (2), -CH₂- positioned between -CH₃ and -CH₂- (2), and -CH₂- positioned between other -CH₂- (14). The rate constant of ALKH is found from $k_{ALKH} = 2k_{CH_3}f_{CH_2} + 2k_{CH_2}f_{CH_3}f_{CH_2} + 14k_{CH_2}f_{CH_2}^2$ where k_i represents a rate constant for group *i* and f_i represents a temperature dependent substituent factor. In this case, $k_{CH_3} = 4.49 \times 10^{-18} T^2 e^{-320/T}$ (cm³ molecule⁻¹ s⁻¹), $k_{CH_2} = 4.50 \times 10^{-18} T^2 e^{-253/T}$ (cm³ molecule⁻¹ s⁻¹), $f_i = e^{E_i/T}$ (dimensionless), $E_{CH_3} = 0$ (K), and $E_{CH_2} = 61.69$ (K). The parameters for k_i and f_i for unsaturated bonds and most functional groups also exist. To convert to ppm⁻¹ min⁻¹ units, multiply by (4.4E+17/T).

Table 5.7. Emissions summary in 10^3 kg/day used in CIT for August 27, 1987.

	NMHC*	NO _x	CO
On Road Vehicles	1229	678	4743
Other Mobile Sources	601	244	730
Ground-level Point Sources	379	123	139
Biogenic Emissions	110	--	--
Other Elevated Point Sources	6	60	8
Power Plants	1	33	6
Total	2326	1138	5626

*Non-methane hydrocarbons

Table 5.8. Upwind boundary condition concentrations (ppb).

Species	
CO	200
NO ₂	1
NO	1
HCHO	3
ALD2	5
KETL	4
O ₃	40
NMHC (ppb C)	100
Speciation*:	
ALKL	0.095
ETHE	0.017
OLEL	0.018
AROH	0.015
AROL	0.016

*Speciation in ppbv per ppb C of NMHC

Table 5.9. Statistical analysis of CACM performance on August 28 for O₃ and NO₂.

Statistical Measure	O ₃	NO ₂
Bias (pphm)	1.5	0.03
Normalized Bias (%)	21	13.8
σ of Residuals (pphm)	5.6	2.8
Gross Error (pphm)	4.0	2.1
Normalized Gross Error (%)	41	52

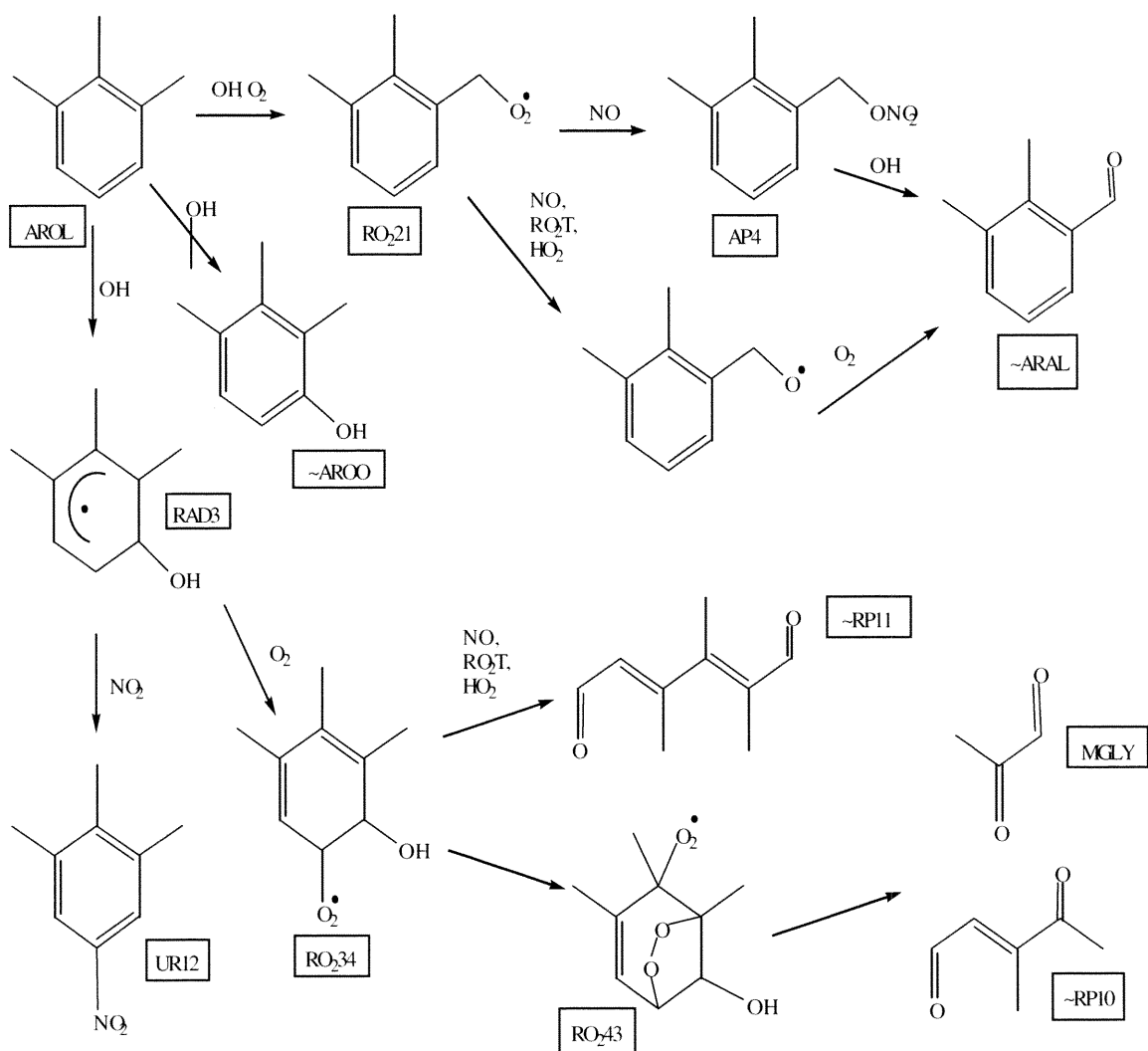


Figure 5.1. An illustrative example of a degradation mechanism for a parent hydrocarbon. That of AROL is shown.

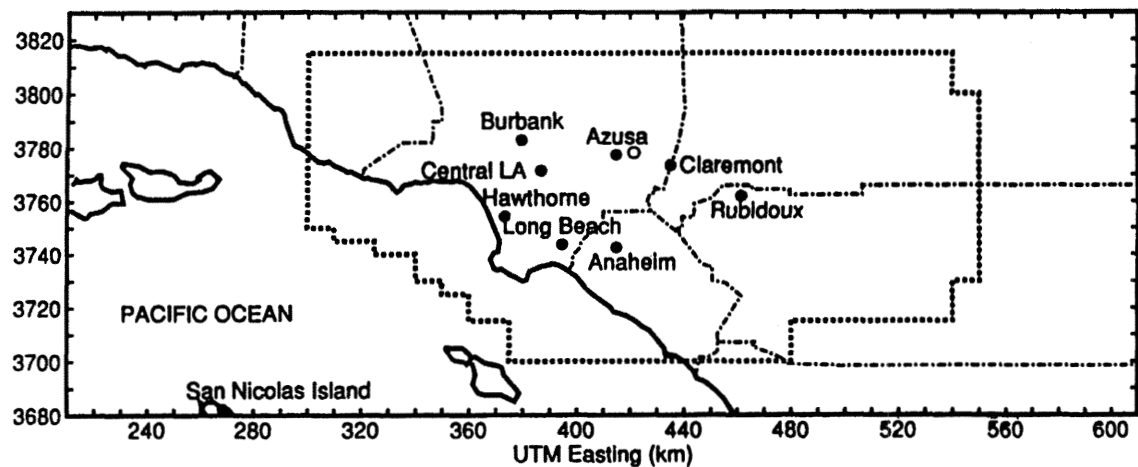


Figure 5.2. A map of the SOCAB. Cities for which data is given are indicated, as is downtown Los Angeles for reference.

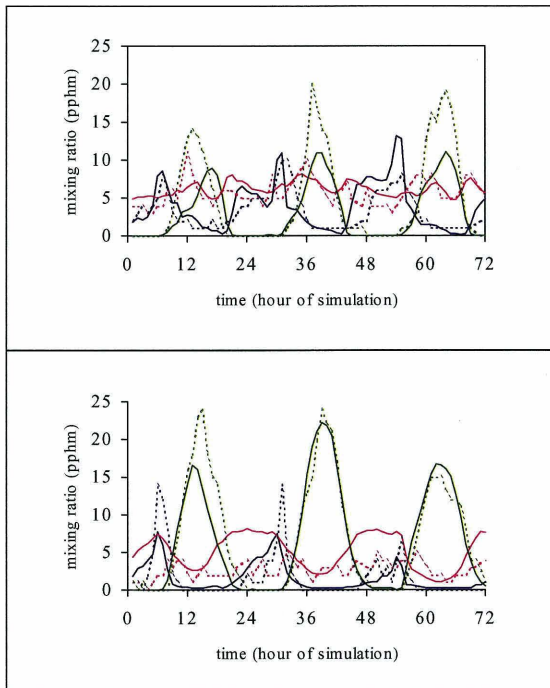


Figure 5.3

Figure 5.4

Figure 5.3. Simulated (solid) versus observed (dashed) NO (blue), NO₂ (red), and O₃ (green) mixing ratios for Pasadena for August 27-29, 1987.

Figure 5.4. Simulated (solid) versus observed (dashed) NO (blue), NO₂ (red), and O₃ (green) mixing ratios for Riverside for August 27-29, 1987.

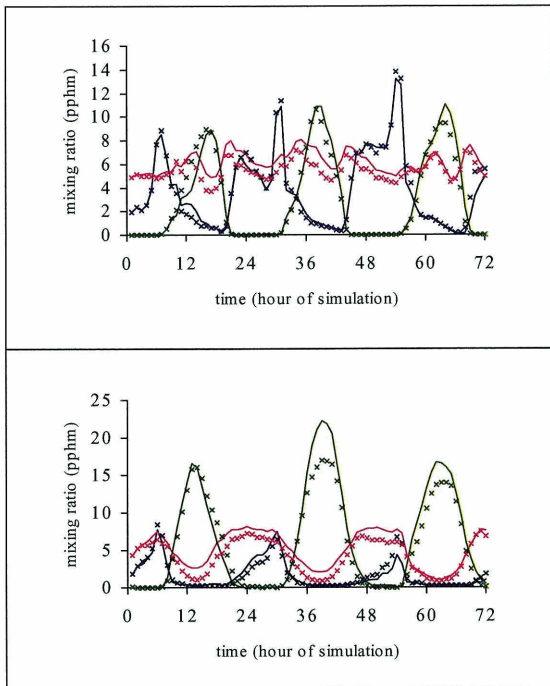


Figure 5.5

Figure 5.6

Figure 5.5. Mixing ratios simulated by CACM (solid) versus those simulated by the extended LCC mechanism (x) [Harley *et al.*, 1993] for Pasadena for August 27-29, 1987. See the caption for Figures 5.3 and 5.4 for color scheme explanation.

Figure 5.6. Mixing ratios simulated by CACM (solid) versus those simulated by the extended LCC mechanism (x) [Harley *et al.*, 1993] for Riverside for August 27-29, 1987. See the captions for Figure 5.3 and 5.4 for color scheme explanation.

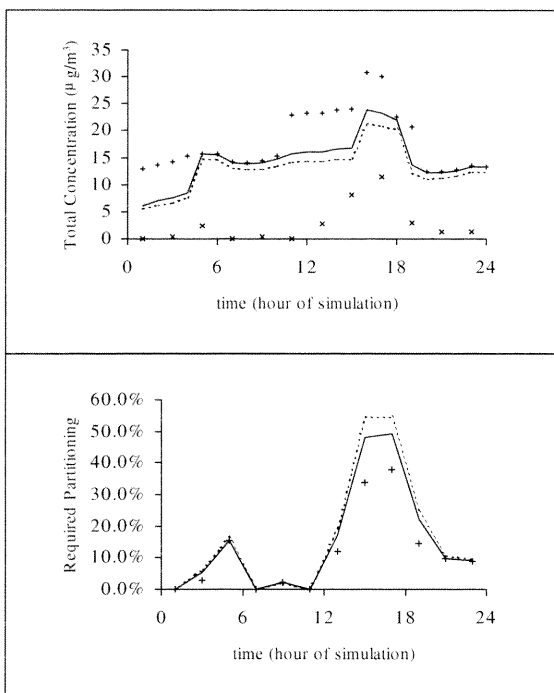


Figure 5.7

Figure 5.8

Figure 5.7. Comparison of total predicted SOA precursor concentration in the base case (solid) versus observed SOA data (x) in Claremont on August 28, 1987. The data of *Turpin and Huntzicker* [1995] were converted from $\mu\text{gC}/\text{m}^3$ to $\mu\text{g}/\text{m}^3$ by multiplying by a factor of 1.2. Also shown is the sensitivity of the total predicted SOA precursor concentrations to the aromatic radical isomerization rate constant and to the yield of direct conversion of certain aldehydes to acids. $b/2$ (+) represents the case in which the base case aromatic radical isomerization rate constant is divided by 2; acid (dashed) represents the case in which the yield of direct conversion of certain aldehydes to acids is divided by 2.

Figure 5.8. Percentage of the total SOA precursor concentration that must partition to account for the observations of *Turpin and Huntzicker* [1995] for the three cases investigated. Solid represents the base case, + represents the $b/2$ case, and dashed represents the acid case.

Chapter 6

Secondary Organic Aerosol: II. Thermodynamic Module for Gas/Particle Partitioning of Molecular Constituents

6.1. Introduction

In both urban and rural atmospheres, organic aerosol (OA) is a significant constituent of particulate matter (PM) [Stevens *et al.*, 1984; White and Macias, 1989; Penner, 1995; *United States Environmental Protection Agency*, 1996; Murphy *et al.*, 1998]. For example, in major cities such as Philadelphia, Los Angeles, and Chicago, OA has been observed to make up 14-44% by mass of the measured PM in summer [*United States Environmental Protection Agency*, 1996]. Understanding the sources and formation of OA is crucial to our ability to model the atmospheric aerosol. OA can be both primary (POA, emitted as aerosol) and secondary (SOA, formed *in situ* in the atmosphere as condensable vapors). Sources of POA include all types of combustion [Schauer, 1998; Schauer *et al.*, 1999ab]. SOA is formed as a result of the oxidation of both anthropogenic and biogenic organic species [Odum *et al.*, 1996, 1997; Hoffmann *et al.*, 1997; Griffin *et al.*, 1999]. Oxidation of these species leads to the formation of products that often contain a high degree of functionality, including hydroxy-, carbonyl, carboxy-, nitrooxy-, and nitro groups (See, for example, Atkinson, [1994, 1997] and references therein, Smith *et al.* [1999], and Yu *et al.* [1999]). Those products with sufficiently low vapor pressures will partition between the gas- and aerosol phases, forming SOA and contributing to the overall PM burden [Pankow, 1994]. Some of these products may also partition to the aerosol aqueous phase [Saxena and Hildemann, 1996].

Inorganic thermodynamic equilibrium models have reached a state where they are now incorporated in atmospheric models. (See, for example, Jacobson *et al.* [1997], Ansari and Pandis [1999], and Zhang *et al.* [2000] and references therein.) However, because of the large number of organic compounds in the atmosphere and because

methods to predict their thermodynamic properties in complex organic-water mixtures pose significant theoretical challenges, current gas-aerosol thermodynamic models for organic atmospheric species do not include the same level of detail as those for inorganic species. Experimentally based gas-particle distribution factors for complex mixtures generated by the photooxidation of aromatic and biogenic hydrocarbons are available [Odum *et al.*, 1996, 1997; Hoffmann *et al.*, 1997; Griffin *et al.*, 1999]. However, for atmospheric models one requires a fundamentally based thermodynamic model that predicts the phase partitioning of individual organic compounds between the gas phase and complex organic-inorganic-water mixtures. Such a model would afford a first-principles prediction of the amount of OA formed from secondary species in the atmosphere and is the subject of this paper.

This paper focuses on a module that predicts the equilibrium partitioning of SOA and that is designed for use in a three-dimensional atmospheric model. Concentrations of secondary organic oxidation products are predicted by a gas-phase chemical mechanism (Part I). The equilibrium partitioning module will be incorporated in a comprehensive gas- and particle-phase air quality model for simulations of a 1993 smog episode in the South Coast Air Basin of California (SOCAB). The following text first reviews the methods used previously to predict SOA in three-dimensional atmospheric models and then presents the new module developed to predict aerosol formation.

6.2 Review of Previous Techniques to Model SOA

The development of source-receptor relationships for secondary PM formation requires the use of three dimensional air quality models with comprehensive treatment of the relevant physical and chemical processes [Seigneur *et al.*, 1999]. Several models

have been developed that include some treatment of SOA formation [*Jacobson et al.*, 1997; *Lurmann et al.*, 1997; *Meng et al.*, 1998; *Sun and Wexler*, 1998; *Pai et al.*, 2000]. However, as discussed below, the approaches used to model SOA formation fail to provide a realistic treatment of the gas/partitioning processes over a wide range of conditions. On the other hand, detailed mechanisms for SOA formation have been developed but have been limited to chemical systems studied in smog chamber experiments [*Barthelme and Pryor*, 1999; *Kamens et al.*, 1999].

6.2.1 Fractional Aerosol Coefficient

The simplest method that attempts to account for the conversion of a given parent species from the gas phase to products in the particle phase via oxidation is based on the fractional aerosol coefficient (FAC). The FAC is defined as the ratio of the SOA formed from a parent organic to the initial amount of that parent species present in a chamber experiment [*Grosjean*, 1992]. Because the technique considers no kinetics, SOA can be treated as if it were emitted. There are a number of problems with the FAC method. Most importantly, it does not take into account the time needed to form SOA in the atmosphere. Also, concentrations of available oxidants, and, therefore, the amount of the parent species that reacts, are not treated explicitly. As a result, the FAC only apply to conditions for which they were derived. In addition, the FAC values do not take into account temperature, relative humidity, or initial particle concentrations. Thus, FAC values cannot provide realistic SOA estimates for air quality modeling and are not currently used in three-dimensional air quality models.

6.2.2 Fixed Aerosol Yield

A second method for estimating SOA formation based on the concentrations of precursors is to assume a fixed SOA yield for a given parent organic. In contrast to the FAC, this approach takes into account the time needed to form SOA and is defined as the amount of organic aerosol mass that forms per amount of the parent organic mass that reacts [Pandis *et al.*, 1992]. Thus, this method takes the reactivity of the parent organic and the availability of oxidants into account. The limitations associated with estimating SOA formation using this method are that there is no dependence of the yield on the existing particle phase, temperature, or relative humidity. In addition, measured yields for a given parent organic are highly variable because of changes in temperature and initial concentrations between experiments [Odum *et al.*, 1996, and references therein]. Given this variation, it is difficult to determine which experimentally determined yield is the most appropriate to use when conditions vary temporally and spatially and deviate significantly from smog chamber conditions.

6.2.3 Saturation of Oxidation Products

The fixed aerosol yield approach is generally used in conjunction with a gas/particle partitioning calculation based on saturation vapor pressure. It is assumed that one product condenses into the particle phase only when its saturation vapor pressure has been reached [Pandis *et al.*, 1992]. The amount of SOA from a given organic parent is thus defined as the difference between the amount of the product that forms and that product's saturation concentration. Attempts have been made to account for the dependence of the product's saturation vapor pressure on temperature through the

Clausius-Clapeyron equation and an estimated heat of vaporization that must be determined experimentally [*Strader et al.*, 1999]. Therefore, this approach has limited usefulness.

6.2.4 Dry Absorptive Partitioning

Recent experimental studies have shown that the formation of organic aerosol under dry conditions is best described by a dynamic equilibrium for species that exist in both the gas- and aerosol phases [*Odum et al.*, 1996, 1997; *Hoffmann et al.*, 1997; *Griffin et al.*, 1999]. Multiple products are formed in constant stoichiometric yield from the oxidation of a parent organic and then partition between an absorptive organic aerosol phase and the gas phase. Based on the premise of an ideal solution in the aerosol phase, the phase distribution of the products is determined by an experimentally-derived partitioning constant that is independent of the composition of the organic aerosol phase. Because of the equilibrium established between the gas and particle phases, species can partition to the absorbing organic phase at concentrations below their individual saturation vapor pressures [*Pankow*, 1994]. The partitioning of an SOA constituent is enhanced by the presence of additional SOA. It has been shown that two surrogate products (described by two mass-based stoichiometric parameters and two equilibrium partitioning coefficients) adequately represents observed aerosol formation from the complex mixture of products resulting from oxidation of a given parent organic [*Odum et al.*, 1996]. A problem with this technique is that these parameters are derived using smog chamber experimental data, which may not be extended to the atmosphere with complete accuracy. Smog chamber concentrations usually exceed ambient concentrations, and the effects of increased humidity and variable temperature have yet to be parameterized.

6.2.5 Henry's Law

One approach used to approximate the formation of SOA in models describing regional air quality is to assume that the secondary organic compounds associated with PM are absorbed only into an aqueous phase. This absorption is governed by Henry's law [Jacobson *et al.*, 1997; Aumont *et al.*, 2000] and activity coefficients of organic solutes are assumed to be unity. In this manner, only water-soluble organic species are accounted for; those that partition via condensation (absorption into an organic media or adsorption to aerosol surfaces) are ignored. Once the liquid water content (LWC) of an existing aerosol is assumed or calculated, the amount of OA present in the particle phase is calculated using Henry's law. If the Henry's law coefficient has not been measured, it can be derived using a group contribution method once the structure of the organic compound of interest is determined [Hine and Mookerjee, 1975; Suzuki *et al.*, 1992]. In addition to considering only those organics that are water-soluble, a limitation associated with this technique is that Henry's law, without activity correction, applies only for solutions that are dilute, which is not a relevant situation for ambient aerosols.

6.3 Partitioning Module Description

The numerous constituents of atmospheric aerosol undergo many processes (reaction, partitioning, etc.) that affect the behavior of the other species present (Figure 6.1). The purpose of this work is to describe a model to account for the phase- and composition distribution of these aerosol constituents. The major feature of this model is the distinction between those organic oxidation products that are considered hydrophilic (water-soluble organic compounds, WSOC) and those that are considered hydrophobic.

Because of the large number of atmospheric organic compounds that fall into each of these categories, it is necessary to choose surrogate compounds to represent species in each group.

Hydrophobic OA constituents partition via absorption into an organic phase (condensation due to low volatility). As shown in Figure 6.1, hydrophilic OA constituents interact with inorganic aerosol constituents such as nitrate, sulfate, ammonium, etc. Therefore, the module that has been developed to predict dissolution of WSOC is used in conjunction with an inorganic gas-aerosol equilibrium model such as SCAPE2 [Kim *et al.*, 1993; Meng *et al.*, 1995] or ISORROPIA [Nenes *et al.*, 1998]. These models are used to predict the equilibrium distribution of inorganic aerosol constituents and the corresponding aerosol LWC and pH. Figure 6.2 shows the ambient constituents, inorganic and organic, modeled in the hydrophilic module. Just as molecular and ion solutes are treated in SCAPE2 or ISORROPIA, the hydrophilic group of organic compounds is divided into two subgroups: those that are electrolytes and those that are molecular solutes. However, because experimental data describing the equilibrium in a mixed inorganic/organic/aqueous system do not exist, the inorganic and organic fractions are treated separately at the moment, united only through the LWC and pH of the aerosol. LWC is used as an iterative variable between the models of the two fractions.

6.3.1 Hydrophobic Module Description

Pankow [1994] gives a detailed derivation of expressions governing the partitioning of organic species between the gas- and particle phases. The partitioning of

compound i between the gas- and particle phases can be described by defining a partitioning coefficient, K_i ($\text{m}^3 \mu\text{g}^{-1}$),

$$K_i = \frac{A_i / \text{TSP}}{G_i} \quad (1)$$

where A_i ($\mu\text{g m}^{-3}$ air) is the concentration of the compound in the aerosol phase, G_i ($\mu\text{g m}^{-3}$ air) is the concentration of the compound in the gas phase, and TSP ($\mu\text{g m}^{-3}$ air) is the concentration of total suspended PM. This partitioning coefficient describes the equilibrium phase distribution of compound i when both adsorptive and absorptive partitioning occur. It has been demonstrated that absorption is the dominant mode of partitioning for organic species in the urban environment [Liang *et al.*, 1997]. To derive an expression for an equilibrium coefficient in which only absorptive partitioning is considered, only that aerosol mass that is part of an absorptive organic mixture is taken into account,

$$K_{i,om} = \frac{A_{i,om} / M_o}{G_i} \quad (2)$$

where the subscript om represents the absorbing organic phase, and M_o ($\mu\text{g m}^{-3}$ air) is the total concentration of the absorptive material, primary and secondary, in the om phase. M_o is assumed to be equal to the product of f_{om} and TSP, where f_{om} is the fraction of the PM that is part of the absorptive media.

To develop a thermodynamic expression for $K_{i,om}$, consider each of the three terms on which it depends functionally. First, the mass concentration of compound i in the om phase is simply given by

$$A_{i,om} = c_{i,om} M_i \quad (3)$$

where $c_{i,om}$ is the molar concentration of compound i in the om phase ($\mu\text{mol m}^{-3}$ air) and M_i is the molecular weight of species i (g mol^{-1}). Similarly, the gas-phase mass concentration of i is given by

$$G_i = c_{i,g} M_i \quad (4)$$

where $c_{i,g}$ is the molar concentration of compound i in the gas phase ($\mu\text{mol m}^{-3}$ air).

Finally, the mass concentration of the om phase is given by

$$M_o = c_{t,om} \overline{M}_{om} \quad (5)$$

where $c_{t,om}$ is the total molar concentration of the om phase ($\mu\text{mol m}^{-3}$ air) and \overline{M}_{om} is the average molecular weight (g mol^{-1}) of the om phase.

For a given air-parcel volume, the mole fraction of compound i in the om phase, x_i , is defined by

$$x_i = \frac{c_{i,om}}{c_{t,om}} \quad (6)$$

Assuming ideality, the molar concentration ($\mu\text{mol m}^{-3}$) of compound i in the gas phase is given by

$$c_{i,g} = \frac{py_i}{RT} \quad (7)$$

where p (atm) is the total pressure, y_i is the mole fraction of compound i in the gas phase, (the partial pressure of compound i in the gas phase, p_i , is defined as the product of p and y_i), R is the ideal gas constant ($0.82 \text{ m}^3 \text{ atm } \mu\text{mol}^{-1} \text{ K}^{-1}$), and T (K) is the absolute temperature. The final expression required is Raoult's law, which is derived from the fact that the activity of compound i in the gas phase must be equal to its activity in the absorptive om phase:

$$p_i = x_i \gamma^{RL}_i p_{L,i}^o \quad (8)$$

where γ^{RL}_i is the activity coefficient of species i in the om phase (pure solvent reference state) and $p_{L,i}^o$ (atm) is its sub-cooled liquid vapor pressure at the temperature of interest. Combining equations (2)-(8) yields a thermodynamic expression for the absorptive partitioning coefficient:

$$K_{i,om} = \frac{760RT}{10^6 M_{om} \gamma_i p_{L,i}^o} = \frac{A_{i,om}/f_{om} \text{TSP}}{G_i} = f(T, x_i) \quad (9)$$

It is seen in equation (9) that the absorptive partitioning of a compound between an *om* phase and the gas phase is strictly a function of temperature (explicitly and implicitly through vapor pressure) and the composition (through both the average molecular weight and the activity coefficient) of the *om* phase. Assuming vapor pressures are known or can be estimated for a given temperature and that activity coefficients can be estimated, e.g., by a group contribution method such as UNIFAC [Fredenslund *et al.*, 1977], it is possible to predict the fraction of each compound ($i = 1$ to n , where n is the number of condensable compounds) that resides in each phase. This is done by solving iteratively a set of implicit simultaneous equations that includes equation (2), equation (9), a mass-balance for each compound (the set total concentration of compound i is equal to the sum of its gas- and particle phase concentrations), and the fact that the sum of $A_{i,om}$ values (and primary organics) must equal M_o . These constraints make modeling SOA formation via thermodynamic principles feasible as the number of equations reduces to n , with n unknowns (each $A_{i,om}$).

The hydrophobic module is shown in more detail in Figure 6.3. Required inputs include the concentration and composition of any non-volatile POA and the total concentrations of the hydrophobic OA constituents. An initial distribution of the hydrophobic organics is assumed, to obtain a first approximation for the mass concentration and composition of the absorbing OA (denoted $M_{o,1}$ in the Figure 6.3). The initial guess for the distribution is determined based on the volatility of the condensing product. From this composition, it is straightforward to calculate the average molecular

weight of the absorbing phase. This composition is also used in UNIFAC to calculate the activity coefficients of the partitioning hydrophobic species. With temperature and a vapor pressure (experimentally determined or estimated using a group contribution method) defined, the next step is to calculate an absorptive partitioning coefficient as in equation (9) for each condensing species. Using these partitioning coefficients with $M_{o,1}$ and each individual total concentration (c_i in Figure 6.3), it is possible to calculate G_i and $A_{i,om}$ (using equation (2)) and compare them to the initial guess. The $n A_{i,om}$ values are the iterated variables. Once the series of $A_{i,om}$ values no longer changes by more than a prescribed small value, the calculations of the hydrophobic module are complete. It is also ensured that the gas-phase concentrations of all compounds do not exceed their saturation vapor pressures.

6.3.2 Hydrophilic Module Description

Partitioning of WSOC between the gas- and aqueous phases is governed by

$$H^{HL}_i = \frac{c_{w,i}}{p_i} = \frac{A_i \gamma^{HL}_i}{M_i(\text{LWC})p_i} \quad (10)$$

where H^{HL}_i ($\mu\text{M atm}^{-1}$) is the Henry's law constant of species i , determined, for example, by a group contribution method, $c_{w,i}$ is its aqueous phase concentration ($\mu\text{mol L}^{-1}$ (of water)), LWC in this case has units of L of water per m^3 of air, and γ^{HL}_i is its activity coefficient in the aqueous mixture (infinite dilution reference state). Note that γ^{HL}_i and γ^{RL}_i are related through γ^{RL}_i at $c_{w,i} = 0$. For organic acids, solubility is enhanced by the dissociation into ions, which is governed by equilibrium acid dissociation constants,

$$K_{a,i} = \frac{\{\text{H}^+\}\{\text{ORG}_i^-\}}{\{\text{ORG}_i\}} \quad (11)$$

where $K_{a,i}$ is the acid dissociation constant of organic species i (ORG_i) and the $\{ \}$ notation represents the activities of the species of interest. Acid dissociation constants can also be estimated by structure-activity relationships.

As shown in equation (10) above, the partitioning of WSOC depends on the activity coefficient of the species in the aqueous mixture. Such activity coefficients measure the deviation from ideality, which is usually significant for highly concentrated ambient aerosols. Various methods can be used to calculate the activity coefficients of ions (See *Kim et al.* [1993] for more detail.), each of which considers only inorganic ion-ion interactions. Limited data for inorganic-organic ion-ion interactions are available. For molecular solutes, UNIFAC can be used to estimate activity coefficients. While UNIFAC was not designed for use with highly polar compounds such as those that are constituents of SOA, it is assumed that the UNIFAC group contribution parameters for functionalities such as COOH , CHO , CH_2 , etc., can be applied to the surrogate molecules. Some parameters are available to treat the interactions between molecular groups and inorganic ions within the UNIFAC framework (e.g., *Kicic et al.* [1991] and *Yan et al.* [1999]). Unfortunately, key inorganic components in the atmosphere, such as ammonium and sulfate, are not included in these studies.

Ideally, the aerosol system would be treated as an interacting mixture of inorganics, organics, and water. Because of the lack of experimental data, however, traditional methods of estimating activity coefficients can not be used for interactions

between inorganic and organic ions. Therefore, a number of assumptions must be made. First and foremost, it is assumed that inorganic and organic solutes do not interact. This allows for the decoupling of the organic partitioning of WSOC from the inorganic model (e.g., SCAPE2), in terms of calculating activity coefficients. Also as a result of this assumption, the formation of organic-inorganic salts is not modeled. Second, it is assumed that the activity coefficients of organic ions are equivalent to those of the corresponding molecular solute. These are clearly approximations, the validity of which future work will address. At this point, they are deemed appropriate for development of an atmospheric model.

The LWC of the aerosol is also a key parameter in determining the Henry's Law partitioning of WSOC. Because of its simplicity, the Zdanovskii-Stokes-Robinson (ZSR) method is used in three-dimensional atmospheric models to determine the water content of the aerosol solution (See, for example, *Meng et al.* [1998].). The basic assumption of the ZSR method is that the water associated with each solute is additive. Therefore, LWC ($\mu\text{g water m}^{-3}$ air) is defined by

$$\text{LWC} = \sum_i \frac{m_i}{m_{i0}(a_w)} \quad (12)$$

where m_i is the molar concentration of species i ($\text{mol } i \text{ m}^{-3}$ of air) and $m_{i0}(a_w)$ is the molality of species i ($\text{mol } i \mu\text{g}^{-1}$ water) in a binary mixture at the water activity of interest (a_w). Polynomial fits for inorganic solute concentrations as a function of water activity have been developed by *Kim et al.* [1993] and *Meng et al.* [1995] based on experimental data. However, this approach is not possible for organic solutes due to lack of activity

measurements. An estimation method must be used to determine water activities for binary or multicomponent organic systems. UNIFAC can be used in this regard to determine the molality of organic solutions at specific water activity, which is equal to the relative humidity at equilibrium [Saxena and Hildemann, 1996]. The water associated with the inorganic and organic components is then considered and used in equation (12) to determine the LWC of the aerosol of interest.

The hydrophilic module is shown in more detail in Figure 6.4. As shown, the required inputs for the hydrophilic module include the SCAPE2 output (LWC and the concentration of hydrogen ions) and the total concentrations of the hydrophilic organics. The first step in the hydrophilic module is to determine the type of calculation that must be performed. As shown in Figure 6.4, if there is no existing aqueous phase, a calculation using both hydrophilic and hydrophobic species in the hydrophobic module is performed. If the relative humidity (RH) is below the deliquescence relative humidity (DRH) of all WSOC species present, the organic phase remains dry. If RH is greater than the DRH of any of the hydrophilic species, a new aqueous phase is formed. If an aqueous phase exists at the start of the calculation, a saturation calculation is performed only if RH is less than the DRH of all species. Otherwise, if RH is greater than the DRH of any species, an aqueous equilibrium calculation is performed. The equilibrium calculation is performed by simultaneously solving mass balance (total concentration, c_i , is equal to the sum of the concentrations in the gas- and aqueous phases), Henry's law (equation (10)), and acid dissociation equations for each species (both ions and molecules) (equation (11)).

Iteration (using a Newton line search method) is required because the activity coefficients are a strong function of the aerosol composition. Once equilibrium values based on the input LWC are reached, an organic-water system is considered so as to calculate the additional amount of water that is taken up as a result of the presence of the hydrophilic organics. The new total LWC and the concentrations of organic ions are passed to SCAPE2 to see if the distribution of the inorganic aerosol constituents is affected. (When a new aqueous phase is formed, the output is not passed to SCAPE2 as the effect of organics on the DRH of inorganic aerosol is currently not known.) If this change in LWC is zero, the output from the hydrophilic module includes the phase distribution of inorganic aerosol constituents, the phase distribution of hydrophilic organic aerosol constituents, and the LWC of the aerosol.

6.3.3 Example Case Studies

6.3.3.1 Hydrophobic Module

In order to demonstrate the hydrophobic portion of the model, both a surrogate SOA compound and a prescribed mixture of POA constituents must be defined. Representative POA constituents have been determined based on measurements made in the Los Angeles Basin [*Rogge et al.*, 1993] and the San Joaquin Valley of California [*Schauer and Cass*, 1998]. Major classes of organic compounds resolved in the analysis of OA include fatty acids, substituted phenols, aromatic acids, alkanes, and, for the San Joaquin Valley, levoglucosan and other sugar derivatives. Surrogate POA constituents are chosen from this group, excluding those that were shown to have affinity toward the

aqueous phase (Table 6.1). Octadecanoic acid is selected as the surrogate hydrophobic SOA constituent.

The first variable investigated in the evaluation of the hydrophobic module is TSP (with f_{om} set to 0.1 for this study in order to match that estimated by *Pankow* [1994]). For a set amount of octadecanoic acid present ($1 \mu\text{g m}^{-3}$), increasing initial TSP (from 10 to $100 \mu\text{g m}^{-3}$) and, therefore, the mass of each POA constituent, results in an increase in the amount of octadecanoic acid that partitions to the aerosol phase from approximately 0.35 to $0.8 \mu\text{g m}^{-3}$ (Figure 6.5). The resulting changes in average molecular weight and activity coefficients lead to a decrease in the partitioning coefficient of octadecanoic acid.

The total concentration of octadecanoic acid was also varied while holding the total TSP constant ($50 \mu\text{g m}^{-3}$). Naturally, increasing the concentration of octadecanoic acid leads to an increase in the amount of the species that partitions to the aerosol (Figure 6.6). The changes in the average molecular weight of the absorbing medium and the activity coefficients lead to increases in the partitioning coefficient as the total acid concentration is increased.

6.3.3.2 Hydrophilic Module

In order to demonstrate the hydrophilic module, malic ($\text{COOH-CH}_2\text{-CHOH-COOH}$) and glyoxalic (CHO-COOH) acids were chosen as surrogate WSOC. The properties of these compounds are given in Table 6.2. Malic acid is very soluble; glyoxalic acid is only sparingly so. Table 6.3 shows the input conditions and predictions from the hydrophilic module. Because of its high solubility, all of the malic acid partitions to the aqueous phase, with the ions being the dominant forms. Glyoxalic acid

tends to remain in the gas phase. For what little amount partitions to the aqueous phase, the ion is again the dominant form.

Sensitivity studies show that the change in LWC as a result of the hydrophilic organics increases as RH increases (Figure 6.7). The change in LWC associated with changes in RH is especially important for malic acid, which exhibits deliquescence behavior at approximately 79% RH. Below this humidity, no additional water is associated with the organic aerosol because of the presence of malic acid. Because malic acid is much more soluble, the amount of water associated with malic acid is orders of magnitude greater than that associated with glyoxalic acid, even though both compounds are present at the same total concentrations.

Sensitivity studies also show the importance of the pH obtained from the inorganic thermodynamic module (Figure 6.8). A lower aerosol pH affects the dissociation of acids, resulting in molecular solutes being favored over the ionized forms. An increased pH results in a higher effective Henry's law constant for the acids, yielding higher organic concentrations. This increase in the organic concentration also leads to an increase in the change in LWC. These changes are especially important for glyoxalic acid. Because of the malic acid's high solubility, pH has little affect on the amount of water associated with this species.

The hydrophilic organic module was also evaluated in conjunction with SCAPE2, using both inorganic and WSOC constituents. The input and simulation results are shown in Table 6.4. The simulation results indicate two main effects of the organic solutes. First, the extra water associated with the WSOC encourages additional partitioning of the inorganics to the aqueous phase. Second, the decrease in pH favors

the dissolution of basic gases (e.g., ammonia) as opposed to acidic gases (e.g., nitric acid). For example, in the case shown in Table 6.4, the final concentration of NH_4^+ is $0.078 \mu\text{mol m}^{-3}$, while in the absence of organics, the concentration of NH_4^+ would be $0.064 \mu\text{mol m}^{-3}$.

6.4. Implementation in Three-Dimensional Atmospheric Models

The integration of the aerosol module in a three-dimensional atmospheric model is shown in Figure 6.9. The first set of inputs includes total inorganic concentrations, relative humidity, and temperature. This information is passed to the inorganic thermodynamic equilibrium model, the output from which includes the phase and composition distribution of the inorganics and the LWC and pH of the inorganic/water aerosol. If the LWC is zero, a calculation using the hydrophobic module is performed first, with the resulting WSOC causing formation of a new aqueous phase under most conditions. The LWC and the pH are then passed to the hydrophilic module, along with total concentrations of the hydrophilic organic oxidation products. The water taken up as a result of the absorption of these organics is calculated, and the total LWC is passed back to SCAPE2 to determine if the additional water affects the distribution of the inorganic species. Once the LWC is internally consistent between the inorganic calculation and the hydrophilic organic calculation, the results are passed to the hydrophobic module, along with total concentrations of the POA constituents and the hydrophobic organic oxidation products. Upon completion of the hydrophobic module, predictions include the LWC, the distribution of all organic oxidation products, and the distribution of the inorganic species.

As discussed above, this module has been tested using simple two or three component mixtures and set concentrations. However, for use in a three-dimensional atmospheric model, the partitioning module is linked to a chemical mechanism that predicts the concentrations of semi- or non-volatile organic oxidation products. As described in Part I, there are 42 compounds specified in the Caltech Atmospheric Chemistry Mechanism (CACM) that are considered capable of forming SOA because of their solubility or low vapor pressures. Predicting the partitioning of that many species (into 8 primary organic species) is deemed at present to be too computationally demanding, especially in light of the lack of thermodynamic data for multi-functional organic species. Therefore, these secondary products are further lumped into one of five hydrophilic groups or into one of five hydrophobic groups. Obviously, the first separation is made on the basis of affinity for water. An organic is considered water-soluble based on the length of the carbon chain (≤ 7 carbons), its solubility (≥ 1 g solute/100g water), and its effective Henry's law coefficient ($\geq 1 \times 10^6$ M atm $^{-1}$). Additionally, those species with 7 or more carbon atoms and three functional groups are considered water-soluble because these compounds exhibit such a high degree of polarity [Saxena and Hildemann, 1996]. Compounds meeting these criteria are defined as hydrophilic and can be further subdivided by size (low or high carbon number), source (anthropogenic or biogenic), and dissociative properties. This process results in five hydrophilic surrogates. The products from CACM that fall into each group are structurally averaged (number of carbon, number and type of functional groups, etc.) to determine the structure of the five surrogates to be used in the hydrophilic module. Five surrogates for the hydrophobic module were determined similarly. The hydrophobic

compounds are divided based on source (anthropogenic versus biogenic), structure (aliphatic versus benzene-based versus naphthalene-based for anthropogenic species), and volatility (for benzene-based anthropogenic species). Reduction of the 42 compounds into 10 (the properties for which are determined using group contribution methods) allows for a substantial reduction in the computational demands of the partitioning module. The 10 compounds are given in Table 6.5. In some cases, the structure of a surrogate was difficult to determine because the averaging technique predicted a fractional number of certain functional groups. This is most important in surrogate B2, in which the aldehyde group could be replaced by either a hydroxy- or a nitro group.

When this module is employed in a three-dimensional application, specification of the composition of the POA and using a set value of f_{om} will be unnecessary. By incorporating the composition of POA emissions in the area to be simulated, these values can be easily calculated. In the studies of the air quality in the SOCAB, for example, it has been determined that the organic fraction of aerosol emissions can be classified into 8 categories: *n*-alkanes, polycyclic aromatic hydrocarbons (PAH), oxygenated PAH, diacids, aliphatic acids, substituted monoaromatics, cyclic petroleum biomarkers (e.g., hopanes), and unresolved organic matter (characterized by highly cyclic and branched petroleum biomarkers) [Schauer, 1998].

6.5 Discussion

Because experimental data on thermodynamic properties of mixed organic-inorganic aqueous solutions are sparse, many necessary assumptions have been made in the development of this partitioning module. First, the module does not account for the

behavior of those organic species that show affinity for both the aqueous and organic phases. If a compound exhibits such behavior, it is chosen as one or the other, which may result in the underprediction of its amount in the aerosol phase. Once additional experimental data are available, compounds that display this behavior can be accounted for explicitly. Second, it is assumed that there is no interaction between aqueous phase inorganics and organics. As thermodynamic data become available, such interactions will be incorporated. Third, the ability of certain hydrophobic organic species to limit water uptake has not been taken into account. Uncertainty associated with UNIFAC and other group contribution methods for estimating thermodynamic properties add to the uncertainty associated with the partitioning module. Predictions of the partitioning module depend, of course, on the input from the gas-phase chemical mechanism, which has inherent uncertainties, as discussed in Part I. Despite these issues, the current module represents the state-of-the-art model for describing SOA formation in a three-dimensional atmospheric model. Of the many improvements that could be made to this module, the most important is the ability to describe the effects of the interactions of the molecules and ions in a mixed inorganic-organic-aqueous aerosol. Current work of the authors is directed toward this goal.

6.6 Conclusions

An organic-inorganic, gas-aerosol module that predicts thermodynamically the formation of secondary organic aerosol (SOA) for use in three-dimensional atmospheric models has been presented. The gas-phase chemical mechanism described in Part I predicts the concentrations of SOA precursors, which are assigned to one of ten surrogate groups based on water affinity, size, source, structure, and volatility. The total

concentrations of these ten surrogates are then passed to the module described here to predict gas-aerosol partitioning. As discussed in Section 2, techniques used previously to predict SOA concentrations in three-dimensional models have been limited in theory or depend on experiments that are specific to a certain set of conditions. The new module represents an improvement over these techniques in that it is theoretically sound, is not based on data specific to one set of experiments, and accounts for different ambient conditions (temperature, oxidant and precursor concentrations, relative humidity, etc.). Like the CACM model described in Part I, the organic gas-aerosol partitioning module conforms with the U.S. Environmental Protection Agency's Models-3 framework [*United States Environmental Protection Agency, 1999*] so that it can be used in that setting.

6.7. References

Ansari, A.S., and S.N. Pandis, An analysis of four model predicting the partitioning of semivolatile inorganic aerosol components, *Aerosol Sci. Technol.*, 31, 129-153, 1999.

Atkinson, R., Gas-phase tropospheric chemistry of volatile organic compounds: 1. Alkanes and alkenes, *J. Phys. Chem. Ref. Data*, 26, 215-290, 1997.

Atkinson, R., Gas-phase tropospheric chemistry of organic compounds, *J. Phys. Chem. Ref. Data, Monograph 2*, 1994.

Aumont, B., S. Madronich, I. Bey, and G.S. Tyndall, Contribution of secondary VOC to the composition of aqueous atmospheric particles: A modeling approach, *J. Atmos. Chem.*, 35, 59-75, 2000.

Barthelmie, R.J., and S.C. Pryor, A model mechanism to describe oxidation of monoterpenes leading to secondary organic aerosol, *J. Geophys. Res.*, 104, 23,657-23,669, 1999.

CRC Handbook of Physics and Chemistry, 77th edition, ed. by David R. Lide, CRC Press,

Boca Raton, FL, 1997.

Fredenslund, A., J. Gmehling, and P. Rasmussen, *Vapor-Liquid Equilibrium Using UNIFAC*, Elsevier, Amsterdam, 1977.

Griffin, R.J., D.R. Cocker III, R.C. Flagan, and J.H. Seinfeld, Organic aerosol formation from the oxidation of biogenic hydrocarbons, *J. Geophys. Res.*, 104, 3555-3567, 1999.

Grosjean, D., *In situ* organic aerosol formation during a smog episode: estimated production and chemical functionality, *Atmos Environ.*, 26A, 953-963, 1992.

Hine, J., and P.K. Mookerjee, The intrinsic hydrophilic character of organic compounds: correlations in terms of structural contributions, *J. Org. Chem.*, 40, 292-298, 1975.

Hoffmann, T., J.R. Odum, F. Bowman, D. Collins, D. Klockow, R.C. Flagan, and J.H. Seinfeld, Formation of organic aerosols from the oxidation of biogenic hydrocarbons, *J. Atmos. Chem.*, 26, 189-222, 1997.

Jacobson, M.Z., Development and application of a new air pollution modeling system 3. Aerosol-phase simulations, *Atmos. Environ.*, 31, 587-608, 1997.

Kamens, R., M. Jang, C.-J. Chien, and K. Leach, Aerosol formation from the reaction of α -pinene and ozone using a gas phase kinetics-aerosol partitioning module, *Environ. Sci. Technol.*, 33, 1430-1438, 1999.

Kicic, I., M. Femeglia, and P. Rasmussen, UNIFAC prediction of vapor-liquid equilibria in mixed solvent-salt systems, *Chem. Eng. Science*, 47, 2775-2780, 1991.

Kim, Y.P., J.H. Seinfeld, and P. Saxena, Atmospheric gas-aerosol equilibrium I. Thermodynamic model, *Aerosol Sci. Technol.*, 19, 157-181, 1993.

Liang, C.K., J.F. Pankow, J.R. Odum, and J.H. Seinfeld, Gas/particle partitioning of semi-volatile organic compounds to model inorganic, organic, and ambient smog aerosols, *Environ. Sci. Technol.*, 31, 3086-3092, 1997.

Lurmann, F.W., A.S. Wexler, S.N. Pandis, S. Musarra, N. Kumar, and J.H. Seinfeld, Modeling urban and regional aerosols – II. Application to California’s South Coast Air Basin, *Atmos. Environ.*, 31, 2695-2715, 1997.

Meng Z., D. Dabdub, and J.H. Seinfeld, Size-resolved and chemically resolved model of atmospheric aerosol dynamics, *J. Geophys. Res.*, 103, 3419-3435, 1998.

Meng, Z., J.H. Seinfeld, P. Saxena, and Y.P. Kim, Atmospheric gas-aerosol equilibrium 4. Thermodynamics of carbonates, *Aerosol Sci. Technol.*, 23, 131-154, 1995.

Middlebrook, A.M., D.M. Murphy, and D.S. Thomson, Observations of organic material in individual marine particles at Cape Grim during the First Aerosol Characterization Experiment (ACE-1), *J. Geophys. Res.*, 103, 16,475-16,483, 1998.

Murphy, D.M., D.S. Thomson, and T.M.J. Mahoney, *In situ* measurements of organics, meteoritic material, mercury, and other elements in aerosols at 5 to 19 kilometers, *Science*, 282, 1664-1669, 1998.

Nenes, A., S.N. Pandis, and C. Pilinis, ISORROPIA: A new thermodynamic equilibrium model for multiphase multicomponent inorganic aerosols, *Aquatic Geochem.*, 4, 123-152, 1998.

Odum, J.R., T.P.W. Jungkamp, R.J. Griffin, R.C. Flagan, and J.H. Seinfeld, The atmospheric aerosol-forming potential of whole gasoline vapor, *Science*, 276, 96-99, 1997.

Odum, J.R., T. Hoffmann, F. Bowman, D. Collins, R.C. Flagan, and J.H. Seinfeld, Gas/particle partitioning and secondary organic aerosol yields, *Environ. Sci. Technol.*, 30, 2580-2585, 1996.

Pai, P., K. Vijayaraghavan, and C. Seigneur, Particulate matter modeling in the Los Angeles Basin using SAQM-AERO, *J. Air Waste Manage. Assoc.*, 50, 32-42, 2000.

Pandis, S.N., R.H. Harley, G.R. Cass, and J.H. Seinfeld, Secondary organic aerosol formation and transport, *Atmos. Environ.*, 26A, 2269-2282, 1992.

Pankow, J.F., An absorption model of the gas/aerosol partitioning involved in the formation of secondary organic aerosol, *Atmos. Environ.*, 28, 189-193, 1994.

Penner, J.E., Carbonaceous aerosols influencing atmospheric radiation: Black and organic carbon in *Aerosol Forcing of Climate: Report of the Dahlem Workshop on Aerosol Forcing of Climate, Berlin 1994*, edited by R.J. Charlson and J. Heintzenberg, Wiley, New York, p. 91-108, 1995.

Rogge, W.F., M.A. Mazurek, L.M. Hildemann, and G.R. Cass, Quantification of urban organic aerosols at a molecular level: Identification, abundance, and seasonal variation, *Atmos. Environ.*, 27, 1309-1330, 1993.

Saxena, P., and L.M. Hildemann, Water-soluble organics in atmospheric particles: a critical review of the literature and application of thermodynamics to identify candidate compounds, *J. Atmos. Chem.*, 24, 57-109, 1996.

Schauer, J.J., M.J. Kleeman, G.R. Cass, and B.R.T. Simoneit, Measurement of emissions from air pollution sources 1. C₁ through C₂₉ organic compounds from meat charbroiling, *Environ. Sci. Technol.*, 33, 1566-1577, 1999a.

Schauer, J.J., M.J. Kleeman, G.R. Cass, and B.R.T. Simoneit, Measurement of emissions from air pollution sources 2. C₁ through C₃₀ organic compounds from medium duty diesel trucks, *Environ. Sci. Technol.*, 33, 1578-1587, 1999b.

Schauer, J.J. *Source Contributions to Atmospheric Organic Compound Concentrations: Emissions, Measurements, and Model Predictions*, Ph.D. Thesis, California Institute of Technology, Pasadena, CA, 1998.

Schauer, J.J., and G.R. Cass, *Source contributions to airborne particles in the San Joaquin Valley during the IMS95 Study, Contract 97-6PM, Draft Final Report*, California Air Resources Board, Sacramento, CA, 1998.

Seigneur, C., P. Pai, P.K. Hopke, and D. Grosjean, Modeling atmospheric particulate matter, *Environ. Sci. Technol.*, 33, 80A-86A, 1999.

Smith, D.F., T.E. Kleindienst, and C.D. McIver, Primary product distributions from the reaction of OH with *m*-, *p*-xylene, 1,2,4- and 1,3,5-trimethylbenzene, *J. Atmos. Chem.*, 34, 339-364, 1999.

Stevens, R.K., T.G. Dzubay, C.W. Lewis, and R.W. Shaw, Jr., Source apportionment methods applied to the determination of the origin of ambient aerosols that affected visibility in forested areas, *Atmos. Environ.*, 18, 261-272, 1984.

Strader, R., F. Lurmann, and S.N. Pandis, Evaluation of secondary organic aerosol formation in winter, *Atmos. Environ.*, 33, 4849-4863, 1999.

Sun, Q., and A.S. Wexler, Modeling urban and regional aerosols near acid neutrality – application to the 24-25 June SCAQS episode, *Atmos. Environ.*, 32, 3533-3545, 1998.

Suzuki, T., K. Ohtaguchi, and K. Koide, Application of principal components analysis to calculate Henry's constant from molecular structure, *Computers Chem.*, 16, 41-52, 1992.

United States Environmental Protection Agency, Web site for Models 3
(<http://www.epa.gov/asmdnerl/models3/index.html>), 1999

United States Environmental Protection Agency, *Air Quality Criteria for Particulate Matter*, EPA/600/P-95/001, 1996.

White, W.H., and E.S. Macias, Carbonaceous particles and regional haze in the Western United States, *Aerosol. Sci. Technol.*, 10, 106-110, 1989.

Yan, W., M. Toppoff, C. Rose, and J. Gmehling, Prediction of vapor-liquid equilibrium in mixed solvent electrolyte systems using the group contribution concept, *Fluid Phase Equilibria*, 162, 97-113, 1999.

Yu, J., D.R. Cocker III, R.J. Griffin, R.C. Flagan, and J.H. Seinfeld, Gas-phase ozone oxidation of monoterpenes: gaseous and particulate products, *J. Atmos. Chem.*, 34, 207-258, 1999.

Zhang, Y., C. Seigneur, J.H. Seinfeld, M. Jacobson, S.L. Clegg, and F.S. Binkowski, A comparative review of inorganic aerosol thermodynamic modules: similarities, differences, and their likely causes, *Atmos. Environ.*, 34, 117-137, 2000.

Table 6.1. Assumed primary organic aerosol composition for validation of the hydrophobic module.

	Fatty Acids	Substituted Phenols	Alkanes	Aromatic Acids
Mass Fraction	0.57	0.11	0.17	0.15
Surrogate Structure	Tetracosanoic Acid (C ₂₄ n-acid)	Acetonyl syringol (2,6-dimethoxy-4-acetonyl-phenol)	Nonacosane (C ₂₉ n-alkane)	Phthalic acid (1,2-Benzene-dicarboxylic acid)

Table 6.2. Properties for malic and glyoxalic acids.

	Malic Acid	Glyoxalic Acid
H_i^*	$2 \times 10^{13} \text{ M atm}^{-1}$	$9 \times 10^3 \text{ M atm}^{-1}$
K_a^+	$3.98 \times 10^{-4} \text{ M}$	$6.61 \times 10^{-4} \text{ M}$
K_{a2}^+	$7.76 \times 10^{-6} \text{ M}$	--

*Henry's Law coefficient, *Saxena and Hildemann [1996]*

⁺Acid dissociation constants, *CRC Handbook of Physics and Chemistry*

K_{a2} represents dissociation of the second acid group of malic acid

Table 6.3. Input and output for the evaluation of the hydrophilic module.

	Input		Output
T	298 K	MA (g)	$2.88 \times 10^{-8} \mu\text{g m}^{-3}$
RH	0.8	MA (aq)	$5.88 \times 10^{-6} \mu\text{g m}^{-3}$
LWC	$1 \mu\text{g m}^{-3}$	MA ⁻ (aq)	$5.56 \times 10^{-4} \mu\text{g m}^{-3}$
pH	5	MA ²⁻ (aq)	$4.28 \times 10^{-4} \mu\text{g m}^{-3}$
MA (t)	1 ng m^{-3}	GA (g)	$1.00 \times 10^{-3} \mu\text{g m}^{-3}$
GA (t)	1 ng m^{-3}	GA (aq)	$1.24 \times 10^{-10} \mu\text{g m}^{-3}$
		GA ⁻ (aq)	$1.48 \times 10^{-8} \mu\text{g m}^{-3}$
		ΔLWC	0.46 ng m^{-3}

Table 6.4. Input and output for the evaluation of the hydrophilic module used in conjunction with SCAPE2.

Input to SCAPE2

Total NH ₃	0.1 $\mu\text{mol m}^{-3}$
Total HNO ₃	0.1 $\mu\text{mol m}^{-3}$
Temperature	298 K
Relative Humidity	0.8

Output of SCAPE2

LWC (inorganic)	15.4 $\mu\text{g m}^{-3}$
pH	2.28

Additional Input to Hydrophilic Module

Total GA	0.1 $\mu\text{mol m}^{-3}$
Total MA	0.1 $\mu\text{mol m}^{-3}$

Output of First Pass of Hydrophilic Module

LWC (organic)	14.4 $\mu\text{g m}^{-3}$
Total organic ions (aq)	0.0071 $\mu\text{mol m}^{-3}$
Total organic molecules (aq)	0.0928 $\mu\text{mol m}^{-3}$
LWC (total)	29.8 $\mu\text{g m}^{-3}$

Output of SCAPE2 and Hydrophilic Module After Iteration

LWC (inorganic)	17.5 $\mu\text{g m}^{-3}$
pH	2.15
LWC (organic)	14.4 $\mu\text{g m}^{-3}$
Total organic ions (aq)	0.0053 $\mu\text{mol m}^{-3}$
Total organic molecules (aq)	0.0947 $\mu\text{mol m}^{-3}$
LWC (total)	31.9 $\mu\text{g m}^{-3}$

Table 6.5. Surrogate organic oxidation products to be used in the partitioning module.

Surrogate	Description	#C	COOH	C=O	CHO	OH	ONO ₂	NO ₂	C=C
A1	WSOC, anthropogenic, dissociative, low #C	2	2						
A2	WSOC, anthropogenic, dissociative, high #C	8	2		1				2
A3	WSOC, anthropogenic, non- dissociative	8			2	1			2
A4	WSOC, biogenic, dissociative	9	1	1		1			1
A5	WSOC, biogenic, non- dissociative	10		1	1	1			
B1	Hydrophobic, anthropogenic, benzene-based, low volatility	9	1(a)			1(a)		1(a)	
B2	Hydrophobic, anthropogenic, benzene-based, higher volatility	9	1(a)		1(a)				
B3	Hydrophobic, anthropogenic, naphthalene- based	12					1		
B4	Hydrophobic, anthropogenic, aliphatic	16				1	1		
B5	Hydrophobic, biogenic, aliphatic	10		1		1			1

(a) attached to the aromatic ring as opposed to a side chain alkyl substituent

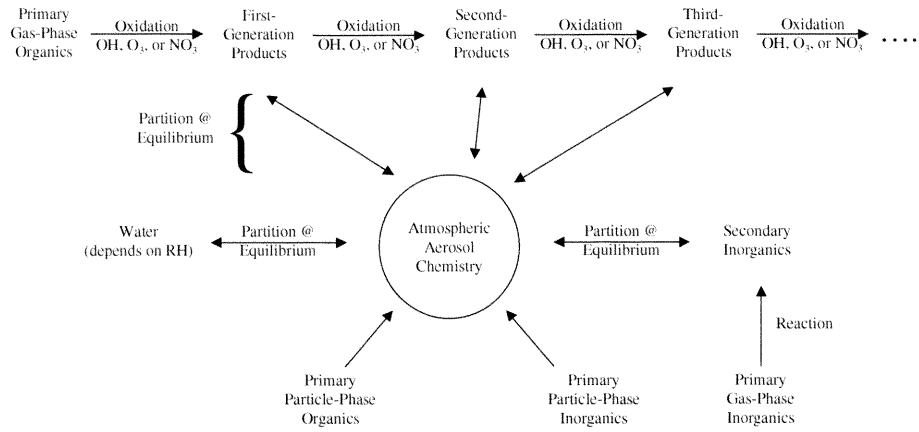


Figure 6.1. Species that partition into the aerosol phase and the processes that affect them. Other factors that influence partitioning include, for example, temperature and mixing height (which affects concentrations).

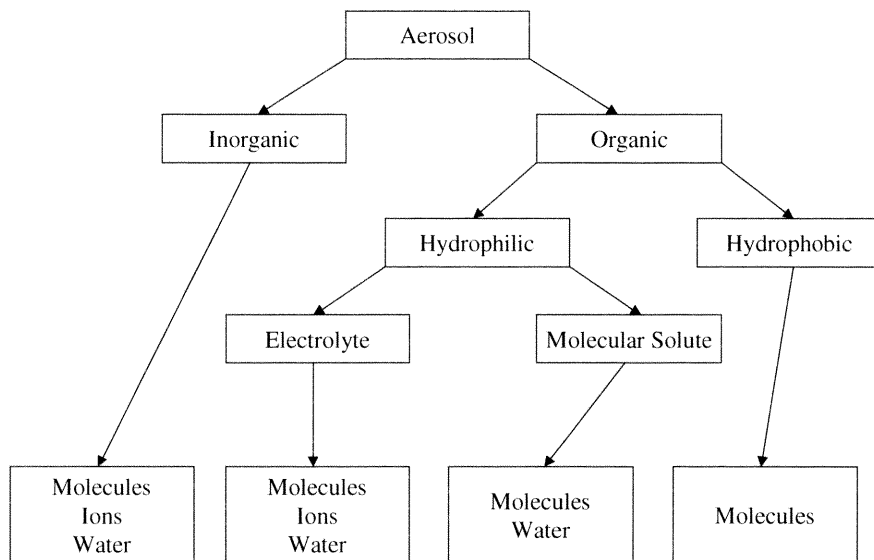


Figure 6.2. Breakdown of aerosol constituents based on their atomic nature, water affinity, and dissociative properties.

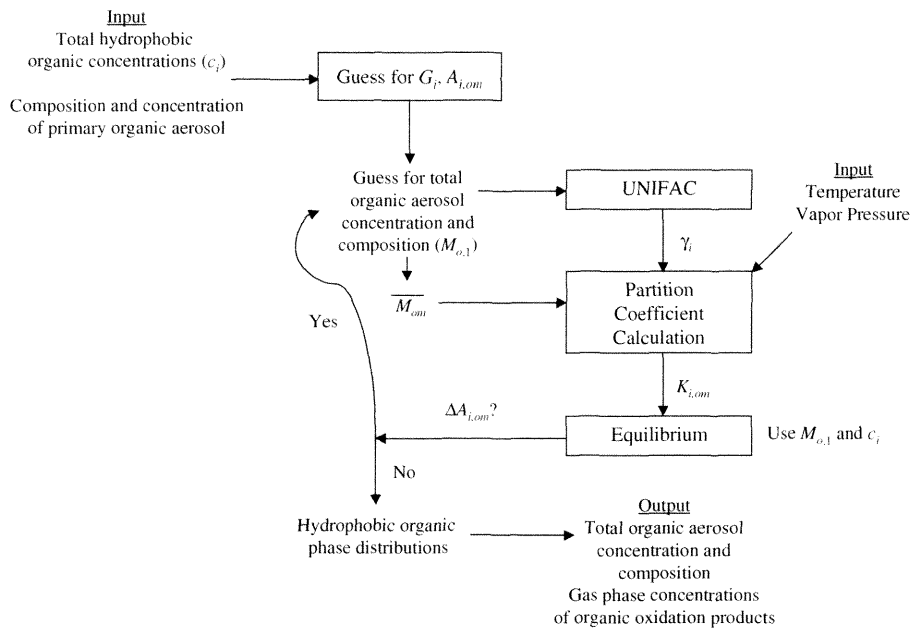


Figure 6.3. Flowsheet for the calculation of the partitioning of hydrophobic organic aerosol constituents between the gas- and aerosol-phases.

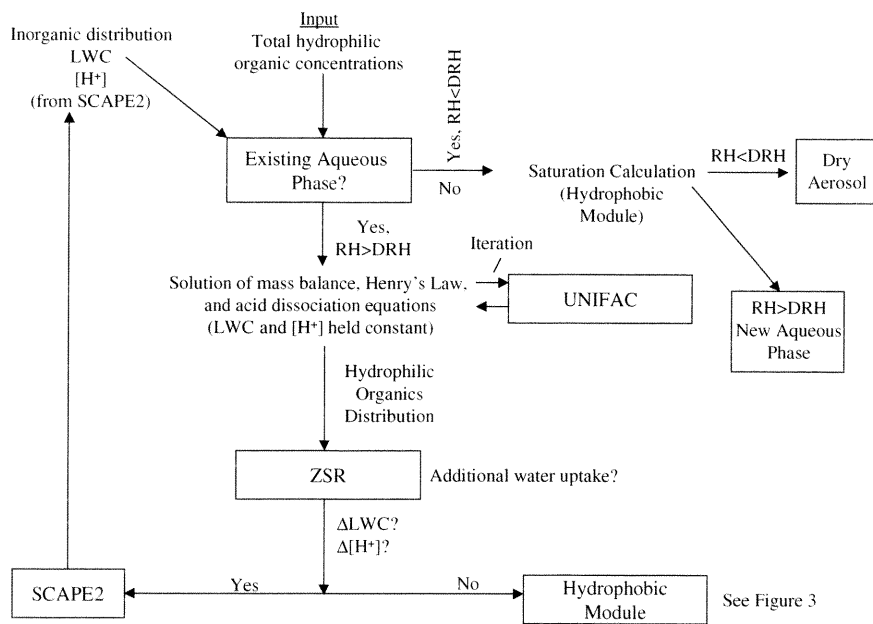


Figure 6.4. Flowsheet for the calculation of the partitioning of hydrophilic organic aerosol constituents between the gas- and aqueous- phases.

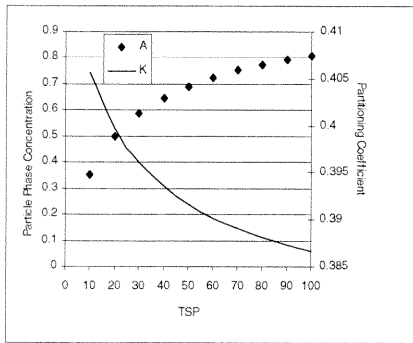


Figure 6.5

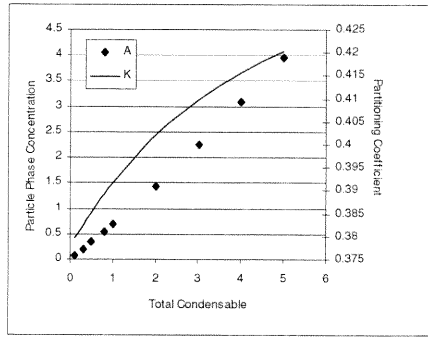


Figure 6.6

Figure 6.5. Particulate concentrations of octadecanoic acid ($\mu\text{g m}^{-3}$) and its partitioning coefficient ($\text{m}^3 \mu\text{g}^{-1}$) as a function of TSP. Total condensable material = $1 \mu\text{g m}^{-3}$.

Figure 6.6. Particulate concentrations of octadecanoic acid ($\mu\text{g m}^{-3}$) and its partitioning coefficient ($\text{m}^3 \mu\text{g}^{-1}$) as a function of the total amount of condensable material. TSP = $50 \mu\text{g m}^{-3}$.

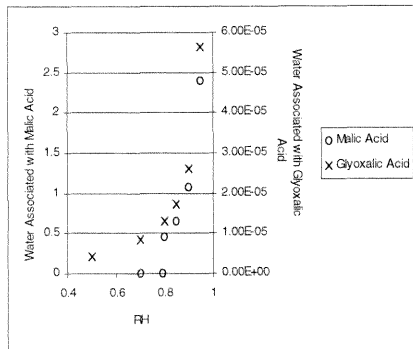


Figure 6.7

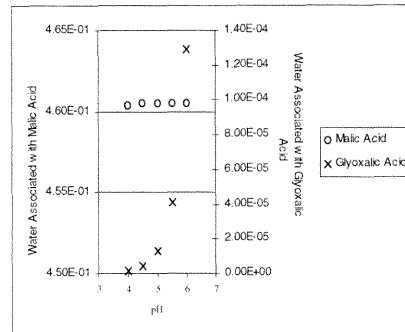


Figure 6.8

Figure 6.7. Sensitivity of the water associated with WSOC (ng m^{-3}) at varying RH.

Initial LWC = $1 \mu\text{g m}^{-3}$, pH = 5, total solute = 1 ng m^{-3} .

Figure 6.8. Sensitivity of the water associated with WSOC (ng m^{-3}) at varying pH.

Initial LWC = $1 \mu\text{g m}^{-3}$, RH = 0.8, total solute = 1 ng m^{-3} .

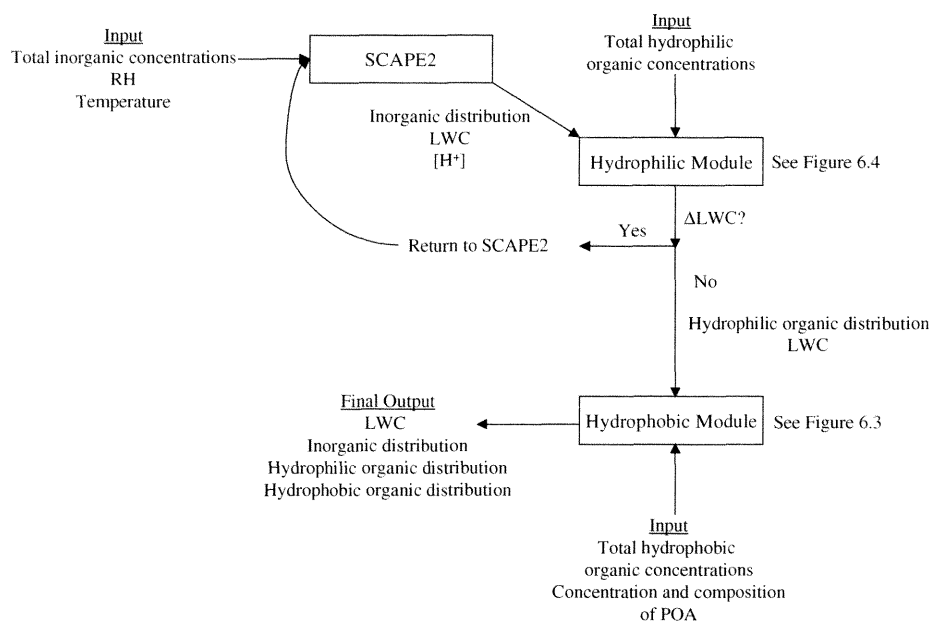


Figure 6.9. Overall flowsheet for the calculation of aerosol water content and the phase distributions of both inorganic and organic aerosol constituents.

Chapter 7

Conclusions

As discussed, the troposphere is a complex system constituted by species that reside in both the gas- and aerosol-phases. These species are either natural or anthropogenic and can be primary or secondary in nature.

Of specific interest in the work presented here are the secondary organic aerosol (SOA) constituents of atmospheric particulate matter. SOA is formed when a volatile parent organic species is oxidized, resulting in products with decreased vapor pressures or increased solubilities because of the functional groups that form as a result of oxidation. These functional groups lead to partitioning to the aerosol phase and may include alcohols, acids, carbonyls, nitro- groups, and nitrooxy- groups. The phase distribution of these species is governed usually by absorption into an organic aerosol phase or by Henry's law if the oxidation product is soluble. While the yields (Y , defined as the amount of SOA mass formed per the amount of parent organic mass reacted) of many parent species have been investigated previously, the two groups of compounds that have been investigated in the context of an absorptive partitioning theory are the aromatics that are constituents of gasoline and the biogenic monoterpenes.

The work presented in this thesis discusses each of these compound groups and how the appropriate yield parameters (stoichiometric factors and equilibrium partitioning coefficients) for a given parent organic are developed using smog chamber experiments. These parameters are used to estimate SOA formation on a global and annual basis from the oxidation of biogenic organic species. In addition, such parameters are used to introduce a new concept, the incremental aerosol reactivity of a parent organic. Finally, methods to simulate SOA formation using this partitioning theory in a three-dimensional atmospheric model are described.

This thesis represents the current state of the art of both laboratory and computational work aimed at understanding the formation of SOA. While a large amount of information is contained within this thesis, there are still many unanswered questions with regard to SOA formation. Subjects currently or soon to be under investigation in the Seinfeld laboratory include the effects of relative humidity (RH) and temperature on SOA yields and the SOA yields of those species that are semivolatile in nature upon emission. The RH study will attempt to quantify the effects of both gas-phase and aerosol-phase water on the partitioning of oxidation products from both biogenic and anthropogenic species. Because temperature must be carefully controlled in order to control relative humidity, the effect of temperature on partitioning will be quantified as well.

Because the field of atmospheric organic chemistry is still relatively young, there are many topics on which work may be focused in the future. First, nucleation of new particles in forest atmospheres has been observed at a number of sites and is temporally correlated to organic aerosol precursor concentrations. However, no quantitative data exist describing the kinetics of the formation of new organic aerosol particles. Variables of interest include composition of the organic mixture to be nucleated, RH, and temperature. The competition between heterogeneous and homogeneous nucleation will need to be investigated in order to develop a parameterization of SOA nucleation for global models from the new data. A second issue that remains open to question is organic acid formation in the atmosphere as current known sources cannot account for observed concentrations. In addition, little is known about the atmospheric behavior of these acids in terms of reactions, solubility, and partitioning to the aerosol phase. Third, further improvements to regional air quality models will need to be made in order to

improve the simulation of SOA. These include incorporation of fog chemistry (which affects sulfate aerosol chemistry and aerosol acidity, thereby affecting partitioning of hydrophilic organic species), inorganic-organic interactions in the aqueous phase, and wet deposition of particles (e.g., incorporation of aerosol into water droplets). In addition, air quality models should find applications in areas other than Los Angeles, as more and more focus is being placed on regional air quality issues in regions outside California. Other topics may include the effects of SO₂ on SOA yields (aerosol-phase sulfate effects on partitioning of organics and gas-phase SO₂ effects on the product distribution resulting from the oxidation of a given parent organic), surface reactions that may occur at the organic aerosol surface (reaction of unsaturated bonds or aldehydes and isomerization of biogenic aerosol components upon exposure to acidic conditions), organic aerosol toxicity (structure effects on toxicity and establishment of a toxicity potential based on the probable oxidation products of a parent organic), and statistical mechanical approaches to describe reactions and molecular properties that affect partitioning of semivolatile organic oxidation products.

Appendix 1

The Atmospheric Aerosol-Forming Potential of Whole Gasoline Vapor

Reference: J.R. Odum, T.P.W. Jungkamp, R.J. Griffin, R.C. Flagan, and J.H. Seinfeld, *Science*, 276, 96-99, 1997.

Abstract

A series of sunlight-irradiated, smog-chamber experiments confirmed that the atmospheric organic aerosol formation potential of whole gasoline vapor can be accounted for solely in terms of the aromatic fraction of the fuel. The total amount of secondary organic aerosol produced from the atmospheric oxidation of whole gasoline vapor can be represented as the sum of the contributions of the individual aromatic molecular constituents of the fuel. The urban atmospheric, anthropogenic hydrocarbon profile is approximated well by evaporated whole gasoline, and thus these results suggest that it is possible to model atmospheric secondary organic aerosol formation.

Several recent epidemiologic studies have consistently reported increased daily mortality associated with exposure to fine particulate air pollution [Schwartz *et al.*, 1996; Shprentz, 1996; Pope *et al.*, 1995]. Fine particulate matter, also known as PM_{2.5} (that is, particles of diameter less than 2.5 μ m), is the respirable fraction of atmospheric particulate matter. An important contribution to the atmospheric fine particulate burden, especially during severe urban smog episodes, is secondary organic aerosol (SOA) [Turpin and Huntzicker, 1991; Turpin *et al.*, 1991]. Like ozone (O₃), SOA is formed from the oxidation of organic compounds. Whereas the oxidation of most hydrocarbons contributes to O₃ formation, SOA is generally formed only from the oxidation of hydrocarbon molecules containing seven or more carbon atoms [Grosjean, 1992; Grosjean and Seinfeld, 1989]. To form SOA, oxidation products must have vapor pressures that are sufficiently low to enable them to partition into the particulate phase.

In an effort to achieve urban and regional O₃ abatement through the reduction of mass emissions of nonmethane hydrocarbons, the 1990 amendments to the U.S. Clean

Air Act mandate the use of reformulated gasoline in motor vehicles. Several recent studies have suggested that a more effective approach to controlling urban O₃ associated with emissions from gasoline usage is to target the emissions of specific fuel components, rather than total nonmethane hydrocarbons, because of the extreme differences in the O₃-forming potential of the hundreds of individual compounds that constitute gasoline

[*Bowman and Seinfeld, 1995; Russell et al., 1995; Calvert et al., 1993; Hoekman, 1992*].

Considering the common link between urban O₃ formation and SOA formation, this approach may also be an effective way to control SOA formation associated with emissions from gasoline usage.

Organic aerosol formation potentials depend on two factors: reactivity of the parent compound and volatility of the product species. The reactivity of the parent species can be directly measured by reaction rate constants. However, because atmospheric chemical reaction pathways for large hydrocarbon molecules are complex and the resulting oxidation products are both numerous and difficult to quantify analytically, a more indirect measure of product volatility, the SOA yield Y , has been used. Traditionally, Y has been defined as the fraction of a reactive organic gas (ROG) that is converted to aerosol by means of atmospheric oxidation processes: $Y = \Delta M_o / \Delta \text{ROG}$, that is, the total mass concentration of organic aerosol, ΔM_o , produced for a given amount of ROG reacted, ΔROG . Yield data have been obtained for dozens of ROGs in controlled smog chamber studies [*Pandis et al., 1991; Wang et al., 1992; Hatakeyama et al., 1991; Izumi and Fukuyama, 1990; Stern et al., 1987; Gery et al., 1985; Leone et al., 1985; Grosjean, 1977*].

The mixture of hydrocarbons that compose gasoline is representative of the atmospheric distribution of anthropogenic hydrocarbons in an urban airshed in terms of both complexity and composition [Harley *et al.*, 1992], and, therefore, determining the atmospheric aerosol-forming potential of whole gasoline vapor is of significant interest. In general, gasoline contains four classes of reactive organics – oxygenates, alkanes, alkenes, and aromatics – which vary widely in their atmospheric reactivity and in the volatility of their atmospheric oxidation products. Our hypothesis is that the atmospheric aerosol-forming potential of whole gasoline vapor can be quantitatively accounted for in terms of the aromatic content of the fuel.

The outdoor smog chamber system used in this study has been described in detail previously [Odum *et al.*, 1996]. It consists of a 60-m³ sealed, collapsible polytetrafluoroethylene (Teflon) bag. Experiments are performed by (1) injecting into the bag (filled with humidified clean air) appropriate concentrations of seed aerosol [(NH₄)₂SO₄, about 5,000 to 10,000 particles per cubic centimeter, an initial aerosol volume of about 5 to 10 μm^3 per cubic centimeter of air], a photochemical initiator [propene, about 150 to 300 parts per billion (ppb)], NO and NO₂, and the single hydrocarbon or hydrocarbon mixture of choice and then (2) allowing the mixture to react under sunlight for 6 to 8 hours. Initial hydrocarbon concentrations ranged from 400 to 5000 $\mu\text{g m}^{-3}$ for the individual aromatic experiments and from 2700 to 7000 $\mu\text{g m}^{-3}$ for the gasoline experiments. Concentrations of NO_x (NO + NO₂) were selected so that HC/NO_x ratios typical of those in an urban environment (5 to 10 ppbC/ppb NO₂) were achieved. The ratio of NO/NO₂ was always set at 2. During the course of the experiment, the concentration of each ROG species is either measured with the use of gas

chromatography or is calculated on the basis of relative rates of reaction, in order to determine ΔROG . Particle number and size are measured continuously throughout the experiment by scanning electrical mobility spectrometers (SEMS) to determine ΔM_o [Wang *et al.*, 1992]. SEMS were used to obtain complete particle number and size distributions with a 1-minute frequency. Time-dependent particle volume concentrations were calculated from these distributions. The time-dependent cumulative organic volume concentration was calculated by subtracting the volume concentration at time t (corrected for deposition) from the initial volume concentration. Total organic mass concentrations were calculated from the total cumulative organic volume concentration assuming the density of the condensed organic phase was 1.0 g cm^{-3} .

Because the oxidation products responsible for forming SOA are semivolatile and partition themselves between the gas and absorbing organic aerosol phases [Odum *et al.*, 1996; Pankow, 1994], SOA yields for individual ROGs (Y) are a function of M_o . This dependence is represented by [Odum *et al.*, 1996]

$$Y = M_o \sum_i \left(\frac{\alpha_i K_{om,i}}{1 + K_{om,i} M_o} \right) \quad (1)$$

where α_i and $K_{om,i}$ are the mass-based stoichiometric coefficient and absorption equilibrium partitioning coefficient of product i , respectively. Parameter K_{om} is an equilibrium constant describing the partitioning of semivolatile organics between the vapor phase and an absorbing organic condense phase: $K_{om} = (F/M_o)/A$, where F and A are a semivolatile compound's concentration in the absorbing organic and vapor phases,

respectively, and M_o is the concentration of the absorbing organic aerosol. Yield data for individual hydrocarbons can be fit well to equation (1) assuming a two-product model (that is, by choosing appropriate values for α_1 , α_2 , $K_{om,1}$, and $K_{om,2}$) [Odum *et al.*, 1996]. Organic aerosol yields were measured as a function of ΔM_o for 17 aromatic species that represent the predominant mass fraction of aromatics present in gasoline (Figure A.1.1). Most of the data can be fit with only two curves. Curve 1 corresponds to propylbenzene and to those species having one or fewer methyl substituents plus one or fewer ethyl substituents, and curve 2 fits species that contain two or more methyl substituents. Curves 3 and 4 fit the only diethylbenzene and methyl-*n*-propylbenzene species that were studied. There is little variation of the yield for different isomers. For example, *o*-, *m*-, and *p*-xylene all exhibit yields that are described by the same curve. It is likely that parent species that are sufficiently similar in nature generate, upon photooxidation, semivolatile products that have similar gas-aerosol partitioning behavior.

From yield curves for individual parent hydrocarbons, like those shown in Figure A.1.1, one can account for the aerosol that is formed from the oxidation of a mixture of two species as the sum of the yields of the individual parent species present in the mixture [Odum *et al.*, 1996]. To ensure that the aerosol formed in a more complex mixture could be accounted for in such a manner, we performed an experiment in which a mixture of five different aromatic species (toluene, *m*-xylene, *m*-ethyltoluene, propylbenzene, and 1,2,4-trimethylbenzene) was photooxidized. The total organic aerosol concentration produced in the chamber was $28 \mu\text{g m}^{-3}$. Using the curves from Figure A.1.1, an appropriate yield value (Y_i) for each of the five aromatics, corresponding to a total organic aerosol mass concentration $\Delta M_o = 28 \mu\text{g m}^{-3}$, is obtained, and each

value is multiplied by the respective reacted ROG concentration (ΔROG_i) to produce an estimate of the amount of SOA attributed to each of the five species. Summing these values yields a total of $29.7 \mu\text{g m}^{-3}$, which is very close to the observed value of $28 \mu\text{g m}^{-3}$ (Table A.1.1). Thus, by using SOA yields for the individual ROGs in conjunction with equation (1), one can account for the aerosol that is produced from the oxidation of a mixture.

We performed 20 smog chamber experiments with 12 different reformulated gasolines obtained from the Auto/Oil Air Quality Improvement Research Program (AQIRP) (Table A.1.2). AQIRP was a cooperative program whose members included three domestic auto companies and 14 petroleum companies, the objective of which was to develop data on the potential improvements in vehicle emissions and air quality, primarily O_3 , from reformulated gasoline, various other alternative fuels, and developments in automotive technology [Burns *et al.*, 1991; Hochhauser *et al.*, 1991]. Molecular speciation of the AQIRP fuels was used to calculate the amount of each ROG (ΔROG_i) in the fuel mixture [Pahl and McNally, 1991]. We accomplished this procedure by quantifying the initial concentration of six to eight calibrated species present in each fuel using gas chromatography. Knowing the initial concentrations of these species, on the basis of the relative mass fractions of all the components in the fuel, we could calculate the initial concentration of every other species present. During the course of each experiment, the concentration time profiles of each of the calibrated species were measured and used along with their hydroxyl radical (OH) rate constants to determine the concentration time profile of OH in the chamber. Hydroxyl radical and O_3 rate constants were taken from review literature [Atkinson, 1994] and the National Institute of Standards

(NIST) chemical kinetics database [NIST, 1994] or, when experimentally not known, were estimated with the structure activity relations (SARs) [Kwok and Atkinson, 1995]. The SAR expressions for alkanes and alkenes were used unchanged; we modified those for aromatics by deriving a new Hammet constant for *meta*- substituents (σ_m^+). We optimized σ_m^+ for the ring addition rate constant (k_{add}) of 15 alkyl-substituted aromatics. The expression derived for use with SAR was $\log_{10}(k_{add})$ (cm³ molecule⁻¹ s⁻¹) = -11.89 - 1.82 $\Sigma \sigma^+$, where $\sigma^+ = \sigma_m^+ + \sigma_{o,p}^+$, with $\sigma_m^+ = -0.190$ for all *meta*-alkyl substituents and Hammet constants for *ortho* and *para* substituents ($\sigma_{o,p}^+$) as used in Kwok and Atkinson [1995]. The quality of the fit for the overall OH rate constant estimates for aromatics was improved to 30% maximum error, compared to 110% using the parameters in Kwok and Atkinson [1995]. Typical OH concentrations were 10⁶ molecules per cubic centimeter. This information, together with measured O₃ concentrations and the OH and O₃ rate constants for all other species, allowed us to determine the reacted amount of each species present in the fuel mixture during the course of an experiment.

The results of these experiments strongly support the hypothesis that aromatics play the predominant role in SOA formation associated with atmospheric oxidation of unburned gasoline. Plotting the ratio of the total SOA concentration produced from a given fuel to the reacted concentration of a fuel's aromatic constituents ($\Delta M_o/\Delta_{\text{aromatic}}$) versus ΔM_o (Figure A.1.2), we see that points for all fuels other than RF-L fall within the range specified by the yield curves that describe the majority of SOA yields from the individual aromatic studies (curves 1 and 2 from Figure A.1.1). If significant amounts of the SOA that was produced originated from species other than the aromatics, then most points would lie above the envelope specified by these two curves. The value of

Δ_{aromatic} was calculated by summing the reacted amount of each aromatic species in a fuel for a given experiment. The ratio of $\Delta M_o/\Delta_{\text{aromatic}}$ is a measure of the SOA yield of a fuel in terms of its aromatic fraction only. For the individual aromatic experiments, $\Delta M_o/\Delta_{\text{aromatic}} = Y$. For most fuels, 92 to 99% of the mass was speciated in AQIRP [Pahl and McNally, 1991]. Only 83% of the mass of fuel RF-L, which was the only high T_{90} AQIRP Phase I fuel used in this study, was speciated in AQIRP. Temperature T_{90} is the distillation temperature at which 90% of the fuel evaporates. It relates to a fuel's heavy-end volatility: Fuels with high T_{90} contain a significant fraction of heavy components. In Phase I of AQIRP, only 143 compounds were speciated, and many of the heavy components (including the aromatics) were not accounted for. In Phase II, 320 compounds were speciated, and many of the heavier aromatics were accounted for. Thus, more than 94% of the carbon, on average, was accounted for in all Phase II fuels (both high and low T_{90}).

Using the curves for the 17 species shown in Figure A.1.1, and assuming that all isomers of a given compound behave similarly, we obtained yield curves for 19 of the 26 aromatics speciated in Phase I of the AQIRP study. These 19 species represented, on average, 96% of Δ_{aromatic} for all fuels other than RF-A and RF-L. Of the 57 speciated aromatic compounds for the AQIRP Phase II fuels, yield curves were available for 28, representing, on average, 95% of Δ_{aromatic} . Obtaining a yield value, corresponding to the amount of SOA formed in an individual experiment, for an individual aromatic (Y_i) and multiplying that value by the reacted amount of the respective aromatic (ΔROG_i) produces an estimate of the amount of SOA attributable to that given aromatic species. Summing these values for all aromatics gives a quantitative estimate of the amount of

SOA ($\Delta M_o = \sum_i \Delta \text{ROG}_i Y_i$) that was produced by the aromatic fraction of each fuel (Figure A.1.3). These results quantitatively support the hypothesis that aromatic content controls a fuel's SOA formation potential. The average ratio of the SOA concentration predicted to be formed from a fuel's aromatic constituents to the observed SOA concentration for all fuels, excluding RF-L, is 1.00 ± 0.16 (1σ). Thus, it is evident that aromatics dominate the process of SOA formation associated with the atmospheric oxidation of whole gasoline vapor. Given the chemical complexity of whole gasoline, the results of this study suggest that SOA formation in an urban airshed can be modeled using yield data such as those presented here.

References

Atkinson, R., Gas-phase tropospheric chemistry of organic compounds, *J. Phys. Chem. Ref. Data, Monograph 2*, 1994.

Bowman, F.B., and J.H. Seinfeld, Atmospheric chemistry of alternate fuels and reformulated gasoline components, *Prog. Energy Combust. Sci.*, 21, 387-417, 1995.

Burns, V.R., J.D. Benson, A.M. Hochhauser, W.J. Koehl, W.M. Kreucher, and R.M. Reuter, *Description of the Auto/Oil Air Quality Improvement Research Program*, SAE Technical Paper No. 912320, Society of Automotive Engineers, Warren, PA, 1991.

Calvert, J.G., J.B. Heywood, R.F. Sawyer, and J.H. Seinfeld, Achieving acceptable air quality: Some reflections on controlling vehicle emissions, *Science*, 261, 37-45, 1993.

Gery, M.W., D.L. Fox, H.E. Jeffries, L. Stockburger, and W.S. Weathers, A continuous stirred tank reactor investigation of the gas-phase reaction of hydroxyl radicals and toluene, *Intl. J. Chem. Kinet.*, 17, 177-216, 1985.

Grosjean, D., *In situ* organic aerosol formation during a smog episode: estimated production and chemical functionality, *Atmos Environ.*, 26A, 953-963, 1992.

Grosjean, D., and J.H. Seinfeld, Parameterization of the formation potential of secondary organic aerosols, *Atmos. Environ.*, 23, 1733-1747, 1989.

Grosjean, D., in *Ozone and Other Photochemical Oxidants*, National Academy of Sciences, Washington, DC, 1977.

Harley, R.A., M.P. Hannigan, and G.R. Cass, Respeciation of organic gas emissions and the detection of excess unburned gasoline in the atmosphere, *Environ. Sci. Technol.*, 26, 2395-2408, 1992.

Hatakeyama, S., K. Izumi, T. Fukuyama, and H. Akimoto, Reactions of ozone with α -pinene and β -pinene in air: yields of gaseous and particulate products, *J. Geophys. Res.*, 96, 947-958, 1989.

Hochhauser, A.M., J.D. Benson, V. Burns, R.A. Gorse, W.J. Koehl, L.J. Painter, B.H. Rippon, R.M. Reuter, and J.A. Rutherford, *The Effect of Aromatics, MTBE, Olefins and T₉₀ on Mass Exhaust Emissions from Current and Older Vehicles – The Auto/Oil Air Quality Improvement Research Program*, SAE Technical Paper No. 912320, Society of Automotive Engineers, Warren, PA, 1991.

Hoekman, S.K., Speciated measurements and calculated reactivities of vehicle exhaust emissions from conventional and reformulated gasolines, *Environ. Sci. Technol.*, 26, 1206-1216, 1992.

Izumi, K., and T. Fukuyama, Photochemical aerosol formation from aromatic hydrocarbons in the presence of NO_x, *Atmos. Environ.*, 24A, 1433-1441, 1990.

Kwok, E.S.C., and R. Atkinson, Estimation of hydroxyl radical reaction rate constants for gas-phase organic compounds using a structure-reactivity relationship: an update, *Atmos. Environ.*, 29, 1685-1695, 1995.

Leone, J.A., R.C. Flagan, D. Grosjean, and J.H. Seinfeld, An outdoor smog chamber and modeling study of toluene-NO_x photooxidation, *Intl. J. Chem. Kinet.*, 17, 177-216, 1985.

NIST Chemical Kinetics Database ver 6.01; W.G. Mallard, F. Westley, J.T. Herron, R.F. Hampson, NIST Standard Reference Data, Gaithersburg, MD, 1994.

Odum, J.R., T. Hoffmann, F. Bowman, D. Collins, R.C. Flagan, and J.H. Seinfeld, Gas/particle partitioning and secondary organic aerosol yields, *Environ. Sci. Technol.*, 30, 2580-2585, 1996.

Pandis, S.N., S.E. Paulson, J.H. Seinfeld, and R.C. Flagan, Aerosol formation in the photooxidation of isoprene and β -pinene, *Atmos. Environ.*, 25A, 997-1008, 1991.

Pankow, J.F., An absorption model of the gas/aerosol partitioning involved in the formation of secondary organic aerosol, *Atmos. Environ.*, 28, 189-193, 1994.

Pahl, R.H., and M.J. McNally, *Fuel blending and analysis for the Auto/Air Quality Improvement Research Program*, SAE Technical Paper No. 902098, Society of Automotive Engineers, Warren, PA, 1991.

Pope III, C.A., D.V. Bates, M.E. Raizenne, Health effects of particulate air pollution – time for reassessment, *Environ. Health Perspect.*, 103, 472-480, 1995.

Russell, A., J. Milford, M.S. Bergin, S. McBride, L. McNair, Y. Yang, W.R. Stockwell, and B. Croes, Urban ozone control and atmospheric reactivity of organic gases, *Science*, 269, 491-495, 1995.

Schwartz, J., D.W. Dockery, and L.M Neas, Is daily mortality associated specifically with fine particles?, *J. Air Waste Manage. Assoc.*, *46*, 927-939, 1996.

Shprentz, D.S., *Breath Taking: Premature Mortality Due to Particulate Air Pollution in 239 American Cities*, National Resources Defense Council, New York, 1996.

Stern, J.E., R.C. Flagan, D. Grosjean, and J.H. Seinfeld, Aerosol formation and growth in atmospheric aromatic photooxidation, *Environ. Sci. Technol.*, *21*, 1224-1231, 1987.

Turpin, B.J., and J.J. Huntzicker, Secondary formation of organic aerosol in the Los Angeles Basin: A descriptive analysis of organic and elemental carbon concentrations, *Atmos. Environ.*, *25A*, 207-215, 1991.

Turpin, B.J., J.J. Huntzicker, S.M. Larson, and G.R. Cass, Los Angeles summer-midday particulate carbon: Primary and secondary aerosol, *Environ. Sci. Technol.*, *25*, 1788-1793, 1991.

Wang, S.-C., S.E. Paulson, D. Grosjean, R.C. Flagan, and J.H. Seinfeld, Aerosol formation and growth in atmospheric organic/NO_x systems – I. Outdoor smog chamber studies of C₇- and C₈- hydrocarbons, *Atmos. Environ.*, *26A*, 403-420, 1992.

Table A.1.1. Estimation of the contributions by individual species to the SOA formed from the photooxidation of a five-hydrocarbon mixture. Values of yield Y are taken from the curves shown in Figure A.1.1 at a value of $\Delta M_o = 28 \mu\text{g m}^{-3}$.

Species	Initial ROG ($\mu\text{g m}^{-3}$)	ΔROG ($\mu\text{g m}^{-3}$)	Y ($\mu\text{g m}^{-3}$)	$\Delta\text{ROG} \times Y$ ($\mu\text{g m}^{-3}$)
Toluene	663	265	0.049	13.0
m-Xylene	330	284	0.027	7.6
m-Ethyltoluene	105	89	0.049	4.4
n-Propylbenzene	40	16	0.049	0.8
1,2,4-Trimethylbenzene	162	147	0.027	3.9
Total				29.7

Table A.1.2. Properties of AQIRP reformulated gasolines. MTBE = the fuel additive methyl tertiary butyl ether; the fuel identification code is derived A(a) = high (low) aromatics, M(m) = high (low) MTBE, O(o) = high (low) olefins, T(t) = high (low) T_{90} , RMH = medium and heavy reformate cut (predominantly C₉- and C₁₀- aromatics), and AH = heavy alkylate cut (heavy paraffins).

Fuel Code	AQIRP Phase	Fuel ID	Aromatics (vol %)	MTBE (vol %)	Olefins (vol %)	T_{90} (°C)
A	I	Industry average	32.0	0.0	9.2	166
F	I	amot	20.0	0.0	3.2	137
G	I	AmOt	44.3	0.0	17.4	141
K	I	Amot	45.7	0.0	4.9	146
L	I	AmOT	47.8	0.0	17.7	181
O	I	AMOt	46.7	14.6	19.3	139
P	I	amOt	20.3	0.0	18.3	140
C2	II	CA Phase II	25.4	11.2	4.1	145
1B	II	Matrix B base	25.3	11.2	15.0	131
2B	II	Base + RMH	35.1	10.4	11.2	157
3B	II	Base + AH	22.1	10.4	13.3	148
4B	II	Base + AH + RMH	32.2	10.2	10.7	168

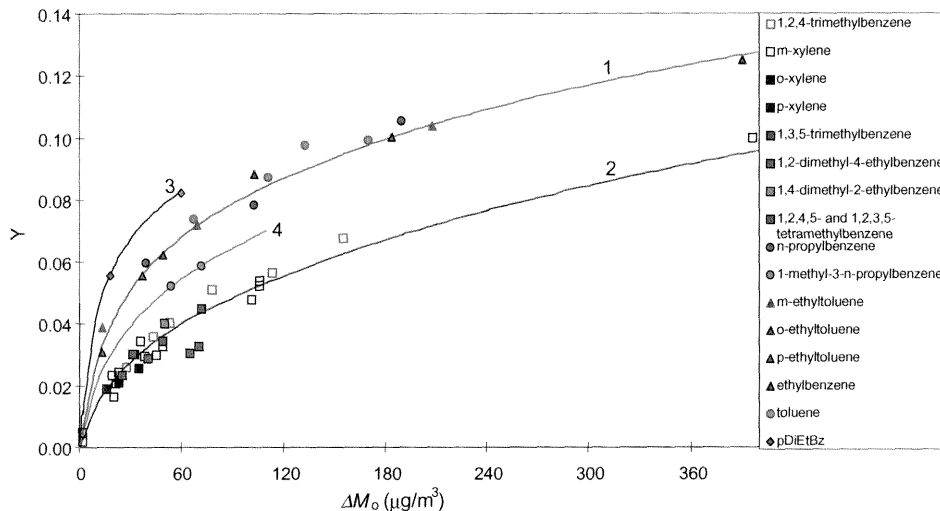


Figure A.1.1. Secondary organic aerosol yield as a function of total organic aerosol mass concentration (ΔM_o) for 17 individual aromatic species. Each point represents an individual experiment. Curves were fit to the data using a two-product model in conjunction with equation (1) by minimizing the weighted squared residuals. Curve 1 is fit with values 0.071, 0.053, 0.138, and 0.0019 for α_1 , $K_{om,1}$, α_2 , and $K_{om,2}$, respectively. The corresponding values are 0.038, 0.042, 0.167, and 0.0014 for curve 2, 0.083, 0.093, 0.22, and 0.001 for curve 3, and 0.05, 0.054, 0.136, and 0.0023 for curve 4.

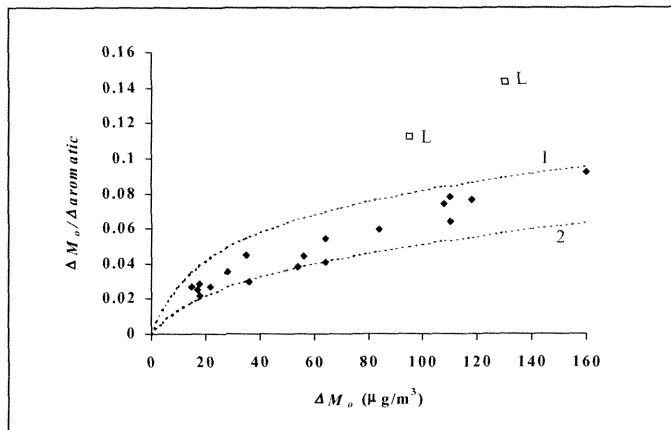


Figure A.1.2. Plot of $\Delta M_o/\Delta\text{aromatic}$ as a function of ΔM_o for 12 different AQIRP gasolines (Table A.1.2). Curves 1 and 2 are taken from Figure A.1.1. $\Delta M_o/\Delta\text{aromatic}$ is equivalent to the SOA yield if $\Delta\text{aromatic}$ is equal to ΔROG . Each point represents an individual experiment. Changes in ΔM_o for an individual fuel were obtained by varying fuel initial concentrations.

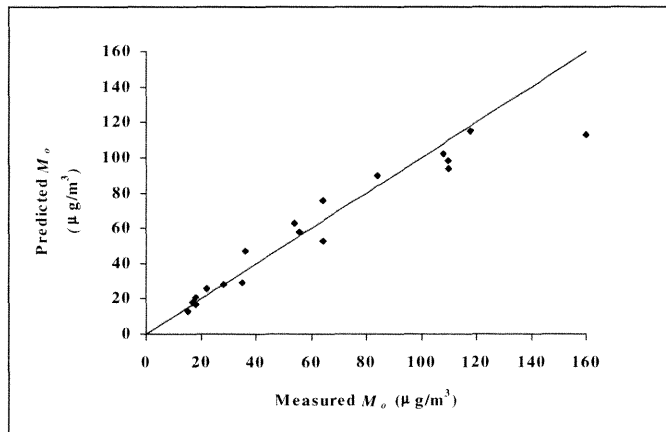


Figure A.1.3. Comparison between observed total SOA concentrations produced from the oxidation of whole gasoline vapor and total SOA concentrations predicted to be formed solely from the fuel's aromatic components.

Appendix 2

Observation of Gaseous and Particulate Products of Monoterpene Oxidation in Forest Atmospheres

Reference: J. Yu, R.J. Griffin, D.R. Cocker III, R.C. Flagan, J.H. Seinfeld, and P. Blanchard, *Geophys. Res. Lett.*, 26, 1145-1148, 1999.

Abstract

Atmospheric oxidation of biogenic hydrocarbons, such as monoterpenes, is estimated to be a significant source of global aerosol. Whereas laboratory studies have established that photochemical oxidation of monoterpenes leads to aerosol formation, there are limited field studies detecting such oxidation products in ambient aerosols. Drawing on prior results of monoterpene product analysis under controlled smog chamber conditions, we have identified organic aerosol components attributable to monoterpene oxidation in two forest atmospheres, Kejimkujik National Park, Nova Scotia, Canada, and Big Bear, San Bernardino National Forest, California, U.S.A. The major identified aerosol products derived from α -pinene and β -pinene oxidation include pinic acid, pinonic acid, norpinonic acid and its isomers, hydroxy pinonaldehydes, and pinonaldehyde, concentrations of which in the aerosol phase are in the sub ng m^{-3} range. Identification of oxidation products in atmospheric aerosol samples serves as direct evidence for aerosol formation from monoterpenes under ambient conditions.

A.2.1 Introduction

The atmospheric aerosol-forming potential of biogenic hydrocarbons was noted as early as 1960 [Went, 1960], and laboratory studies have established that atmospheric oxidation of monoterpenes and sesquiterpenes leads to aerosol formation [Hoffmann *et al.*, 1997; Griffin *et al.*, 1999]. Production of biogenic secondary organic aerosols on a global basis is estimated to range between 30 and 270 Tg year⁻¹, a magnitude comparable to the production of biogenic and anthropogenic sulfate aerosols [Andreae and Crutzen, 1997].

Monoterpenes are important constituents of aerosol-forming biogenic compounds [Griffin *et al.*, 1999]. Despite numerous field measurements of gas-phase monoterpenes [e.g., Roberts *et al.*, 1983; Zimmerman *et al.*, 1988; Clement *et al.*, 1990; Biesenthal *et al.*, 1998], there are few field studies in which their oxidation products have been measured. Recent advances in analytical methods have now made it possible to detect and identify such secondary organic aerosol components, which generally have multiple polar oxygenated functional groups [Yu *et al.*, 1998; 1999]. Ambient measurements of biogenic hydrocarbon oxidation products in the atmospheric aerosol provide the link that establishes the importance of this source to global tropospheric aerosol. We present here measurements of monoterpene-derived aerosol components in two forest atmospheres, Kejimkujik National Park, Nova Scotia, Canada, and San Bernardino National Forest, California, U.S.A.

A.2.2 Ambient Sampling and Analysis

The measurement site in Kejimkujik National Park ($44^{\circ}26' N$, $62^{\circ}12' W$) is situated in the Atlantic province of Nova Scotia. The park is in a forest consisting of a mixture of two-thirds coniferous and one-third deciduous trees [Bottenheim *et al.*, 1994]. Ambient mixing ratios of α -pinene and β -pinene were determined on-line using a Hewlett-Packard GC/MS [Biesenthal *et al.*, 1998]. Aerosol samples were collected in July, 1996, over a period of two to three days at a flow rate of 10 L min^{-1} on 47 mm quartz fiber filters. Since the aerosol samples were collected in a field campaign that did not include characterizing semivolatile organics as one of its goals, adequate sampling devices were not implemented to minimize sampling artifacts for semivolatiles. Collection of two filter samples analyzed in this work commenced on July 5 and July 8,

based on a sampled air volume of 26.94 and 44.72 m³, respectively. The diurnal temperature during the sampling period ranged from 11 to 21°C, and the relative humidity from 13% to 50% [Leaitch *et al.*, 1999].

The measurement site in the San Bernardino National Forest is located in Big Bear Valley (34°13' N, 116°49' W), CA, at an elevation of 2150 meters. Lodgepole pines, pinion pines, oaks, and Douglas firs are major tree species in this area. Hourly measurements of gas-phase monoterpenes were achieved by collecting 300 L of air on Tenax tubes, and were then analyzed by a Hewlett-Packard GC/MS following thermal desorption using a Tekmar AeroTrap Desorber 6000. Two types of aerosol sampling devices were deployed, one consisting of one or two denuders followed by a Teflon impregnated glass fiber filter, and the other one consisting of two 47 mm filters--a Teflon impregnated glass fiber filter followed by a glass fiber filter. Two sampling trains were set up for each type of sampling device. The sampling train with two denuders was used to quantify denuder collection efficiency. Samples were collected from 19:00 PDT Aug. 31 to 13:00 PDT Sep. 1, 1998, at a flow rate of 22 L min⁻¹. The back filter in the two-filter set-up was used for assessing filter adsorption of gaseous semivolatile organics. Ambient temperature during the sampling period varied from 18 to 32°C, and relative humidity ranged from 20% to 59%.

Denuder samples were extracted on-site, and all samples were stored at 0°C before analysis. The procedure for extraction, subsequent processing, and analysis of denuder and filter samples has been described elsewhere [Yu *et al.*, 1999]. The extracts of denuder and filter samples were derivatized by (2,3,4,5,6-pentafluorobenzyl) hydroxy amine (PFBHA) and N, O-bis (trimethylsilyl)-trifluoroacetamide. By this procedure,

carbonyl functional groups of the oxidation products were converted into oximes, and carboxyl and hydroxyl function groups were converted into trimethylsilyl (TMS) groups. The resulting derivatives were then analyzed by GC/MS, using both electronic ionization (EI) and chemical ionization (CI) modes for identification and quantification. Blank filters in both studies were treated and analyzed following the same procedures applied to the sample filters. Quantification of products for which authentic standards do not exist was achieved by using surrogate compounds that have the same functional groups and approximate carbon numbers [Yu *et al.*, 1999].

A.2.3 Results and Discussion

A.2.3.1 Identification of Monoterpene Oxidation Products

Oxidation products of α -pinene and β -pinene in the ambient samples were identified by comparing GC chromatograms and mass spectra of the ambient samples with those obtained from controlled chamber experiments. Table A.2.1 lists the chemical structures of the monoterpene oxidation products observed.

Established products from oxidation of α -pinene and β -pinene include pinic acid, norpinic acid, pinonaldehyde, norpinonaldehyde, hydroxy pinonaldehydes, pinonic acid, norpinonic acid, hydroxy pinonic acid, hydroxy pina ketones, and nopinone. An unidentified product (denoted X_1), having two carbonyl groups and a molecular weight of 198 as determined from its EI and CI mass spectra, is observed in both laboratory generated aerosol in the α -pinene/ O_3 system and ambient aerosols at both sites. Besides oxidation products derived from α -pinene and β -pinene, a compound denoted X_2 , detected in samples from both sites, is identified as a C_9 dioxo mono-carboxylic acid,

having a molecular weight of 186. Figure A.2.1 displays the CI mass spectrum for the PFBHA and TMS derivative of this compound X₂. The molecular weight and some structural information can be determined from the mass spectrum [Yu *et al.*, 1998]. Ozone oxidation of limonene could lead to the formation of a C₉ dioxo mono-carboxylic acid, 3-acetyl-6-oxo-heptanoic acid, as illustrated in Figure A.2.2 [Horie *et al.*, 1994; Neeb *et al.*, 1997]. The mass spectrum shown in Figure A.2.1 is consistent with that expected for this compound.

A.2.3.2 Kejimkujik Samples

Table A.2.2 lists mixing ratios of three monoterpenes and concentrations of various monoterpene oxidation products in the aerosol phase in two filter samples collected in Kejimkujik National Park. All the identified oxidation products are detected at the sub-nanogram m⁻³ level. The presence of monoterpene oxidation products in filter samples correlates with the observation that aerosol volume increased with the decrease in α -pinene and β -pinene during the same sampling period at this same site [Leaitch *et al.*, 1999].

A.2.3.3 Big Bear Samples

Table A.2.3 lists the mixing ratios of six monoterpenes and the concentrations of various monoterpene oxidation products detected in both the gas and aerosol phases in the San Bernardino National Forest of California. The denuder/filter set-up at this site allowed simultaneous determination of semi-volatile compounds in both gas and particulate phases. Species collected by the denuder represent those in the gas phase. Denuder collection efficiencies for the products in Table A.2.3 range from 0.88 to 1.0.

Gas-phase concentrations as determined from denuder samples have been corrected for the denuder collection efficiency for each product. As evident in Table A.2.3, the monoterpene oxidation products at this site predominately exist in the gas phase. A number of oxidation products were detected solely in the gas phase due to either their high volatility (e.g., nopinone, hydroxy pina ketones, and norpinonaldehyde) or to such a low concentration in the air that the amount partitioned to the aerosol phase is below detection limit (e.g., norpinonic acid and hydroxy pinonic acid).

Comparison of filter samples in the presence and absence of a denuder in front of the sampling train indicates that the filter-only technique suffers a positive sampling artifact. Semivolatile products are also detected on the back filter in the filter-only setup, which is evidence for filter adsorption of gaseous semivolatile organics. Concentrations obtained via the filter-only technique are 120%-137% higher than those obtained using the denuder/filter sampling device for sampling conditions employed at the Big Bear site. *McDow and Huntzicker* [1990] observed a significant increase of positive artifact with decreasing filter face velocity for a quartz fiber filter. They estimated that at low organic carbon concentrations, the correction factor due to adsorption could exceed 50% at a sampling face velocity of 40 cm s^{-1} . Considering the lower face velocity ($\sim 20 \text{ cm s}^{-1}$), the positive artifact observed at the Big Bear site is in general agreement with the results of *McDow and Huntzicker* [1990]. Therefore, the filter-only technique is not adequate for measurements of biogenic oxidation products in the aerosol phase. Concentrations derived from the two Kejimkujik filter samples likely overestimate the actual aerosol concentrations for this reason.

A.2.4 Comparison with Prior Field Studies

Previous field measurements of particulate-phase terpene oxidation products have been limited to pinonaldehyde, pinonic acid, and nopinone. A recent study has also measured ambient concentrations of pinic acid and norpinonic acid [Kavouras *et al.*, 1999]. *Yokouchi and Ambe* [1985] measured pinonaldehyde concentrations of 2-3 ng m⁻³ in aerosol samples collected in the cedar forest at Kiyosumi and in the pine forest at Tsukuba in Japan in summer time. *Satsumabayashi et al.* [1990] detected pinonaldehyde at 30 ng m⁻³ and 100 ng m⁻³ at two mountainous sites in central Japan. *Calogirou et al.* [1997] observed pinonaldehyde near Ispra, Italy, at 90 ng m⁻³ using DNPH-coated cartridges. Since an ozone scavenger was used in this study, which also collected particles, this concentration reflects that in the gas-phase. *Kavouras et al.* [1998] reported aerosol concentrations for pinonic acid, nopinone, and pinonaldehyde ranging from 9-140, 0.3-13.2, and 0.17-32.1 ng m⁻³, respectively, at a forest site in Portugal. In the most recent study, *Kavouras et al.* [1999] deployed a denuder/filter sampling device to measure monoterpene oxidation products in both gas and aerosol phases in a conifer forest located in Pertouli in Central Greece. They reported diurnal particulate concentrations for pinonic acid, pinic acid, norpinonic acid, pinonaldehyde, and nopinone to be 1.0-25.7, 0.4-4.4, 0.2-5.4, 0.2-1.2, and 0-0.4 ng m⁻³, respectively. In this study, simultaneous measurements of Aitken nuclei also provided evidence that the photooxidation products from biogenic precursors play a role in forming new particles.

Considering the many factors influencing concentrations of aerosol-phase monoterpene oxidation products, the wide variability of ambient concentrations among the six studies is not surprising. Pinonaldehyde, for example, was measured in all six

studies with concentrations ranging from under detection limit to 100 ng m⁻³.

Concentrations of precursor monoterpenes and atmospheric oxidants govern formation rate of the products. The higher mixing ratios of α -pinene (0-3.2 ppbv) and β -pinene (0-1.4 ppbv) may partly account for the more plentiful oxidation products in the aerosol phase in the study of *Kavouras et al.* [1999]. The aerosol-phase fraction of a semi-volatile organic compound, such as any of the monoterpene oxidation products, is known to be controlled by available organic aerosol mass and the compound's gas-aerosol partitioning coefficient, which, in turn, is a function of temperature and the overall aerosol chemical composition [*Odum et al.*, 1996; *Jang et al.*, 1997; *Jang and Kamens*, 1999; *Yu et al.*, 1999]. Besides these factors intrinsic to aerosol formation, sampling artifacts can also introduce variability in the reported concentrations. For example, as noted earlier, the filter-only technique suffers a positive artifact from adsorption of gas-phase semi-volatiles onto the filter surface, whereas volatilization of aerosol-phase semi-volatiles introduces a negative artifact, which depends on sampling rate and filter area [*McDow and Huntzicker*, 1990]. In addition, a number of products (e.g., pinonaldehyde and norpinonic acid) do not have available commercial standards, and different surrogate compounds have been used to estimate their concentrations.

A.2.5 Conclusions

We have detected in two forest atmospheres a number of gas- and aerosol-phase products from oxidation of α -pinene and β -pinene, including pinic acid, norpinic acid, pinonic acid, norpinonic acid and its isomers, pinonaldehyde, norpinonaldehyde, hydroxy pinonaldehydes, hydroxy pinonic acid, and nopinone. In addition, a C₉ dioxo carboxylic acid, detected at both sites, is postulated to be 3-acetyl-6-oxo-heptanoic acid, a product

expected from ozone oxidation of limonene. Identification of monoterpene oxidation products in aerosol samples serves as direct evidence for aerosol formation from monoterpenes under ambient conditions.

A.2.6 References

Andreae, M. O., and P.J. Crutzen, Atmospheric aerosols: Biogeochemical sources and role in atmospheric chemistry, *Science*, 276, 1052-1055, 1997.

Biesenthal, T.A., J.W. Bottenheim, P.B. Shepson, and P.C. Brickell, The chemistry of biogenic hydrocarbons at a rural site in eastern Canada, *J. Geophys. Res.*, 103, 25,487-25,498, 1998.

Bottenheim, J.W., A. Sirois, K.A. Brice, and A.J. Gallant, Five years of continuous observation of PAN and ozone at a rural location in Eastern Canada, *J. Geophys. Res.*, 99, 5333-5352, 1994.

Calogirou, A., M. Duane, D. Kotzias, M. Lahaniati, and B.R. Larsen, Polyphenylenesulfide NOXON, an ozone scavenger for the analysis of oxygenated terpenes in air, *Atmos. Environ.*, 13, 2741-2751, 1997.

Clement, B., M.L. Riba, R. Leduc, M. Haziza, and L. Terres, Concentration of monoterpenes in a maple forest in Quebec, *Atmos. Environ.*, 24A, 2513-2516, 1990.

Griffin, R.J., D.R. Cocker, R.C. Flagan, and J.H. Seinfeld, Organic aerosol formation from the oxidation of biogenic hydrocarbon., *J. Geophys. Res.*, 104, 3555-3568, 1999.

Hoffmann, T., J.R. Odum, F. Bowman, D. Collins, D. Klockow, R.C. Flagan, and J.H. Seinfeld, Formation of organic aerosols from the oxidation of biogenic hydrocarbons, *J. Atmos. Chem*, 26, 189-222, 1997.

Horie, O., P. Neeb, S. Limbach, and G.K. Moortgat, Formation of formic acid and organic peroxides in the ozonolysis of ethene with added water vapor, *Geophys. Res. Lett.*, 21, 1523-1526, 1994.

Jang, M., and R.M. Kamens, Newly characterized products and composition of secondary aerosols from the reaction of α -pinene with ozone, *Atmos. Environ.*, 33, 459-474, 1999.

Jang, M., R.M. Kamens, K.B. Leach, and M.R. Strommen, A thermodynamic approach using group contribution methods to model the partitioning of semivolatile organic compounds on atmospheric particulate matter, *Environ. Sci. Technol.*, 31, 2805-2811, 1997.

Kavouras, I.G., N. Mihalopoulos, and E.G. Stephanou, Formation of atmospheric particles from organic acids produced by forests, *Nature*, 395, 683-686, 1998.

Kavouras, I.G., N. Mihalopoulos, and E.G. Stephanou, Formation and gas/particle partitioning of monoterpenes photooxidation products over forests, *Geophys. Res. Lett.*, 26, 55-58, 1999.

Leaitch, W.R., J.W. Bottenheim, T.A. Biesenthal, S.M. Li, P.S. K. Liu, K. Asalien, H. Dryfhout-Clark, F. Hopper, and F. Brechtel, A case study of gas-to-particle conversion in an eastern Canadian Forest, *J. Geophys. Res.*, 104, 8095-8111, 1999.

McDow, S.R., and J.J. Huntzicker, Vapor adsorption artifact in the sampling of organic aerosol: Face velocity effects, *Atmos. Environ.*, 24A, 2563-2571, 1990.

Neeb, P., F. Sauer, and O. Horie, Formation of hydroxymethyl hydroperoxide and formic acid in alkene ozonolysis in the presence of water vapor, *Atmos. Environ.*, 31, 1417-1423, 1997.

Odum, J.R., T. Hoffmann, F. Bowman, D. Collins, R.C. Flagan, and J.H. Seinfeld, Gas/particle partitioning and secondary organic aerosol yields, *Environ. Sci. Technol.*, 30, 2580-2585, 1996.

Roberts, J.M., F.C. Fehsenfeld, D.L. Albritton, and R.E. Sievers, Measurement of monoterpane hydrocarbons at Niwot Ridge, Colorado, *J. Geophys. Res.*, 88, 667-678, 1983.

Satsumabayashi, H., H. Kurita, Y. Yokouchi, and H. Ueda, Photochemical formation of particulate dicarboxylic acids under long-range transport in Central Japan, *Atmos. Environ.*, 24A, 1443-1450, 1990.

Went, F.W., Blue hazes in the atmosphere, *Nature*, 187, 641-643, 1960.

Yokouchi, Y., and Y. Ambe, Aerosols formed from the chemical reaction of monoterpenes and ozone, *Atmos. Environ.*, 19, 1271-1276, 1985.

Yu, J., R.C. Flagan, and J.H. Seinfeld, Identification of products containing -COOH, -OH, and -C=O in atmospheric oxidation of hydrocarbons, *Environ. Sci. Technol.*, 32, 2357-2370, 1998.

Yu, J., D.R. Cocker III, R.J. Griffin, R.C. Flagan, and J.H. Seinfeld, Gas-phase ozone oxidation of monoterpenes: Gaseous and particulate products, *J. Atmos. Chem.*, 104, 3555-3568, 1999.

Zimmerman, P.R., J.P. Greenberg and C.E. Westberg, Measurement of atmospheric hydrocarbons and biogenic emission fluxes in the Amazon boundary layer, *J. Geophys. Res.*, 93, 1407-1416, 1988.

Table A.2.1. Monoterpene oxidation products detected at forest sites.

Name	Structure	note
$C_8H_{12}O_4$		
norpinic acid		a, b MW=172
$C_9H_{14}O_4^*$		
pinic acid		c, d MW=186
$C_9H_{14}O^*$		
nopinone		e, f MW=138
$C_9H_{14}O_2$		
hydroxy pina		e, f ketones
MW=154		
$C_9H_{14}O_3$		
norpinonic acid		a, d & its isomers
MW=170		
$C_{10}H_{16}O_3^*$		
pinonic acid		g, d MW=184

Table A.2.1. (continued) Monoterpene oxidation products detected at forest sites.

Name	Structure	note
$C_{10}H_{16}O_4$		
hydroxy pinonic acid		a, h
MW=200		
$C_9H_{14}O_2$		
norpinonaldehyde		g, f
MW=154		
$C_{10}H_{16}O_2$		
pinonaldehyde		g, d
MW=168		
$C_{10}H_{16}O_3$		
hydroxy pinonaldehydes		g, d
MW=184		
X_1	two carbonyl groups	g, d
MW=198		
X_2	e.g.	
$C_9H_{14}O_4$		i, d
MW=186		

Table A.2.1. (continued) Monoterpene oxidation products detected at forest sites.

^{*} identification confirmed with an authentic standard.

^a known product of O₃ oxidation of α -pinene and β -pinene.

^b detected in Kejimkujik samples.

^c known product of O₃ oxidation of α -pinene, β -pinene, sabinene and Δ^3 -carene.

^d detected in Kejimkujik and Big Bear samples.

^e known product of O₃ oxidation of β -pinene.

^f detected in Big Bear denuder samples.

^g known product of O₃ oxidation of α -pinene.

^h detected in Big Bear denuder and filter samples.

ⁱ possible product of O₃ oxidation of limonene.

Table A.2.2. Monoterpene oxidation products in filter samples collected in Kejimkujik National Park, Nova Scotia.

monoterpene	mixing ratio (pptv)	product	conc. (ng m ⁻³)	
			960705 ^a	960708 ^a
α-pinene	88-283	147-642	norpinic acid ^b	0.34
β-pinene	69-401	209-864	pinic acid	0.48
camphene	60-442	156-561	norpinonic acid & its isomers ^c	0.24
			pinonic acid	0.39
			pinonaldehyde ^d	0.19
		hydroxy pinonaldehydes ^c	0.12	ND ^e
		X ₁ ^d	0.12	0.13
		X ₂ ^c	0.19	0.13

^a Dates when aerosol samples commenced

^b Quantified using the calibration factor and recovery for pinic acid.

^c Quantified using the calibration factor and recovery for pinonic acid.

^d Quantified using the calibration factor and recovery for 5-methyl-cyclohexane-1,3-dione.

^e Not detectable.

Table A.2.3. Gaseous and particulate monoterpene oxidation products in samples collected in San Bernardino National Forest, California.

monoterpene	mixing ratio (pptv)	product	conc.(ng m ⁻³) ^a	
	range	avg.	gas	aerosol
α-pinene	22 – 119	63	pinic acid	11.5
β-pinene	16 - 111	50	norpinonic acid & its isomers	12.3
limonene	13 - 63	27	pinonic acid	202.4
camphene	7 - 76	36	norpinonaldehyde	4.7
Δ ³ -carene	2 - 21	10	pinonaldehyde	280
junipene	0 - 8	5	hydroxy pinonaldehydes	16.8
			X ₁	3.3
			X ₂	17.8
			hydroxy pinonic acid	9.0
			hydroxy pina ketones	18.0
			nopinone & isomers ^c	132.9
				ND

^a average values of two samples.

^b Not detectable.

^c Possible isomers include primary carbonyl products from ozone oxidation at the external C=C bond in limonene and camphene.

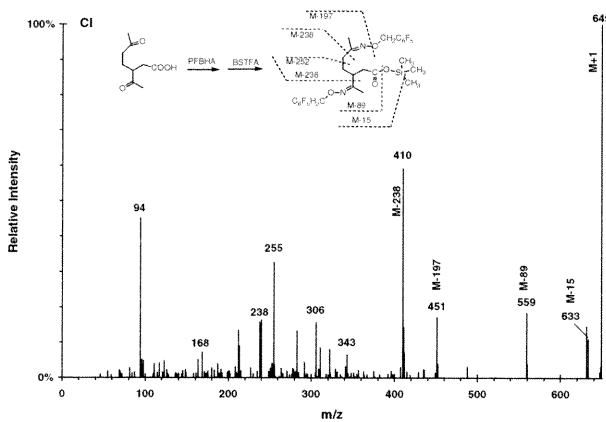


Figure A.2.1. Chemical ionization mass spectrum for the derivative of a C₉ dioxo carboxylic acid compound detected in aerosol samples.

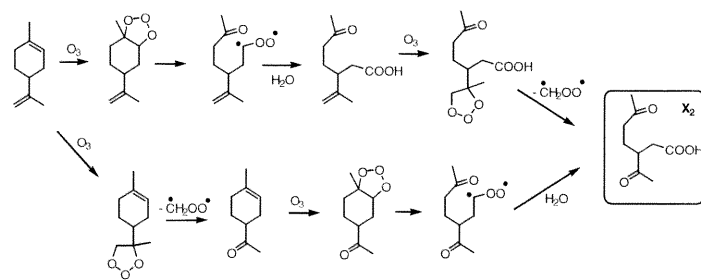


Figure A.2.2. Formation pathways for a C₉ dioxo carboxylic acid product from oxidation of limonene.

Appendix 3

Gas-phase Ozone Oxidation of Monoterpenes: Gaseous and Particulate Products

Reference: J. Yu, D.R. Cocker III, R.J. Griffin, R.C. Flagan, and J.H. Seinfeld, *J. Atmos. Chem.*, 34, 207-258, 1999.

Abstract

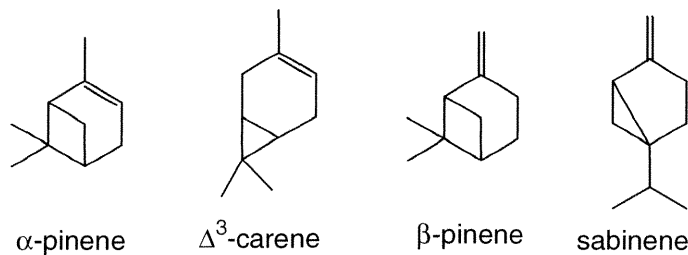
Atmospheric oxidation of monoterpenes contributes to formation of tropospheric ozone and secondary organic aerosol, but their products are poorly characterized. In this work, we report a series of outdoor smog chamber experiments to investigate both gaseous and particulate products in the ozone oxidation of four monoterpenes: α -pinene, β -pinene, Δ^3 -carene, and sabinene. More than ten oxygenated products are detected and identified in each monoterpene/O₃ reaction by coupling derivatization techniques and GC/MS detection. A denuder/filter pack sampling system is used to separate and simultaneously collect gas and aerosol samples. The identified products, consisting of compounds containing carbonyl, hydroxyl, and carboxyl functional groups, are estimated to account for about 34-50%, 57%, 29-67%, and 24% of the reacted carbon mass for β -pinene, sabinene, α -pinene, and Δ^3 -carene, respectively. The identified individual products account for >83%, ~100%, >90%, and 61% of the aerosol mass produced in the ozone reaction of β -pinene, sabinene, α -pinene, and Δ^3 -carene. The uncertainty in the yield data is estimated to be $\sim \pm 50\%$. Many of the products partition between gas and aerosol phases, and their gas-aerosol partitioning coefficients are determined and reported here. Reaction schemes are suggested to account for the products observed.

A.3.1. Introduction

Emissions of biogenic organic compounds have been estimated to dominate over those from anthropogenic sources on a global basis [Guenther *et al.*, 1995]. As important constituents of biogenic VOC emissions, the C₁₀H₁₆ monoterpenes contribute to formation of tropospheric ozone and secondary organic aerosol (SOA) [Kamens *et al.*,

1981; Chameides *et al.*, 1988; Pandis *et al.*, 1991; Zhang *et al.*, 1992; Hoffmann *et al.*, 1997; Griffin *et al.*, 1999]. Whereas the rate constants of monoterpenes with OH radicals, NO₃ radicals, and O₃ are reasonably well established, the reaction products are less well understood [Atkinson, 1997; Calogirou *et al.*, 1999]. Information on both gaseous and particulate products is important to elucidate the mechanism of oxidation and to understand the formation of secondary organic aerosol.

In a previous paper, we reported the identification of ozone oxidation products of α -pinene and Δ^3 -carene (see below for chemical structures) [Yu *et al.*, 1998]. In this work we have investigated ozone oxidation products of two additional bicyclic monoterpenes, β -pinene and sabinene, for which little product information is known.



At an initial β -pinene mixing ratio of several ppmv, nopinone is the only product that has previously been clearly identified from O₃ oxidation of β -pinene, besides low-molecular products such as formaldehyde, CO, and CO₂ [Hatakeyama *et al.*, 1989; Grosjean *et al.*, 1993; Hakola *et al.*, 1994]. For the sabinene/O₃ reaction, sabina ketone is the only known product [Hakola *et al.*, 1994].

Few studies have been carried out to determine yields of gaseous and particulate products from ozone oxidation of the monoterpenes, and to our knowledge, no study has been reported to examine gaseous and particulate oxidation products simultaneously. The semi-volatile nature of many of the oxidation products dictates that they partition

between the gas and aerosol phases. The filter-only technique, which is the most common aerosol sampling method, results in positive artifacts from adsorption of gaseous semi-volatile compounds on the filter [McDow and Huntzicker, 1990; Hart and Pankow, 1994]. We have employed a denuder/filter pack system to separate gaseous and particulate semivolatile compounds and to minimize sampling artifacts. Using this sampling device, we have measured the product yields from the ozone oxidation of the four monoterpenes in both gas and aerosol phases and determined their gas-aerosol partitioning coefficients.

Detection and identification of products from oxidation of biogenic hydrocarbons are hindered by the fact that many contain functional groups such as carbonyl and carboxylic acids that are poorly resolved by standard gas chromatography. We have recently reported a method to detect and identify organics containing -C=O (aldehyde and ketone), -OH (hydroxy), and -COOH (carboxyl) groups [Yu *et al.*, 1998]. In this method, -C=O groups are derivatized using O-(2,3,4,5,6-pentafluorobenzyl) hydroxy amine (PFBHA) and -COOH and -OH groups are derivatized using a silylation reagent, N,O-bis(trimethylsilyl)-trifluoroacetamide (BSTFA), to give trimethylsilyl (TMS) derivatives. The resulting derivatives are easily resolved by a GC column and identified by their chemical ionization (CI) and electronic ionization (EI) mass spectra. The CI mass spectra of these derivatives exhibit several pseudo-molecular ions, allowing unambiguous determination of molecular weights. The EI mass spectra allow functional group identification by exhibiting ions characteristic of each functional group: m/z 181 for carbonyl and m/z 73 and 75 for carboxyl and hydroxy groups. In addition, each functional group is associated with a unique set of pseudo-molecular ions in CI spectra.

The PFBHA-carbonyl derivatives give rise to pseudo-molecular ions at m/z M+181, M-181 and M-197, whereas the TMS derivatives of OH/COOH containing compounds have pseudo-molecular ions at m/z M+73, M-15 and M-89. We refer the reader to *Yu et al.* [1998] for a detailed description of the mass spectra fragment patterns.

A.3.2. Experimental Section

A.3.2.1 Smog chamber experiments and sample collection

Samples were collected from a series of β -pinene/ O_3 , sabinene/ O_3 , α -pinene/ O_3 , and Δ^3 -carene/ O_3 experiments conducted in the dark in a 60-m³ Teflon reactor, which has been described previously [Hoffmann *et al.*, 1997; Griffin *et al.*, 1999]. When fully inflated, the reactor has a surface to volume ratio (S/V) of 1.8 m⁻¹. This reactor was normally divided in the center so that two experiments could be run under identical environmental conditions. The temperature in the reactor was maintained between 305 and 310 K to approximate that of a typical afternoon smog chamber experiment. To achieve this, the entire reactor was covered with an insulating cover as well as a black tarpaulin. In addition, four Holmes (Milford, MA) Model HFH-501FP space heaters were placed in the open area underneath the reactor. In a typical experiment, seed particles of $(NH_4)_2SO_4$ were injected into the chamber to obtain initial particle concentrations of approximately 9,000-17,000 particle cm⁻³. The initial size distribution of the seed aerosol was centered around 100 nm. The aerosol size distribution and total number concentrations of each side of the reactor were monitored at a one-minute frequency using a TSI (St. Paul, MN) Model 3071 cylindrical scanning electrical mobility spectrometer (SEMS) and a TSI Model 3760 condensation nucleus counter (CNC).

Particle losses in the SEMS, SEMS response functions, particle charging efficiencies, CNC charging efficiencies, and particle deposition in the reactor have been taken into account in the analysis of the aerosol data [Wang *et al.*, 1992]. The initial monoterpene mixing ratio ranged from 50 to 110 ppbv, and an appropriate amount of 2-butanol was also added to the reactor to scavenge >95% of OH radicals produced from the monoterpene-O₃ reaction [Chew and Atkinson, 1996; Atkinson, 1997]. Finally, ozone was injected to the reactor using an Enmet Corporation (Ann Arbor, MI) Model 04052-011 O₃ generator until the O₃ mixing ratio reached approximately four times that of the initial hydrocarbon for all experiments except one α -pinene/O₃ and one β -pinene/O₃ experiment, in which excessive hydrocarbon was established in the reactor. Table A.3.1 summarizes the initial conditions of each experiment.

Reactor air was withdrawn through a sampling system consisting of a glass annular denuder (University Research Glassware, Chapel Hill, NC) followed by a 47 mm Pallflex Teflon impregnated glass fiber filter at a flow rate of 25 L min⁻¹ for 1 h. The denuder is 40 cm long and consists of 5 annular channels with 2 mm space between channels. The sand-blasted denuder walls were coated with sub-micron XAD-4 particles beforehand using the procedure described by Gundel *et al.* [1995].

A.3.2.2 Sample treatment and analysis

Denuder and filter samples were spiked with 10 μ L of 40 ng/ μ L tricosane in dichloromethane (DCM) immediately after sample collection. Filters were soxhlet-extracted with 160 mL 1:1 acetonitrile and DCM solvents for 12-16 hrs. Before extraction, 150 μ L of 19 mM PFBHA acetonitrile/aqueous solution (a minimum amount of water was used to dissolve PFBHA·HCl) was added to the soxhlet extractor along with

the extraction solvents. Denuders were extracted with 4 x 40 mL of a solvent mix made of DCM, acetonitrile, and hexane (50%: 38%: 12%) by manually inverting the denuder 40 times. After addition of 150 μ L of 19 mM PFBHA solution, the denuder extracts were left at room temperature overnight. Then both the filter and denuder extracts were reduced to *ca.* 5 mL by rotary evaporation. The extracts were blown to nearly dryness under a gentle N₂ stream, followed by reconstitution with 280 μ L 1:1 hexane and DCM solvent mixture, and addition of 20 μ L of BSTFA and 10 μ L of 3 ng/ μ L 1-phenyldodecane (injection internal standard). The mixtures were then heated at 70°C for 2.5 hrs. After cooling briefly, 20 μ L of the mixture was injected for GC/MS analysis.

A Varian Saturn 2000 gas chromatograph/ ion trap mass spectrometer was used for both EI and methane CI analysis. The GC temperature was programmed at 60°C for 1 min, to 250°C at 10°C/min, to 300°C at 5°C/min, and held at 300°C for 10 min. Samples were injected in the splitless injection mode. The injector was switched to split mode 1 min after an injection was made. The injector port temperature was programmed at 60°C for 1 min, ramped to 320°C at 180°C/min, and held at 320°C until the end of the analysis. The mass range was 50 - 650 amu. A 30m x 0.25 mm x 0.25 μ m DB-5 fused silica column was used for all samples.

A.3.2.3 Denuder and filter collection efficiencies

The collection efficiency of the 40-cm long denuder was determined by connecting this denuder and a 20-cm long denuder in series (the limited space between the sampling port and the ground can only accommodate a 20-cm long denuder). The collection efficiency was calculated as $A_L/(A_L+A_S)$, where A_L and A_S represent the

amounts collected by the long and the short denuders, respectively. Semi-volatile products can volatilize from a filter due to changes in gas/particle equilibrium conditions as a result of the denuder stripping off gas-phase semi-volatiles. The filter "blow-off" was collected by a pre-baked glass fiber filter placed downstream from the Teflon filter. The filter collection efficiency was then calculated as $F_t/(F_t+F_g)$, where F_t and F_g represent the amounts collected by the front Teflon filter and the rear glass fiber filter, respectively. The collection efficiencies were computed using the photooxidation products of α -pinene/NO_x in the outdoor reactor under sunlight irradiation. The reaction mixture contained pinic acid, pinonic acid, norpinonic acid, 2,2-dimethyl-3-formyl-cyclobutyl-methanoic acid, pinonaldehyde, and norpinonaldehyde. Table A.3.2 lists the denuder and filter collection efficiencies for each individual product. The results indicate that a 20-cm long denuder is sufficient to collect any breakthrough from the first denuder.

A.3.2.4 Recoveries of denuder and filter samples

Recoveries of select compounds were determined by spiking on filters and denuders known amounts of liquid standards and the recovery standard tricosane. The same extraction and concentration procedures as those described in Section A.3.2.2 were then applied.

Relative recoveries for select multifunctional compounds versus the recovery standard tricosane are given in Table A.3.3. 2-Hydroxy-cyclohexanone is included to serve as a surrogate for hydroxy pina ketones and hydroxy sabina ketones, and the two dicarbonyls, 5-methyl-1,3-cyclohexanedione and 5-isopropyl-1,3-cyclohexanedione, act as surrogates for dicarbonyl compounds, such as pinonaldehyde and norpinonaldehyde. Two dicarboxylic acids, heptanedioic acid and octanedioic acid, and one keto acid, 7-

oxo-octanoic acid, are included to test whether compounds with the same type of functional groups exhibit similar recoveries. Comparison of the recoveries of heptanedioic and octanedioic acid with that of pinic acid, a C₉ cyclic dicarboxylic acid, shows that the three dicarboxylic acids exhibit similar recoveries for both denuder and filter samples. The two keto acids, 7-oxo-octanoic acid and pinonic acid, also have similar recoveries. This adds confidence to the assumption that the recoveries for those compounds without available standards can be approximated with those of known standards that have similar functional groups.

For each compound tested, the denuder samples show lower recovery than filter samples. This indicates the mouth washing extraction technique performed on denuders is not as efficient in extracting the polar compounds as the soxhlet extraction method performed on filter samples. The large standard deviations associated with the recoveries are likely a result of a number of factors including extraction efficiency, volatilization during rotary evaporation, and losses from transfer and surface adsorption. Absolute recovery of a given compound is obtained by multiplying its relative recovery by that of tricosane in individual samples. All the denuder and filter samples have been corrected with the recoveries determined here.

A.3.3 Product Identification

The newly developed analytical derivatization method [*Yu et al.*, 1998] allows for detection and identification of three types of products: (1) those containing only carbonyl group(s) (e.g., simple aldehydes, ketones and dicarbonyls), (2) those containing only OH/COOH groups (e.g., dicarboxylic acids), and (3) those containing both carbonyl and OH/COOH groups (e.g., oxoacids and hydroxy carbonyls). Here OH/COOH denotes the

presence of hydroxy or carboxy functional groups since the mass spectra for the TMS derivatives often can not differentiate between these two functional groups. Two types of ion chromatograms are constructed: m/z 181 ion chromatogram and m/z 73 and 75 ion chromatogram. Type (1) compounds show peaks only in the 181 ion chromatogram, type (2) compounds exhibit peaks only in the 73 and 75 ion chromatogram, and type (3) compounds show peaks in both chromatograms. The classification for each product is further substantiated by the unique pseudo-molecular ions in the CI mass spectra.

A.3.3.1 Products from ozone oxidation of β -pinene

Figure A.3.1a is the reconstructed m/z 181 ion chromatogram, showing carbonyl-containing products from the β -pinene/ O_3 reaction. Figure A.3.1b is the reconstructed m/z 73 and 75 ion chromatogram, displaying all products bearing OH/COOH groups. Table A.3.4 lists molecular weight (MW), chemical structure, and the pseudo-molecular ion fragments in the CI mass spectra that are used to obtain molecular weight for the products. Product names are derived using the newly proposed nomenclature for terpene oxidation products by *Larsen et al.* [1998].

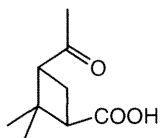
Among the products, compounds P_1 and P_2 are type (2) products, i.e., only contain OH/COOH groups. Compound P_1 is tentatively identified as norpinic acid (2,2-dimethyl-cyclobutane-1,3-dicarboxylic acid). The CI spectrum shows ions at m/z 389, 317, 301, 227, and 117, corresponding to $M+73$, $M+1$, $M-15$, $M-89$, and $M-117$ (Figure A.3.2- P_1). The m/z $M+73$ ion is an adduct ion resulting from the addition of the $[\text{Si}(\text{CH}_3)_3]^+$ fragment ion to a neutral molecule. The m/z $M+1$ ion is the protonated molecular ion. The ions at m/z $M-15$, $M-89$, and $M-117$ are fragment ions resulting from loss of CH_3 , $\text{OSi}(\text{CH}_3)_3$ and $\text{C}(\text{O})\text{OSi}(\text{CH}_3)_3$ from the neutral molecules. Compound P_2 is

identified as pinic acid, which has been confirmed by comparison with an authentic standard obtained from Aldrich (Figure A.3.2-P₂).

Compounds P₃, P₁₀, and P₁₁ have carbonyl groups, but no OH/COOH groups (type 1 compounds), as indicated by their presence in Figure A.3.1a and absence in Figure A.3.1b. Compound P₃ is positively identified as nopinone (pina ketone) by comparison with an authentic standard. There are two GC peaks corresponding to nopinone, as PFBHA forms two geometric isomers with a given nonsymmetrical carbonyl [Le Lacheur *et al.*, 1993; Yu *et al.*, 1995]. The relative intensity of the pseudo-molecular ions from two isomers of a PFBHA derivative may vary, but the mass fragment patterns are similar. Therefore, only one spectrum is given to illustrate the identification of a given carbonyl-PFBHA derivative. Figure A.3.2-P₃ shows the CI spectrum of the second nopinone peak, with pseudo-molecular ions at *m/z* 514, 362, 334, 152 and 136, corresponding to M+181, M+29, M+1, M-181, and M-197. The *m/z* M+181 ion is an adduct ion formed between a neutral molecule and the fragment ion [C₆F₅CH₂]⁺. The *m/z* M+29 ion is an adduct ion resulting from the addition of the methane reagent ion [C₂H₅]⁺ to a neutral molecule. The ions at *m/z* M-181 and M-197 are fragment ions arising from loss of C₆F₅CH₂ and C₆F₅CH₂O fragments from the neutral molecules. Compound P₁₀ is tentatively identified as 2,2-dimethyl-cyclobutane-1,3-dicarboxaldehyde, with a MW of 530 for its PFBHA derivative (Figure A.3.2-P₁₀). Compound P₁₁ is tentatively identified as 3-oxo-pina-ketone, a diketone (Figure A.3.2-P₁₁). Its PFBHA derivative has a MW of 542 when both carbonyl groups are derivatized. In addition, two peaks in Figure A.3.1a are ascribed to the mono-derivative of 3-ketono pinone, with a MW of 347. For a dicarbonyl, PFBHA may derivatize only one of the

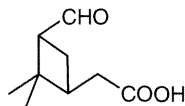
two carbonyl groups and leave the other intact if unfavorable derivatization conditions occur. Among unfavorable conditions are steric hindrance and insufficient amount of derivatization agent and reaction time.

Compounds P₄, P₅, P₆, P₇, P₈, and P₉ have both carbonyl and OH/COOH groups (type 3 compounds), indicated by their presence in both Figures A.3.1a and A.3.1b. Compound P₄ is tentatively identified as a hydroxy substituted nopinone, 3-hydroxy-pina ketone or 1-hydroxy-pina ketone. The derivatized form of P₄ has a MW of 421 (See Figure A.3.2-P₄ for its CI mass spectrum.). Compound P₅ is tentatively identified as 2,2-dimethyl-3-formyl-cyclobutyl-methanoic acid, having a MW of 423 for its derivatized form (Figure A.3.2-P₅). Three peaks, labeled P₆ in Figure A.3.1, are identified to have a MW of 437, indicated by the presence of several pseudo-molecular ions in their CI spectrum at *m/z* 510, 438, 348, 256, and 240, corresponding to M+73, M+1, M-89, M-181, and M-197 (Figure A.3.2-P₆). The observation of three peaks indicates that at least two isomers with the same number and type of functional groups are present. The following three isomers are possible candidates with structures consistent with the EI and CI mass spectra fragment patterns:



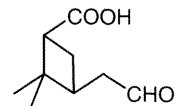
norpinonic acid

(3-acetyl-2,2-dimethyl cyclobutylmethanoic acid)



pinalic-4-acid

(2,2-dimethyl-3-formyl cyclobutylmethanoic acid)



pinalic-3-acid

(2,2-dimethyl-3-formylmethyl cyclobutylmethanoic acid)

Further differentiation among the three isomers is impossible on the basis of CI and EI mass spectra. Figure A.3.2-P₆ shows ion fragment patterns using pinalic-4-acid as an

example. Compound P₇ is identified as *cis*-pinonic acid, and the identification has been confirmed by comparison with an authentic standard. The CI mass spectrum of its derivative is shown in Figure A.3.2-P₇. Compound P₈ is tentatively identified as hydroxy norpinonic acid, with a MW of 525 for its derivative (Figure A.3.2-P₈). Compound P₉ is tentatively identified as hydroxy pinonic acid, with a MW of 539 for its derivative (Figure A.3.2-P₉).

Some of the products observed here have been reported in previous studies. Nopinone has long been identified as a major product in the β -pinene/O₃ reaction [Hull, 1981; Hatakeyama *et al.*, 1989; Grosjean *et al.*, 1993, Hakola *et al.*, 1994]. Using GC/MS and nuclear magnetic resonance (NMR) analyses, Hull [1981] also positively identified 3-hydroxy-pina ketone and 3-oxo-pina ketone and had indirect evidence for the formation of 1-hydroxy-pina ketone. Products that are reported here for the first time include pinic acid, norpinic acid, 2,2,-dimethyl-3-formyl-cyclobutyl methanoic acid, norpinonic acid and its isomers, pinonic acid, hydroxy norpinonic acid, hydroxy pinonic acid, and 2,2-dimethyl-cyclobutane-1,3-dicarboxaldehyde.

A.3.3.2 Products from ozone oxidation of sabinene

Carbonyl bearing products of the sabinene/O₃ reaction are shown in Figure A.3.3a, and OH/COOH bearing products are shown in Figure A.3.3b. Table A.3.5 lists the MWs and chemical structures of these products. Most products are analogous to those identified in the β -pinene/O₃ reaction, and their methane CI mass spectra are similar to those in the β -pinene/O₃ reaction. The CI mass spectra are given only for the products unique in the sabinene/O₃ reaction (Figure A.3.4). Interested readers can get from us the mass spectra data for those analogous products.

Among the products, compound S₁, S₂, and S₃ contain only OH/COOH groups (type 2 compounds). Compound S₁ is tentatively identified as norsabinic acid on the basis of that it shows a MW of 316 for its derivative, and elutes at an earlier retention time than that of norpinic acid. The CI spectrum of compound S₂ indicates a MW of 330 for its TMS derivative. S₂ elutes from the GC column earlier than pinic acid. It is tentatively identified as sabinic acid, the analogue of pinic acid derived from sabinene. Compound S₃ is pinic acid, confirmed by authentic standard. The observation of pinic acid as a product in the sabinene/O₃ reaction is also reported by *Glasius et al.* [1998]. It is not likely that pinic acid is a residue resulting from the previous chamber experiment, which was a β -pinene/O₃ experiment. Between chamber experiments, clean air of more than 15 times the bag volume passes through the reactor. More experiments are needed to verify this observation.

Compounds S₄ and S₁₁ are found to contain only carbonyl groups (type 1 compounds), indicated by their presence in Figure A.3.3a and absence in Figure A.3.3b. Both EI and CI spectra indicate a MW of 333 for compound S₄. It is tentatively identified as sabina ketone. This product is identified as a major product by *Hakola et al* [1994]. Compound S₁₁ is tentatively identified as 3-oxo-sabina ketone. The mono-derivative of this diketone is also present.

Compounds S₅, S₆, S₇, S₈, S₉, S₁₀, and S₁₂ have both carbonyl and OH/COOH groups (type 3 compounds), indicated by their presence in both Figure A.3.3a and Figure A.3.3b. Compound S₅ is tentatively identified as 2-(2-isopropyl)-2-formyl-cyclopropyl-methanoic acid, as its CI spectrum shows a MW of 423 for its PFBHA and TMS derivative. Three peaks are ascribed to S₆, and their CI spectra indicate a MW of 421. S₆

is therefore tentatively identified as hydroxy sabina ketones (3-hydroxy and 1-hydroxy sabina ketone). Four peaks are assigned to S_7 , which has a MW of 437. Similar to the P_7 peaks in the β -pinene/ O_3 samples, S_7 could be two of the three isomers listed in Table A.3.5. Further differentiation is not possible based on the mass spectra data. Peak S_8 shows a MW of 495 (Figure A.3.4- S_8). Table A.3.5 lists one of the possible candidates that matches the MW and functional group types. Three peaks, with a MW of 525 determined from their CI mass spectra, are assigned to S_9 . Three of all possible structures are listed in Table A.3.5. S_{10} is determined to have a MW of 539 for its derivatized form. Two peaks are ascribed to compound S_{12} , with a MW of 590 for its derivatized forms. One EI spectrum is given in Figure A.3.4- S_{12} . Their CI spectra are weak, but the protonated molecular ion is present. One postulated structure is listed in Table A.3.5.

A comparison of the products from β -pinene/ O_3 and sabinene/ O_3 reveals that there are nine analogous product pairs in the two reaction systems: norpinic acid/norsabinic acid, pinic acid/sabinic acid, nopinone/sabina ketone, P_5/S_5 , hydroxy pina ketones/hydroxy sabina ketones, P_6/S_7 , P_8/S_9 , P_9/S_{10} , and 3-oxo-pina ketone/3-oxo-sabina ketone (Tables A.3.4 and A.3.5). These analogous products suggest that they are derived from a common moiety between the two parent reactants, i.e., an external unsaturated bond to the six-member ring. The sabinene/ O_3 reaction also produces two unique products (S_8 and S_{12}), correspondents of which are not observed in the β -pinene/ O_3 reaction.

A.3.3.3 Products from ozone oxidation of α -pinene

Identification of ozone oxidation products of α -pinene, based on a collection of $\sim 0.36\text{ m}^3$ reactor air in an impinger, has been described by *Yu et al.* [1998]. The collection of a larger air volume (1.5 m^3) by the denuder/filter system in this work allows detection of six additional minor products. For completeness, Table A.3.6 shows the structures of all the identified products. The six additional products identified include norpinic acid (A_1), (2,2-dimethyl-3-acetyl)-cyclobutyl formate (A_3), hydroxy pinonic acid (A_7), A_{11} , A_{13} , and A_{14} (See Table A.3.6.). Figures A.3.5a and A.3.5b are the GC chromatograms for carbonyl and COOH/OH bearing products, respectively. Some of the products in the α -pinene/ O_3 reaction are also observed in the β -pinene/ O_3 system, apparently as a result of the common moieties shared by α -pinene and β -pinene. Unique products in the α -pinene/ O_3 reaction include A_3 , and A_9 - A_{14} . Their CI spectra are displayed in Figure A.3.6.

The tentative identifications of (2,2-dimethyl-3-acetyl)-cyclobutyl formate (A_3), norpinonaldehyde (A_9), pinonaldehyde (A_{10}), and hydroxy pinonaldehydes (A_{12}) are based on their mass spectra and reasonable postulation of the gas-phase α -pinene/ O_3 reaction mechanism [*Yu et al.*, 1998]. A possible structure for A_{14} is suggested based on its mass spectrum. For A_{11} and A_{13} , only their MW and some functionality information are given in Table A.3.6, as it is difficult to suggest possible candidates.

A number of recent product studies of the α -pinene/ O_3 reaction have also revealed some of the products observed in this work [*Hoffmann et al.*, 1998; *Glasius et al.*, 1998,1999; *Jang and Kamens*, 1998]. Using HPLC/ atmospheric pressure chemical ionization (APCI) mass spectrometry, *Hoffmann et al.* [1998] reported the observation of

pinic acid, norpinic acid, pinonic acid, and evidence for an adduct of pinic acid and norpinic acid. Such a binary diacid adduct, if existing, would likely dissociate when undergoing the heating treatment (70°C for 2.5 hrs) used for the silylation derivatization.

Glasius et al. [1999], using HPLC/ electrospray ionization and APCI mass spectrometry, reported observation of pinonic acid, pinic acid, norpinic acid, hydroxy pinonic acid, and pinalic-4-acid. *Jang and Kamens* [1998], using derivatization techniques and GC/MS detection similar to this work, tentatively identified norpinic acid, pinic acid, norpinonic acid, pinonic acid, 2,2-dimethyl-3-formyl-cyclobutyl-methanoic acid, norpinonaldehyde, pinonaldehyde, pinalic-3-acid, hydroxy pinonic acid, and A₁₄. Compounds A₃, A₁₁ and A₁₃ are reported here for the first time.

A.3.3.4 Products from ozone oxidation of Δ^3 -carene

Identification of ozone oxidation products of Δ^3 -carene based on impinger samples has been described by *Yu et al.* [1998]. Using the denuder/filter pack collection system, we have identified additional products in small yields. Figures A.3.7a and A.3.7b are the GC chromatograms of the derivatized products in a denuder sample. Table A.3.7 lists the structures of these products and the pseudo-molecular ions in their CI mass spectra, which are used to determine MWs. Due to lack of authentic standards, all the products are tentatively identified on the basis of their mass spectra and possible reaction mechanism. Many of the products in the Δ^3 -carene/O₃ reaction are analogous in structure to those in the α -pinene/O₃ reaction. The CI mass spectra of the products that do not have analogous products in the α -pinene/O₃ reaction are given in Figure A.3.8.

The CI mass spectra for C₇ and C₈ have been shown in the previous paper [Yu *et al.*, 1998].

Additional products identified in the denuder sample include nor-caric acid (C₁), pinic acid (C₃), C₄, C₅, and C₁₀. For C₄, C₅, and C₁₀, we are not currently able to suggest possible chemical structures, so only their MW and the presence of functional group types are given in Table A.3.7. These three products do not have corresponding analogues in the α -pinene/O₃ reaction. On the other hand, four products, A₃, A₁₁, A₁₃, and A₁₄, are found unique to the α -pinene/O₃ reaction. This is not unexpected as minor reaction pathways may take place at locations other than the C=C bond.

The observation of pinic acid in the Δ^3 -carene/O₃ reaction is not expected. Glasius *et al.* [1998] also observed trace amount of pinic acid in their Δ^3 -carene/O₃ reaction systems.

A.3.4. Product Yields

Yields of the above-identified products have been determined or estimated. For products with standards, the calibration factor, extraction recovery, and collection efficiency have been determined using the standards. For products that do not have available authentic standards, their yields are estimated using the calibration factor, and the recovery and collection efficiency of surrogate compounds. The surrogate compounds are chosen to have the same type of functional groups and approximate carbon numbers as the products that the surrogates represent. Table A.3.8 lists the available standards and the products for which the standards serve as surrogates. For example, pinic acid serves as the surrogate for norpinic acid, 3-caric acid, nor-3-caric acid, sabinic acid, and norsabinic acid. Carbonyl bearing products (type 1 compounds)

are quantified using the m/z 181 ion, products bearing COOH/OH groups (type 2 compounds) are quantified using the m/z 73 and 75 ions, and for those products that contain both carbonyl and COOH/OH groups (type 3 compounds), the sum of three ions at m/z 181, 73 and 75 is used for their quantification. The selection of surrogates on the basis of functional group types is justified by the use of the above functional group specific ions for quantification. The estimated calibration factors have a $\sim\pm30\%$ uncertainty. The other sources that contribute to the uncertainty associated with product yields include uncertainties for collection efficiency ($\sim\pm4\%$), extraction efficiency ($\sim\pm15\%$) and sample volume ($\pm5\%$). After considering all contributing sources, the uncertainty associated with product yields is estimated to be $\sim\pm50\%$.

Our calculation of gaseous product yields ignores wall loss processes, as we estimate that the loss of an oxygenated product resulting from wall loss processes is likely less than 15% at 300 min after its formation. *Grosjean* [1985] measured the wall loss rates for five oxygenated species, biacetyl, pyruvic acid, *o*-cresol, benzaldehyde, and benzoic acid, in a Teflon chamber with a S/V of 3.8 m^{-1} . The first three compounds had an unmeasurable wall loss rate while benzaldehyde and benzoic acid had wall loss rates of 3.4×10^{-4} and $10.8 \times 10^{-4}\text{ min}^{-1}$, respectively. *Hallquist et al.* [1997] measured the wall loss rates for pinonaldehyde and caronaldehyde to be $(2.4-4.2) \times 10^{-3}\text{ min}^{-1}$ in a borosilica glass reactor with a S/V of 14.3 m^{-1} . If one assumes wall loss processes are similar on borosilica glass and Teflon surfaces, one could calculate that the two dicarbonyls have a wall loss rate of $(3-5) \times 10^{-4}\text{ min}^{-1}$, comparable to that for benzoic acid ($5 \times 10^{-4}\text{ min}^{-1}$), in the present Teflon reactor with a S/V of 1.8 m^{-1} . Using the wall loss rate for benzoic acid, which has the highest wall loss rate among all the tested oxygenated species, we

estimate that about 86% of an oxygenated product remains in the gas phase at 300 min after its formation, if we assume that wall loss is the only loss process. A more detailed study of gas-phase product yields needs experimentally determined wall loss rates for each product, which unfortunately can not be readily accomplished as many products lack commercially available standards.

The organic aerosol mass generated in each experiment was obtained from the aerosol volume measured by SEMS/CNC and assuming a SOA density of 1 g cm⁻³. The SOA yield (Y) was then calculated by

$$Y = \frac{\Delta M_o}{\Delta HC} \quad (1)$$

where ΔM_o is the organic aerosol mass concentration (μg m⁻³) produced for a given amount of hydrocarbon reacted, ΔHC (μg m⁻³). The estimated uncertainty in the measured SOA yield is roughly ±12%, with SOA density uncertainty assumed to be ±10%.

A.3.4.1 β-Pinene

Table A.3.9 shows yields of individual products in gas and aerosol phases, as well as the total yields in two β-pinene/O₃ experiments. The yield of nopinone in the gas-phase is determined from measurements made by an on-line GC/FID, as GC/FID provides more accurate and frequent measurements of nopinone. As an example, Figure A.3.9 shows the amount of nopinone formed against the amount of β-pinene reacted for the experiment carried out on June 11, 1998 (side B). The gas-phase yield of nopinone

was determined to be 17.0% and 15.8% in the 6/11/98b and 6/17/98b experiments, respectively. Nopinone resides almost exclusively in the gas phase; trace amounts were detected in the filter samples. Previously reported nopinone yields vary from 22% [Grosjean *et al.* 1993] and 23 ± 5% [Hakola *et al.*, 1994] to 40 ± 2% [Hatakeyama *et al.*, 1989]. The much higher nopinone yield in the study by Hatakeyama *et al.* [1989] is possibly due to the presence of other carbonyl products that were reported as nopinone, as their measurement of nopinone was based on FTIR absorption spectroscopy at the 1740 cm⁻¹ -C=O stretch frequency.

Only one study in the literature [Hull, 1981] reported yields for individual products other than nopinone in the β -pinene/O₃ reaction. In this study, Hull [1981] estimated the total molar yields of three major products: nopinone (10%), 3-hydroxy-pina-ketone (28%), and 3-oxo-pina-ketone (7%). The total molar yield for 3-hydroxy-pina ketone in the present work is estimated to be 7.3% and 9.0% in the two experiments, lower than Hull's [1981] result. Our yield for 3-oxo-pina-ketone is estimated to be 1.8% and 7.7%. In his study, Hull [1981] used high mixing ratios for β -pinene (275 to 440 ppmv) and ozone (179 to 270 ppmv), and no OH scavenger. The very different reaction conditions may account for the different product yields.

The identified products account for 34% and 50% of the reacted β -pinene carbon mass in the 6/11/98b and 6/17/98b experiments, respectively. Products with a yield exceeding >1% include nopinone (15.8-17.0%), hydroxy pina ketones (7.3-9.0%), 3-oxo-pina-ketone (1.8-7.7%), norpinonic acid and its isomers (5.9-16.5%), and pinic acid (2.6-3.7%). The identified products are estimated to account for 98% and 83% of the organic aerosol mass formed in the two β -pinene/O₃ experiments. Norpinonic acid and its

isomers, pinic acid, and hydroxy pina ketones are SOA components that contribute to more than 10% of the organic aerosol mass.

The 6/17/98b experiment has a much higher percentage of reacted β -pinene accounted for by the identified products than the 6/11/98b experiment, as two major products, norpinonic acid and its isomers and 3-oxo-pina-ketone, were observed to have much higher gas-phase yields in the 6/17/98b experiment (Table A.3.9). The two β -pinene/ O_3 experiments were conducted under different initial conditions, i.e., ozone was present in an excess amount in the 6/11/98b experiment whereas β -pinene is in excess in the 6/17/98b experiment (Table A.3.1). The variation between the two experiments can not be accounted for by measurement error alone. It is possible the different initial reaction conditions are responsible for the variation, but a satisfactory explanation is not possible without further experiments designed to systematically examine the effects of different reaction conditions on product yields.

The functional group distribution of SOA components from the β -pinene/ O_3 experiments is comparable to results obtained by *Palen et al.* [1992] using Fourier transform infrared spectrometry (FTIR). *Palen et al.* [1992] analyzed aerosol samples generated from an experiment with 8 ppmv O_3 and 14.5 ppmv β -pinene. Their results indicated that an average aerosol-phase product molecule contained one ketone group, 0.7 alcohol groups, and 0.4 carboxylic groups. For the 6/17/98 β -pinene/ O_3 experiment where excessive β -pinene was used, our GC/MS analysis showed that the average aerosol molecule contained about one ketone group, 0.2 alcohol groups, and 0.8 carboxylic groups.

A.3.4.2 Sabinene

Table A.3.10 shows yields of individual products in the gas and aerosol phases, as well as the total yields of both phases in the sabinene/O₃ experiment. Identified products in both the gas and aerosol phases account for 57% of the reacted sabinene carbon mass. Products with a molar yield exceeding 1% include sabina ketone (47%), hydroxy sabina ketone (7%), norsabinonic acid and its isomers (5%), pinic acid (1%), and sabinic acid (1%).

All the products added together account for 100% of the organic aerosol mass formed. The 100% yield is rather fortuitous, and it is associated with an uncertainty factor resulting from the approximations made for response factors and SOA density. Aerosol components that make up more than 10% of the aerosol mass are norsabinoic acid and its isomers, hydroxy sabina ketones, sabinic acid, sabina ketone, and pinic acid.

The estimated yield of sabina ketone in this work is in agreement with that, 50±9%, measured by *Hakola et al.* [1994]. *Glasius et al.* [1998] reported molar yields of sabinic acid and pinic acid in aerosol phase at 1.1% and 1.4%. Our yields for the two dicarboxylic acids in the aerosol phase are 0.4% and 0.3%. As we will discuss in section A.3.5, the absolute aerosol yield of a particular product depends on the temperature and the organic aerosol mass concentration in each system in which SOA is generated. Without the knowledge of the temperature and organic aerosol mass concentration in the system of *Glasius et al.* [1998], it is difficult to make a meaningful comparison.

A.3.4.3 α -Pinene

Table A.3.11 shows yields of individual products in the gas and aerosol phases, as well as the total yields of both phases, in three α -pinene/O₃ experiments. Identified products in both the gas and aerosol phases account for 29-67% of the reacted α -pinene

carbon mass. Products with a molar yield exceeding 1% include pinonaldehyde (6-19%), norpinonic acid and its isomers (4-13%), hydroxy pinonaldehydes (2-11%), pinonic acid (2-8%), pinic acid (3-6%), hydroxy pinonic acid (1-4%), (2,2-dimethyl-3-acetyl)-cyclobutyl formate (1-4%), and norpinonaldehyde (1-3%).

In the 6/17/98a experiment, a much higher percentage of reacted α -pinene is accounted for by the identified products, as the four major products, pinonaldehyde, hydroxy pinonaldehydes, pinonic acid, and norpinonic acid and its isomers, are measured to have much higher yields than those in the experiments 6/9/98a and 6/9/98b. While measurement errors may account for part of the variation, the different reaction conditions also likely contribute to the variation. The 6/17/98a experiment is different from the experiments 6/9/98a and 6/9/98b in two aspects: 1) excessive α -pinene was used in the 6/17/98a experiment while excessive ozone was present in the prior two experiments, and 2) the denuder/filter sample was started 53 min after the initiation of the α -pinene/O₃ in the 6/19/98a experiment while in the other two experiments denuder/filter samples were collected more than 290 min after ozone oxidation of α -pinene started. One explanation is that the polar nature of the products makes them susceptible to be lost to the reactor wall by adsorption, as demonstrated for pinonaldehyde and caronaldehyde by *Hallquist et al. [1997]* in their experimental chamber. Actual product yields may be higher after accounting for wall loss, but wall loss does not account for all the yield variation. It is noted that for both the α -pinene/O₃ and the β -pinene/O₃ experiments, higher gas-phase yields were measured when excess monoterpene was present in the reaction systems. Presently we do not have a satisfactory explanation for this observation.

Four previous studies have reported yields of some of the above products. The gas-phase yield of pinonaldehyde was measured to be $14.3\pm2.4\%$ [Alvarado *et al.*, 1998] and $19\pm4\%$ [Hakola *et al.*, 1994]. In this work, the yield is estimated to be 5.7-18.1%, in general agreement with the values reported in the two previous studies. Hull [1981] reported total yields in both phases for four major products: pinonic acid (27%), pinonaldehyde (15%), hydroxy pinonaldehyde (7%), and norpinonic acid (7%). We have measured or estimated the yields in both phases to be 2.1-7.9%, 6.5-19.0%, 1.8-11.2%, and 4.2-12.6%, respectively. The yield of pinonic acid measured by Hull [1981] is much higher than our yield. In Hull's [1981] study, no OH scavenger was added, and the mixing ratios of α -pinene used ranged from 110 to 509 ppmv, which is more than 1000 times higher than those in this work. It is difficult to make meaningful comparisons considering the very different reaction conditions investigated in the two studies. In the absence of OH scavengers, Hatakeyama *et al.* [1989] measured aldehyde yield in the gas-phase to be $51\pm6\%$ by FTIR absorption spectroscopy. In this study we have identified ten products with aldehyde functional group(s), i.e., pinonaldehyde, norpinonaldehyde, hydroxy pinonaldehydes (A₁₂), norpinonic acid and isomers (A₅), A₄, A₈, A₁₁, A₁₂, A₁₃, and A₁₄. The sum of yields for all these aldehyde products in the gas phase ranges from 14-45%. If one considers that the absence of OH scavenger would increase yields of aldehyde products such as pinonaldehyde, yield data from this study may be consistent with the result obtained by Hatakeyama *et al.* [1989].

All the products added together account for 90-111% of the organic aerosol mass formed. The larger than 100% aerosol yield reflects the uncertainties associated with the estimated response factors for those products without available standards, and the

assumption that SOA has a density of 1 g cm^{-3} . At 306-308 K, major aerosol components that make up more than 10% of the organic aerosol mass include pinic acid, hydroxy pinonaldehydes, pinonic acid, norpinonic acid and its isomers, and hydroxy pinonic acid.

Among all the monoterpenes, ozone oxidation of α -pinene is the most frequently studied reaction for its aerosol products. In previous studies, the molar yield of pinic acid and pinonic acid in the aerosol phase was measured to range from 0.2% to 1%, and 0.1-0.3%, respectively [Christoffersen *et al.*, 1998; Glasius *et al.*, 1998]. The temperature and organic aerosol mass in their systems were not reported.

A.3.4.4 Δ^3 -Carene

Table A.3.12 shows the gas and aerosol phase yields of the individual products, as well as the total yields of both phases in two Δ^3 -carene/ O_3 experiments. Identified products in both the gas and aerosol phases account for 24% of the reacted Δ^3 -carene carbon mass. Products with a molar yield exceeding 1% include caronaldehyde (8%), 3-caronic acid (4%), hydroxy caronaldehydes (3%), nor-3-caronic acid and isomers (2%), C_5 (2%), 3-caric acid (2%), hydroxy-3-caronic acid (1%), and pinic acid (1%). Caronaldehyde has been identified as a major product in a previous study with a yield of $\leq 8\%$ in the gas phase [Hakola *et al.*, 1994]. Here the gas-phase caronaldehyde yield is estimated to be 7.8%.

All the products added together account for 61% of the organic aerosol mass formed. Major aerosol products that contribute to $>10\%$ of organic aerosol mass are 3-caronic acid and 3-caric acid. Glasius *et al.* [1998] reported three aerosol products, 3-

caric acid, 3-caronic acid, and nor-3-caric acid, with aerosol phase yields of 0.5-5%, 0.1-0.7%, and 0.08-0.1%, respectively.

A.3.5 Gas-Particle Partitioning

Many products identified in this study are detected in both gas and aerosol phases. Gas-particle partitioning for semi-volatile organic compounds has been successfully described by the equilibrium relation:

$$K_{om,i} = \frac{F_i}{A_i \Delta M_o} \quad (2)$$

where $K_{om,i}$ is the gas-particle partitioning coefficient of species i , A_i is the gas phase concentration ($\mu\text{g m}^{-3}$) of compound i , and F_i is the concentration of compound i ($\mu\text{g m}^{-3}$) in the aerosol phase [Odum *et al*, 1996]. A_i and F_i can be determined directly from denuder and filter samples, and ΔM_o is obtained from aerosol size distribution measurements. Table A.3.13 lists the gas-particle partitioning coefficients of aerosol components generated in the ozone oxidation of the four monoterpenes.

Gas-particle partitioning coefficients of semi-volatile compounds depend on their vapor pressures [Pankow, 1987]:

$$K_{om,i} = \frac{760RT}{MW_{om} 10^6 \zeta_i P_{L,i}^o} \quad (3)$$

where R is the ideal gas constant ($8.206 \times 10^{-5} \text{ m}^3 \text{ atm mol}^{-1} \text{ K}^{-1}$), T is temperature (K), MW_{om} is the number-averaged molecular weight of the organic matter (om) phase (g mol⁻¹), ζ_i is the molar fraction scale activity coefficient of compound i in the om phase, and $p^o_{L,i}$ is the sub-cooled liquid vapor pressure (mm Hg) of compound i . Sub-cooled liquid vapor pressures of the major products in the β -pinene/O₃ and α -pinene/O₃ systems have been estimated using a modification of the Clausius-Claperyron equation [Schwarzenbach *et al.*, 1993] (Table A.3.14). Measured $K_{om,i}$ values versus the estimated $p^o_{L,i}$ are shown in Figure A.3.10. As Figure A.3.10 illustrates, the lower the vapor pressure, the higher the corresponding $K_{om,i}$. For example, hydroxy pinonic acid, as a result of the presence of three polar functional groups, has the lowest vapor pressure (~ 10^{-5} mm Hg) among all identified products, and consequently exhibits the highest $K_{om,i}$ value. On the other hand, the vapor pressure of pinonaldehyde and 3-oxo-pina ketone are higher than the -COOH bearing products, which correlates with the lowest $K_{om,i}$ values (Table A.3.13). Nopinone has an even higher vapor pressure than 3-oxo-pina ketone and is, as a result, expected to reside mainly in the gas-phase. Only trace amounts of nopinone were detected in any filter samples, confirming the influence of vapor pressure on the partitioning between the gas and aerosol phases. Similar trends are observed for SOA products in the ozone oxidation of the other two monoterpenes.

The aerosol phase fraction ϕ_i of a semi-volatile product is given by

$$\phi_i = \frac{F_i}{F_i + A_i} = \frac{\Delta M_o K_{om,i}}{1 + \Delta M_o K_{om,i}} \quad (4)$$

As equation (4) indicates, ϕ_i is controlled by the aerosol organic matter concentration ΔM_o available for absorption and the gas-aerosol partitioning coefficient $K_{om,i}$, which is a function of temperature and compound-dependent. Consequently, SOA chemical composition is a function of organic matter concentration and temperature. Figure A.3.11 illustrates the dependence of ϕ_i on ΔM_o , using pinic acid as an example. The temperature dependence of SOA chemical composition was demonstrated by *Jang and Kamens* [1998], who observed that for SOA generated in the α -pinene/ O_3 reaction, the more volatile SOA components reside in the particle phase to a much greater extent under cold conditions than warmer conditions. When reporting aerosol yield of an individual product and composition of SOA, it is necessary to include the organic aerosol mass concentration and associated temperature.

The yield of an individual product i in the aerosol phase (Y_i) can be expressed as:

$$Y_i = \Delta M_o \frac{\alpha_i K_{om,i}}{1 + K_{om,i} \Delta M_o} \quad (5)$$

where α_i is the individual mass-based stoichiometric coefficient of i . The overall SOA yield Y is then just the sum of the individual yields,

$$Y = \sum_i Y_i = \Delta M_o \sum_i \left(\frac{\alpha_i K_{om,i}}{1 + K_{om,i} \Delta M_o} \right) \quad (6)$$

Using equation (6), a two-product model has successfully described the overall SOA yield Y as a function of stoichiometric coefficient α_i and partitioning coefficients $K_{om,i}$ of

two hypothetical products, and ΔM_o , the total organic aerosol mass concentration [*Odum et al.*, 1996, 1997ab; *Hoffman et al.*, 1997; *Griffin et al.*, 1999].

One of the major assumptions underlying the derivation of equations (5) and (6) is that the total amount of a product is proportional to the amount of the parent hydrocarbon reacted. If this assumption holds, the SOA yield at any time $Y(t)$, should be described by equation (6). Figure A.3.12a shows the $Y(t)$ values as a function of organic aerosol mass for the 6/09/98a and 6/09/98b α -pinene/ O_3 experiments. The experimentally determined time-dependent yield curves for both experiments can be closely represented by using equation (6) and assuming two hypothetical products with $\alpha_1 = 0.262$, $K_{om,1} = 0.030$, $\alpha_2 = 0.062$, and $K_{om,2} = 0.0028$ (Figure A.3.12a). On the other hand, a yield curve can also be constructed for each experiment by using equation (6) and the experimentally determined α_i and $K_{om,i}$ values for the individual aerosol-phase products. The resulting curves fit well the experimental SOA yield curves (Figure A.3.12a). Since the denuder/filter samples were taken at the end of the two experiments (Table A.3.1), the α_i and $K_{om,i}$ values obtained from these samples represent the SOA composition and product distribution between gas and aerosol phases at the end of the experiments. The fact that they also predict the SOA yields during earlier stages of the experiments indicates that in the α -pinene/ O_3 system, the SOA composition and product distribution between gas and particle phase remains relatively unchanged over time. This is in agreement with the time profiles of α -pinene mixing ratio and organic aerosol mass concentration ΔM_o (Figure A.3.12b). As Figure A.3.12b shows, after most of the α -pinene is oxidized, the aerosol mass remains almost constant, which indicates that the SOA mass arises from either primary products or secondary products formed relatively rapidly.

Conversely, if the total amount of a product that is generated in the reaction is not proportional to the amount of the parent hydrocarbon reacted throughout an experiment, e.g., the relative chemical composition changes over the course of the experiment, one set of α_i and $K_{om,i}$ values will not describe the SOA yields over the reaction time. The time-dependent SOA yield in the sabinene/O₃ reaction appears to be such an example (Figure A.3.13a). As shown in Figure A.3.13a, a two-product model, using equation (6) and assuming two hypothetical products with $\alpha_1 = 0.041$, $K_{om,1} = 0.154$, $\alpha_2 = 0.51$, and $K_{om,2} = 0.0005$, describes the time-dependent aerosol yield reasonably well up to $\Delta M_o \sim 15 \mu\text{g/m}^3$, which corresponds to a reaction time of ~ 100 min and 99% sabinene consumption. The $Y(t)$ curve computed using equation (6) and the α_i , and $K_{om,i}$ values for multiple actual products fits well the measured aerosol yields at the later stage, but represents poorly the early-stage yields. The denuder/aerosol sample was taken 232 minutes after the reaction started, therefore the measured α_i , and $K_{om,i}$ values of individual products reflect the SOA composition in the later stage of the experiment. The above analysis suggests that slowly forming secondary or tertiary products play a role in the aerosol formation in the sabinene/ O₃ reaction. The contribution of secondary products is further evidenced by the time profiles of sabinene mixing ratio and organic aerosol mass concentration ΔM_o . As shown in Figure A.3.13b, at ~ 100 min, while nearly all the sabinene is reacted, the organic aerosol mass continues to grow.

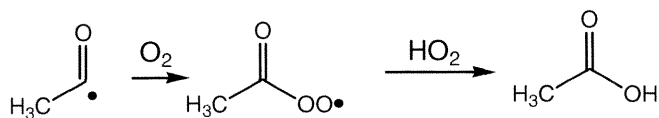
For reaction systems such as α -pinene/O₃ reaction, one set of α_i and $K_{om,i}$ values is sufficient to describe the kinetics of aerosol formation. On the other hand, for reaction systems such as the sabinene/O₃ reaction, more than one set of α_i and $K_{om,i}$ values are necessary to describe the evolution of aerosol mass.

A.3.6. Mechanisms of product formation

Based on known reaction mechanisms for alkene-O₃ reactions, it is possible to propose reaction schemes to account for most of the observed products.

A.3.6.1 β -pinene / O₃ reaction

Figure A.3.14 shows reaction sequences leading to the products in the β -pinene/O₃ reaction. The reaction of β -pinene with O₃ proceeds by initial O₃ addition to the C=C bond to yield an energy-rich ozonide, which rapidly decomposes to form nopinone and a C₉ biradical. Many of the observed products are formed from the subsequent reactions of the C₉ biradical. The energy-rich C₉ biradical undergoes isomerization to give rise to two enehydroperoxides (EN₁ and EN₂) with excess energies. This is the so-called hydroperoxide channel. The formation of hydroxy pina ketones (P₄) are a result of stabilization of EN₁ and EN₂ through collision [Niki *et al.*, 1987; Martinez and Herron, 1987, 1988; Atkinson, 1997]. One additional pathway for EN₂ is to produce 3-oxo-pina ketone (P₁₁) by loss of a H₂ molecule. This pathway is not operative for EN₁ because the OH group is attached to a tertiary C, and no H-atom is available for loss of a H₂ molecule. It is postulated that the energized 3-hydroxy pina ketone could undergo unimolecular dissociation to form an acetyl-like radical I₁ and I₂. For the acetyl radical, it has been established that its subsequent reactions with O₂ and HO₂ radical lead to the formation of acetic acid [Niki *et al.*, 1985; Moortgat *et al.*, 1989].



Similarly, the reaction of I_1 and I_2 with O_2 and subsequently with HO_2 would lead to P_6 .

I_2 can also lose a molecule of CO to form I_3 , which reacts with O_2 , and a peroxy radical

RO_2 to form I_4 . It follows that I_4 loses one H -atom to an O_2 molecule to produce P_{10} .

The formation of P_5 , norpinic acid (P_1), and pinic acid (P_2) is presupposed to result from oxidation of their corresponding aldehydes, P_{10} , P_5 and P_6 , respectively, although the explicit oxidation mechanism is unclear.

The formation pathway for a possible candidate of P_8 is proposed to arise from I_5 , which can be formed from isomerization of I_1 . It is difficult to construct plausible formation pathways for pinonic acid and hydroxy pinonic acid.

A.3.6.2 Sabinene / O_3 reaction

Figure A.3.15 depicts reaction pathways that account for most of the products observed from the sabinene/ O_3 reaction. The many pairs of analogous products in the sabinene/ O_3 and β -pinene/ O_3 reactions are easily explained by the same reaction pathways derived from O_3 attack of the external $\text{C}=\text{C}$ bond.

The observation of pinic acid in the sabinene/ O_3 reaction is difficult to explain in terms of plausible gas-phase reaction mechanisms. It is not clear whether aerosol surface plays a role in the formation of pinic acid via heterogeneous reactions. There is evidence that isomerization of monoterpenes can take place on acidic surfaces [Pio and Valente, 1998]. In addition, Coeur *et al.* [1997] observed that ~ 70% of sabinene isomerizes to other monoterpenes of lower ring tension when it is sampled onto Tenax TA or Carboxen

sorbents. Sabinic acid may undergo similar isomerization to pinic acid on particle surfaces.

As the chemical structures of the two unique products, S₈ and S₁₂, in the sabinene/O₃ reaction remain uncertain, we do not attempt to propose formation mechanisms for them.

A.3.6.3 α -Pinene / O₃ and Δ^3 -carene / O₃

The formation mechanisms of products from ozone oxidation of α -pinene have been described in an earlier paper [Yu *et al.*, 1998]. Here we only discuss the formation pathways for the newly identified products (Figure A.3.16). The formation of A₃ arises from isomerization of the Criegee biradical, known as the ester channel [Atkinson, 1997]. Hydroxy pinonic acid is postulated to result from its aldehyde precursor, 10-hydroxy-pinonaldehyde (A₁₂). We do not yet attempt to propose formation mechanism for A₁₁, A₁₃ and A₁₄, as their chemical structures are not yet known.

The formation pathways for most of the products in the Δ^3 -carene/O₃ reaction (Figure A.3.17) are similar to those in the α -pinene/O₃ reaction, as a result of the internal C=C bond common to both reactants. Those products unique to the Δ^3 -carene/O₃ reaction do not have obvious routes of formation. The presence of pinic acid in the Δ^3 -carene/O₃ reaction system may derive from similar routes to those responsible for the formation of pinic acid in the sabinene/ O₃ reaction system.

A.3.7. Summary and Conclusions

This study has identified a substantial fraction of the particulate products from ozone oxidation of each of the four monoterpenes: α -pinene, β -pinene, Δ^3 -carene, and

sabinene. β -Pinene and sabinene are structurally analogous in that both are bicyclic and have an external unsaturated bond where ozone oxidation takes place. α -Pinene and Δ^3 -carene also share one common structural moiety, an internal unsaturated bond. A number of analogous product pairs, including major products, have been identified for each pair of monoterpenes. These products are consistent with the established understanding of the mechanism of ozone-alkene reactions. In addition to expected products, a number of products having minor yields that are unique to each monoterpenes have also been detected. One interesting finding that is yet to be explained is the presence of pinic acid in both the sabinene/O₃ and Δ^3 -carene/O₃ reactions.

Yields of individual products in both the gas and aerosol phases have been determined or estimated, thus providing a direct measure of the gas-particle partitioning of each product. The identified products account for a significant fraction of the secondary organic aerosol for each of the parent hydrocarbons. Identified products, in both gas and aerosol phases, are estimated to account for about 34-50%, 57%, 29-67%, and 24% of the total reacted carbon mass for β -pinene, sabinene, α -pinene, and Δ^3 -carene, respectively. Whereas these percentages exceed those of previous studies, a significant fraction of the monoterpenes reacted still remains unaccounted for. As the yields of many products are estimated using the response factor of surrogates, an improved mass balance awaits authentic standards or new analytical techniques that do not require authentic standards. Based on experimentally measured gas-particle partitioning coefficients of individual oxidation products, it is possible to evaluate the extent to which overall aerosol yields observed in smog chamber experiments can be

represented by the stoichiometric yields and gas-particle partitioning of the individual products.

Based on the nature and yield of various aerosol components, products such as pinic acid, pinonic acid, norpinonic acid, hydroxy pinonic acid, and hydroxy pinonaldehydes can act as molecular markers for secondary organic aerosol derived from biogenic sources.

A.3.8 References

Alvarado, A., E.C. Tuazon, S.M. Aschmann, R. Atkinson, and J. Arey, Products of the gas-phase reactions of $O(^3P)$ atoms and O_3 with α -pinene and 1,2-dimethyl-1-cyclohexene, *J. Geophys. Res.*, 103, 25,541-25,551, 1998.

Arey, J., R. Atkinson, and S.M. Aschmann, Product study of the gas-phase reactions of monoterpenes with the OH radical in the presence of NO_x , *J. Geophys. Res.*, 95, 18,539-18,546, 1990.

Atkinson, R., Gas-phase tropospheric chemistry of volatile organic compounds: 1. alkanes and alkenes., *J. Phys. Chem. Ref. Data*, 26, 215-290, 1997.

Atkinson, R., and W.P.L. Carter, Kinetics and mechanisms of the gas-phase reactions of ozone with organic compounds under atmospheric conditions, *Chem. Rev.*, 84, 437-470, 1984.

Calogirou, A., B.R. Larsen, and D. Kotzias, Gas phase terpene oxidation products: A review, *Atmos. Environ.*, 33, 1423-1439, 1999.

Chameides, W. L., R.W. Lindsay, J. Richardson, and C.S. Kiang, The role of biogenic hydrocarbons in urban photochemical smog: Atlanta as a case study, *Science*, 241, 1473-1475, 1988.

Chew, A. A., and R. Atkinson, OH radical formation yields from the gas-phase reaction of O₃ with alkenes and monoterpenes, *J. Geophys. Res.*, 101, 28,649-28,653, 1996.

Christoffersen, T. S., J. Hjorth, O. Horie, N.R. Jensen, D. Kotzias, L.L. Molander, P. Neeb, L. Ruppert, R. Winterhalter, A. Virkkula, K. Wirtz, and B.R. Larsen, *cis*-Pinic acid, a possible precursor for organic aerosol formation from ozonolysis of α -pinene, *Atmos. Environ.*, 32, 1657-1961, 1998.

Coeur, C., V. Jacob, I. Denis, and P. Foster, Decomposition of α -pinene and sabinene on solid sorbents, Tenax TA, and Carboxen, *J. Chromatogr.*, 786, 185-187, 1997.

Glasius, M., M. Duane, and B.R. Larsen, Analysis of polar terpene oxidation products in aerosols by liquid chromatography ion trap mass spectrometry (MSⁿ), *J. Chromatogr.*, 833, 121-135, 1999.

Glasius, M., M. Lahaniati, A. Calogirou, D. DiBella, N.R. Jensen, J. Hjorth, M. Duane, D. Kotzias, and B.R. Larsen, Carboxylic acids in secondary aerosols from O₃ and OH oxidation of cyclic monoterpenes, In Proceedings of the fifth EUROTRAC Symposium, Garmish-Partenirchen, March 23-27, 1998.

Griffin, R. J., D.R. Cocker III, R.C. Flagan, and J.H. Seinfeld, Organic aerosol formation from the oxidation of biogenic hydrocarbon, *J. Geophys. Res.*, 104, 3555-3567, 1999.

Grosjean, D., Wall loss of gaseous pollutants in outdoor Teflon chamber, *Environ. Sci. Technol.*, 19, 1059-1065, 1985.

Grosjean, D., E.L. William II, E. Grosjean, J.M. Andino, and J.H. Seinfeld, Atmospheric oxidation of biogenic hydrocarbons: reaction of ozone with β -pinene, D-limonene and *trans*-caryophyllene, *Environ. Sci. Technol.*, 27, 2754-2758, 1993.

Guenther, A., C.N. Hewitt, D. Erickson, R. Fall, C. Geron, T. Graedel, P. Harley, L.

Klinger, and M. Lerdau, A global model of natural volatile organic compound emissions, *J. Geophys. Res.*, 100, 8873-8892, 1995.

Gundel, L.A., V.C. Lee, K.R.R. Mahanama, R.K. Stevens, and J.M. Daisey, Direct determination of the phase distributions of semi-volatile polycyclic aromatic hydrocarbons using annular denuders, *Atmos. Environ.*, 29, 1719-1733, 1995.

Hakola, H., J. Arey, S.M. Aschmann, and R. Atkinson, Product formation from the gas-phase reactions of OH radicals and O₃ with a series of monoterpenes, *J. Atmos. Chem.*, 18, 75-102, 1994.

Hallquist, M., I. Wängberg, and E. Ljungström, Atmospheric fate of carbonyl oxidation products originating from α -pinene and Δ^3 -carene: Determination of rate of reaction with OH and NO₃ radicals, UV absorption cross sections, and vapor pressure, *Environ. Sci. Technol.*, 31, 3166-3172, 1997.

Hart, K. M., and J.F. Pankow, High-volume air sampler for particle and gas sampling. 2. Use of backup filters to correct for the adsorption of gas-phase polycyclic aromatic hydrocarbons to the front filter, *Atmos. Environ.*, 28, 655-661, 1994.

Hatakeyama, S., K. Izumi, T. Fukuyama, and H. Akimoto, Reactions of ozone with α -pinene and β -pinene in air: Yields of gaseous and particulate products, *J. Geophys. Res.*, 94, 13,013-13,024, 1989.

Hoffmann, T., R. Bandur, U. Marggraf, and M. Linscheid, Molecular composition of organic aerosols formed in the α -pinene/O₃ reaction: Implication for new particle formation processes, *J. Geophys. Res.*, 103, 25,569-25,578, 1998.

Hoffmann, T., J.R. Odum, F. Bowman, D. Collins, D. Klockow, R.C. Flagan, and J.H. Seinfeld, Formation of organic aerosols from the oxidation of biogenic hydrocarbons,

J. Atmos. Chem., 26, 189-222, 1997.

Hull, L.A., Terpene ozonolysis products, in J.J. Bufalini and R.R. Arnts (eds), *Atmospheric Biogenic Hydrocarbons Vol. 2, Ambient Concentrations and Atmospheric Chemistry*, Ann Arbor Science, Ann Arbor, 161-185, 1981.

Jang, M., and R.M. Kamens, Newly characterized products and composition of secondary aerosols from the reaction of α -pinene with ozone, *Atmos. Environ.*, 33, 459-474, 1998.

Kamens, R.M., H.E. Jeffries, M.W. Gery, R.W. Wiener, K.G. Sexton, and G.B. Howe, The impact of α -pinene on urban smog formation: an outdoor smog chamber study, *Atmos. Environ.*, 15, 969-981, 1981.

Larsen, B.R., M. Lahaniati, A. Calogirou, and D. Kotzias, Atmospheric oxidation products of terpenes: a new nomenclature, *Chemosphere*, 37, 1207-1220, 1998.

LeLacheur, R.M., L.B. Sonnenberg, P.C. Singer, R.F. Christman, and M.J. Charles, Identification of carbonyl compounds in environmental samples, *Environ. Sci. Technol.*, 27, 2745-2753, 1993.

Martinez, R.I., and J.T. Herron, Stopped-flow studies of the mechanisms of ozone-alkene reactions in the gas-phase: Tetramethylethylene, *J. Phys. Chem.*, 91, 946-953, 1987.

Martinez, R.I., and J.T. Herron, Stopped-flow studies of the mechanisms of ozone-alkene reactions in the gas phase: *trans*-2-Butene, *J. Phys. Chem.*, 92, 4644-4648, 1988.

McDow, S.R., and J.J. Huntzicker, Vapor adsorption artifact in the sampling of organic aerosol: Face velocity effects, *Atmos. Environ.*, 24A, 2563-2571, 1990.

Moortgat, G.K., B. Veyret, and R. Lesclaux, Kinetics of the reaction of HO₂ with CH₃C(O)O₂ in the temperature range 253-368K, *Chem. Phys. Lett.*, 160, 443-447,

1989.

Niki, H., P.D. Maker, C.M. Savage, and L.P. Breitenbach, FTIR study of the kinetics and mechanism for Cl-atom-initiated reactions of acetaldehyde, *J. Phys. Chem.*, 89, 588-591, 1985.

Niki, H., P.D. Maker, C.M. Savage, L.P. Breitenbach, and M.D. Hurley, FTIR spectroscopic study of the mechanism for the gas-phase reaction between ozone and tetramethylethylene, *J. Phys. Chem.*, 91, 941-946, 1987.

Odum, J.R., T. Hoffmann, F. Bowman, D. Collins, R.C. Flagan, and J.H. Seinfeld, Gas/particle partitioning and secondary organic aerosol yields, *Environ. Sci. Technol.*, 30, 2580-2585, 1996.

Odum, J.R., T.P.W. Jungkamp, R.J. Griffin, R.C. Flagan, and J.H. Seinfeld, The atmospheric aerosol-forming potential of whole gasoline vapor, *Science*, 276, 96-99, 1997a.

Odum, J.R., T.P.W. Jungkamp, R.J. Griffin, H.J.L. Forstner, R.C. Flagan, and J.H. Seinfeld, Aromatics, reformulated gasoline, and atmospheric organic aerosol formation, *Environ. Sci. Technol.*, 31, 1890-1897, 1997b.

Palen, E.J., D.T. Allen, S.N. Pandis, S.E. Paulson, J.H. Seinfeld, and R.C. Flagan, Fourier transformation infrared analysis of aerosol formed in the photooxidation of isoprene and β -pinene, *Atmos. Environ.*, 26A, 1239-1251, 1992.

Pandis, S.N., S.E. Paulson, J.H. Seinfeld, and R.C. Flagan, Aerosol formation in the photooxidation of isoprene and β -pinene, *Atmos. Environ.*, 25A, 997-1008, 1991.

Pankow, J. F., Review and comparative analysis of the theories on partitioning between the gas and aerosol particulate phases in the atmosphere, *Atmos. Environ.*, 21, 2275-

2283, 1987.

Pio, C.A., and A.A. Valente, Atmospheric fluxes and concentrations of monoterpenes in resin-tapped pine forest, *Atmos. Environ.*, 32, 683-691, 1998.

Rechsteiner, C.E., Jr., Boiling Point, in Lyman, W.J., Reehl, W.F., and Rosenblatt, D.H. (eds), *Handbook of Chemical Property Estimation Methods*, American Chemical Society, Washington D.C., 1990.

Schwarzenbach, R.P., P.M. Gschwend, and D.M. Imboden, Environmental Organic Chemistry, John Wiley & Sons, New York, 70-75, 1993.

Wang, S-C., S.E. Paulson, D. Grosjean, R.C. Flagan, and J.H. Seinfeld, Aerosol formation and growth in atmospheric organic/NO_x systems- I. Outdoor smog chamber studies of C₇- and C₈-hydrocarbons, *Atmos. Environ.*, 26A, 403-420, 1992.

Yu, J., R.C. Flagan, and J.H. Seinfeld. Identification of Products Containing -COOH, -OH, and -C=O in atmospheric oxidation of hydrocarbons, *Environ. Sci. Technol.*, 32, 2357-2370, 1998.

Yu, J., H.E. Jeffries, and R.M. LeLacheur, Identifying airborne carbonyl compounds in isoprene atmospheric photooxidation products by their PFBHA oximes using gas chromatography/ion trap mass spectrometry, *Environ. Sci. Technol.*, 29, 1923-1932, 1995.

Zhang, S-H, M. Shaw, J.H. Seinfeld, and R.C. Flagan, Photochemical aerosol formation from α -pinene and β -pinene, *J. Geophys. Res.*, 97, 20,717-20,729, 1992.

Table A.3.1. Initial conditions and results of ozone-terpene reactions.

HC	Date	T (K)	O ₃ initial ppbv	HC initial ppbv	HC final ppbv	ΔHC ppbv	Sample start time (min)	ΔM _o μg m ⁻³	Aerosol yield
α-pinene	6/9/98a	308	237	59.2	2.2	57.0	291	54.2	0.176
	6/9/98b	308	269	67.2	2.1	65.1	339	65.1	0.186
	6/17/98a	306	74	107.1	62.0	45.1	53	38.8	0.159
β-pinene	6/11/98b	307	352	87.9	10.0	77.9	388	18.9	0.045
	6/17/98b	306	56	104.6	79.8	24.8	303	11.2	0.083
Δ ³ -carene	6/15/98b	306	360	89.9	0.4	89.5	299	63.3	0.130
sabinene	6/15/98a	306	370	92.4	0.0	92.4	232	17.6	0.035

Table A.3.2. Denuder and filter collection efficiencies of selected products.

Compound	Collection efficiency (%)	
	denuder	filter
pinic acid	98.7 ± 0.2	0.85
2,2-dimethyl-3-formyl-cyclobutyl	97.1 ± 1.9	NA [*]
methanoic acid		
norpinonic acid	94.0 ± 4.0	NA
pinonic acid	97.8 ± 1.3	0.59
norpinonaldehyde	95.8 ± 1.0	0.89
pinonaldehyde	97.7 ± 0.5	0.95

^{*} Not available.

Table A.3.3. Relative recoveries of select multifunctional compounds vs. recovery standard.

Compound	Denuder samples	Filter samples
	N=6 [*]	N=5 [*]
pinic acid	0.66±0.04	0.80±0.07
pinonic acid	0.67±0.19	0.74±0.14
2-hydroxy-cyclohexanone	0.64±0.10	0.74±0.07
5-methyl-1,3-cyclohexanedione	0.41±0.06	0.61±0.08
5-isopropyl-1,3-cyclohexanedione	0.44±0.04	0.63±0.10
7-oxo-octanoic acid	0.66±0.12	0.83±0.07
heptanedioic acid	0.69±0.05	0.77±0.17
octanedioic acid	0.59±0.05	0.82±0.14

^{*} Number of experiments conducted.

Table A.3.4. Products from ozone oxidation of β -pinene.

Name	Structure	Pseudo-molecular ions in CI mass spectrum
P ₁ : C ₈ H ₁₂ O ₄ norpinic acid MW=172 deri. MW=316 [‡]		M+73: 389 M+1: 317 M-15: 301 M-89: 227 M-117: 199
P ₂ : C ₉ H ₁₄ O ₄ [*] pinic acid MW=186 deri. MW=330		M+73: 403 M+1: 331 M-15: 315 M-89: 241
P ₃ : C ₉ H ₁₄ O [*] nopinone MW=138 deri. MW=333		M+181: 514 M+29: 362 M+1: 334 M-181: 152 M-197: 136
P ₄ : C ₉ H ₁₄ O ₂ hydroxy pina ketone MW=154 deri. MW=421		M+181: 602 M+1: 422 M-15: 406 M-89: 332 M-197: 224
P ₅ : C ₈ H ₁₂ O ₃ 2,2-dimethyl-3-formyl-cyclobutyl-methanoic acid MW=156 deri. MW=423		M+73: 496 M+1: 424 M-15: 408 M-89: 334 M-117: 306 M-181: 242 M-197: 226
P ₆ : C ₉ H ₁₄ O ₃ norpinonic acid and its isomers MW=170 deri. MW=437		M+73: 510 M+1: 438 M-15: 422 M-89: 348 M-117: 320 M-181: 256 M-197: 240
P ₇ : C ₁₀ H ₁₆ O ₃ [*] pinonic acid MW=184 deri. MW=451		M+73: 524 M+1: 452 M-89: 362 M-181: 270 M-197: 254 M-238: 213
P ₈ : C ₉ H ₁₄ O ₄ hydroxy norpinonic acids MW=186 deri. MW=525	e.g. 	M+73: 598 M+1: 526 M-15: 510 M-89: 436 M-181: 344 M-197: 328

Table A.3.4. (continued) Products from ozone oxidation of β -pinene.

Name	Structure	Pseudo-molecular ions in CI mass spectrum
P ₉ : C ₁₀ H ₁₆ O ₄ hydroxy pinonic acid MW=200 deri. MW=539		M+73: 612 M+1: 540 M-15: 524 M-89: 450 M-181: 358 M-197: 342 M-326: 213
P ₁₀ : C ₈ H ₁₂ O ₂ 2,2-dimethyl-cyclobutane-1,3-dicarboxaldehyde MW=140 deri. MW=530		M+1: 530 M-181: 349 M-197: 333 M-224: 306
P ₁₁ : C ₉ H ₁₂ O ₂ 3-oxo-pina ketone MW=152 deri. MW=542 mono-deri. MW=347		M+29: 571 M+1: 543 M-197: 345

[‡] deri. denotes derivative.

^{*} identification confirmed with an authentic standard.

Table A.3.5. Products from ozone oxidation of sabinene.

Name	Structure	Pseudo-molecular ions in CI mass spectrum
S ₁ : C ₈ H ₁₂ O ₄ MW=186 deri. MW=330		M+73: 389 M+1: 317 M-15: 301 M-89: 227 M-117: 199
S ₂ : C ₉ H ₁₄ O ₄ sabinic acid MW=186 deri. MW=330		M+73: 430 M+1: 331 M-15: 315 M-89: 241 M-117: 225
S ₃ : C ₉ H ₁₄ O ₄ pinic acid MW=186 deri. MW=330		M+73: 403 M+1: 331 M-15: 315 M-89: 241
S ₄ : C ₉ H ₁₄ O sabina ketone MW=138 deri. MW=333		M+181: 514 M+29: 362 M+1: 334 M-181: 152 M-197: 136
S ₅ : C ₈ H ₁₂ O ₃ 2-(2-isopropyl)-2-formylcyclopropyl-methanoic acid MW=156 deri. MW=423		M+73: 496 M+1: 424 M-15: 408 M-89: 334 M-181: 242 M-197: 226
S ₆ : C ₉ H ₁₄ O ₂ hydroxy sabina ketones MW=154 deri. MW=421		M+181: 602 M+1: 422 M-15: 406 M-89: 332 M-197: 224 M-212: 210
S ₇ : C ₉ H ₁₄ O ₃ norsabinonic acid and its isomers MW=170 deri. MW=437		M+197: 634 M+181: 618 M+73: 510 M+1: 438 M-15: 422 M-89: 348 M-197: 240

Table A.3.5. (continued) Products from ozone oxidation of sabinene.

Name	Structure	Pseudo-molecular ions in CI mass spectrum
S ₈ : C ₈ H ₁₂ O ₃ MW=156 deri. MW=495	e.g. 	M+89: 584 M+1: 496 M+29: 524 M-15: 480 M-89: 406 M-147: 348 M-197: 298
S ₉ : C ₉ H ₁₄ O ₄ hydroxy norsabinonic acid MW=186 deri. MW=525	e.g. 	M+73: 598 M+1: 526 M-15: 510 M-89: 436 M-197: 328
S ₁₀ : C ₁₀ H ₁₆ O ₄ MW=200 deri. MW=539	e.g. 	M+73: 612 M+1: 540 M-15: 524 M-89: 450 M-181: 358 M-197: 342
S ₁₁ : C ₉ H ₁₂ O ₂ 3-oxo-sabina ketone MW=152 deri. MW=542		M+29: 571 M+1: 543 M-197: 345
S ₁₂ : C ₆ H ₈ O ₃ MW=128 deri. MW=590	e.g. 	EI spectrum M: 590 M-15: 575 M-181: 409 M-197: 393

* identification confirmed with an authentic standard.

Table A.3.6. Products from ozone oxidation of α -pinene.

Product	Structure	Product	Structure
A ₁ : C ₈ H ₁₂ O ₄ norpinic acid MW=172 deri. MW=316		A ₈ : C ₈ H ₁₂ O ₂ 2,2-dimethyl- cyclobutyl-1,3- dicarboxaldehyde MW=140	
A ₂ : C ₉ H ₁₄ O ₄ [*] pinic acid MW=186 deri. MW=330		A ₉ : C ₉ H ₁₄ O ₂ norpinonaldehyde MW=154 deri. MW=544	
A ₃ : C ₁₀ H ₁₆ O ₃ (2,2-dimethyl-3-acetyl)- cyclobutyl formate MW=184 deri. MW=379		A ₁₀ : C ₁₀ H ₁₆ O ₂ pinonaldehyde MW=168 deri. MW=558	
A ₄ : C ₈ H ₁₂ O ₃ 2,2-dimethyl-3-formyl- cyclobutyl-methanoic acid MW=156 deri. MW=423		A ₁₁ : C ₁₁ H ₁₈ O ₂ MW=182 deri. MW=572	two carbonyl groups
A ₅ : C ₉ H ₁₄ O ₃ norpinonic acid and isomer MW=170 deri. MW=437		A ₁₂ : C ₁₀ H ₁₆ O ₃ hydroxy pinonaldehydes MW=184 deri. MW=646	
A ₆ : C ₁₀ H ₁₆ O ₃ [*] pinonic acid MW=184 deri. MW=451		A ₁₃ MW=198 deri. MW=588	two carbonyl groups
A ₇ : hydroxy pinonic acid MW =200 deri. MW=539		A ₁₄ : C ₁₀ H ₁₄ O ₃ MW=198 deri. MW=660	e.g.

* identification confirmed with an authentic standard.

Table A.3.7. Products from ozone oxidation of Δ^3 -carene.

Product	Structure	Pseudo-molecular ions in CI mass spectrum
C ₁ : C ₈ H ₁₂ O ₄ nor-3-careic acid MW=172 deri. MW=316		M+1: 317 M-15: 301 M-89: 227 M-117: 199
C ₂ : C ₉ H ₁₄ O ₄ 3-careic acid MW=186 deri. MW=330		M+147: 477 M+73: 403 M+29: 359 M+1: 331 M-15: 315 M-89: 241 M-117: 213
C ₃ : C ₉ H ₁₄ O ₄ pinic acid* MW=186 deri. MW=330		M+73: 403 M+1: 331 M-15: 315 M-89: 241 M-117: 213
C ₄ : MW=118 deri. MW=457	one carbonyl and two OH/COOH groups	M+181: 638 M+1: 458 M-15: 442 M-89: 368 M-117: 340 M-197: 260
C ₅ : MW=142 deri. MW=337	one carbonyl group, no OH/COOH groups	M+181: 518 M+1: 338 M-17: 320 M-197: 140
C ₆ : C ₈ H ₁₂ O ₂ MW=140 deri. MW=423		M+1: 424 M-89: 334 M-197: 226
C ₇ : C ₉ H ₁₄ O ₃ 3-norcaronic acid and isomers MW=170 deri. MW=437		M+73: 510 M+1: 437 M-89: 348 M-181: 256 M-197: 240
C ₈ : C ₁₀ H ₁₆ O ₃ 3-caronic acid MW=184 deri. MW=451		M+73: 524 M+1: 452 M-89: 362 M-181: 270 M-197: 254 M-197: 254 M-211: 240

Table A.3.7. (continued) Products from ozone oxidation of Δ^3 -carene.

Product	Structure	Pseudo-molecular ions in Cl mass spectrum
$C_9: C_{10}H_{16}O_3$ hydroxy 3-caronic acid MW=184 deri. MW=539	e.g. 	M+1: 540 M-89: 450 M-197: 342
$C_{10}:$ MW=128 deri. MW=518	two carbonyl groups, no OH/COOH groups	M+1: 519 M-181: 337 M-197: 321 M-224: 294
$C_{11}: C_9H_{14}O_2$ norcaronaldehyde MW=154 deri. MW=544		EI spectrum: M: 544 M-181: 363 M-197: 347
$C_{12}: C_{10}H_{16}O_2$ caronaldehyde MW=168 deri. MW=558		M+29: 587 M+1: 559 M-181: 377 M-197: 361 M-238: 320
$C_{13}: C_{10}H_{16}O_3$ hydroxy 3-caronic aldehydes MW=184 deri. MW=646		M+1: 647 M-197: 449

* identification confirmed with an authentic standard.

Table A.3.8. Products and their surrogates for quantification.

Standard	Products surrogated for			
	β -pinene/O ₃	sabinene/O ₃	α -pinene/O ₃	Δ^3 -carene/O ₃
pinic acid	norpinic acid	sabinic acid, norsabinic acid	norpinic acid	3-caric acid, nor-3-caric acid
pinonic acid	P ₅ , norpinonic acid and its isomers, hydroxy norpinonic acid, hydroxy pinonic acid	sabinonic acid, norsabinonic acid and its isomers, S ₈ , S ₉ , S ₁₀	A ₄ , norpinonic acid and its isomers, hydroxy pinonic acid,	3-caronic acid, nor-3-caronic acid and its isomers, C ₆ , C ₉
2-hydroxy-cyclohexanone	hydroxy pina ketones	hydroxy sabina ketones		
5-methyl-1,3-cyclohexanedione	P ₁₀ , 3-oxo-pina ketone	3-oxo-sabina ketone, S ₁₂	pinonaldehyde, norpinonaldehyde, A ₈ , A ₁₁ , hydroxy pinonaldehydes, A ₁₃ , A ₁₄	C ₁₀ , norcaronaldehyde, caronaldehyde, hydroxy caronaldehydes
nopinone		sabina ketone	A ₃	C ₅

Table A.3.9. Gaseous and particulate product yields in the β -pinene/O₃ reaction (6/11/98b).

Product	Molar yield (%)			Aerosol yield by mass (%)
	Gas	Aerosol	Total	
pinic acid	1.7	0.91	2.6	1.2
norpinic acid	0.23	0.11	0.35	0.17
pinonic acid	0.41	0.10	0.52	0.14
norpinonic acid and its isomer	4.6	1.3	5.9	1.7
hydroxy-pina-ketones	6.6	0.66	7.3	0.74
3-oxo-pina-ketone	1.8	0.02	1.8	0.02
2,2-dimethyl-cyclobutane-1,3-dicarboxaldehyde	0.35	ND	0.35	ND
nopinone	17.0	trace	17.0	trace
hydroxy norpinonic acid	0.58	0.1	0.68	0.14
hydroxy pinonic acid	0.26	0.17	0.43	0.25
total molar yield	33.5	3.4	36.9	4.4
carbon-based total yield			34.2	
Aerosol yield measured by SEMS and CNC				4.5

Table A.3.9. (continued) Gaseous and particulate product yields in the β -pinene/ O_3 reaction (6/17/98b).

Product	Molar yield (%)			Aerosol yield by mass (%)
	Gas	Aerosol	Total	
pinic acid	2.5	1.2	3.7	1.6
norpinic acid	0.17	0.09	0.27	0.12
pinonic acid	0.56	0.19	0.74	0.25
norpinonic acid and its isomer	14.3	2.2	16.5	2.7
hydroxy-pina-ketones	7.9	1.1	9.0	1.3
3-oxo-pina-ketone	7.6	0.11	7.7	0.12
2,2-dimethyl-cyclobutane-1,3-dicarboxaldehyde	0.29	ND	0.29	ND
nopinone	15.8	trace	15.8	trace
hydroxy norpinonic acid	0.98	0.24	1.2	0.33
hydroxy pinonic acid	0.16	0.15	0.31	0.20
total molar yield	50.3	5.3	55.6	6.6
carbon-based total yield			50.1	
Aerosol yield measured by SEMS and CNC				8.3

Table A.3.10. Gaseous and particulate product yields in the sabinene/O₃ reaction.

Product	Molar yield (%)			Aerosol yield by mass (%)
	Gas	Aerosol	Total	
pinic acid	1.1	0.29	1.4	0.39
sabinic acid	0.80	0.39	1.2	0.53
norsabinic acid	0.18	0.07	0.25	0.09
norsabinonic acid and its isomers	3.6	1.1	4.7	1.4
hydroxy-sabina-ketones	6.6	0.43	7.0	0.53
3-oxo-sabina-ketone	0.50	0.01	0.51	0.01
S ₅ [*]	0.15	0.11	0.26	0.13
sabina ketone	46.2	0.43	46.6	0.43
S ₈ [*]	0.54	ND	0.54	ND
S ₉ [*]	0.75	ND	0.75	ND
S ₁₀ [*]	0.12	0.02	0.14	0.03
total molar yield	60.5	2.9	63.4	3.5
carbon-based total yield			57.0	
	Aerosol yield measured by SEMS and CNC			3.5

^{*} See Table A.3.5 for possible candidate structures.

Table A.3.11. Gaseous and particulate product yields in the α -pinene/ O_3 reaction.

Product	Molar yield (%)									Aerosol yield (%) by mass		
	Gas			Aerosol			Total					
	6/9a	6/9b	6/17	6/9a	6/9b	6/17	6/9a	6/9b	6/17	6/9a	6/9b	6/17
Experiment												
pinic acid	1.2	2.1	2.7	1.8	3.9	2.8	3.0	6.0	5.5	2.5	5.3	3.9
norpinic acid	0.04	0.03	0.04	0.08	0.09	0.05	0.1	0.1	0.09	0.1	0.1	0.06
hydroxy pinonaldehydes	1.4	0.8	9.2	2.4	1.1	2.0	3.8	1.9	11.2	3.3	1.4	2.8
pinonic acid	0.8	0.6	6.6	1.7	1.6	1.3	2.5	2.2	7.9	2.3	2.1	1.8
norpinonic acid & isomer	2.2	5.4	9.8	2.1	4.8	2.8	4.3	10.2	12.6	2.6	5.9	3.4
pinonaldehyde	9.6	5.7	18.1	0.8	0.3	0.9	10.4	6.0	19.0	1.0	0.4	1.1
nor-pinonaldehyde	1.1	1.5	2.4	0.1	0.2	0.2	1.2	1.7	2.6	0.2	0.2	0.2
2,2-dimethyl-cyclobutane-1,3-dicarboxaldehyde	0.4	0.3	1.6	ND	ND	ND	0.4	0.3	1.6	0	0	0
hydroxy pinonic acid	0.8	0.2	1.6	2.1	1.3	2.1	2.9	1.5	3.7	3.1	1.9	3.1
A_3^*	1.5	0.6	3.8	ND	ND	ND	1.5	0.6	3.8	ND	ND	ND
A_{13}^*	0.06	0.02	0.1	0.08	0.12	0.1	0.14	0.1	0.2	0.1	0.2	0.1
A_{14}^*	0.03	trace	0.03	0.55	0.48	0.8	0.6	0.5	0.8	0.7	0.6	1.1
total molar yield	19.1	17.2	56.0	11.7	13.9	13.0	30.8	31.0	69.1	15.9	18.1	17.6
carbon-based total yield							29.9	29.1	66.8			
Aerosol yield measured by SEMS and CNC										17.6	18.6	15.9

* See Table A.3.6 for possible candidate structures.

Table A.3.12. Gaseous and particulate product yields in the Δ^3 -carene/O₃ reaction.

Product	Molar yield (%)			Aerosol yield by mass (%)
	Gas	Aerosol	Total	
pinic acid	0.83	0.33	1.2	0.46
3-caric acid	0.64	1.3	1.9	1.8
nor-3-caric acid	0.07	ND	0.07	ND
hydroxy caronaldehydes	3.0	0.19	3.2	0.25
3-caronic acid	2.7	1.5	4.2	2.1
nor-3-caronic acid and isomers	1.8	0.54	2.3	0.68
caronaldehyde	7.8	0.67	8.5	0.83
norcaronaldehyde	trace	trace	trace	trace
hydroxy 3-caronic acid	0.47	0.69	1.2	1.0
C ₄ [*]	0.31	0.39	0.70	0.54
C ₅ [*]	2.3	0.24	2.5	0.25
C ₁₀ [*]	0.22	ND	0.22	ND
total molar yield	20.1	5.9	26.0	7.9
carbon-based total yield			24.4	
Aerosol yield measured by SEMS and CNC				13.0

^{*}See Table A.3.7 for possible candidate structures.

Table A.3.13. Gas-particle partitioning coefficients ($\text{m}^3 \mu\text{g}^{-1}$) of individual products at 306-308 K.

α -Pinene/ O_3		Δ^3 -Carene/ O_3		β -Pinene/ O_3		Sabinene/ O_3	
Compound	$K_{om, i}$	Compound	$K_{om, i}$	Compound	$K_{om, i}$	Compound	$K_{om, i}$
pinic acid	0.028 ± 0.001	3-caric acid	0.033	pinic acid	0.035 ± 0.009	sabinic acid	0.027
hydroxy pinon-aldehydes	0.019 ± 0.013	hydroxy caron-aldehydes	0.0010	hydroxy pina-ketones	0.0091 ± 0.0054	hydroxy sabina ketones	0.0037
pinonic acid	0.030 ± 0.005	3-caronic acid	0.0090				
norpinonic acid and its isomers	0.013 ± 0.005	nor-3-caronic acid	0.0047	norpinonic acid and its isomers	0.014 ± 0.001	nor-sabinonic acid and its isomers	0.018
pinon-aldehyde	0.0012 ± 0.0003	caronaldehyde	0.0014	3-oxo-pina ketone	0.0010 ± 0.0005	3-oxo-sabina ketone	0.0012
hydroxy pinonic acid	0.040 ± 0.010	hydroxy caronic acid	0.0231	hydroxy pinonic acid	0.066 ± 0.026	sabina ketone	0.00053
A_{13}	0.025 ± 0.003			hydroxy norpinonic acid	0.016 ± 0.009		

Table A.3.14. Sub-cooled liquid vapor pressure estimates.

Compound	T_b (K) ^a	Vapor pressure estimates at 306K ^b	
		mm Hg	ppmv
hydroxy pinonic acid	606	1.9×10^{-5}	0.048
pinic acid	601	5.1×10^{-5}	0.067
hydroxy pinonaldehydes	577	2.4×10^{-4}	0.32
pinonic acid	572	8.4×10^{-4}	0.45
norpinonic acid & isomers	558	8.4×10^{-4}	1.1
hydroxy pina ketone	542	2.2×10^{-3}	2.9
pinonaldehyde	530	4.4×10^{-2}	58
3-oxo-pina ketone	521	6.9×10^{-2}	91
nopinone	482	4.7×10^{-1}	620

^a T_b , boiling point at 1 atm if decomposition would not occur, estimated using Meissner's method [Rechsteiner, 1990]. T_b is needed to estimate vapor pressure. Meissner's method underestimates the T_b for each of C₅-C₁₀ *n*-alkanoic acids by ~6.5%, therefore a correction formula is obtained by a linear regression ($r^2=0.994$) for C₅-C₁₀ *n*-alkanoic acids, and applied to the compounds of unknown T_b . This correction is also justified for carbonyl-containing compounds. For example, Meissner's method estimates that the T_b for nopinone is 453K before correction and 485K after correction, which agrees well with the experimental value 482K.

^b Sub-cooled liquid vapor pressures are estimated using a modification of the Clausius-Claperyron equation [Schwarzenbach *et al.*, 1993].

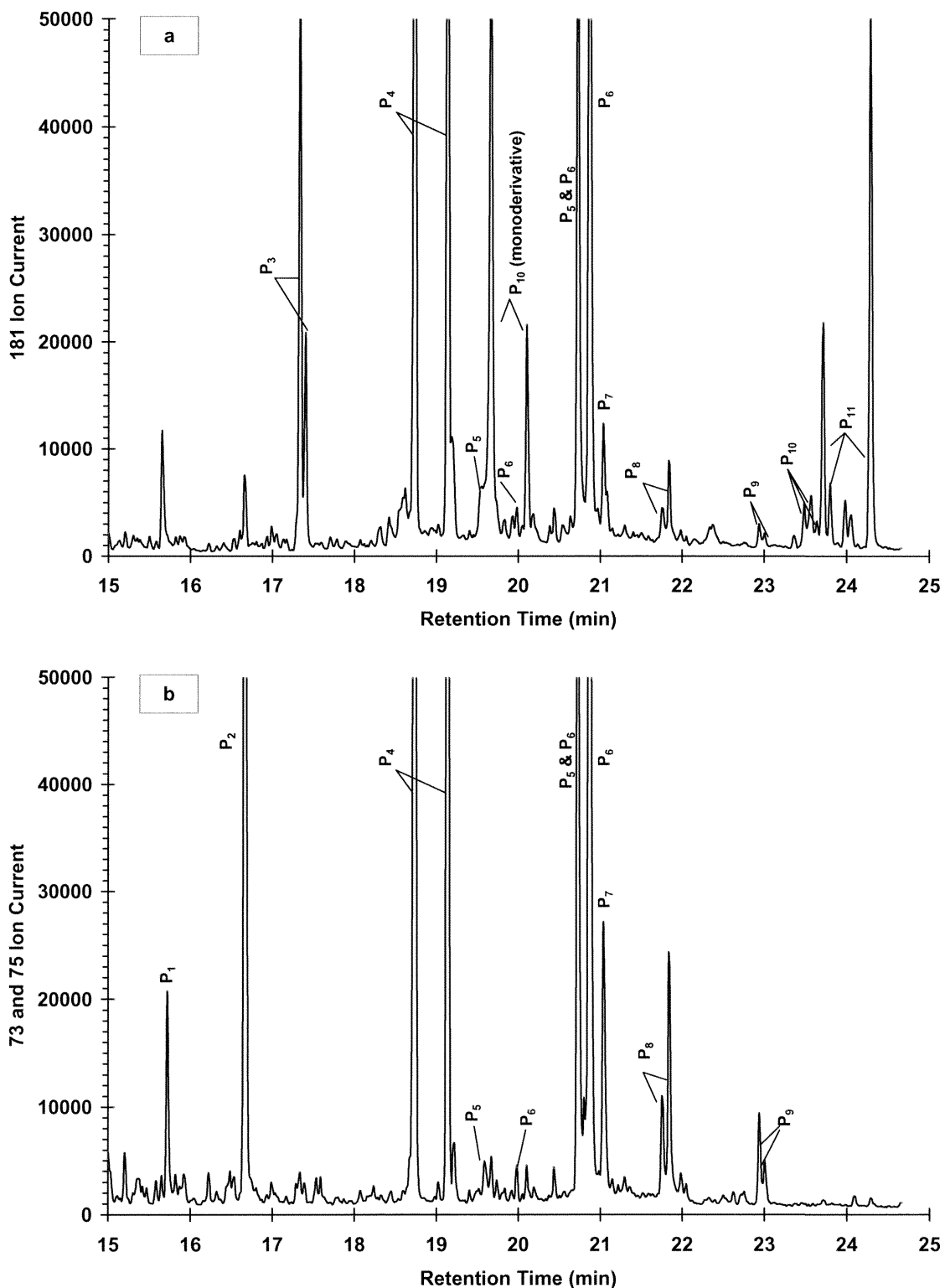


Figure A.3.1. Chromatogram of products from β -pinene/ O_3 reaction; see Table A.3.4 for peak identification. Top: Products containing carbonyl groups. Bottom: Products containing OH/COOH groups.

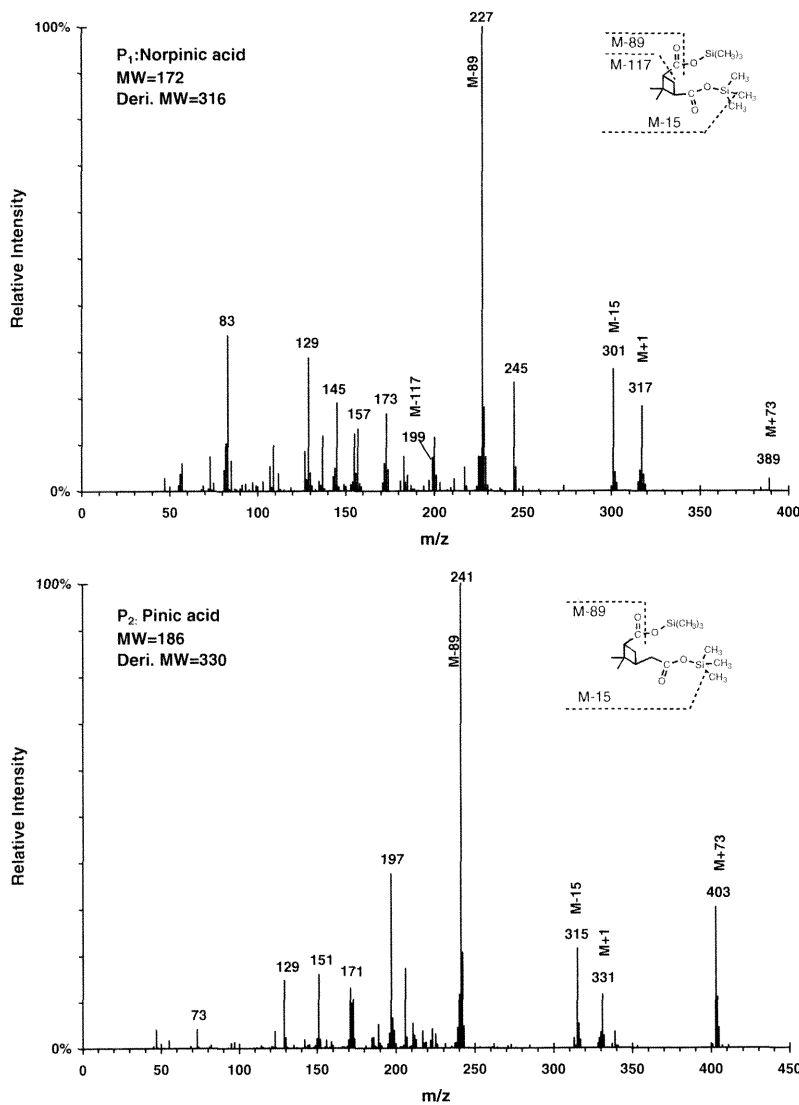


Figure A.3.2. Methane CI mass spectra for the derivatives of products from ozone oxidation of β -pinene.

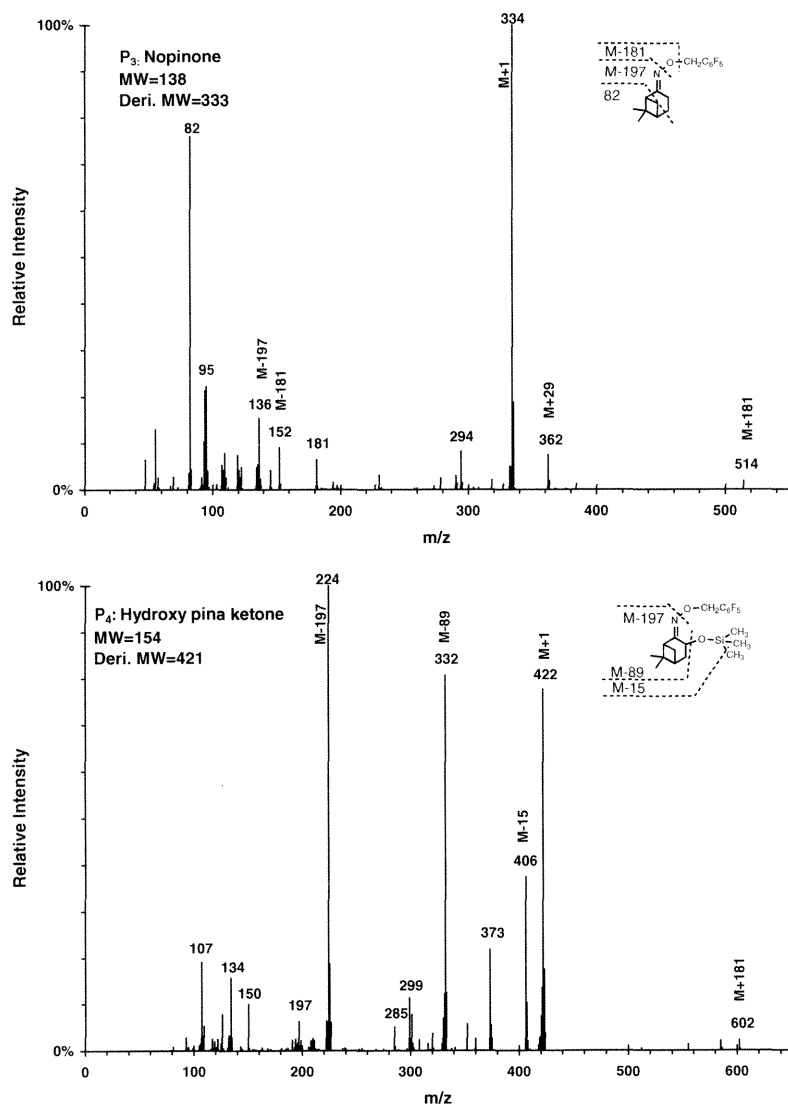


Figure A.3.2. (continued) Methane CI mass spectra for the derivatives of products from ozone oxidation of β -pinene.

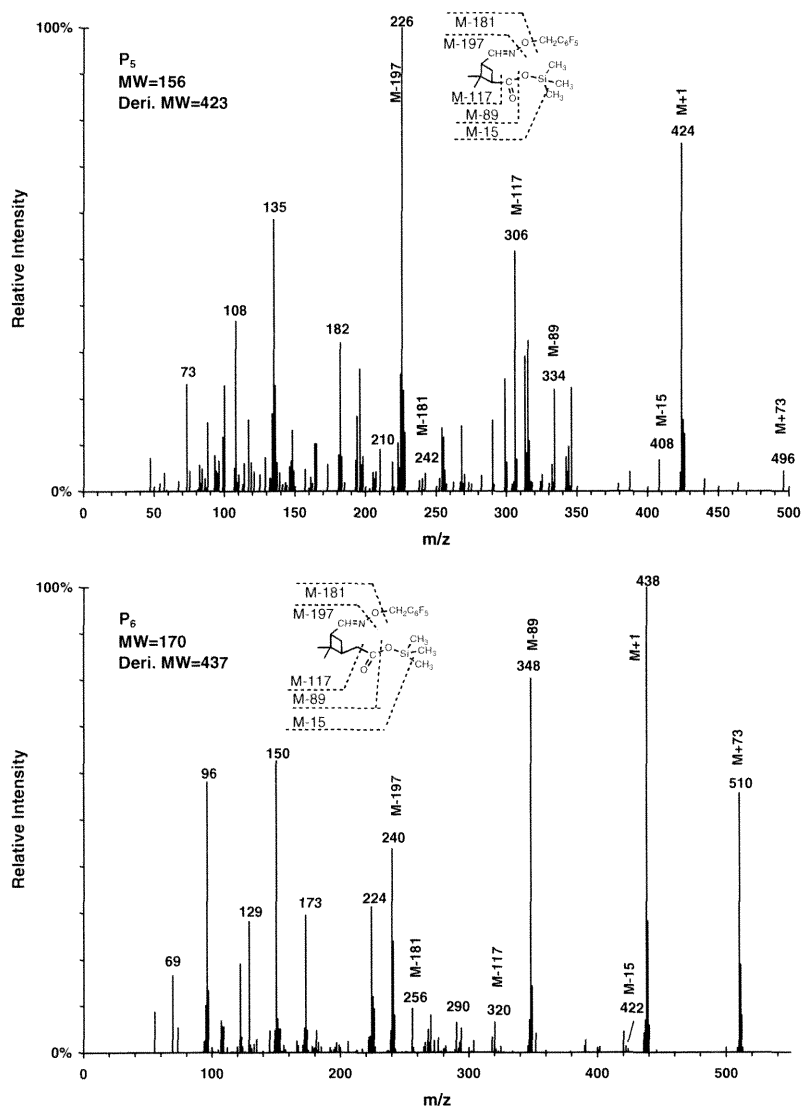


Figure A.3.2. (continued) Methane CI mass spectra for the derivatives of products from ozone oxidation of β -pinene.

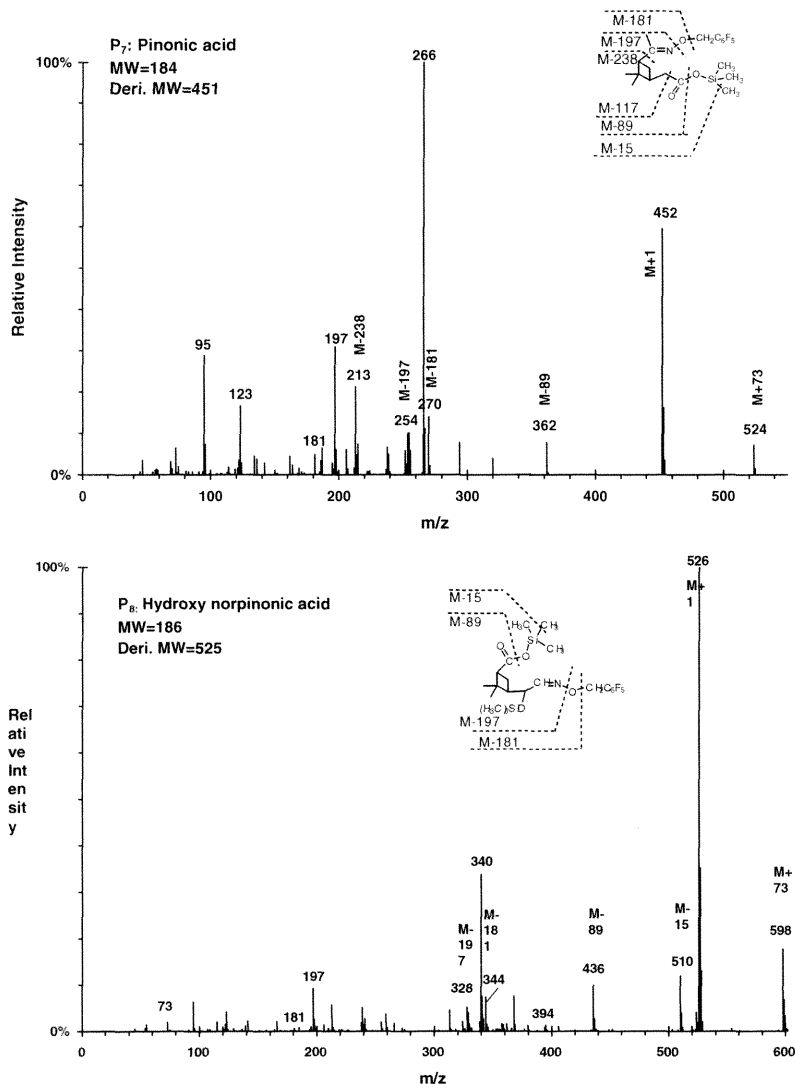


Figure A.3.2. (continued) Methane CI mass spectra for the derivatives of products from ozone oxidation of β -pinene.

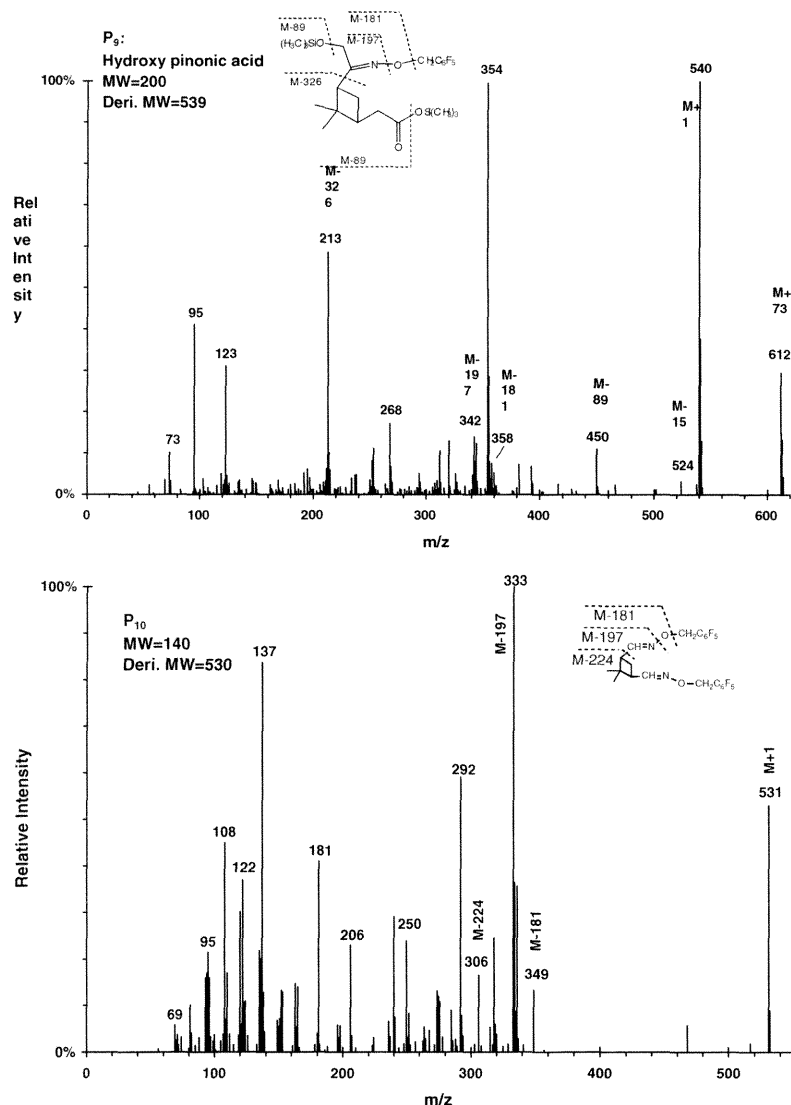


Figure A.3.2. (continued) Methane CI mass spectra for the derivatives of products from ozone oxidation of β -pinene.

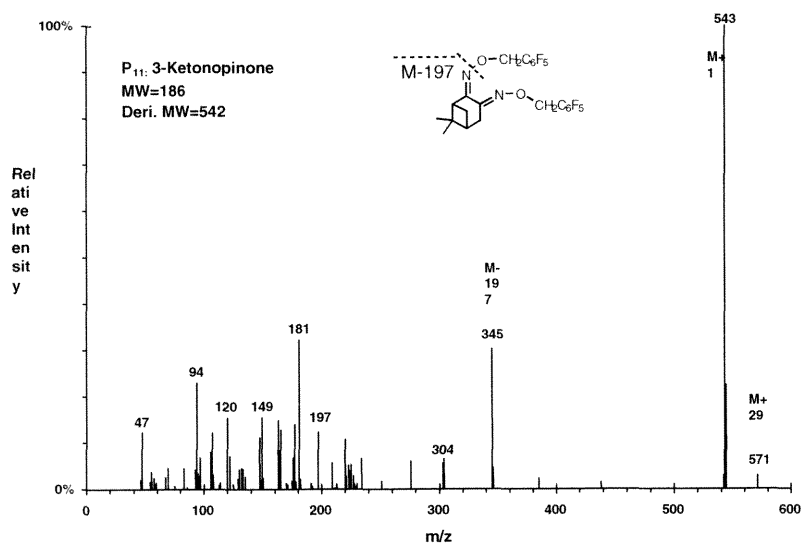


Figure A.3.2. (continued) Methane CI mass spectra for the derivatives of products from ozone oxidation of β -pinene.

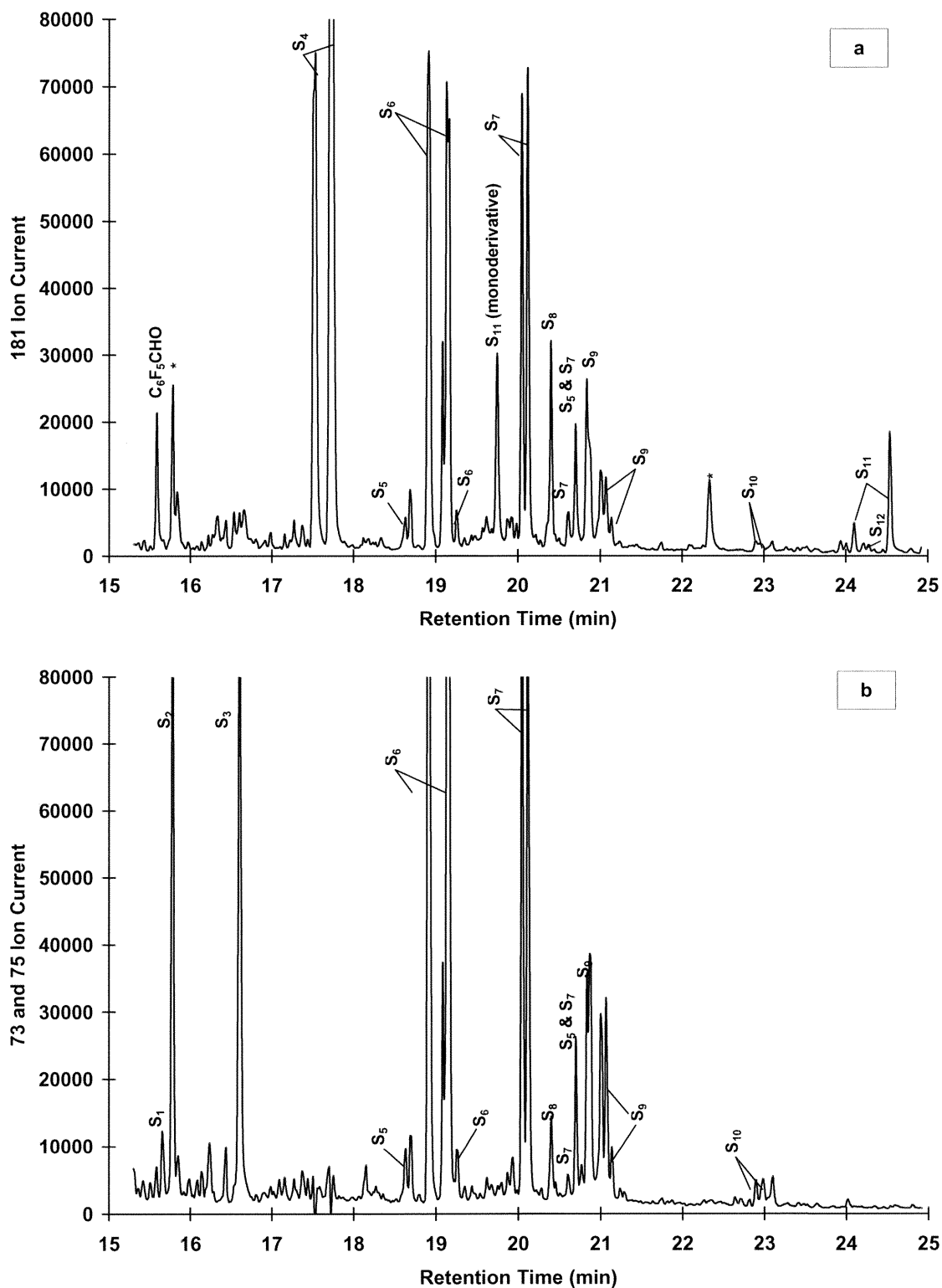


Figure A.3.3. Chromatogram of products from sabinene/O₃ reaction; see Table A.3.5 for peak identification. Top: Products containing carbonyl groups. Bottom: Products containing OH/COOH groups. (*: present in blank samples).

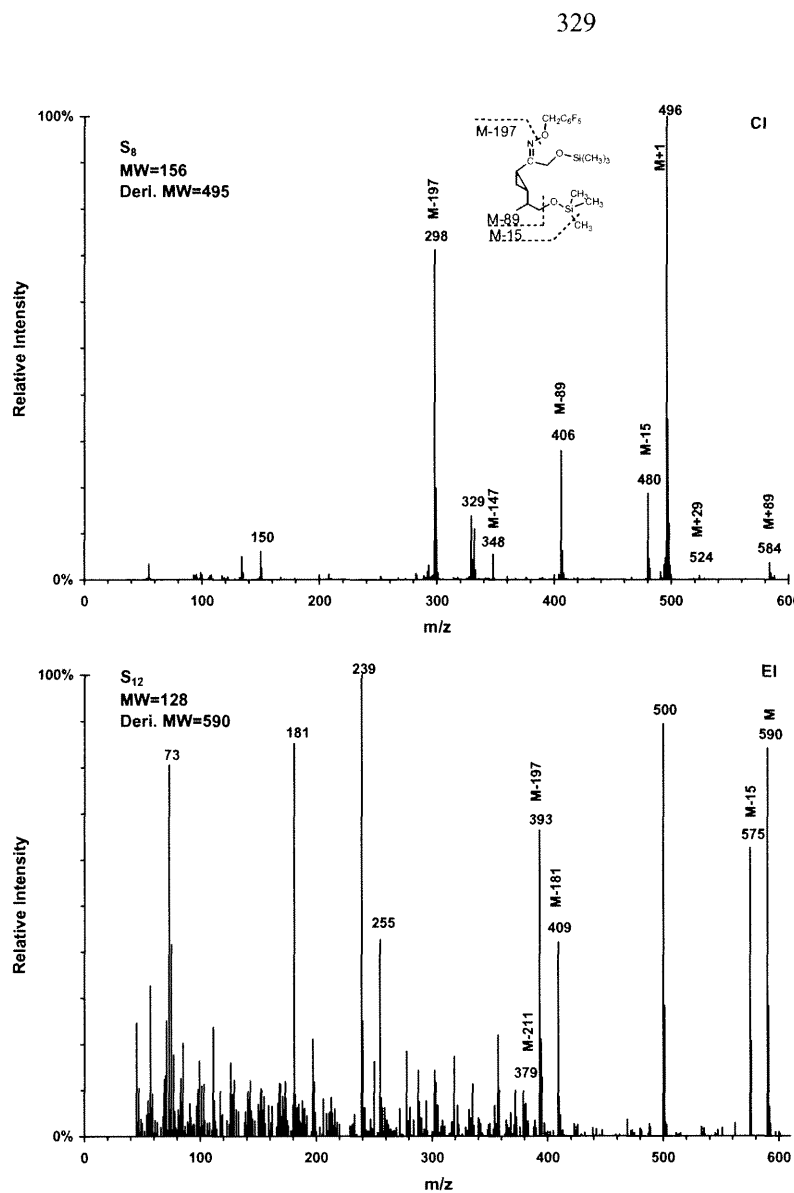


Figure A.3.4. Mass spectra for the derivatives of two products (S₈ and S₁₂) from ozone oxidation of sabinene.

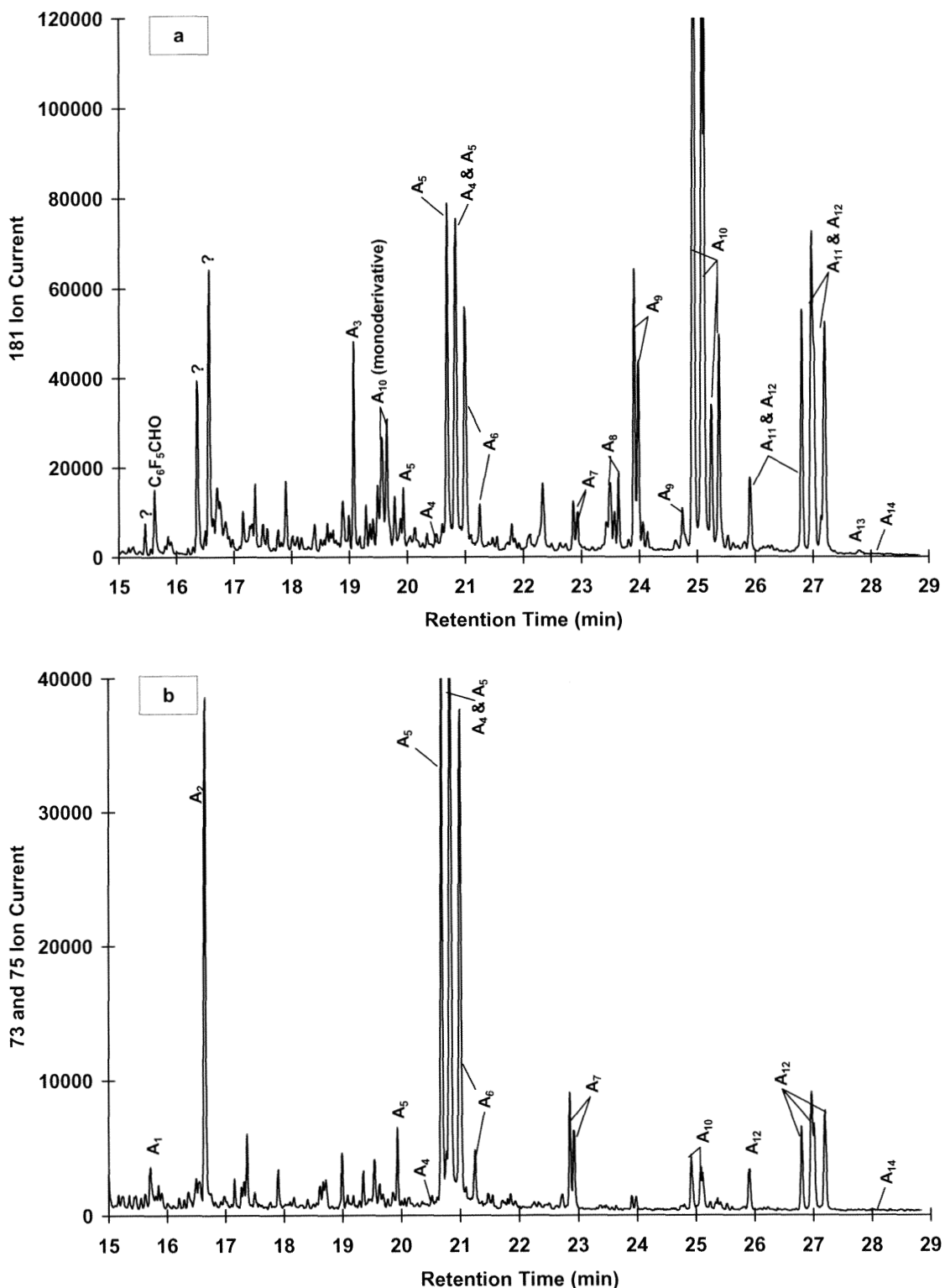


Figure A.3.5. Chromatogram of products from α -pinene/O₃ reaction, see Table A.3.6 for peak identification. Top: Products containing carbonyl groups. Bottom: Products containing OH/COOH groups.

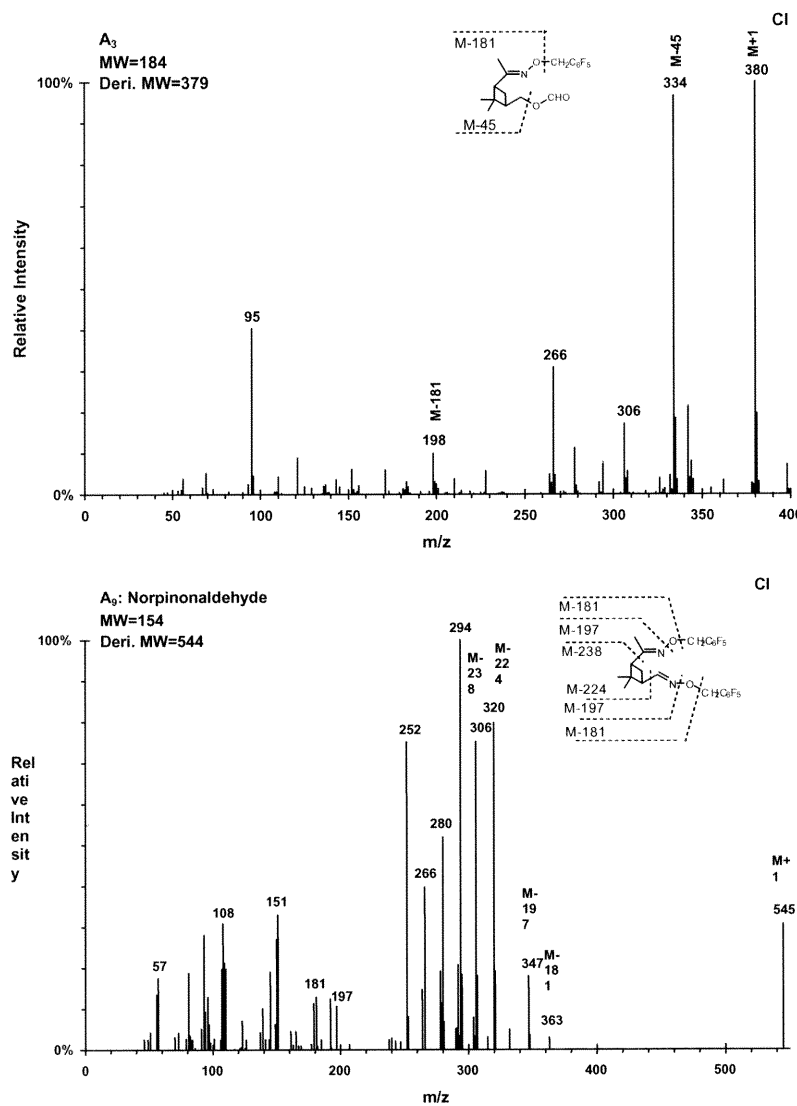


Figure A.3.6. Mass spectra for the derivatives of products from ozone oxidation of α -pinene.

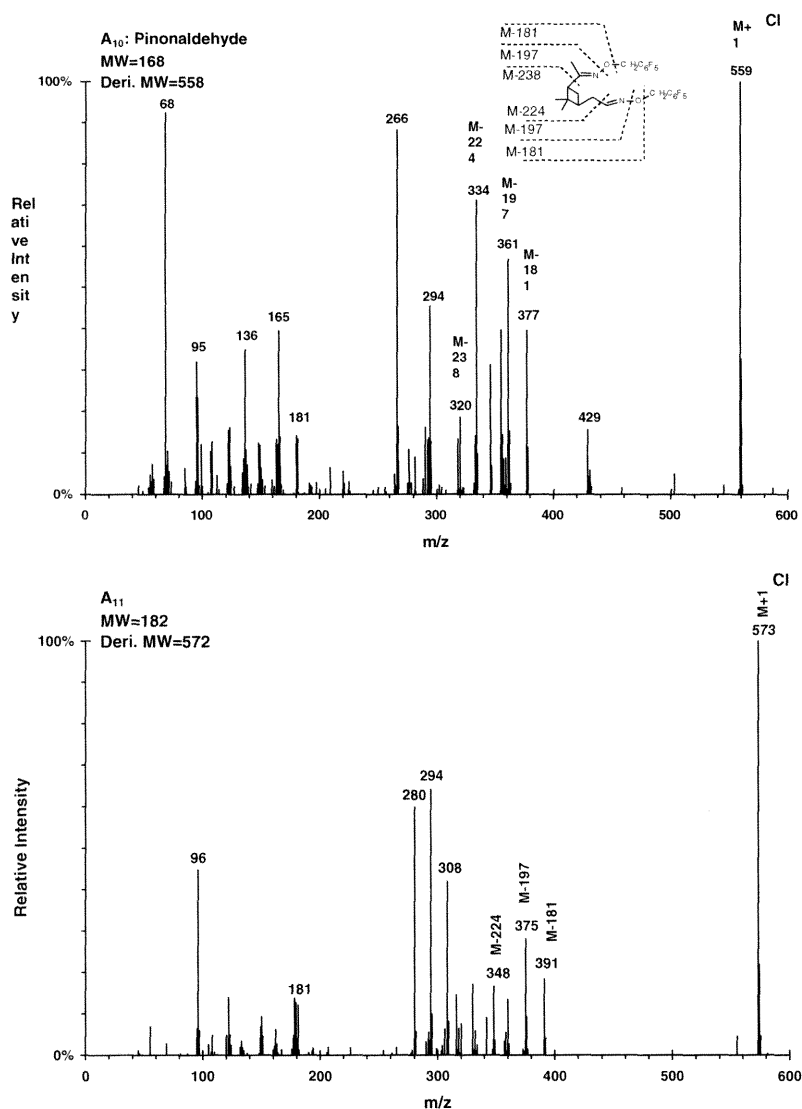


Figure A.3.6. (continued) Mass spectra for the derivatives of products from ozone oxidation of α -pinene.

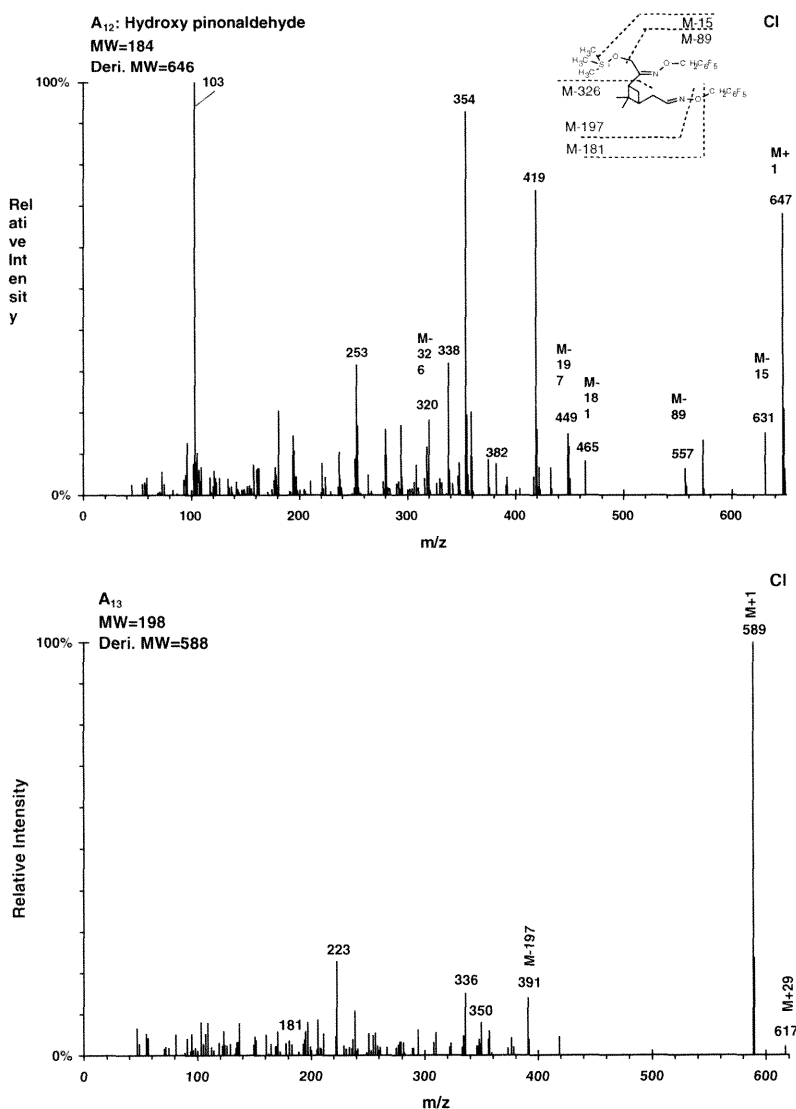


Figure A.3.6. (continued) Mass spectra for the derivatives of products from ozone oxidation of α -pinene.

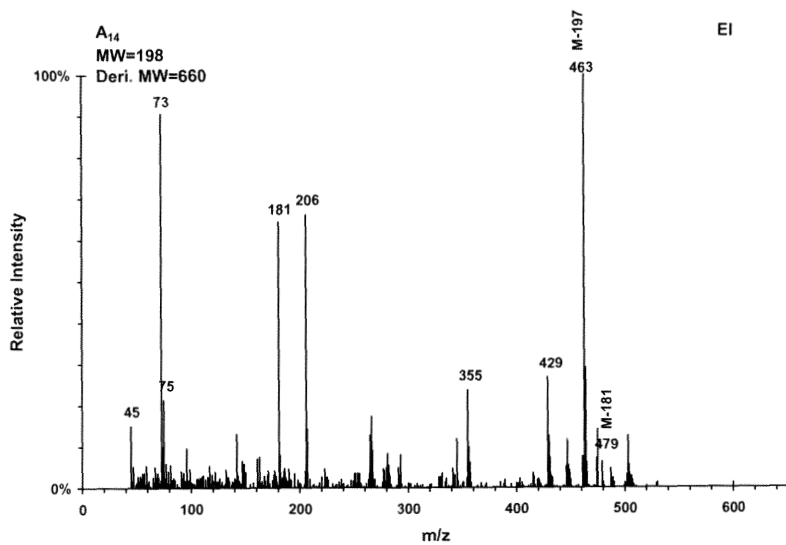


Figure A.3.6. (continued) Mass spectra for the derivatives of products from ozone oxidation of α -pinene.

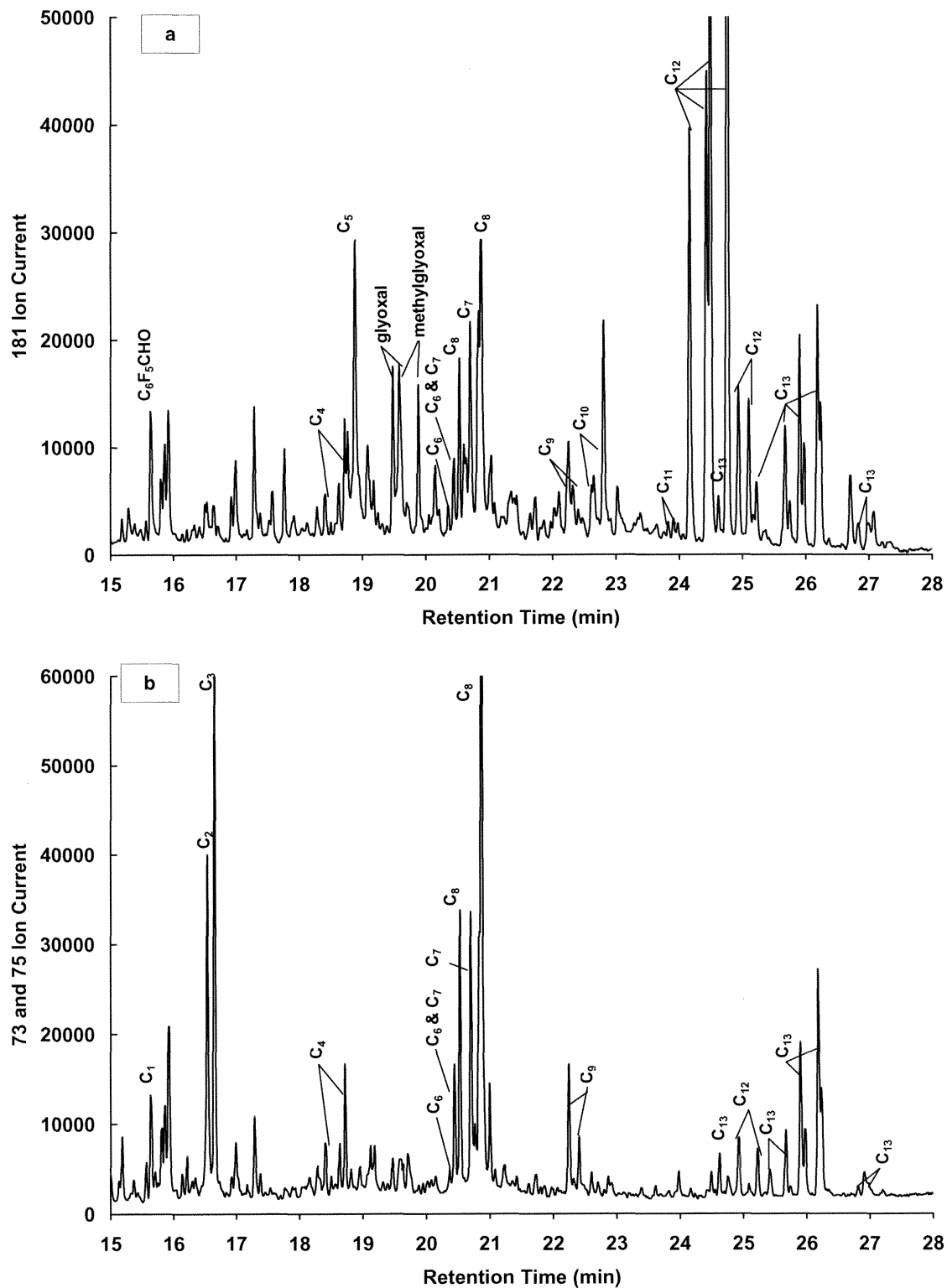


Figure A.3.7. Chromatogram of products from Δ^3 -carene/O₃ reaction; see Table A.3.7 for peak identification. Top: Products containing carbonyl groups. Bottom: Products containing OH/COOH groups.

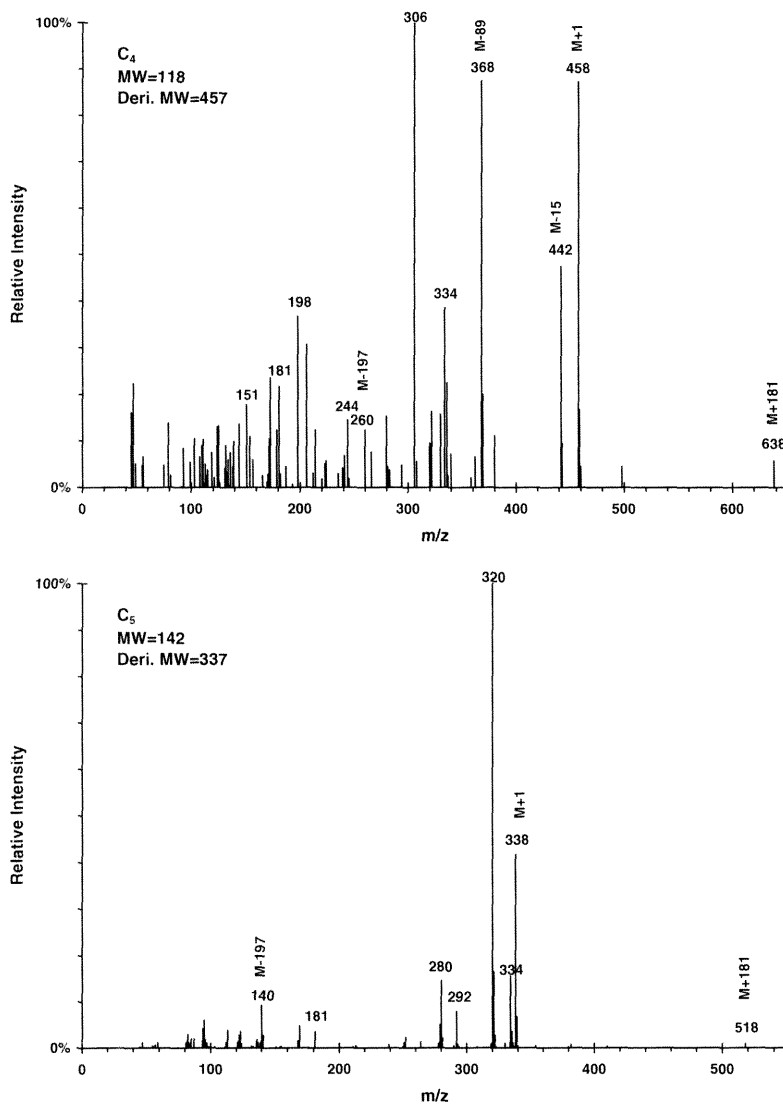


Figure A.3.8. Methane CI mass spectra for the derivatives of products from ozone oxidation of Δ^3 -carene.

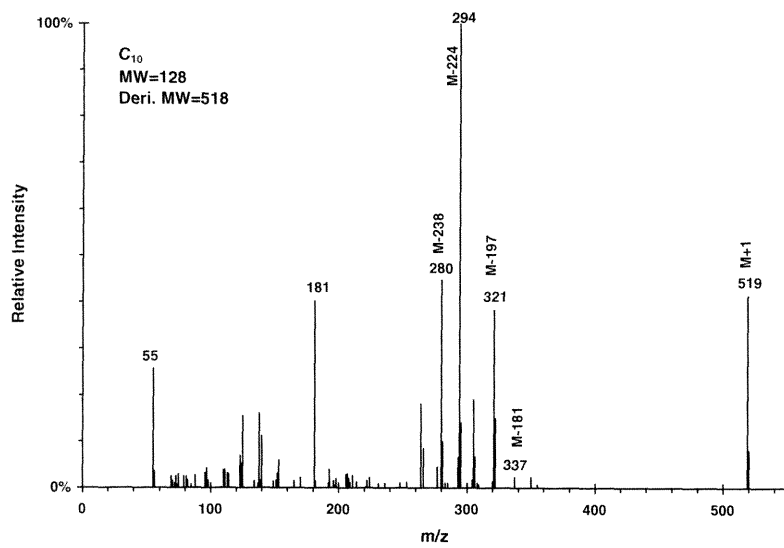


Figure A.3.8. (continued) Methane CI mass spectra for the derivatives of products from ozone oxidation of Δ^3 -carene.

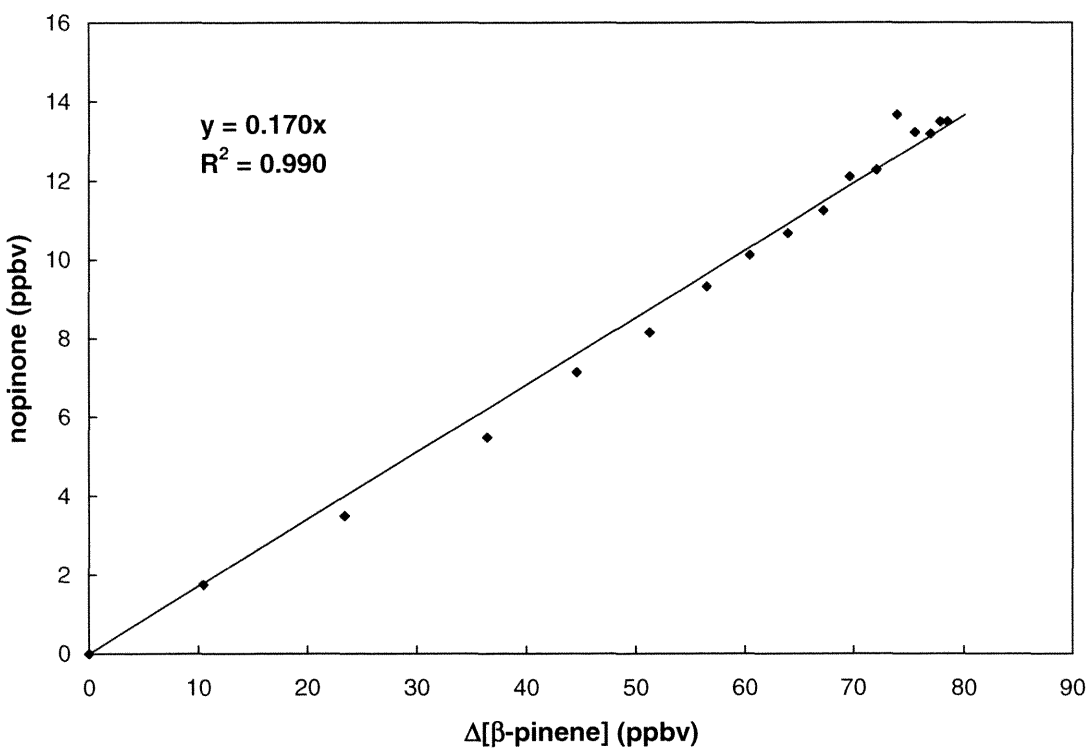


Figure A.3.9. Amount of nopinone formed versus the amount of β -pinene reacted.

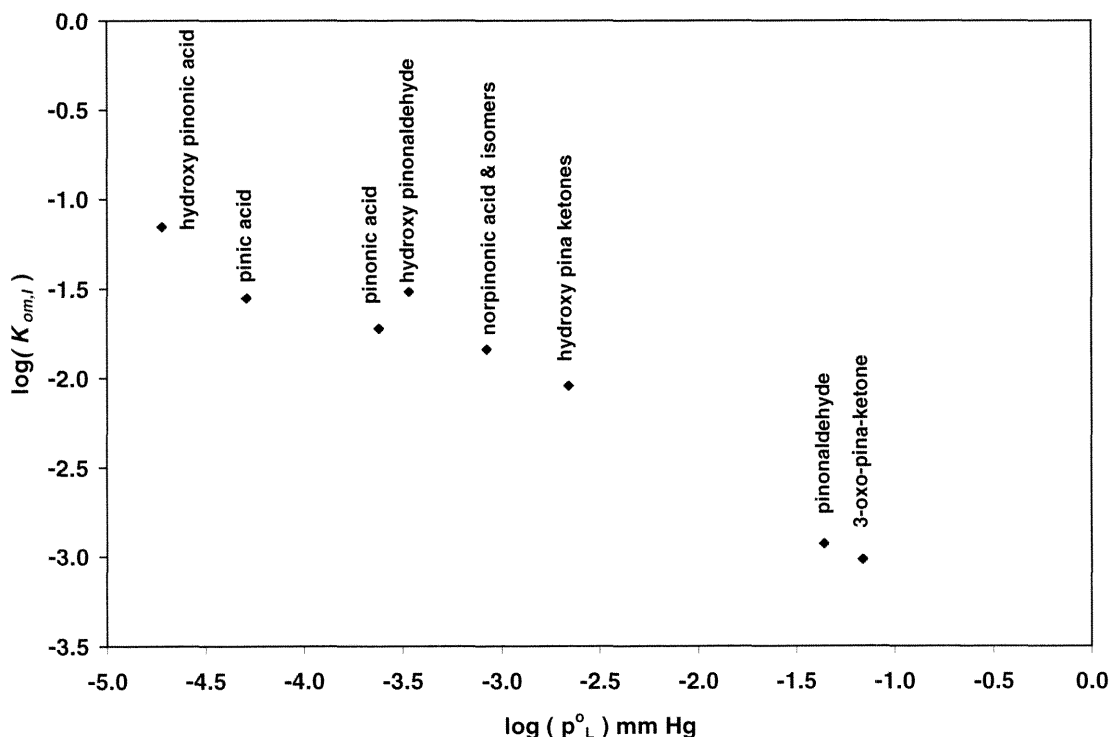


Figure A.3.10. Measured $\log(K_{om,i})$ versus estimated $\log p_L^0$ for the major products in the β -pinene/ O_3 and α -pinene/ O_3 systems.

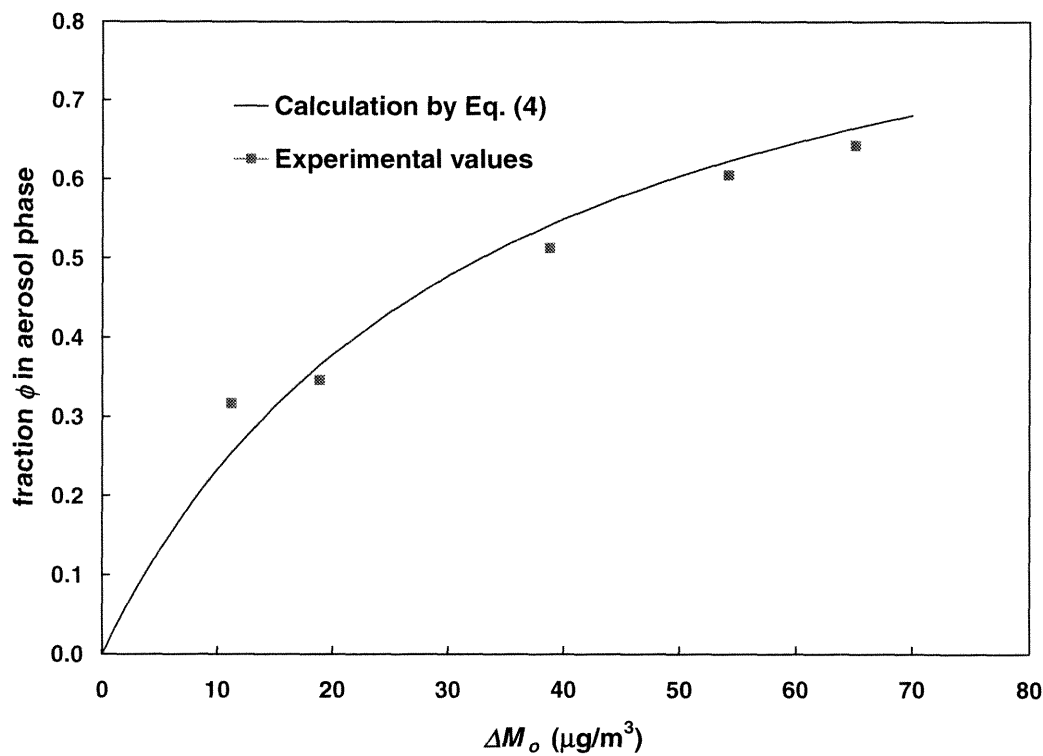


Figure A.3.11. Fraction of pinic acid in aerosol phase as a function of organic aerosol mass concentration. (The curve is generated using an average K_{om} value for pinic acid determined in all α -pinene/ O_3 and β -pinene/ O_3 experiments.)

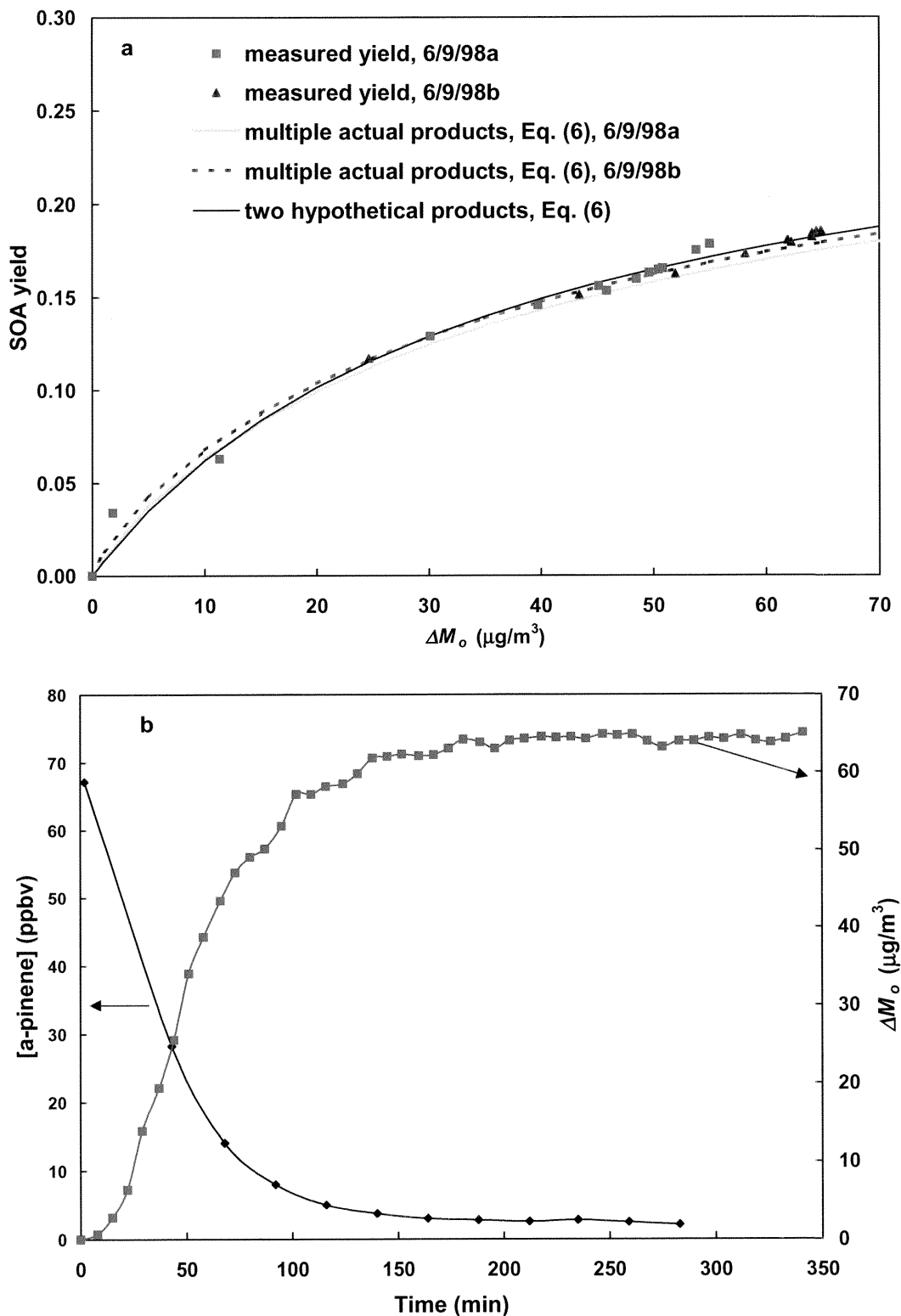


Figure A.3.12. Top: Time-dependent secondary organic aerosol yields as a function of organic aerosol mass for two α -pinene/O₃ experiments. Bottom: α -Pinene mixing ratio and organic aerosol mass concentration as a function of time in the 6/9/98b experiment.

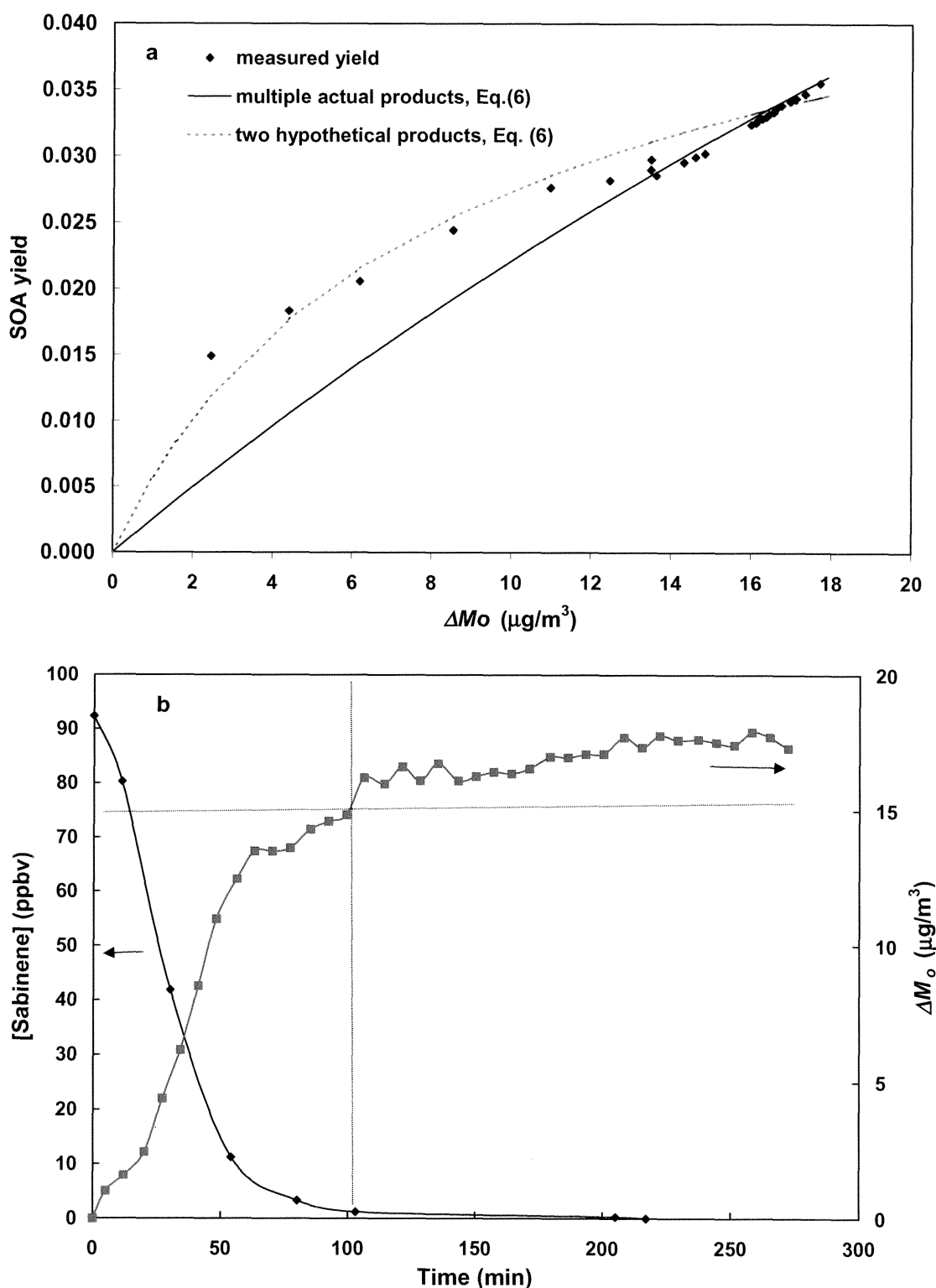


Figure A.3.13. Top: Time-dependent secondary organic aerosol yields as a function of organic aerosol mass concentration for the sabinene/O₃ reaction. Bottom: Sabinene mixing ratio and organic aerosol mass concentration as a function of time.

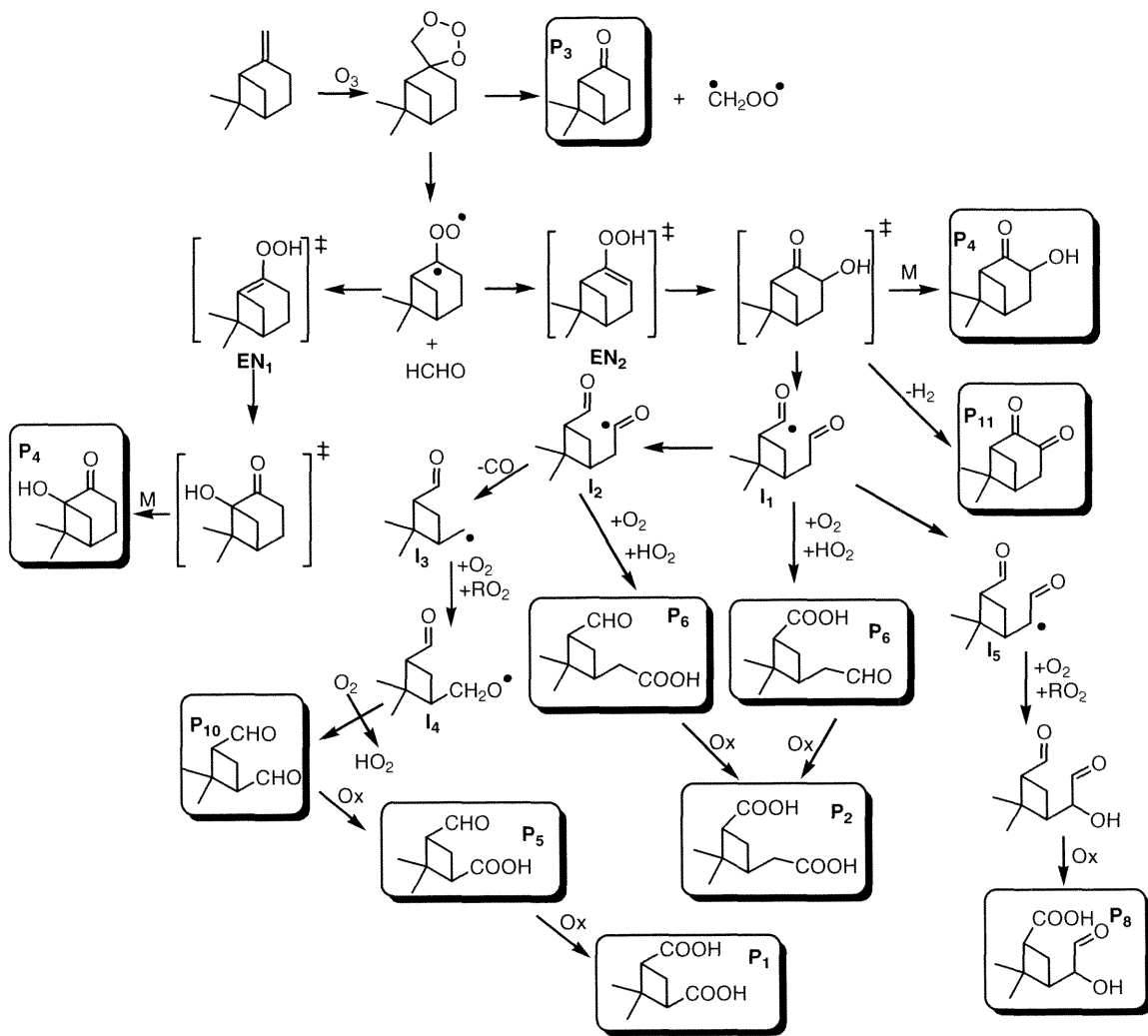


Figure A.3.14. Reaction mechanism of $\text{O}_3/\beta\text{-pinene}$ reaction. (Ox denotes oxidant)

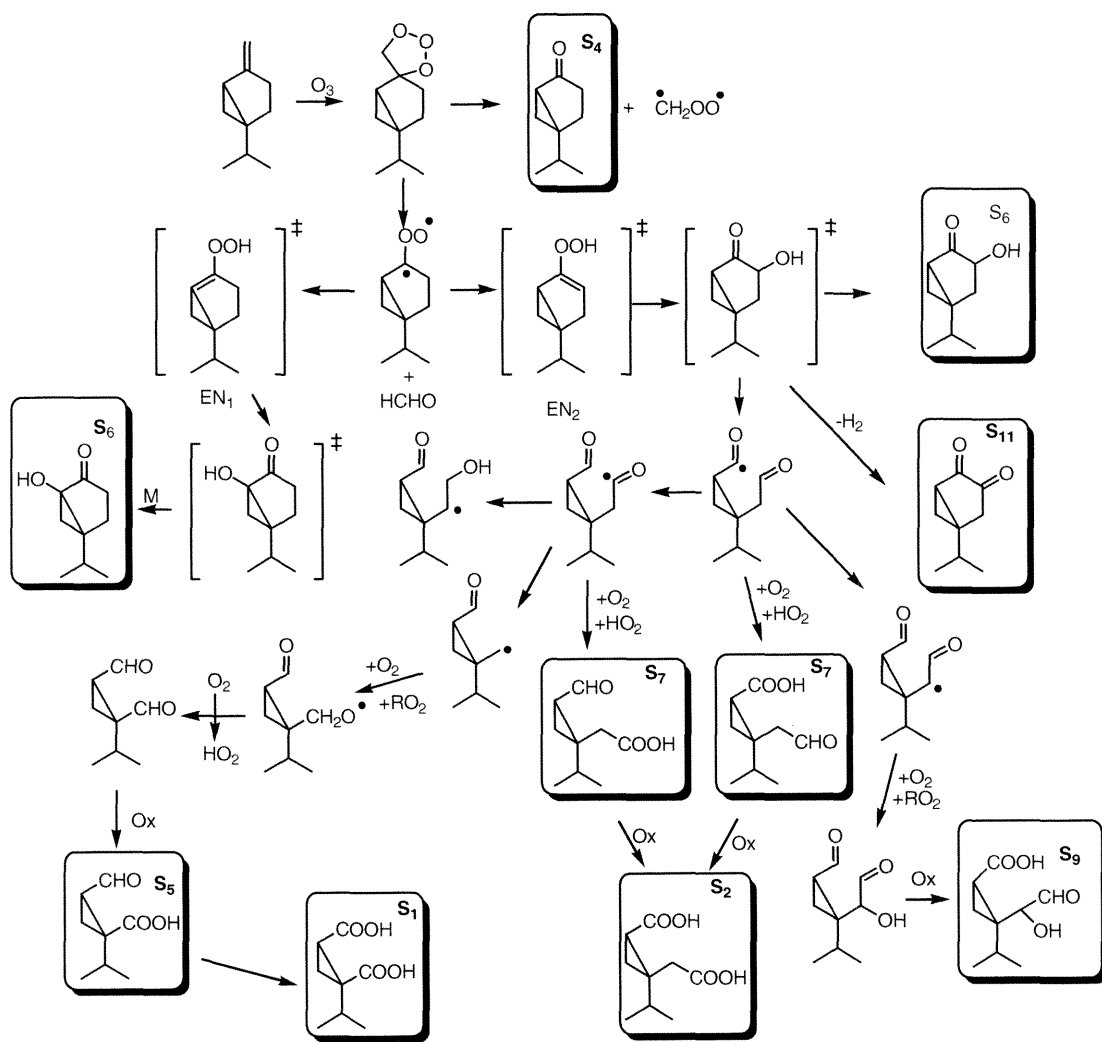


Figure A.3.15. Reaction mechanism of O_3 /sabinene reaction. (Ox denotes oxidant)

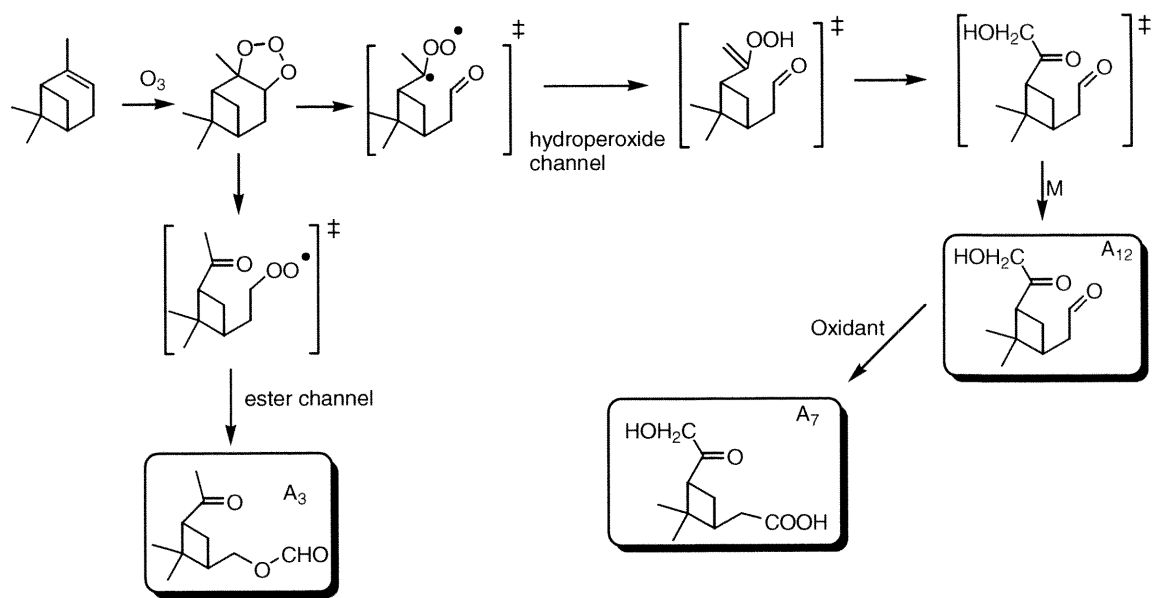


Figure A.3.16. Formation mechanism of A_3 and A_7 in the O_3/α -pinene reaction.

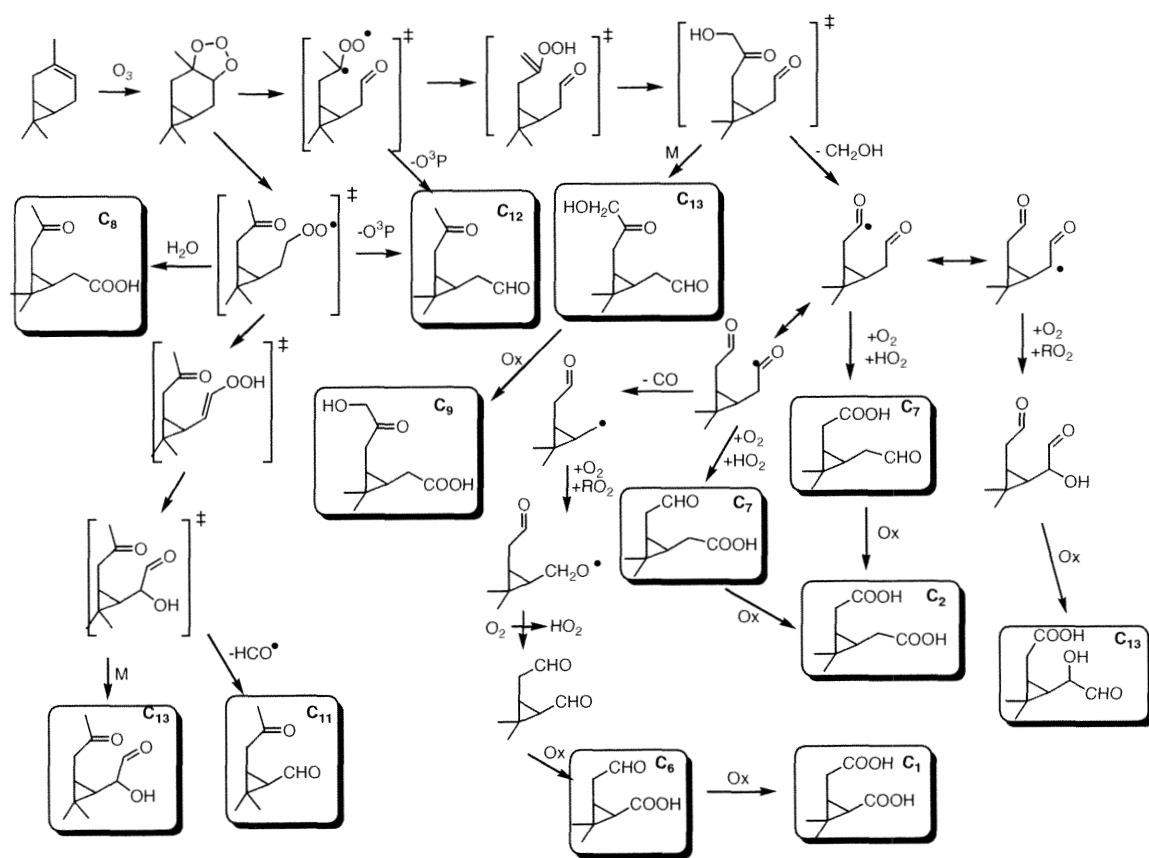


Figure A.3.17. Reaction mechanism of O_3/Δ -3-carene reaction. (Ox denotes oxidant)